DIMETHYL ETHER FROM SYNTHESIS GAS OVER BIFUNCTIONAL HYBRID CATALYST MIXTURES

A THESIS SUBMITTED TO
THE GRADUATE SCHOOL OF NATURAL AND APPLIED SCIENCES
OF
MIDDLE EAST TECHNICAL UNIVERSITY

BY

AYŞEGÜL BAYAT

IN PARTIAL FULFILLMENT OF THE REQUIREMENTS
FOR
THE DEGREE OF MASTER OF SCIENCE
IN
CHEMICAL ENGINEERING

DECEMBER 2013

Approval of the thesis:

DIMETHYL ETHER FROM SYNTHESIS GAS OVER BIFUNCTIONAL HYBRID CATALYST MIXTURES

submitted by **AYŞEGÜL BAYAT** in partial fulfillment of the requirements for the degree of **Master of Science in Chemical Engineering Department, Middle East Technical University** by,

Prof. Dr. Canan Özgen _____
Dean, Graduate School of **Natural and Applied Sciences**

Prof. Dr. Deniz Üner _____
Head of Department, **Chemical Engineering**

Prof. Dr. Timur Doğu _____
Supervisor**, Chemical Engineering Dept., METU**

Examining Committee Members:

Prof. Dr. Göknur Bayram _____
Chemical Engineering Dept., METU

Prof. Dr. Timur Doğu _____
Chemical Engineering Dept., METU

Assoc. Prof. Dr. Naime Aslı Sezgi _____
Chemical Engineering Dept., METU

Assoc. Prof. Dr. Sena Yaşyerli _____
Chemical Engineering Dept., Gazi University

Assoc. Prof. Dr. Dilek Varışlı _____
Chemical Engineering Dept., Gazi University

Date: 10.12.2013

I hereby declare that all information in this document has been obtained and presented in accordance with academic rules and ethical conduct. I also declare that, as required by these rules and conduct, I have fully cited and referenced all material and results that are not original to this work.

Name, Last name: AYŞEGÜL BAYAT

Signature:

ABSTRACT

DIMETHYL ETHER FROM SYNTHESIS GAS OVER BIFUNCTIONAL HYBRID CATALYST MIXTURES

Bayat, Ayşegül

M.Sc., Department of Chemical Engineering

Supervisor : Prof. Dr. Timur Doğu

December 2013, 192 pages

Due to increasing prices of crude oil based transportation fuels and ascending rate of global warming caused by high emission levels of conventional fuels with excessive use, alternative fuels have been considered as alternates. Dimethyl ether (DME) has received growing attention as an alternative clean fuel with low NO_x formation and particulate emission, smokeless combustion and high cetane number. DME is mainly synthesized by two methods. In the first method, synthesis gas which is a mixture of carbon monoxide and hydrogen is converted to methanol over a copper-based catalyst; then, methanol dehydration takes place in the presence of a solid acid catalyst, resulting in the production of DME. The second method is direct synthesis of DME from synthesis gas, which is a single step process that requires catalysts having two active sites for methanol synthesis and methanol dehydration. In this work, direct synthesis of DME from synthesis gas was investigated using different catalyst mixtures containing methanol synthesis and dehydration components.

Bifunctional catalyst mixtures containing copper-based methanol synthesis catalysts and commercial γ-Al_2O_3 methanol dehydration catalyst were tested in a high pressure, fixed bed flow reactor system. The reaction conditions were selected as 50 bar, temperature range of 200-300^oC with a feed gas composition of H_2/CO=50/50 based on volume ratio. The highest CO conversion was achieved as 15.6% at 300^oC using alumina promoted catalyst mixture. Bifunctional catalyst mixtures containing

alumina and zirconia promoted catalysts yielded the best DME selectivities of 68.8% and 66.4%, respectively, at 200^{o}C. Zirconia promoted catalyst (CZZr) was found to be the most stable copper-based catalyst. Catalyst mixture containing zirconia promoted catalyst calcined at higher temperature showed high initial DME selectivity of 73.9% at 225^{o}C which decreased sharply at higher temperatures.

In the second part of the work, mesoporous alumina (MA) was successfully synthesized with surface area of 322 m^2/g. Commercial methanol synthesis catalyst (MSC) and CZZr were separately mixed with MA at the same reaction conditions. The activity test of MSC + MA showed that both CO conversion and DME selectivity increased with temperature and reached 36.6% and 55.8%, respectively, with a DME yield of 20.4% at 300^{o}C. To increase the acidic strength, Silicotungstic acid (STA) was impregnated on MA (STA@MA). The amount of STA@MA was also increased. The highest CO conversion, DME selectivity and DME yield were achieved as 49.4%, 60.8% and 30.1%, respectively, at 300^{o}C by using MSC + STA@MA.

MSC + STA@MA was tested using different volumetric flow rate ratios of H_2, CO and CO_2. The overall DME selectivity obtained with 10% of CO_2 containing feed gas was 90% at 275^{o}C and decreased to 82.2% and 78.2% with increasing CO_2 to 25% and 40%, respectively. The feed gas mixture containing 10% of CO_2 could be considered as the best feed gas composition.

Experimental CO conversion and CO and CO_2 compositions were compared with the predicted equilibrium values. None of the experimental results exceeded their corresponding equilibrium CO conversion, CO and CO_2 compositions.

Results proved that, synergetic effect of occurrence of methanol synthesis and dehydration reactions simultaneously in the same system considerably enhanced DME yield.

Keywords: Dimethyl ether synthesis, Bifunctional catalyst, Direct synthesis, Mesoporous Alumina, Silicotungstic acid, Carbon Dioxide

ÖZ

İKİ FONKSİYONLU HİBRİT KATALİZÖR KARIŞIMLARI KULLANARAK SENTEZ GAZINDAN DİMETİL ETER ÜRETİMİ

Bayat, Ayşegül
Yüksek Lisans, Kimya Mühendisliği Bölümü
Tez Yöneticisi : Prof. Dr. Timur Doğu

Aralık 2013, 192 sayfa

Petrolden elde edilen yakıtların fiyatlarının sürekli artması ve bu yakıtların aşırı kullanımınından dolayı artan emisyon miktarlarının küresel ısınmanın hızlanmasına neden olmasından dolayı, bu yakıtlara alternatif olacak yakıtlar göz önünde bulundurulmaya başlanmıştır. Dimetil eter (DME) düşük NO_x dönüşümü ve partikül salınımına, dumansız yanma ve yüksek setan sayısına sahip olması sebebiyle dikkat çekmektedir. DME iki farklı yöntem ile sentezlenebilir. Birinci yöntemde, karbon monoksit ve hidrojen karışımı olan sentez gazı bakır içeren katalizör varlığında metanole dönüştürülür ve ardından katı asit katalizör varlığında oluşan metanolden dehidrasyon ile dimetil eter sentezlenir. İkinci yöntem ise sentez gazından doğrudan DME sentezidir. Bu yöntem tek adım içerir ve metanol sentez ve dehidrasyonu için iki aktif bölgeye sahip katalizör kullanımını gerektirir. Bu çalışmada, metanol sentez ve dehidrasyon bileşenleri içeren farklı katalizör karışımları kullanılarak sentez gazından doğrudan DME sentezi incelenmiştir.

Bakır bazlı metanol sentez katalizörleri ve ticari γ-Al_2O_3 metanol dehidrasyon katalizörü içeren iki fonksiyonlu katalizör karışımları yüksek basınçlı, sabit yataklı reaktör sisteminde test edilmiştir. Reaksiyon şartları olarak 50 bar basınç, 200-300^oC sıcaklık aralığı ve hacim oranına göre H_2/CO=50/50 içeren besleme gazı bileşimi seçilmiştir. En yüksek karbon monoksit dönüşümü aluminyum promotör içeren katalizör kullanılarak 300^oC'de %15,6 olarak elde edilmiştir. Aluminyum ve

zirkonyum promotör bulunan katalizörleri içeren iki fonksiyonlu katalizör karışımları ile 200^{o}C'de sırası ile %68,8 ve %66,4 olmak üzere en iyi DME seçiciliklerine ulaşılmıştır. Zirkonyum promotör içeren katalizör (CZZr) en kararlı bakır bazlı metanol sentez katalizörü olarak belirlenmiştir. Zirkonyum promotör içeren ve yüksek sıcaklıkta kalsine edilmiş katalizör içeren karışım 225^{o}C'de %73,9 ile yüksek DME seçiciliği göstermiş ama yüksek sıcaklıkta seçicilik hızla azalmıştır.

Çalışmanın ikinci kısmında, mezogözenekli aluminyum (MA) 322 m^2/g yüzey alanı ile başarı ile sentezlenmiştir. Ticari methanol sentezi katalizörü (MSC) ile CZZr aynı reaksiyon şartlarında ayrı ayrı MA ile karıştırılmıştır. MSC + MA'nın aktivite sonucu gösterdi ki CO dönüşümü ve DME seçiciliği sıcaklıkla artmış ve sırası ile %36,6 ve %55,8'e yükselmiş ve 300^{o}C'de %20,4 DME verimi elde edilmiştir. Asidik kuvveti artırmak için MA üzerine Silicotungstik asit (STA) yüklenmiştir (STA@MA). Ayrıca, STA@MA miktarı da artırılmıştır. 300^{o}C'de en yüksek CO dönüşümü, DME seçiciliği ve DME verimi sırası ile %49,4, %60,8 ve %30,1 olarak MSC + STA@MA kullanılarak elde edilmiştir.

H_2, CO ve CO_2 gazlarının farklı hacimsel akış hızı oranları kullanılarak MSC + STA@MA test edilmiştir. %10 CO_2 içeren besleme gazı ile 275^{o}C'de %90 toplam DME seçicliği elde edilmiş ve bu değer CO_2 yüzdesinin %25 ve %40'a yükseltilmesi ile sırası ile %82,2 and %78,2'ye düşmüştür. %10 CO_2 içeren besleme gazı en iyi besleme gaz bileşimi olarak belirlenmiştir.

Deneysel olarak elde edilen CO dönüşümü ile CO and CO_2 komposizyonları tahmin edilen denge değerleri ile kıyaslanmıştır. Deneysel sonuçların hiçbiri kendilerine karşılık gelen denge CO dönüşümü ile CO and CO_2 komposizyonlarını geçmemiştir.

Sonuçlar kanıtladı ki, methanol sentez ve dehidrasyon reaksiyonlarının aynı sistemde eş zamanlı olarak meydana gelmesi ile oluşan sinerji DME verimini önemli ölçüde artırmıştır.

Anahtar Kelimeler: Dimetil Eter sentezi, İki fonksiyonlu katalizör, Doğrudan sentez, Mezogözenekli aluminyum, Silikotungstik asit, Karbondioksit

To my family

ACKNOWLEDGEMENTS

I would like to present my sincere thanks and deepest gratitude to my supervisor Prof. Dr. Timur Doğu for allowing me to be a part in his research group, for his continuous support, encouragement and inspiration. I also would like to thank him for his endless guidance to every single part for the last two years.

I would like to offer my sincere thanks to Assoc. Prof. Dr. Naime Aslı Sezgi for her great support, valuable suggestions and advices not only for this study but also for in every aspects.

I would like to present my sincere and special thanks to Seval Gündüz for her endless support and for being there whenever I needed. This work would not be completed without her great contribution, help and friendship.

I would like to offer my sincere thanks to Arzu Arslan for her kindness, great support and friendship. I would like to express my sincere thanks to Gökhan Çelik for his great support and advices during this work. I would like to thank Canan Şener for her great advices.

I would like to thank my friend Burçin İkizer for her support, advice and friendship throughout this work. I would like to thank my friends Özgen Yalçın, Tuğçe Kırbaş and Erdem Balık.

I would like to present my special thanks to my family. There are not enough words to express my sincere gratitude for their continuous and everlasting support and encouragement throughout my life. I would not be able to conclude this work without their faith in me. I would like to thank my mother Kerime Bayat, my father Mustafa Bayat and my dear sister Ayça Bayat for always being there.

TABLE OF CONTENTS

LIST OF FIGURES

FIGURES

LIST OF TABLES

TABLES

NOMENCLATURE

C_p: Heat Capacity (J/mol.K)

DME: Dimethyl Ether

DRIFTS: Diffuse Reflectance Infrared Fourier Transform Spectroscopy

EtOH: Ethanol

FA: Formic Acid

G: Gibbs Free Energy (kJ/mol)

H: Enthalpy (kJ/mol)

IUPAC: International Union of Pure and Applied Chemistry

K: Equilibrium Constant

K_P: Equilibrium Constant based on Partial Pressure

K_φ: Equilibrium Constant based on Fugacity

MW: Molecular weight (g/mol)

MCM: Mobil Composition of Matter

MeOH: Methanol

$\dot{n}$: Molar flow rate

n: Mole

P: Pressure (bar)

Q: Volumetric flow rate (ml/min)

R: Gas constant (8.314 J/mol.K)

S, $\underline{S}$: Selectivity

SBA: Santa Barbara Amorphous

T: Temperature (°C)

TEM: Transmission Electron Microscopy

V: Volume (m^3)

X: Conversion

XRD: X-Ray Diffraction

y: Molar composition

Y: Yield

Z: Compressibility Factor

φ: Fugacity (bar)

CHAPTER 1

INTRODUCTION

The excessive use of fossil fuel sources Such as coal, natural gas and petroleum oil results in rapid depletion of the reserves and more importantly environmental pollution and greenhouse effect due to carbon dioxide emissions [1]. Therefore, the effort for development of new, clean, non-petroleum based alternative fuels together with more sustainable energy technologies evolves because of diminishing trend in fossil fuel resources followed by fast increment in the prices of oil and natural gas as well as impact of strict environmental laws and regulations on the production and use of these resources [2, 3]. Recently, DME has received significant attention as a potential alternative to diesel fuel.

DME can replace the conventional fuels due to its good fuel characteristics and environmentally friendly properties. Therefore, it can also be utilized for many industrial and household applications. Physical and fuel properties of DME are presented and compared with other fuels in Chapter 2. Application areas of DME are also mentioned in addition to possible setbacks for application.

In Chapter 3, the literature survey on the synthesis methods of dimethyl ether is given. DME is mainly synthesized by two methods. In the first method, methanol is produced from synthesis gas then, dehydrated to DME. In the second method, DME is directly synthesized from synthesis gas using a bifunctional catalyst with two active sites. One type of site is for methanol synthesis function and for this function mainly copper and zinc containing catalysts are used. The other type active site is for methanol dehydration function and solid acid catalysts, such as γ-Al_2O_3, aluminum silicates and zeolites are used. In this chapter, the important aspects and development

of catalytic materials for the direct synthesis of DME, methanol synthesis and methanol dehydration processes are also presented.

In Chapter 4, thermodynamic analyses are performed in order to determine the operating parameters for DME synthesis. Due to the exothermic nature of methanol synthesis reaction, thermodynamic limitations occur which reduces the carbon monoxide conversion. The direct DME synthesis overcomes the thermodynamic limitations of methanol synthesis reaction; however, the amount of methanol produced is important for being converted to DME. Equilibrium conversions of methanol synthesis reaction and direct DME synthesis reactions are plotted with respect to different temperatures and pressures.

In Chapter 5, the mesoporous catalytic material that was used in this study is introduced and the parameters that affect the catalytic performance of the material are investigated. The characterization techniques applied in this study are also given.

The synthesis procedures of the mesoporous material are explained and the characterization techniques applied to the synthesized materials are presented in Chapter 6. The high-pressure flow system, which was used to test the prepared bifunctional catalysts for the direct synthesis of DME from syngas, is described in detail.

In Chapter 7, the characterization results of synthesized catalysts are given and the results of existing methanol synthesis catalysts are summarized. In Chapter 8, the activity results of all of the studies performed throughout the thesis work are illustrated. The activity test results involve conversions and selectivities with respect to changes in temperature and different conditions. In Chapter 9, thermodynamic analyses were performed to compare the activity results with equilibrium. Finally, conclusions are given in Chapter 10.

CHAPTER 2

IMPORTANCE OF DIMETHYL ETHER

The energy requirement of the world depends on the fossil fuel sources such as coal, natural gas and petroleum oil. Among them, petroleum oil is heavily used as oil based fuel for transportation. The excessive use of these sources, which are not renewable, results in rapid depletion of the reserves and more importantly environmental pollution and greenhouse effect due to carbon dioxide emissions [1]. Therefore, the effort for development of new, clean, non-petroleum based alternative fuels together with more sustainable energy technologies evolves because of diminishing trend in fossil fuel resources followed by fast increment in the prices of oil and natural gas as well as impact of strict environmental laws and regulations on the production and use of these resources [2, 3].

Due to the limitations of fossil fuels, green energy sources such as solar, geothermal, wind, and tidal energies and also synthetic sources such as biomass energy, hydrogen and fuel cells, and gas-to-liquid coal gasification have gained much interest recently. For being environmental friendly and involving the capabilities of high energy density and commercialization, synthetic energy sources, in particular, have become pioneers for the consideration as an alternative, non-petroleum energy sources [2, 4]. Alcohols and ethers are gaining importance especially for transportation purposes; among them, dimethyl ether (DME) can replace the existing transportation fuels [5].

Dimethyl ether, with a chemical formula of CH_3OCH_3, is the simplest ether compound and an invisible gas at room temperature and pressure which can be liquefied at 6 atm (at room temperature) or at -6^{o}C (atmospheric pressure) having a vapor pressure of 5 atm at 20^{o}C. Being a volatile organic compound, DME is non-

toxic, non-teratogenic, non-carcinogenic and non-mutagenic. It burns with a visible blue flame and possesses a sweet ether-like odor. DME is not corrosive for metal however it is not inert for rubber and its by-products [4, 6-9].

Recently, DME has received more attention as a potential alternative to diesel fuel to be used in compression ignition engines due to its good fuel characteristics. The physical properties of dimethyl ether and other alternative fuels are compared in Table 1. The combustion quality of diesel fuel during combustion ignition is measured by the cetane number and DME has higher cetane number (55 - 60) as compared to the conventional diesel fuel having the cetane number of 55. As compared to the conventional fuels, DME emits less air polluting materials such as NOx, CO, hydrocarbons, particulate matters and soot, and it also provides lower engine noise [4, 10]. Its high cetane number, low boiling point (-24.9^{o}C), and high oxygen content (35 wt%) provide smokeless combustion and instant vaporization during injection which requires lower fuel injection pressures; less than 300 atm compared to 2000 atm as for modern diesel engines [8]. The auto-ignition temperature (350^{o}C) of DME is similar to that of conventional diesel fuel. Due to fast fuel/air mixing provided by low boiling point, ignition delay is reduced, that is especially useful for the vehicles started at cold [1].

DME may be considered as an alternative fuel for diesel engines with minor modifications on the fuel system. However, the fuel volume, when DME is used, needs to be larger, since the energy density per volume of DME is lower than that of diesel and gasoline. In order to travel same distance, the necessary volume of DME for the storage tank is about 1.7 times the volume of diesel fuel for the storage tank. Studies show that the vehicles with the ordinary diesel engines having a modification in the fuel injection systems showed the same performance with a significant reduction in exhaust emission as compared to diesel fuels [8].

Table 1. Comparison of physical properties of dimethyl ether and other alternative fuels * (Adapted from [7, 11])

Properties	*DME*	*Diesel*	*Gasoline*	*Methanol*	*Ethanol*	*Methane*	*Propane*	*Butane*
Chemical Structure	CH_3OCH_3	$C_{14}H_{30}$	C_7H_{16}	CH_3OH	C_2H_5OH	CH_4	C_3H_8	C_4H_{10}
Molecular Weight, g/mol	46	-	100	32	46	16	44	58
Liquid density, g/cm^3	0.67	0	0.73-0.76	0.79	0.79	0.42	0.49	0.57
Vapor pressure, bar	5.3	-	-	0.13	0.06	0.05	9.30	2.40
Explosion limit, vol %	3.4 -18.6	0.6-6.5	1.4-7.6	6.7-36	3.3-19	5-15	2.1-9.4	1.9-8.4
Cetane number	55-60	40-55	5-20	5	40,50	0	5	10
Normal Boiling point, °C	-24.9	125-400	38-204	64	78	-162	-42	-0.5
Net Calorific Value, kcal/kg	6900	10200	-	4800	-	12000	11100	10900
Sulfur content, ppm	0	~250	~200	0	0	7-25	-	-
Carbon Content, wt.%	30.8	87	85.5	37.5	29.4	74	81.8	82.8
Specific gravity of gas	1.6	-	-	1.1	1.6	0.6	1.5	2.0
Ignition Temperature, K	350	-	228	385	365	540	470	430
Heat of evaporation, kJ/mol	21.5	-	-	35.2	38.9	8.2	18.7	22.3

* Values are at standard temperature and pressure

DME can replace LPG in household-use for heating and cooking due to great energy carrier potential. Since DME has similar properties with LPG, DME can be transported using the infrastructures for LPG both through land and ocean. DME can also be stored in the existing equipment that is used for LPG. However, this storage equipment requires minor modifications to the parts such as pumps, seals, and gaskets. These kinds of modifications are also necessary for the existing LPG refilling stations in order to be used for DME since it would cost less rather than building a new facility [7]. This application can be considered especially for people who live in the rural areas in developing countries, such as China, India and Brazil to fulfill the need for portable fuel [12].

DME can be preferred as an environmentally friendly aerosol spray and refrigerant instead of traditional chlorofluorocarbon (CFCs, Freon) and newer R-134a (HFC-134a). Due to low toxicity and an average lifetime in the atmosphere of approximately 5 days, DME has zero ozone depletion potential (ODP) and lower globe warming potential (GWP). Therefore, it is not harmful to the atmosphere and can be used in aerosol-based household products such as hair sprays and dyes, personal care mousses, antiperspirants, and room air fresheners [13-15].

DME, which can also be used as turbine fuel for power generation, provides high efficiency and significant reduction in NO_x and CO levels as compared to methane and liquid naptha. Having the properties of easy transportation and volatility, DME is also a hydrogen source for fuel cells that is produced by catalytic reforming and hydrolysis at low temperatures [7]. DME can be preferred instead of methanol as the reactant to produce hydrocarbons such as light olefins, BTX aromatics, and valuable chemicals such as methyl acetate, dimethyl sulphate [16].

DME can be synthesized from carbon containing materials such as natural gas, crude oil, coal and biomass (i.e. agricultural residues). Synthesis gas (syngas) which is a mixture of carbon monoxide and hydrogen is first produced from these carbonaceous materials and then converted to DME by two methods. The first method is the conventional two-step process in which methanol is produced from syngas and then

dehydrates to DME in sequential reactors. The second method is the one-step process in which syngas is directly converted to DME in a single reactor [4, 7]. The production of DME possesses the advantage of relieving from the dependence on crude oil and being producible from renewable sources, since syngas and methanol can be obtained from biomass [17].

The greenhouse effect has become an important global issue and much attention is paid on the reduction on greenhouse gases by development of new catalytic systems that provide efficient usage and recycling of these gases especially CO_2 released due to extensive consumption of fossil fuels. Capturing and then transforming CO_2 into alternative liquid fuels; methanol and DME, and important chemicals such as urea, salicylate is an attractive subject. Production of methanol from CO_2 containing syngas would provide reduction in CO_2 emission and significant enhancement in the economy of the overall process [18, 19].

There are some difficulties in application of DME as fuel due to its physical properties such as low boiling temperature, high vapor pressure, high compressibility and lower viscosity approximately by a factor 20 as compared to diesel fuel. Therefore, leakage problems in pumps and fuel injectors, choke of vapor in fuel lines may be seen. Additives that are used for diesel fuel could be used to solve these problems [6, 7].

CHAPTER 3

SYNTHESIS METHODS OF DIMETHYL ETHER

In this chapter, the literature survey on the synthesis methods of dimethyl ether is given with important aspects and development of catalytic materials for the direct synthesis of DME, methanol synthesis and methanol dehydration processes.

3.1. DIRECT SYNTHESIS OF DIMETHYL ETHER

DME can be synthesized via two methods and for whichever method is preferred, first syngas may be produced from several feed stocks such as natural gas, coal, oil or biomass via gasification or steam/dry reforming reactions. The first method is the conventional two-step process that is known as the indirect method. In this process, methanol is first synthesized from syngas by hydrogenation of CO and CO_2 over copper-based catalyst, and then dehydrated to DME over solid-acid catalysts in sequential reactors. The second method is the one-step process and known as the direct method. In direct method, methanol synthesis and dehydration reactions occur in a single reactor. The direct synthesis of DME from syngas requires bifunctional catalyst or physically admixed catalysts which possess two kinds of active sites; one site for the methanol synthesis provided by metallic function containing as CuO, ZnO, Al_2O_3, and Cr_2O_3 and one site for the methanol dehydration to DME provided by solid acid function such as γ-Al_2O_3, HZSM-5, HY zeolites, or SAPO's [1, 20-24].

The reactions that take place in the direct synthesis of DME are represented in reactions (1) - (6). There are two overall reactions; reaction (1) is the combination of methanol synthesis reactions (3) and (4), methanol dehydration reaction (5) and water-gas shift reaction (6). The other overall reaction (2), on the other hand,

includes all the reactions except for water-gas shift reaction. Copper-based catalyst also catalyzes the water-gas shift reaction as well as methanol synthesis reaction [24, 25].

$3CO + 3H_2 \leftrightarrow CH_3OCH_3 + CO_2$	ΔH_{rxn} = - 246 kJ/mol	(1)
$2CO + 4H_2 \leftrightarrow CH_3OCH_3 + H_2O$	ΔH_{rxn} = - 205 kJ/mol	(2)
$CO + 2H_2 \leftrightarrow CH_3OH$	ΔH_{rxn} = - 90 kJ/mol	(3)
$CO_2 + 3H_2 \leftrightarrow CH_3OH + H_2O$	ΔH_{rxn} = - 49 kJ/mol	(4)
$2CH_3OH \leftrightarrow CH_3OCH_3 + H_2O$	ΔH_{rxn} = - 25 kJ/mol	(5)
$CO + H_2O \leftrightarrow CO_2 + H_2$	ΔH_{rxn} = - 41 kJ/mol	(6)

Direct synthesis of dimethyl ether generally occurs at a temperature range of 240°C-280°C and at a pressure range of 30 bar-70 bar. Since the reactions are exothermic, control of temperature and removal of heat from the reactor are vital in order to reach high conversion of syngas [26]. Generally, the standard condition is chosen as 260^{o}C and 50 bar, since methanol synthesis catalyst deactivates significantly when the temperature is selected above 270^{o}C. [27]

In the direct synthesis process, the number of independent reactions is three since the CO_2 hydrogenation reaction (4) can be obtained by reactions (3) and (6). Therefore, the main reactions in this process are considered to be CO hydrogenation (3), methanol dehydration (5) and water-gas shift (6) reactions. The thermodynamic equilibrium limitation exists for methanol synthesis reaction, therefore, high pressure and low temperature is needed to achieve a suitable syngas conversion. However, the direct synthesis of DME is thermodynamically and economically more favorable due to in situ removal of methanol by dehydration reaction. Therefore, the system becomes independent of thermodynamic limitation of methanol synthesis reaction.

The direct synthesis exhibits a synergistic system in which higher syngas conversion and productivity is obtained than the conventional process would provide. The synthesized methanol dehydrates to DME and water through reaction (5) and shifts the equilibrium to the right-hand side. Water is removed by water-gas shift reaction (6) to accelerate reaction (5) and to be consumed to produce extra hydrogen to be used in reaction (3). Due to the synergetic effect, one product of a step becomes a reactant for another step and high syngas conversion can be achieved [27-29].

The direct synthesis of DME from syngas has certain advantages over conventional two-step process both thermodynamically and economically. The direct synthesis relieves the system from thermodynamic equilibrium constraint caused by methanol synthesis reaction itself and syngas conversion highly enhances. In addition, the cost of production of DME by single-step process could be lower than that of two-step process. The two-step process has the disadvantage of the requirement of a secondary reactor for dehydration. Furthermore, methanol dehydration to DME is also expensive because methanol is a valuable chemical. Due to the synergy within the reactions in the direct synthesis, higher productivity is achieved in a single reactor. However, separation of the products of the direct synthesis is difficult and expensive than the conventional method. Nevertheless, the one-step process is getting more academic and also industrial interest due to its superiority [3, 30, 31].

In the last five decades, the concentration of CO_2 in the atmosphere has evolved by 20% due to excessive consumption of fossil fuels in the industrial, commercial and commune applications. In order to control and reduce the CO_2 amount in the atmosphere in the next four decades, the development of legal regulations, that would be applied globally, is a prolonged process. Furthermore, the new technologies needs to be developed to capture, recycle, reuse, limit and control the excess emission of CO_2 and to produce valuable products such as DME, urea and hydrocarbons [32, 33]. Although utilization of expensive hydrogen for chemical reduction of carbon dioxide into new products may seem unreasonable, the catalytic hydrogenation of carbon dioxide over solid catalysts is advantageous than other

methods such as electrochemical, photochemical, and biochemical methods since very high and selective conversion can be achieved [34].

The direct synthesis of DME from carbon dioxide and hydrogen involves three reactions as well; methanol synthesis (4), methanol dehydration (5) and reverse water-gas shift reaction (7). The synergetic effect of the reactions is also present and methanol produced by reaction (4) is in situ removed by reaction (5) and the overall reaction (8) is shifted to the right-hand side using a bifunctional catalyst having two active sites. For the overall reaction (8), methanol synthesis (4) and methanol dehydration reactions (5) were considered [2].

$$CO_{2(g)} + 3H_{2(g)} \leftrightarrow CH_3OH_{(g)} + H_2O_{(g)} \qquad \Delta H_{298} = -49.46 \text{ kJ/mol} \qquad (4)$$

$$2CH_3OH_{(g)} \leftrightarrow CH_3OCH_{3(g)} + H_2O_{(g)} \qquad \Delta H_{298} = -23.51 \text{ kJ/mol} \qquad (5)$$

$$CO_{2(g)} + H_{2(g)} \leftrightarrow CO_{(g)} + H_2O_{(g)} \qquad \Delta H_{298} = +41.17 \text{ kJ/mol} \qquad (7)$$

$$2CO_{2(g)} + 6H_{2(g)} \leftrightarrow CH_3OCH_{3(g)} + 3H_2O_{(g)} \qquad \Delta H_{298} = -122.43 \text{ kJ/mol} \qquad (8)$$

When the feed gas containing CO_2 and H_2 is used, the CO_2 hydrogenation and reverse water-gas shift reactions are dominant and produce significant amount of water of about 30–40%. For the feed gas containing both CO and CO_2 with a higher ratio of CO, the overall CO hydrogenation becomes the main reaction [32]. However, at low temperatures, CO_2 hydrogenation is the main reaction since the CO hydrogenation is slower [35]. Adding small amount of CO_2 in the feed mixture enhances methanol synthesis and reduces the required pressure for the process [36]. In addition, the studies show that the suitable ratio of CO/CO_2 also reduces the apparent activation energy of methanol synthesis reaction [37, 38]. However, high CO_2 content in the feed gas reduces CO conversion due to inhibition of water-gas shift reaction followed by reduction in CO hydrogenation to methanol [24].

Bae et al. [21] investigated the effect of γ-Al_2O_3 preparation method, weight ratio of methanol synthesis to γ-Al_2O_3 and aging time of the hybrid catalyst at H_2-deficient condition; $CO/CO_2/H_2$ = 41/21/38 vol % at 250°C and 40 bar. γ-Al_2O_3 catalysts prepared by aluminum nitrate (AN) and aluminum isopropoxide (AIP) provided similar CO conversions and DME selectivities but different CO_2 and MeOH formation. The possible reason for this result was determined as that γ-Al_2O_3 with AN possessed stronger acidic sites than that of with AIP however, due to possibility of micropore blockage during synthesis, γ-Al_2O_3 catalysts with AN had smaller surface area than with AIP. As the weight ratio of methanol synthesis to dehydration catalyst was decreased from 5 to 1, selectivities of MeOH, DME, CO_2 and CO conversion were observed to decrease from 66.1% to 25.5%, increase from 7.9% to 44.0%, increase from 25.1% to 30.2% and decreased from 29.3% to 17.8%. It was determined that methanol dehydration catalyst amount favored DME selectivity while methanol synthesis catalyst favored CO conversion. Best catalytic performance was obtained with the hybrid catalyst aged for 6 h for highest CO conversion, best MeOH and DME yields and lowest CO_2 formation.

Kim et al. [39] investigated the effect of Si/Al ratio on activity of Na-ZSM-5 and H-ZSM-5 catalysts methanol and DME synthesis having a feed composition of H_2/CO = 1.5. The results indicate that Si/Al ratio was inversely related to the acidic strength of ZSM-5 catalyst and highest methanol dehydration rate was obtained with H-ZSM-5(30). According to the direct synthesis results, the DME yield and CO conversion were higher for the hybrid catalyst with Na-ZSM-5(30) which were 27.8% and 45.5% at 280°C respectively. As the weight ratio of Na-ZSM-5(50) in the catalyst mixture was selected as 40 wt% the highest CO conversion, DME yield and selectivity of CO to DME were obtained. However all of which decreased at higher Na-ZSM-5(50) composition which caused methanol dehydration rate to increase, methanol synthesis rate to decrease. Lower methanol yield was obtained with the mixed catalyst with Na-ZSM-5(30) than with Na-ZSM-5(50), indicating that methanol formed on the Na-ZSM-5(30) dehydrated quickly to DME.

Yoo et al. [20] studied the catalytic performances of solid acid catalysts which were SAPO type catalysts with different acidic strength and pore structure. The reaction conditions were 260°C and 42 bar with a feed mixture of $H_2/CO = 1.5$ and the results indicated that solid acid catalysts that possessed strong acid sites such as SAPO-34 and -18 presented high initial activity however their activity decreased rapidly due to formation of coke deposited within the pores. The catalytic stability of the solid acid catalysts that possessed moderate acid sites and good pore structure such as SAPO-5 and -11 were much higher and hydrocarbon formation was insignificant. The CO conversion and DME selectivity reached maximum values of 55% and 63% respectively at the solid acid amount of 10%.

Nie et al. [40] prepared core-shell structured CuO–ZnO@H-ZSM-5 (CZ@H) catalysts by homogeneous precipitation through urea hydrolysis. At 260°C and 20 bar using 0.5 g of catalyst, the performances of catalysts having different weight ratio of CZ to H were compared and best results were obtained using CZ@H(7.5) that provided CO conversion of 53.2% and DME selectivity of 69.6% which was higher that of admixed catalyst as 65.1%. It was seen that as the gas hourly space velocity increased, CO conversion and CO_2 selectivity decreased however DME selectivity remained at similar values. This can be attributed to the high acid strength and good cooperation of methanol synthesis and dehydration functions. The excellent core-shell structure and high Cu dispersion over the surface were found to benefit the high catalytic activity.

Naik et al. [33] studied the performances and stability of admixed catalyst containing $6CuO–3ZnO–Al_2O_3$ (MSC) and γ-Al_2O_3 and H-ZSM-5 at 260^{o}C, 50 bar with $H_2/CO_2 = 3$ in fixed-bed and slurry reactors. Using MSC/H-ZSM-5 catalyst, the selectivities of DME, CO and MeOH were obtained as 65%, 33% and 2% respectively in the fixed-bed reactor. In the slurry reactor, the values were obtained as 53%, 42% and 5% respectively. The catalyst 6CuO–3ZnO–Al2O3/γ-Al_2O_3 mostly promoted reverse-water-gas-shift (RWGS) reaction with very low selectivity to DME, and a low conversion of CO_2. The other catalyst, $6CuO-3ZnO-1Al_2O_3$/H-ZSM-5, showed much higher conversion of CO_2 with higher selectivity to DME in

both, fixed-bed and slurry reactors, while MSC/γ-Al_2O_3 presented lower activity and stability. Selectivities were obtained as 82% for CO, 15% for methanol and 3% for DME in the fixed-bed reactor and of 58% for CO, 38% for methanol and 4% for DME in the slurry reactor. The results indicated that H-ZSM-5 was more stable than γ-Al_2O_3 and did not deactivate in the presence of water. Fixed-bed reactor was better for water removal from the surface of the catalyst since catalyst was suspended in hydrocarbon oil, which causes resistance for water removal in the slurry reactor.

Sierra et al. [16] studied the regeneration of CuO-ZnO-Al_2O_3/γ-Al_2O_3 catalyst which were used for DME synthesis at 275^{o}C, 30 bar with H_2/CO molar ratio in the feed of 3/1. The used catalyst was regenerated with O_2 diluted with He (5% of O_2) and selection of regeneration temperature was important for effective removal of coke and to avoid irreversible catalyst deactivation due to Cu sintering. The study revealed that two types of coke were deposited on the catalyst; one of them formed on the metallic sites, the other one formed on the Al_2O_3 support. By, coke combustion was not complete but initial activity of catalyst was regained. This could be due to efficient combustion of coke on the metallic sites but incomplete of coke located on the Al_2O_3 support. Regeneration at 350^{o}C resulted in Cu sintering while regeneration at 325^{o}C restored the initial activity of the catalyst.

Fei et al. [41] studied the effect of modification of HY zeolite-supported Cu–Mn–Zn catalysts. The modified HY zeolites were also compared for methanol dehydration activity at 245^{o}C and the results showed that the activity and stability of Zr- and Ni-modified HY zeolite were higher than that of Fe-, Co-, and Cr-modified HY zeolite which were deactivated because of carbon deposition since they possessed higher amount of strong acid sites. Direct DME synthesis was performed at 245^{o}C and 20 bar with feed gas mixture of H_2/CO = 1.5. As the weight ratio of Zr–HY in Cu–Mn–Zn/Zr–HY catalyst was increased up to 25%, both DME selectivity and CO conversion increase and at 25% the highest DME selectivity and CO conversion were achieved as 67.5% and 71.4%, respectively. However at higher ratios, both DME selectivity and CO conversion decreased due to deep dehydration of methanol and DME to hydrocarbons.

Chen et al. [10] compared the effects of reaction temperature, pressure, CO_2 concentration in the feed and ZSM-5 amount on the synthesis on DME synthesis. As the ratio of CO_2/CO in the feed was increased from 0 to 0.5, reverse WGSR was favored and H_2 conversion increased at low temperatures according to thermodynamic analysis. However, at higher temperatures, DME formation was suppressed due to presence of high CO_2 concentration and high temperature and MeOH selectivity increased. Increase of pressure 20 atm to 40 atm using the feed gas mixture with 5 vol.% of CO_2 presented positive effect on CO conversion and DME selectivity, both of which increased from 29.4% and 87% to 57.1% and 90%, respectively. DME yield decreased as CO_2 content increased from 5% to 16%. As the amount of ZSM-5 catalyst increased, DME yield was enhanced slightly.

Sofianos et al. [42] investigated different methanol dehydration components such as alumina, amorphous silica-alumina, Y zeolite, mordenite, or ZSM-5 zeolites at 40 bar with a temperature range of 180 to 325^{o}C. Amorphous silica-alumina presented higher oxygenates (MeOH and DME) yield and CO conversion due to its higher acidic strength at low temperatures as compared to γ-alumina. As the temperature increased, CO conversion and oxygenate yield increased as well for all dehydration catalyst up to 275^{o}C above which conversion and yield decreased except for H-ZSM-5 and high amounts of by-products such as CO_2 and hydrocarbons were obtained as major products. It was seen that DME synthesis was thermodynamically favorable as compared to methanol synthesis reaction. Furthermore, presence of small amount of CO_2 in the feed mixture was observed to benefit stability, CO conversion and DME selectivity.

Ramos et al. [12] studied the performances of different methanol dehydration catalysts such as alumina, H-ZSM-5, tungsten–zirconia and sulfated-zirconia that were physically mixed with a commercial methanol synthesis catalyst with synthesis gas of H_2/CO = 1 at 250^{o}C and 50 bar. Presence of a solid acid catalyst shifted methanol synthesis that, as a consequence, increased CO conversion in the direct synthesis of DME. It could be concluded that DME synthesis rate was dependent on the acid strength and number of its acid sites of the acid catalyst. H-ZSM-5 possessed

higher amount of Brønsted acid sites than that of sulfated-zirconia and tungsten–zirconia which had the lowest amount. However similar amount of Lewis acid sites were present for the catalysts. According to the performances of the admixed catalysts containing H-ZSM-5 and sulfated-zirconia, methanol synthesis reaction controlled the overall reaction rate. The reason could be the similar CO conversion values even though their acidic strengths were different. For the mixtures containing alumina or tungsten–zirconia, CO conversion was related to the solid-acid property. Therefore, for these mixtures, methanol dehydration rate determined the overall DME rate. As DME selectivities were compared, highest values were obtained with H-ZSM-5 and sulfated-zirconia approximately 62%. It could be inferred that dehydration of methanol was not efficient on weak acid sites.

Mao et al. [43] investigated the effect of sulfate content and calcination temperature on the catalytic performance of γ-Al_2O_3. Sulfate content with a range of 0-15 wt.% was impregnated on γ-Al_2O_3 with calcination temperature range of 350–750^oC. The reaction conditions were 40 bar and 260°C with the feed mixture of $H_2/CO/CO_2$ = 66/30/4. According to the results, as the sulfur content was increased from 0 to 10%, DME selectivity and CO conversion were enhanced due to increase in the strength of the acid sites. Further increase in sulfur content such as 15 wt.%, resulted in slight decrease of DME selectivity and significant formation of byproducts such as CO_2 and hydrocarbons which were produced due to the stronger acid sites presented in the modified γ-Al_2O_3 at this sulfur content. As the calcination temperature increased up to 550^oC, DME selectivity was favored along with reduction in CO_2 selectivity, which favored WGR, followed by increment in CO conversion. Over 550^oC some content of sulfate was lost therefore catalytic activity of the catalyst was not sufficient for methanol dehydration so; DME formation reduced and amount of methanol increased.

Jiang et al. [44] synthesized mesoporous copper-alumina (Cu-γ-Al_2O_3) with different copper contents in a one-pot reaction with evaporation induced self assembly process. The synthesized material was reported to have well distributed copper particles on mesoporous alumina network. The material that was calcined at 400^oC

possessed a surface area of 265 m^2/g and amorphous wall with low hydrothermal stability and that was calcined at 800^oC possessed crystalline Cu-γ-Al_2O_3 walls with higher catalytic activity for methanol dehydration. One gram of the catalyst was tested at 50 bar and temperatures from 280 to 325^oC with feed gas containing 6 mL/min of CO, 12 mL/min of H_2 and 2 mL/min of N_2. CO conversion was 63%, which was close to the equilibrium conversion of 78%, with DME selectivity of 73% at 295^oC. Due to good cooperation of methanol synthesis and dehydration functions, the produced methanol was immediately converted to DME. The study also showed that the synthesized catalyst was highly active even without ZnO which was considered to be essential for the activity of methanol synthesis catalyst.

3.2. METHANOL SYNTHESIS REACTION

Methanol has attracted much attention over a hundred years. It is an important raw material and has been used for production of many valuable chemicals such as acetic acid, methyl tert-butyl ether (MTBE), formaldehyde, chloromethane and several solvents. Methanol has been considered as an environmentally friendly alternative fuel which can be used for fuel cells in transportation and mobile devices [34, 38, 45]. Methanol has high octane number, which provides good antiknock performance, high volatility and burning of fuel with an excess of air. The volumetric energy density capacity of methanol is only half of the capacities of gasoline or diesel; however, methanol can also be used as a mixture with gasoline or diesel. In addition, by methanol-to-olefins (MTO) process, ethylene or propylene can be produced by methanol and be converted to hydrocarbon fuels [46].

Syngas, which was used to be produced from coal, included sulfur compounds that were poison for methanol synthesis reaction. BASF developed a new catalyst containing zinc oxide and chromium oxide that was highly resistant to sulfur. The process proceeded at high pressure and high temperature, which were 250-350 bar and 320-425^oC. Then, in 1960s, ICI used a new highly selective copper oxide and zinc oxide catalyst which reduced the operating conditions to 50-100 bar and 200-270 ^oC [47].

The reactions involved in methanol synthesis from synthesis gas are CO hydrogenation (3) and CO_2 hydrogenation (4) reactions and water-gas shift reaction (6) over CuO–ZnO-support catalyst [45].

$$CO + 2H_2 \leftrightarrow CH_3OH \qquad \Delta H_{rxn} = -90 \text{ kJ/mol} \qquad (3)$$

$$CO_2 + 3H_2 \leftrightarrow CH_3OH + H_2O \qquad \Delta H_{rxn} = -49 \text{ kJ/mol} \qquad (4)$$

$$CO + H_2O \leftrightarrow CO_2 + H_2 \qquad \Delta H_{rxn} = -41 \text{ kJ/mol} \qquad (6)$$

Due to exothermic and thermodynamically limited nature of the overall methanol synthesis reaction, temperature control and heat exchange are important parameters for process and reactor design and also only 15–25% of CO_x conversion is achieved [45]. Reaction heat could be removed from the reaction system and an efficient catalyst that has good catalytic properties could be developed in order to overcome thermodynamic limitations on the syngas conversion and methanol yield [38].

Generally, copper oxide zinc oxide based catalysts are used for methanol synthesis and they are in the form of agglomerated nanoparticles [19, 36]. Even though metallic copper is considered as the active site for methanol synthesis, there is no consensus on the mechanism of the reaction. It is believed by some researches that carbon monoxide is adsorbed on Cu while hydrogen and water are adsorbed on ZnO sites, then reaction takes place on copper surface [19, 34, 38]. Among many mechanisms for methanol synthesis, in the most accepted one, the adsorbed hydrogen atoms are added continuously to adsorbed carbon monoxide atoms for CO hydrogenation. On the other hand, for CO_2 hydrogenation, methanol forms through formate species (HCO_2) which is adsorbed on copper [46].

The active sites for methanol synthesis are metallic copper clusters which need to be highly dispersed for high activity [22, 33, 38]. Therefore, addition of ZnO as support increases copper dispersion and number of active sites for the reactants [10, 48]. Agglomeration of Cu particles is prevented and long term stability of the catalyst is

conserved. Copper species are significantly affected by poison present in feed gas. The poison; H_2S, could be removed in the form of zinc sulfide on ZnO.

Zirconium oxide can also be used as support instead of zinc oxide since zirconia is strong, thermally resistant and highly stable. Zirconium oxide is a better support than others and provides uniform dispersion of CuO on ZrO_2 surface which could enhance catalytic activity of the catalyst. SiO_2 could also be used as a catalyst support due to its good acid-base nature, porous nature and thermal stability. However, catalysts with silica support are almost inactive for methanol synthesis with low methanol selectivity. Therefore, other metal oxides could also be added on the silica support as a promoter to enhance the catalytic activity of the catalyst [38].

The catalytic activity, selectivity and stability of copper-based catalyst are affected by reaction conditions. Therefore, modification of the catalyst with metal oxides could be necessary. Al_2O_3 is generally used as a promoter and inhibits the agglomeration of active sites by forming zinc aluminate. Moreover, surface area of the catalyst is increased, the dispersed Cu/ZnO structure is preserved and the sintering of Cu particles during the reaction is prevented due to presence of Al_2O_3 promoter [10, 38]. Zirconia can also be used as a promoter for copper-based catalysts since ZrO_2 improves catalytic activity at low pressures and temperatures by increasing surface area and dispersion of copper particles [22, 38]. Pore structure and active surface of the copper-based catalyst could be modified by chromia addition which benefits activity and selectivity of the catalyst [38]. CeO_2 might not be selected as promoter since ceria reduces the surface area and metal surface area of Cu–ZnO complex due to its lower chemical and thermal stability [18].

Cu/Zn hydroxy carbonates are formed during the synthesis of the copper-based catalyst by coprecipitation method. Copper dispersion is improved due to the presence of these precipitate phases such as aurichalcite $(Cu, Zn)_5(CO_3)_2(OH)_6$ with atomic dispersion of copper in zinc hydroxy carbonate and zincianmalachite $(Cu, Zn)_2(OH)_2CO_3$ with atomic substitution of copper in zinc in a malachite phase. CuO

crystallites are formed due to presence of Cu/Zn hydroxy carbonates during calcination and Cu^o nanoparticles are formed during subsequent reduction [48].

Baltes et al. [48] investigated the effect of synthesis conditions such as pH, precipitation temperature, and calcination temperature on structure, morphology and activity of the prepared methanol synthesis catalyst. The $Cu/ZnO/Al_2O_3$ catalysts were prepared by coprecipitation method and tested at 45 bar, 245^oC with the feed gas mixture of $H_2/CO/CO_2$ = 70/24/6. As the surface areas of the synthesized catalysts which were in the range of 2-110 m^2/g were compared, the lowest surface area was obtained at pH of 4-5 and low precipitation temperatures of 30-40^oC. Higher precipitation temperature and close to neutral pH had positive effect on surface area and productivity, therefore, best catalyst having high surface areas of 90-110 m^2/g was obtained at 70^oC and pH 6–8. According to the XRD patterns of calcined materials, catalysts prepared at pH 4.5-5 at 30-40◦C possessed large CuO crystallites and low productivity. However catalysts prepared at pH 6 at 70^oC had smaller CuO and ZnO crystals and Cu was found in the form of copper or copper/zinc hydroxy carbonates in the phases of malachite and zincianmalachite [rosasite, $(Cu,Zn)_2(OH)_2CO_3$]. The presence of hydroxy carbonates could be due to incomplete decomposition during calcination and promoted the performance of the catalyst. Optimum calcination temperature was determined to be 300^oC above which methanol productivity decreased rapidly because of thermal sintering of CuO particles. As the aging time increased up to 1 hour, activity of the catalyst increased as well due to increased interaction of Cu and ZnO crystals. At longer aging times, lower activity was observed which could be due to formation of larger crystallites.

Lim et al. [46] performed a kinetic study to investigate the reaction rates of CO and CO_2 hydrogenation using $Cu/ZnO/Al_2O_3/ZrO_2$ catalyst. According to the activity test, $Cu/ZnO/Al_2O_3/ZrO_2$ provided higher CO conversion and methanol selectivity, which were 35.8% and 94.1% respectively as compared to $Cu/ZnO/Al_2O_3$ at 250^oC and 50 bar. The high activity was found to be due to Zr addition providing smaller metallic copper particles and high metallic surface area. According to kinetic studies using $Cu/ZnO/Al_2O_3/ZrO_2$, methanol formation was affected by the hydrogenation

rates of CO and CO_2. It was observed that hydrogenation rate of CO_2 was lower than that of CO. Presence of CO_2 in the feed retarded WGS reaction followed by inhibition of methanol dehydration to DME and as a result, methanol selectivity increased.

Pontzen et al. [32] compared CO_2-based syngas and CO-based syngas for methanol synthesis at 250°C and 80 bar. As the CO_2-based syngas was used, both CO_2 hydrogenation and reverse water-gas shift reactions generated water, therefore amount of water was higher and approximately 30–40% as compared to CO-based syngas. The byproduct formation was about 0.2% which was relatively insignificant compared to CO-based process and purity of methanol was higher.

Bonura et al. [18] investigated the effect of promoter on catalyst structure and catalytic activity for CO_2 hydrogenation at 30 bar with a temperature range of 180-240°C with the feed composition of $CO_2/H_2/N_2$ = 3/9/1. It was concluded that ZnO promoted structural and catalytic properties of the metallic Cu. When ceria was used instead of zirconia, metal surface area and surface are of Cu–ZnO were reduced. For Cu–ZnO catalysts, increase in ceria content resulted in reduced CO_2 conversion and methanol yield due to ineffective promotion of the surface area catalyst structure as compared to zirconia.

Inui et al. [34] studied the effect of modification of Cu-Zn with precious metals and gallium oxide for CO_2 and CO hydrogenation at 270°C, 80 atm. Two different feed gas compositions were used; $CO/CO_2/H_2$ = 3/22/75 as CO_2-rich syngas and $CO/CO_2/H_2$ =30/3/67 as CO-rich syngas. Using CO_2-rich syngas, Ga_2O_3 modified catalyst enhanced the methanol synthesis with 25.1% conversion of CO_2 to methanol and CO selectivity decreased. Pd modification caused CO_2 conversion to methanol and CO to increase. With CO-rich syngas, modification with gallium oxide and Pd promoted CO conversion as well.

Zhang et al. [36] developed the long carbon nanotubes intercrossed Cu/Zn/Al/Zr catalyst for hydrogenation of CO/CO_2. The carbon nanotubes possessed very good

thermal conductivity as compared to conventional Cu/Zn/Al catalyst having low thermal conductivity. Carbon nanotube arrays were prepared by coprecipitation of Cu/Zn/Al/Zr oxides with carbon nanotubes. The catalytic activity of the array was compared with Cu/Zn/Al/Zr and commercial Cu/Zn/Al catalyst under CO-rich syngas with the ratio of $H_2/CO = 2$ with 5% CO_2 at 230^oC and under CO_2-rich syngas with the ratio of $H_2/CO_2 = 3.0$ at 240^oC. Results indicated that carbon nanotubes promoted hydrogen spillover in which hydrogen molecules dissociated on metal part of the catalyst and hydrogen atoms attached on the metal or support. Therefore, CO and CO_2 conversions were enhanced to be 54.5% and 21.5% respectively.

Sloczynski et al. [35] studied the effect of modification of $Cu/ZnO/ZrO_2$ with B, Ga, In, Gd, Y, Mn and Mg oxides on the structure and catalytic activity. The catalysts were prepared by coprecipitation with basic carbonates and by complexing with citric acid. Copper dispersion and resistance to sintering were higher for the coprecipitated catalysts than that of the citric method. Addition of Ga promoted these properties as well. MnO and B_2O_3 also provided high dispersion of CuO, which then sintered during activity tests. Gd also promoted dispersion slightly however Y was inefficient. As far as the methanol productivities were concerned, Ga_2O_3 addition provided the best methanol yield, whereas, In_2O_3 addition presented the lower activity, in addition, the coprecipitated catalysts showed better performance than that of the citric method. Catalyst performance could be promoted by adding ZrO_2 on $Cu/ZnO/Al_2O_3$ or replacing ZrO_2 by Al_2O_3. As a result, methanol synthesis was enhanced by inhibition of adsorption of water on the catalyst.

3.3. METHANOL DEHYDRATION REACTION

Conventionally DME is synthesized by methanol dehydration reaction (5) over solid acid catalysts between 250-300^oC and at atmospheric pressures or up to 18 bar. The different solid acid catalysts available of methanol dehydration are γ-Al_2O_3, zeolite materials such as chabazite, mordenite, SAPO, H-ZSM-5, H-Y, Amberlyst 35,

Nafion, mesoporous aluminosilicate and nanocomposite Nafion-silica. Formaldehyde formation through reaction (9) is also observed as byproduct [49-52].

$$2CH_3OH_{(g)} \leftrightarrow CH_3OCH_{3(g)} + H_2O_{(g)} \quad (5)$$

$$CH_3OH_{(g)} \leftrightarrow CH_2O + H_{2(g)} \quad (9)$$

It is believed that the total number of acidic sites and their strength of a methanol dehydration catalyst affect the catalytic activity for carbon monoxide conversion, DME selectivity and stability [21, 49]. DME formation proceeds with weak and medium acidity, while, the strong acid sites promotes dehydration of alcohols or deep hydrogenation of DME to hydrocarbons [31, 53, 54]. The formed hydrocarbon could possess long carbon chains which could lead to coke formation and deactivation [1]. It is also known that Lewis acid sites could strongly adsorbs water and carbon dioxide that could be formed via methanol reforming of water-gas shift reaction over the strong acid sites [21]. However, the mechanism of the contribution of Brønsted or Lewis acid sites on methanol dehydration to DME is still unclear [28]. The majority of the researches reached a consensus that Brønsted acid sites with benign acid sites are responsible for methanol dehydration to DME, especially at low temperatures, whereas, Lewis acid sites favor formation of olefins from alcohols [15, 50, 52, 55]. However, Xu et al. [53] concluded that both Brønsted and Lewis acid sites were effective in methanol dehydration to DME. Small addition of water to methanol as feed stream, small activity decrease was observed for H-ZSM-5 catalyst. Water is known to adsorb preferentially over Lewis acid sites. They indicated that if only Brønsted acid sites were effective, the presence of water would not disturb the activity. Similarly, if only Lewis acid sites were effective, the presence of water would cause significant reduction in the activity. Some studies indicate that Lewis acid sites were responsible for methanol dehydration to DME, strong Brønsted acid sites caused formation of hydrocarbons from DME and alcohols [28, 31]. Brønsted acid sites or Lewis acid–base pair sites are believed to be important for dehydration reactions. For the mechanism based on Brønsted acid sites, the strength of the sites

could be controlled to prevent hydrocarbons. For the mechanism based on Lewis acidity, an alcohol molecule and an alkoxide anion are adsorbed on an acidic site and a basic site, respectively, over an adjacent acid–base pair sites [12].

The theoretical analysis of DME synthesis mechanism from methanol over zeolite protons was investigated by Blaszkowski and van Santen [56]. Two possible mechanisms were examined using density functional theory (DFT) calculations. The first one was based on the mechanism proposed by Kubelkova et al. [57] at which the methoxonium ion, $H_3COH_2^+$, was formed by transfer of surface proton to adsorbed methanol on zeolite. A methyl group remained bonded to the surface due to dehydration of methoxonium ion and formed dimethyl ether by interacting with another methanol molecule. The second mechanism was based on the study of Bandiera and Naccache [58] at which two methanol molecules were adsorbed on Brønsted acid and adjacent Lewis basic sites. Two surface species $[CH_3{\cdot}OH_2]^+$ and $[CH_3O]^-$ were formed and react to yield dimethyl ether and water. According to the DFT results, the second mechanism was favorable due to lower activation energy of the limiting step found as compared to the first mechanism.

γ-Al_2O_3 is generally used due to its lower price, easy availability and capability of less byproduct formation [54]. γ-Al_2O_3 has good initial activity for methanol dehydration; however, deactivation is rapid as the reaction proceeds. The deactivation could be due to hydrophilic nature of γ-Al_2O_3. Significant amount of water is produced during the direct synthesis of DME and water is competitively adsorbed more than methanol on γ-Al_2O_3 surface, especially on Lewis acid sites. As a result, catalyst activity decreases significantly [59, 60]. The acid strength of γ-Al_2O_3 is very low; therefore, degradation by coke, due to formation of light olefins and heavy hydrocarbons from methanol and DME, is reduced [37, 23]. However, methanol dehydration capacity of γ-Al_2O_3 is very low at 260^{o}C which is the optimum reaction temperature for methanol synthesis reactions. Higher reaction temperature is not favorable due to thermodynamic limitations and catalyst stability of the hybrid catalyst could be reduced due deactivation caused by copper sintering at high

temperatures. Modification of γ-Al_2O_3 could be considered to enhance the catalytic activity [43].

H-ZSM-5 zeolite offers very good methanol dehydration activity at optimum reaction conditions due its very high Brønsted acidity and stability. However, very strong acidic sites tend to produce hydrocarbons which reduce selectivity of DME. Some of the hydrocarbons results in formation of coke which blocks zeolite pores and causes deactivation. H-ZSM-5 zeolite could be modified with proper amount of Na, MgO or Fe in order to moderate the number and strength of Brønsted sites within the zeolite [1, 9, 61]. H-ZSM-5 zeolite is not susceptible to the presence of water formed by methanol dehydration and water-gas shift reaction due to its hydrophobic nature and hydrothermal stability. Therefore, catalyst deactivation due to water is not as significant as in γ-Al_2O_3 [19, 49, 53, 60].

SAPO zeolites could also be used for methanol dehydration. SAPO-34 and -18 have relatively higher surface area with three-dimensional pore structure and possess strong acid sites. Therefore, their catalytic activities are initially high and then decrease very fast due to coke formation within the pores. The formed carbonaceous materials could cause plugging the pores, which are very small, and followed by diffusion limitations and blockage of the active sites. SAPO-5 and -11 possess very low surface area with unidimentional pore structure. The catalytic activities of the catalysts are also very low. However, these catalysts are very stable due to their moderate acidic strengths which are unfavorable for coke formation [20].

Mesoporous silicate materials (M41S family) with ordered pore structures possess very high surface area and very narrow pore size distribution. Due to their larger pores as compared to microporous zeolites, the reacting molecules diffuse easily to the active site and the materials are less sensitive to deposition of coke. Due to their inert nature and low catalytic activity, metals, metal oxides or acids could be incorporated into MCM-41 type materials to improve the acid strength. Utilization of these materials is limited due to poor hydrothermal stability [1, 50, 51]. Mesoporous materials (SBA family) with ordered pore structures such as SBA-15 have very

narrow pore size distribution and high surface area. Its thicker pore walls promote the hydrothermal stability of SBA-15 to be higher as compared to MCM-41 [1].

Nafion, which is a perfluorinated sulfonic acid ion-exchange resin, could be used as solid acid catalyst due to its chemical and thermal stability provided by its fluorocarbon backbone. Although the resin has good properties such as very high acid strength, insolubility in polar solvents and high resistance to chemicals, the disadvantage of utilization of nafion evolves from low surface area and nonporous structure [52].

Heteropolyacid (HPA) catalysts are extensively employed as a solid acid catalyst for acid-catalyzed reactions such as methanol dehydration to DME. Keggin type heteropolyacids, as shown in Figure 1, contain an anion with a general formula of $[XM_{12}O_{40}]^{n-}$ where X is the heteroatom, mostly P^{+5}, Si^{+4}, B^{+3} and M is the addenda atom, commonly molybdenum and tungsten. Their catalytic activities are very high due to presence of high Brønsted acidity which is stronger than many acids like H_2SO_4 and HCl. Their acceptable redox properties with very high proton mobility allow them to be used for selective oxidation reactions. Although heteropolyacids have very good properties, they have some setbacks that limit their performances. They have very low surface area that is less than 1 m^2/g, and are nonporous and soluble in polar a solvent which makes them to be used in vapor phase reactions. Therefore, heteropolyacids could be impregnated on high surface area support catalyst and their salts which are insoluble in water could be synthesized to improve its catalytic performance [50, 51, 62-64].

Figure 1. The primary structure of Keggin HPA's [64]

The most common heteropolyacids are tungstophosphoric acid (TPA), silicotungstic acid (STA) and molybdophosphoric acid (MPA). When the acid strengths of these heteropolyacids were compared, it was found that the acid strength of TPA was the highest while that of MPA was the least [65]. Therefore, it can be concluded that the better performance of STA is depends on some other factors. STA possesses four Keggin protons which is higher than that of TPA which is three [66]. STA and TPA also have different thermal stabilities. TPA, which has hexahydrate structure ($H_3PW_{12}O_{40}.6H_2O$) at room temperature, forms anhydrous TPA by water removal at higher temperatures and decomposes between 180 and 330^oC. However, STA ($H_4SiW_{12}O_{40}$), which is at anhydrous form at room temperature, presents more stability than TPA over 200^oC [67, 68]. Incorporation of STA into catalytic support prevents solubility in polar solvents, therefore, the activity of STA does not decrease and it also provides high catalytic surface area [69]. Calcination temperature affects catalytic activity of heteropolyacid incorporated catalyst. Calcination at temperatures higher than 400^oC results in decrease in activity of STA incorporated catalysts due to significant loss of Brønsted acidity. For TPA incorporated catalysts, the acidity loss occurs at lower calcination temperatures [50, 69].

Xu et al. [53] studied the performances of several solid acid catalysts such as γ-Al_2O_3, H-ZSM-5, amorphous silica-alumina and titania modified alumina and zirconia for methanol dehydration to DME. At low temperature of 150^oC, γ-Al_2O_3 presented 6.3% of methanol conversion, which increased exponentially with temperature and reached approximately 90% at 250^oC. Different amounts of water were added to the feed stream to investigate the effect of water on dehydration. According to the results, presence of water resulted in decrease of methanol conversion from 17.5% to 5.8% at 188^oC. The result could be interpreted as the excess water blocked the active sites of γ-Al_2O_3 due to the competitive adsorption of water and methanol on the surface. Titania modified alumina presented similar catalytic behavior with γ-Al_2O_3 due to their similar acidic strengths. To reduce coke formation due to strong acid sites, Na^+ ions were added to titania modified alumina and the catalytic stability was enhanced. Zirconium oxide possessed less acid sites

than γ-Al_2O_3 therefore; methanol conversion of 41% was obtained at 325°C having DME selectivity of approximately 99%. Titania modification of zirconia increased methanol conversion to 60% at 325°C. H-ZSM-5 was not significantly affected by presence of water as γ-Al_2O_3 did, due to higher Brønsted and Lewis acid sites. H-ZSM-5 presented highest methanol conversion of 78% and DME selectivity of 100% at 190°C. Amorphous silica-alumina was very stable with high selectivity of DME even though strong acid sites presented.

Yaripour et al. [59] compared the performances of γ-Al_2O_3 and aluminosilicates with different silica contents prepared by coprecipitation method at atmospheric pressure and 300^{o}C. γ-Al_2O_3 yielded DME selectivity of 63.23% but deactivated rapidly. Silica modification increased catalytic activity up to 6 wt.% of silica loading by enhancing surface acidity, CO conversion and DME selectivity reached 86.4% and 75.6%, respectively. 6 wt.% of silica loading prevented formation of byproducts and severe deactivation. Higher silica loading had adverse effect due to coverage of the acid sites.

Vishwanathan et al. [60] studied the effect on Na modification on H-ZSM-5 catalysts for methanol dehydration. Na was impregnated on H-ZSM-5 with ratios of varying from 0 to 80 mol% and catalysts were tested at 230-340^{o}C with a feed rate of 0.25 ml/min. Strong acid sites of H-ZSM-5 favored hydrocarbon formation followed by deactivation due to coking. Therefore Na was added on H-ZSM-5 in order to reduce the acidic strength. It was seen that higher Na content enhanced DME yield and best Na content was determined as 80%, which yielded 100% selectivity for DME between 230-340^{o}C with high resistance to coke formation. On the other hand, unmodified H-ZSM-5 showed DME selectivities of 97 and 94% at 270 and 320^{o}C, respectively.

Çiftçi et al. [50] investigated the different synthesis procedures of tungstophosphoric acid (TPA) impregnated silicate structured mesoporous MCM-41 type catalytic materials which were then tested for methanol and ethanol dehydration to DME, DEE and ethylene. Activity tests were conducted with 0.2 g of catalyst at different

temperatures, 200-400^{o}C. TPA impregnated MCM-41-like mesoporous catalyst (TPA@MCM-41) was very stable and very active for both ethanol and methanol dehydration. For the ethanol dehydration reaction, ethanol fractional conversion reached to 1.0 at 300^{o}C. Below 220^{o}C, selectivity of ethylene was lower than that of DEE, however above 220^{o}C, ethylene selectivity increased up to 1.0 due to decomposition of DEE which was caused by the Lewis acid sites contribution at high temperature. In the case of the methanol dehydration reaction, as the temperature was increased from 150-220^{o}C, methanol conversion rapidly increased from 0.17 to 0.79 and DME yield reached a maximum, both of which then decreased due to catalyst deactivation caused by coke formation. Selectivity of DME was found almost 1.0 up to 300^{o}C, however at higher temperatures, formaldehyde and methane was formed due to decomposition of DME. Using TRC-W40, fractional conversion of ethanol reached 1.0 at 400^{o}C and selectivity of DEE was almost 0.9 at 200^{o}C and then decreased while ethylene selectivity increased at higher temperatures. In methanol dehydration, DME selectivities were obtained as 1.0 at 250^{o}C and 0.97 at 180^{o}C along with some formaldehyde. TRC-W40 did not lose its activity due to deactivation caused by coke formation; however, its catalytic activity was lower than that of TPA@MCM-41 due to its lower acidic strength. The results revealed that the dehydration capacity of the catalyst were more significant than the dehydrogenation capacity.

Varışlı et al. [62] synthesized various mesoporous aluminosilicate with different Al/Si atomic ratios between 0.03 and 0.18 using hydrothermal synthesis route and studied the effect of silicotungstic acid impregnation on the synthesized materials. According to the activity tests performed between 200-400^{o}C, the catalysts with Al/Si ratio of 0.09 and 0.18 yielded methanol conversions of 0.78 and 0.72 at 400^{o}C, respectively. The catalytic activity of the catalyst having higher Al/Si ratio was lower since its surface area was lower compared to the catalyst with Al/Si ratio 0.09. In addition, DME selectivities also decreased with increasing Al/Si ratio below 300^{o}C above which selectivity of DME reached 100%. Below 300^{o}C, significant amount of formaldehyde was produced as byproduct, however, above 300^{o}C, formaldehyde

selectivity became less than 1%. Silicotungstic acid impregnation to aluminosilicate enhanced catalytic activity and surface area of the catalyst. 84% of methanol conversion and about 97% of DME selectivity were obtained at 250^{o}C along with high stability.

Tokay et al. [1] synthesized alumina impregnated SBA-15 by a one-pot hydrothermal procedure. The catalytic performance of the catalyst was compared with aluminosilicate with Al/Si ratio of 0.1 at a temperature range of 120-450^{o}C at atmospheric pressure. Alumina impregnation decreased the surface area and pore volume of SBA-15. According to the results, alumina impregnated SBA-15 had stronger Brønsted and Lewis acid sites than aluminosilicate therefore, methanol conversion of alumina impregnated SBA-15 was higher and reached 80% at 350^{o}C. However, both catalysts yielded similar DME selectivity, which approached to 100%, and low formaldehyde selectivities, which reached to 0 at 350^{o}C.

Çiftçi et al. [51] synthesized a novel STA incorporated silicate structured mesoporous catalysts with different W/Si atomic ratios by one-pot hydrothermal synthesis route. The synthesized catalysts were calcined at 350ºC since higher temperature calcination, above 400ºC caused loss of protons of STA. W/Si atomic ratios of mesoporous silicate structured were adjusted as for 0.16, 0.33, 0.47 and 0.78 for TRC-62, TRC-75, TRC-82 and TRC-92 catalysts, respectively and activity tests were performed at 180-350ºC. The surface areas of the catalysts decreased with the increase in W/Si ratios, however, TRC-62 presented the lowest activity since lower content of STA resulted in weaker Brønsted acidity. TRC-75 showed the best catalytic activity with DME selectivity of almost 100% and methanol conversion of 60% due to its better intensities of Brønsted acidities and well dispersion of STA to the catalyst. Operation at high temperatures, such as above 250ºC, caused deactivation by formation of coke. The catalysts restored its initial activity easily by regeneration.

CHAPTER 4

THERMODYNAMIC ANALYSIS

In order to determine the operating parameters for DME synthesis, thermodynamic analysis of the reactions needs to be made. DME synthesis requires high pressure (30 bar and above) and moderate temperatures (200°C-300°C) to reach high conversion. However, the carbon monoxide conversion cannot exceed the equilibrium conversion at a specific temperature and pressure. For this purpose, in this section, thermodynamic analyses of the direct DME synthesis reactions (Reaction 1 and 2) and the methanol synthesis reaction (Reaction 3) were performed with feed composition containing equimolar amount of carbon monoxide and hydrogen.

$3CO + 3H_2 \leftrightarrow CH_3OCH_3 + CO_2$ ΔH_{rxn} = - 246 kJ/mol (1)

$2CO + 4H_2 \leftrightarrow CH_3OCH_3 + H_2O$ ΔH_{rxn} = - 205 kJ/mol (2)

$CO + 2H_2 \leftrightarrow CH_3OH$ ΔH_{rxn} = - 90 kJ/mol (3)

For the thermodynamic analysis, constant pressure heat capacity values were obtained from literature and listed in Table 2 [70]. Heat capacity of any species as a function of temperature can be represented by Equation 4.1.

$$C_{P,T} = a + b \times T + c \times T^2 + d \times T^3 \ \ [J/molK]\,, T[K] \qquad 4.1.$$

Table 2. The molar heat capacity coefficients of species involved in DME synthesis [70]

Species	a	b × 10^2	c × 10^5	d × 10^9
H_2	29.088	- 0.192	0.400	- 0.870
CO	28.142	0.167	0.537	- 2.221
CO_2	22.243	5.977	- 3.499	7.464
H_2O	32.218	0.192	1.055	- 3.593
CH_3OH	19.038	9.146	- 1.218	- 8.034
CH_3OCH_3	17.02	17.91	- 5.234	- 1.918

The constant pressure heat capacity with respect to temperature is required to calculate the heat of reaction at a specific temperature and the expression is given in Equation 4.2. The molar heat capacity coefficients are multiplied with the stoichiometic coefficients and then added.

$$C_p = \Delta a + \Delta b \times T + \Delta c \times T^2 + \Delta d \times T^3 \quad 4.2.$$

Standard enthalpies and Gibbs free energies of formation for the species at reference temperature of 25°C are given in Table 3 in order to determine the reaction enthalpy and equilibrium constants.

Table 3. Standard enthalpies and Gibbs energies of formation of the species at 298.15 K in gas phase [70]

Species	$\Delta H°_f$, kJ/mol	$\Delta G°_f$, kJ/mol
H_2	0	0
CO	-110.5	-137.2
CO_2	-393.5	-394.4
H_2O	-241.8	-228.6
CH_3OH	-200.7	-162.0
CH_3OCH_3	-184.2	-113.0

Heat of reaction of a reaction as a function of temperature can be calculated according to Equation 4.3.

$$\Delta H^{o}_{rxn} = \Delta H^{o}_{298} + \int_{298}^{T} (\Delta a + \Delta b * T + \Delta c * T^2 + \Delta d * T^3) dT \quad 4.3.$$

Temperature dependence of thermodynamic equilibrium constant in differential form is given by Van't Hoff's Equation 4.4. Then the equilibrium constant is calculated by integrating the Van't Hoff relation over the studied range of temperature.

$$\frac{dlnK}{dT} = \frac{\Delta H^{\circ}_{rxn}}{R * T^2} \quad 4.4.$$

When integrating the Van't Hoff's Equation, equilibrium constant at reference temperature is needed and can be calculated as:

$$K_{298} = exp(-\Delta G^{\circ}/RT) \quad 4.5.$$

When the Van't Hoff's Equation is integrated, the following expression is obtained:

$$K = K^{o}_{298} * \exp\left(\int_{298}^{T} \frac{\Delta H^{o}_{rxn}}{R * T^2} dT \right) \quad 4.6.$$

DME and methanol synthesis reactions are operated at high pressure; therefore, non-idealities were taken into account using Peng-Robinson equation of state. The derivation of fugacity coefficient of the species was given in Appendix A. Fugacity coefficient at different pressures and temperatures were calculated and given in Appendix A. The equilibrium constant can also be defined in terms of the equilibrium constants based on partial pressures and fugacity coefficients as given in Equation 4.7.

$$K = K_\phi * K_P \tag{4.7.}$$

$$K_\phi = \prod_{i=1}^{c} (\phi_i)^{v_{ij}} \tag{4.8.}$$

$$K_P = \prod_{i=1}^{c} (P_i)^{v_{ij}} \tag{4.9.}$$

K_ϕ and K_P for all of the reactions are written as follows:

for Reaction 1:

$$K_\phi = \frac{\phi_{CH_3OCH_3} * \phi_{CO_2}}{\phi_{CO}^3 * \phi_{H_2}^3} \tag{4.10.}$$

$$K_p = \frac{P_{CH_3OCH_3} * P_{CO_2}}{P_{CO}^3 * P_{H_2}^3} = \frac{y_{CH_3OCH_3} * y_{CO_2}}{y_{CO}^3 * y_{H_2}^3 * P^4} \tag{4.11.}$$

for Reaction 2:

$$K_\phi = \frac{\phi_{CH_3OCH_3} * \phi_{H_2O}}{\phi_{CO}^2 * \phi_{H_2}^4} \tag{4.12.}$$

$$K_p = \frac{P_{CH_3OCH_3} * P_{H_2O}}{P_{CO}^2 * P_{H_2}^4} = \frac{y_{CH_3OCH_3} * y_{H_2O}}{y_{CO}^2 * y_{H_2}^4 * P^4} \tag{4.13.}$$

for Reaction 3:

$$K_\phi = \frac{\phi_{CH_3OH}}{\phi_{CO} * \phi_{H_2}^2} \tag{4.14.}$$

$$K_p = \frac{P_{CH_3OH}}{P_{CO} * P_{H_2}^2} = \frac{y_{CH_3OH}}{y_{CO} * y_{H_2}^2 * P^2} \tag{4.15.}$$

By taking 100 mole/hour basis, the equilibrium composition calculations for each reaction were tabulated as in Tables 4, 5, and 6.

Table 4. The equilibrium composition calculations for Reaction 1

$(3CO + 3H_2 \leftrightarrow CH_3OCH_3 + CO_2)$

Species	**Inlet Flow Rate**	**Outlet**	**Outlet Composition, y_i**
CO	50	$50-50*x_{eq}$	$[50*(1-x_{eq})] / [100-(200/3)*x_{eq}]$
H_2	50	$50-50*x_{eq}$	$[50*(1- x_{eq})] / [100-(200/3)*x_{eq}]$
CH_3OCH_3	-	$(50/3)*x_{eq}$	$[(50/3)*x_{eq}] / [100-(200/3)*x_{eq}]$
CO_2	-	$(50/3)*x_{eq}$	$[(50/3)*x_{eq}] / [100-(200/3)*x_{eq}]$
Total	*100*	$100-(200/3)*x_{eq}$	

Table 5. The equilibrium composition calculations for Reaction 2

$(2CO + 4H_2 \leftrightarrow CH_3OCH_3 + H_2O)$

Species	**Inlet Flow Rate**	**Outlet**	**Outlet Composition, y_i**
CO	50	$50-(50/2)*x_{eq}$	$[50*(1- x_{eq}/2)] / [100-50*x_{eq}]$
H_2	50	$50-50*x_{eq}$	$[50*(1- x_{eq})] / [100-50*x_{eq}]$
CH_3OCH_3	-	$(50/4)*x_{eq}$	$[(50/4)*x_{eq}] / [100-50*x_{eq}]$
H_2O	-	$(50/4)*x_{eq}$	$[(50/4)*x_{eq}] / [100-50*x_{eq}]$
Total	*100*	$100-50*x_{eq}$	

Table 6. The equilibrium composition calculations for Reaction 3

$(CO + 2H_2 \leftrightarrow CH_3OH)$

Species	**Inlet Flow Rate**	**Outlet**	**Outlet Composition, y_i**
CO	50	$50-(50/2)*x_{eq}$	$[50- 25*x_{eq})] / [100-50*x_{eq}]$
H_2	50	$50-50*x_{eq}$	$[50*(1- x_{eq})] / [100-50*x_{eq}]$
CH_3OH	-	$(50/2)*x_{eq}$	$[25*x_{eq}] / [100-50*x_{eq}]$
Total	*100*	$100-50*x_{eq}$	

In order to calculate the equilibrium conversions, fugacity coefficients and outlet compositions involving equilibrium conversions were inserted in equation 4.7. Then, the equilibrium constant obtained from equation 4.7 was equalized to the equilibrium constant obtained from equation 4.6. By solving these equations, equilibrium conversions were found. Equilibrium conversions with respect to temperature and pressure for methanol synthesis reaction with equimolar mixture of carbon monoxide and hydrogen is presented in Figure 2.

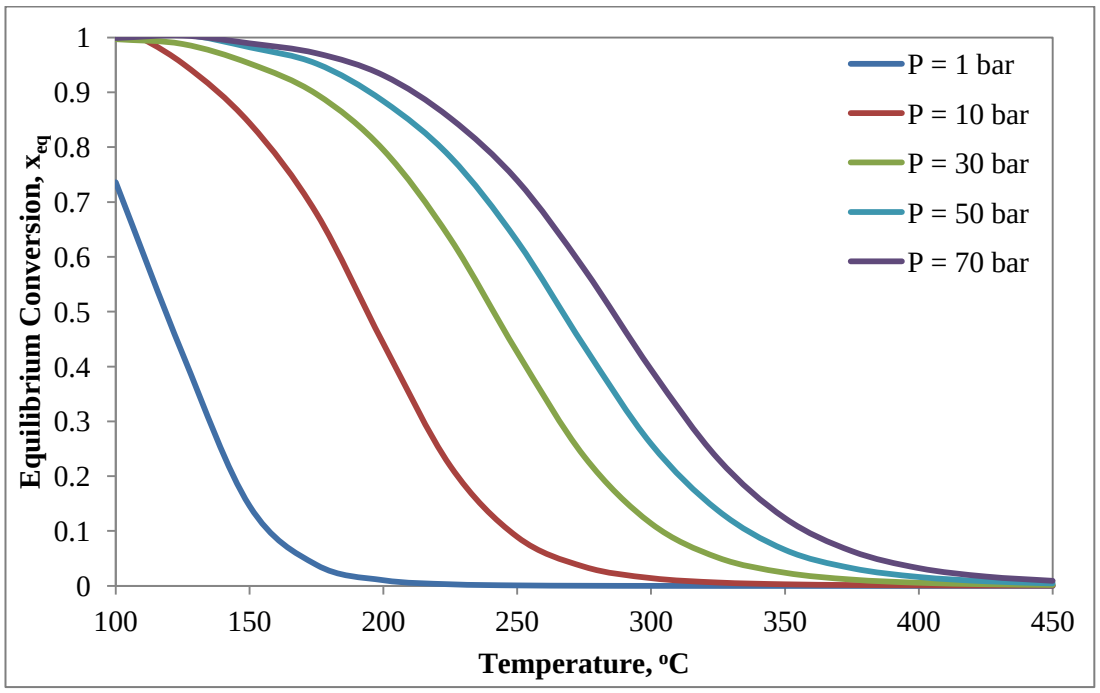

Figure 2. The equilibrium conversion curves with respect to temperature and pressure for Reaction 3 ($CO + 2H_2 \leftrightarrow CH_3OH$) with a feed ratio of H_2:CO=1:1

Due to the exothermic nature of the methanol synthesis reaction, equilibrium conversion decreases as temperature increases. At atmospheric pressure, conversion is zero within the temperature range at which methanol synthesis catalyst is active. As seen from the figure, increase in the pressure promotes conversion according to the Le Chatelier's principle. Equilibrium conversions with respect to temperature and pressure for DME synthesis reactions are given in Figures 3 and 4.

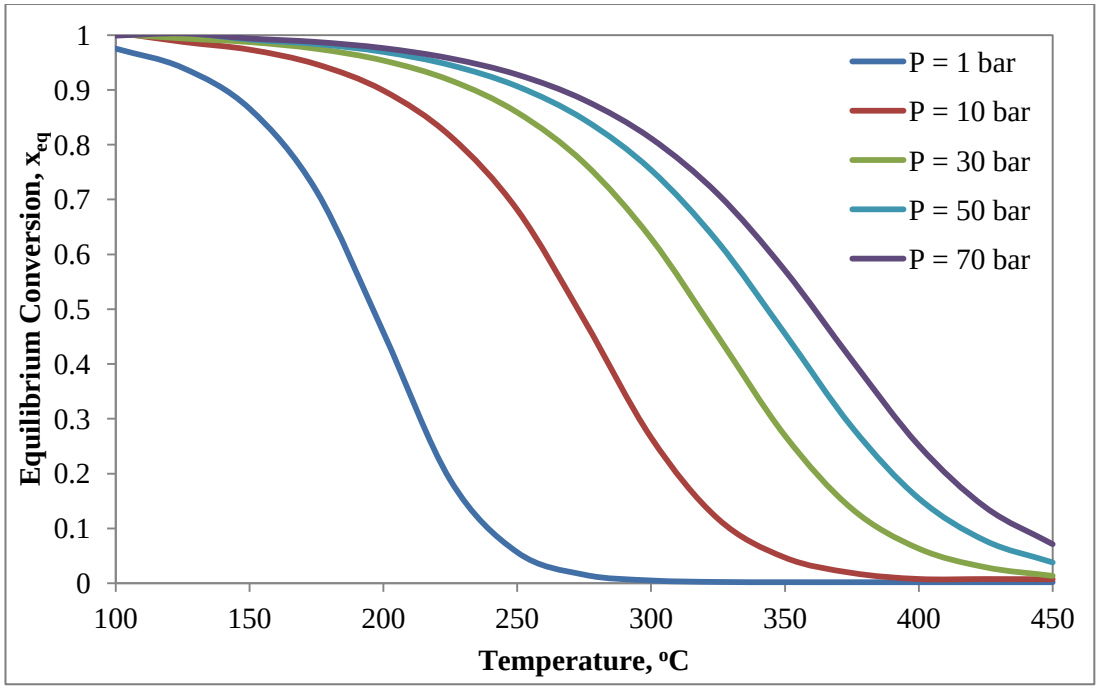

Figure 3. The equilibrium conversion curves with respect to temperature and pressure for Reaction 1 ($3CO + 3H_2 \leftrightarrow CH_3OCH_3 + CO_2$) with a feed ratio of H_2:CO=1:1

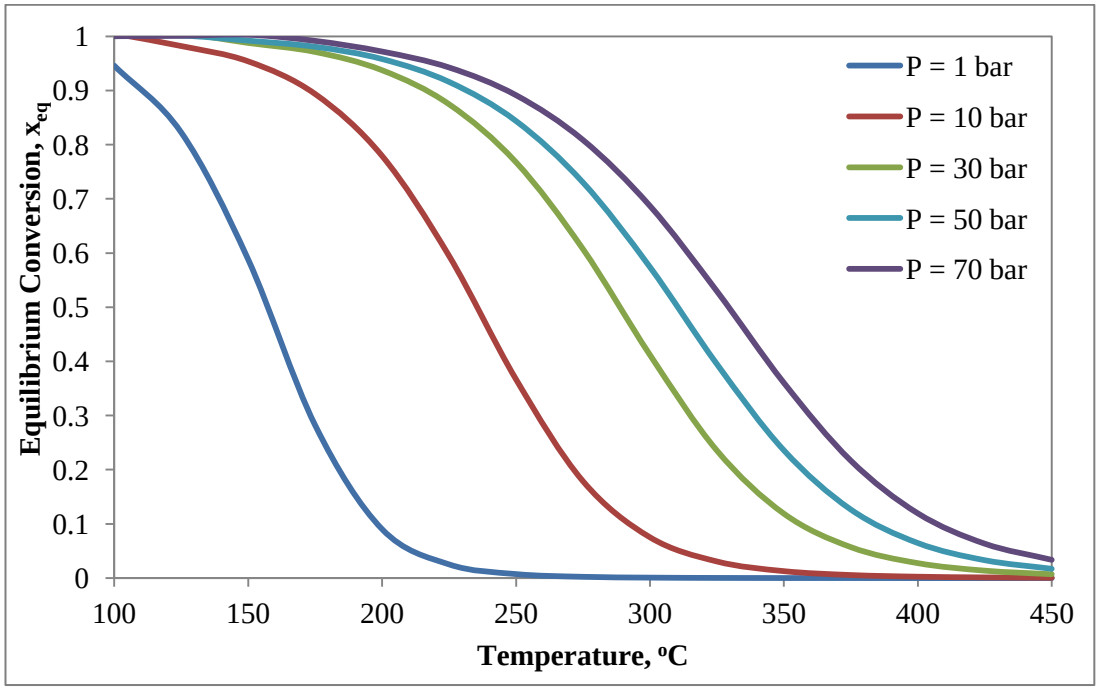

Figure 4. The equilibrium conversion curves with respect to temperature and pressure for Reaction 2 ($2CO + 4H_2 \leftrightarrow CH_3OCH_3 + H_2O$) with a feed ratio of H_2:CO=1:1

The equilibrium conversion curves with respect to temperature for Reactions 1, 2, and 3 at 50 bar are given in Figure 5. As seen from the figure, the direct DME synthesis reactions overcome the thermodynamic equilibrium limitation of the methanol synthesis reaction since the equilibrium conversions are higher than that of the methanol synthesis reaction at a given temperature.

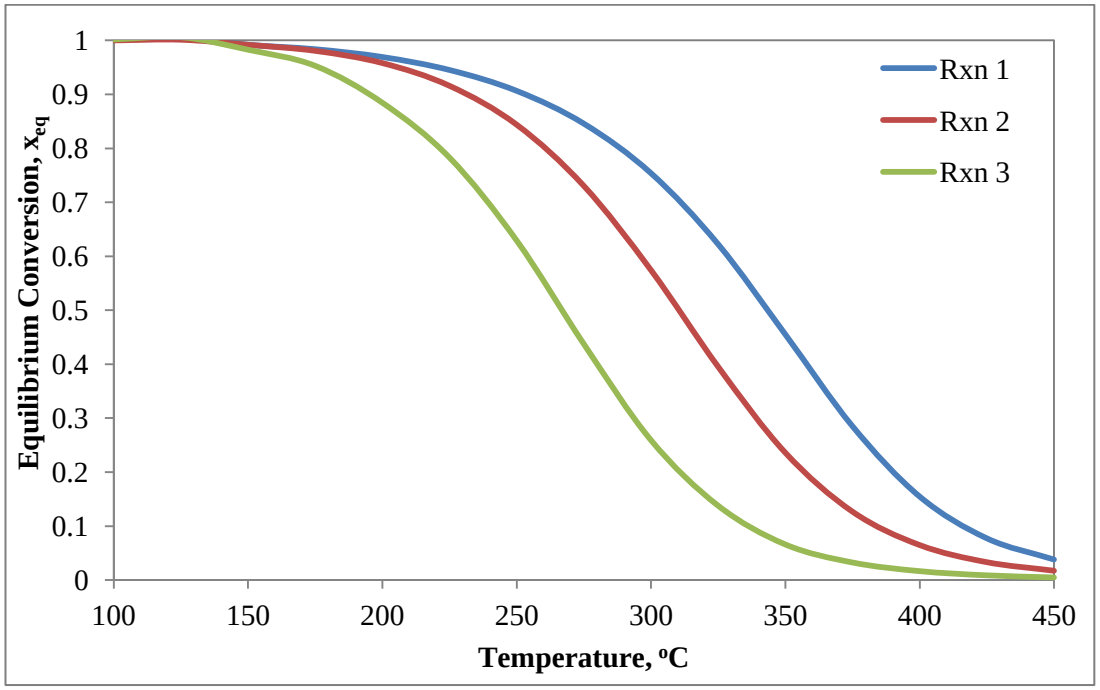

Figure 5. The equilibrium conversion curves with respect to temperature for Reactions 1, 2 and 3 at 50 bar for a feed ratio of H_2:CO=1:1

According to the thermodynamic analyses, conversion increased with pressure up to 50 bar. Further pressure increase did not affect the conversion significantly and also could increase compression cost and feed gas consumption and be hazardous. Therefore, the operating pressure was selected as 50 bar for the direct DME synthesis process.

CHAPTER 5

MESOPOROUS MATERIALS

Direct synthesis of dimethyl ether from synthesis gas requires a bifunctional catalyst with two functional groups, one for methanol synthesis and one for methanol dehydration function. In this study, ordered mesoporous alumina was selected for methanol dehydration function due to high thermal stability, large surface areas and narrow pore-size distributions [71]. The characterization methods applied in this study are also presented. The catalysts that have been synthesized for the methanol synthesis function in the study conducted by Çelik [11] are directly used.

5.1. POROUS MATERIALS

Porous materials can be classified into three groups according to IUPAC definition; such as microporous, mesoporous and macroporous materials [72]. The pore diameters of microporous, mesoporous and macroporous materials are less than 2 nm, between 2-50 nm and larger than 50 nm, respectively.

Microporous materials, especially zeolites, attract much attention in industrial areas such as oil refining, petrochemistry and chemical synthesis. They can also be applied as adsorbents and their performances in catalytic applications depend on high surface area and adsorption capacity, properties of controlled adsorption that vary from hydrophobic to hydrophilic type and generation of active sites in the framework. In addition, their channel structure can be shape selective to promote the given catalytic reaction towards the desired product, avoiding the side reactions [73].

However, the very small pore diameter of zeolites limits their usage in many applications involving molecules larger than 1-1.2 nm. In addition, they are susceptible to pore plugging due to coking, which causes deactivation. Therefore, catalytic materials within mesoporous range have gained many interest due to high thermal stability and large surface areas, tunable pore sizes so that the diffusion properties and the available active sites are promoted [20, 72, 74].

The first mesoporous material, which was MCM (Mobil Composition of Matters)-41/48, was synthesized successfully by Mobil Oil Corporation (USA) in 1992 and opened a new pathway to develop mesoporous materials for various applications like catalytic, energy, biomedical and environmental supports [75, 76].

5.2. MESOPOROUS ALUMINA

Mesoporous alumina is a new type of porous material and very favorable as industrial catalyst and catalyst support due to its wide application areas such as petroleum refinement and emission control processes due to its tunable pore diameters from 2 to 10 nm, large surface areas reaching 700 m^2/g and moderate Lewis acidity [75] and high stability. However, the synthesis conditions of mesoporous alumina strongly affect the ordered structure and thermal stability of material [71, 77, 78]. Many studies were reported for synthesis of mesoporous alumina. Pinnavaia et al. [79] synthesized pseudo-lamellar mesostructured γ-alumina with crystalline walls. Zhao et al. [80] obtained a partly ordered mesoporous alumina using aluminum tri-tert-butoxide as the main inorganic precursor material and anhydrous aluminum chloride as the pH adjusting agent. Somorjai et al. [81] synthesized ordered mesoporous alumina having amorphous walls with the sol-gel synthesis procedure. Sanchez et al. [82] obtained ordered nanocrystalline γ-Al_2O_3 films having contracted fcc mesopores using the dip-coating method. Zhang et al. [79] synthesized an ordered crystalline mesoporous alumina using CMK-3 the hard template which was a multistep and long procedure. Yuan et al. [71] developed an easy and reproducible method for highly ordered mesoporous aluminas having amorphous and/or crystalline γ-phase walls using evaporation-induced self assembly

process using triblock copolymers as the soft templates. Using this process, mesoporous aluminas could be synthesized to possess 2D hexagonal structure with *p*6*mm* hexagonal symmetry, high thermal stability up to 1000^{o}C, higher surface area up to 400 m^2/g, pore volumes of approximately 0.70 cm^3/g, narrow pore-size distribution and high Lewis acidity strength provided by aluminum atoms in tetrahedral and octahedral coordination sites [71, 77]. Yuan et al. investigated the effect of the calcination temperature on the structure and obtained that at 400^{o}C, the mesostructure possessed amorphous wall, which was converted to γ-Al_2O_3 phase with crystalline walls between 800-1000^{o}C, and mesoporous structure was destroyed at 1100^{o}C. The surface area of mesoporous alumina was found as 434 m^2/g at 400^{o}C and decreased with increasing calcination temperature. Pore diameter also decreased however narrow pore-size distributions were preserved as the calcination temperature increased [71].

Poly(alkyleneoxide) triblock copolymers are used widely as structure directing agents due to low cost, biodegradability and commercial availability. Different triblock copolymers such as P123 ($EO_{20}PO_{70}EO_{20}$), F127 ($EO_{106}PO_{70}EO_{106}$), and F68 ($EO_{77}PO_{29}EO_{77}$) have different EO/PO ratios and different molecular weights of 5800, 12600 and 8400, respectively. Therefore, mesoporous aluminas with different structures and pore sizes could be synthesized. The surfactant having higher molecular weight results in larger pore sizes. P123 and F127 promote formation of ordered mesostructure, on the other hand, F68 results in formation of a wormlike structure [71, 77, 78]. These nonionic surfactants do not ionize in water and possess a hydrophilic and a slight hydrophobic component due to polycondensation of ethylene oxide and propylene oxide, respectively [76].

In evaporation induced self-assembly (EISA) method, as given in Figure 6, the amphiphilic structure directing agent composed of hydrophobic and hydrophilic parts and aluminum precursor are homogeneously dispersed in alcohol/water mixture. During the evaporation, the surfactant concentration increases and above the critical micelle concentration (cmc), the surfactant molecules arranges into micelles in which hydrophobic parts are covered by hydrophilic parts. Further increase in the surfactant

concentration organizes the micelles into liquid crystal mesophases to form 2D structures. The inorganic aluminum precursor assembles on the hydrophilic part of the surfactant to form a metal oxide network by hydrogen, covalent and van der Waals interactions bonds via hydrolysis and polymerization. The aging process and subsequent drying solidifies and locks the amorphous alumina phase over the surfactant and the mesoporous alumina is obtained by the removal of the organic surfactant by calcination or extraction [74, 76, 83].

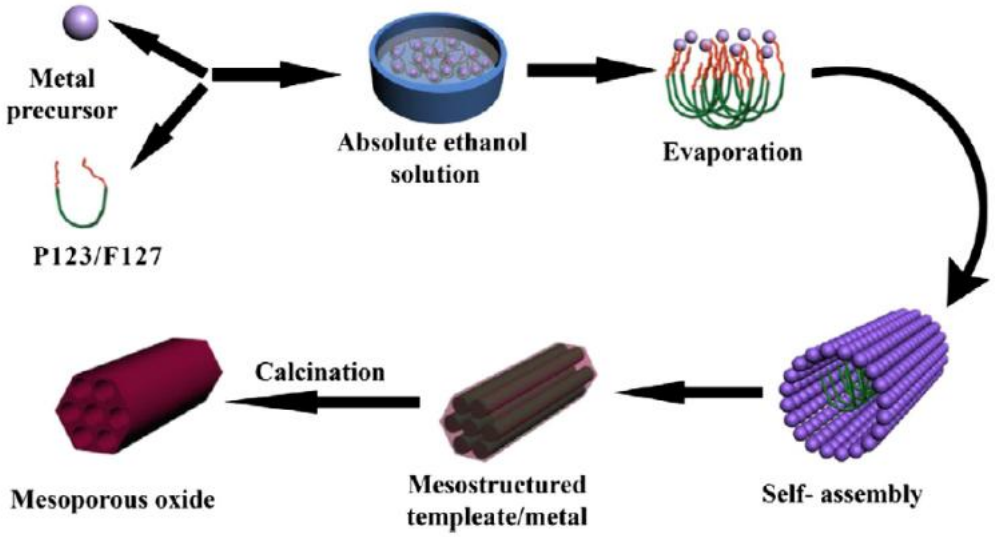

Figure 6. Schematic model for EISA method [76]

Mesophase formation is affected by complex-forming capability of structure directing agents, ions and acids. As the surfactant is dissolved in solvent and metal source, alumina in this case, is added; crown-ether type complexes, as shown in Figure 7, are formed after hydrolysis and condensation due to connection of the metal ions alkylene oxide structures by coordination bonds. Alumina ions are bonded to the hydrophilic poly(ethyleneoxide) functional groups promoted by the presence of an acid such as HNO_3, HCl with hydrogen-bonding, covalent and van der Waals interactions [71, 84].

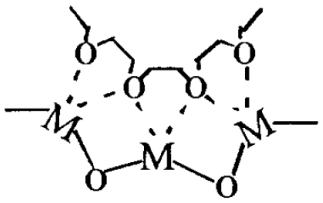

Figure 7. Crown-ether-type complexes [84]

The EISA process is performed in alcohol solution containing a concentrated acid; a non-aqueous media, to slow down the hydrolysis and condensation rate of the aluminum precursor and also redox reaction, phase transformation [76]. The low amount of water present in the concentrated acid and ethanol is sufficient for the slow and controlled hydrolysis of the aluminum precursor since large water content destroys the structure due to the tendency of alumina precursor for precipitation and crystallization to bulk oxide phase [74, 84].

NO_3^- has weak complex-forming capability therefore; the self-assembly process is not significantly affected by the presence of NO_3^- ions. When hydrochloric acid is used instead of nitric acid, the balance of the organic-inorganic interface is destroyed and the assembly process is disturbed due to the strong coordination of chloride ions with aluminum ions. This might result in formation of long-range disordered mesostructures [71].

Volatility of the acid is important for hydrolysis and condensation, which have to be slow to form a robust mesostructure rather than a hard structure. The acid, which is removed by evaporation, controls the inorganic polymerization since dilute solutions are used. The volatility of HNO_3 is lower than that of HCl; therefore, the acidity of the solution reduces more slowly as HNO_3 evaporates and the hydrolysis of alumina and the self-assembly process are not significantly disturbed [71]. The solvent is also required to be evaporated slowly to prevent phase separation between the inorganic and organic species and to provide high cross-linking between the components [81].

5.3. CHARACTERIZATION TECHNIQUES

5.3.1. X-Ray Diffraction (XRD)

X-ray diffraction method is applied to determine the pore structure and crystalline phases of the synthesized material. In the short range of the XRD pattern of mesoporous alumina, a strong (100) diffraction peak around and a weaker (110) peak are observed and are a proof of ordered mesostructure with *p*6*mm* hexagonal symmetry [77]. X-ray diffraction method is also used for fresh and used catalyst in order to determine particle size of agglomerated copper crystals that could cause catalyst deactivation.

5.3.2. Nitrogen Physisorption (BET)

The surface area and pore size distribution of a porous material are determined by nitrogen physisorption (adsorption) method. Surface areas are calculated by the Brunauer–Emmet–Teller (BET) equation using nitrogen adsorption-desorption isotherms at -196^{o}C (77K) and the mesopore sizes are estimated by the Barrett–Joyner–Halenda method [78]. In a typical nitrogen adsorption isotherm of mesoporous alumina, a sharp step in the mesoporous range with relative pressure (P/P_o) between 0.5 and 0.8 indicates the liquid condensation of N_2 at 77 K and uniform mesopores [77].

5.3.3. Transmission Electron Microscopy (TEM)

Transmission Electron Microscopy is a useful method for visualization of pore orderings of the materials. The presence of dislocations and other defects in crystal structure can be determined. The image of the structure, channels, pores and the hexagonal structure of the material is captured as the high-energy electron beam transmits through the sample [72].

5.3.4. Diffuse Reflectance Infrared Fourier Transform Spectroscopy (DRIFTS)

Diffuse Reflectance Infrared Fourier Transform Spectroscopy (DRIFTS) of pyridine adsorbed samples can be used to determine the characteristics of the acid sites of the synthesized materials. This method provides the information about the relative strengths of the Brønsted and Lewis acid sites. A spectrum is obtained with analyzing the reflected infrared (IR) beam from the catalyst surface. The difference between the spectra of the pyridine-adsorbed catalyst and not-adsorbed catalyst identifies the Brønsted and Lewis acidities. The presence of Brønsted acid sites indicated with bands observed at 1490, 1540 and 1640 cm^{-1}, which are due to contribution of pyridinium ions that means pyridine chemisorbed on Brønsted acid sites. For Lewis acid sites, the bands present at 1445, 1490 and 1595 cm^{-1} which are coordinatively bound pyridine that means pyridine interacting with Lewis acid sites [31, 52, 62]. Mesoporous alumina mostly includes large amount of Lewis acid sites [71].

CHAPTER 6

EXPERIMENTAL

In this study, mesoporous alumina and silicotungstic acid impregnated mesoporous alumina were synthesized as methanol dehydration catalysts. Bifunctional catalysts were prepared by physical mixture of previously prepared methanol synthesis catalysts [11] and synthesized mesoporous materials. In this chapter, the synthesis procedures are explained and the characterization techniques of the synthesized materials are presented. The high-pressure flow system, which was used to test the prepared bifunctional catalysts for the direct synthesis of DME from syngas, is described in detail.

6.1. SYNTHESIS OF CATALYSTS

6.1.1. Synthesis of Mesoporous Alumina

Mesoporous alumina was synthesized by evaporation-induced self assembly process reported by Yuan et al. [71]. The following chemicals were used for the synthesis:

- Surfactant: Pluronic P123, Poly(ethylene glycol) - block - poly(propylene glycol) - block - poly(ethylene glycol), $EO_{20}PO_{70}EO_{20}$, MW = 5800 – Sigma-Aldrich
- Alumina source: Aluminum isopropoxide, $C_9H_{21}O_3Al$ – MERCK
- Acid source: Nitric acid, HNO_3 – MERCK
- Solvent: Ethanol, C_2H_5OH – Sigma-Aldrich

There are four main steps for mesoporous alumina synthesis, which are preparation of the synthesis solution, hydrolysis, evaporation and calcination.

For the synthesis, 4 g of Pluronic P123 was dissolved in 30 mL of ethanol. Solution was stirred continuously at 375 rpm at room temperature until clear solution was obtained. In a separate vessel, 6.4 mL of 65 wt. % nitric acid and 20 mL of ethanol were added on 8 g of aluminum isopropoxide and stirred continuously at 200 rpm at room temperature until no solid particle remained. Then, aluminum isopropoxide solution was added dropwise on P123 solution and the resultant mixture was stirred for about 18 hours at room temperature and put into oven at 60 °C for solvent evaporation for 2 days of aging. The solution formed a light-yellow solid that was placed into a quartz tube having a membrane filter for calcination for removal of the surfactant from the structure. Calcination was performed in a tubular furnace from ambient temperature to 700^{o}C with heating rate of 1^{o}C/min and kept at 6 hours in dry air. At the end of the calcination, solid material inside the quartz tube was cooled to room temperature under the flow of dry air and finally white, powder material was obtained. The steps in synthesis procedure are presented in Figure 8.

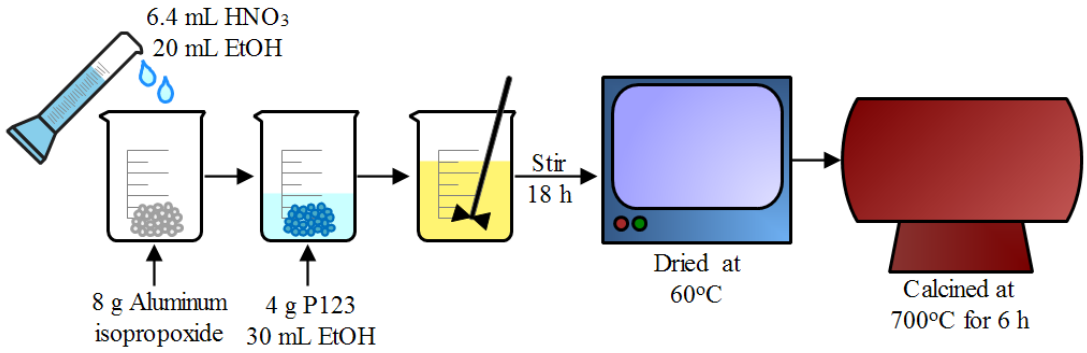

Figure 8. The synthesis procedure for mesoporous alumina

6.1.2. Synthesis of Silicotungstic Acid Impregnated Mesoporous Alumina

Silicotungstic acid (STA) was impregnated on mesoporous alumina (MA) according to procedure presented in study of Varışlı et al. [55]. STA amount was chosen to be 10 wt% of the amount of MA. Therefore, STA to MA weight ratio was determined as 0.1. The chemicals used for impregnation are presented below:

- Heteropolyacid: Silicotungstic acid hydrate 99.9%, $H_4SiW_{12}O_{40}$ – Sigma-Aldrich
- Solvent: Deionized water Millipore Ultra - Pure Water System, Milli-QPlus

1 g of mesoporous alumina was stirred continuously in 15 mL of deionized water and in a separate vessel; 0.1 g of STA was dissolved in 10 mL of deionized water. Then STA solution was added on MA solution and the resultant mixture was stirred at 30°C for 47 hours. Then, the mixture was dried at 70°C without mixing. The solid material was calcined from ambient temperature to 350°C with heating rate of 1°C/min and kept at 6 hours in dry air. The obtained catalyst was named as STA@MA. The impregnation procedure is presented in Figure 9.

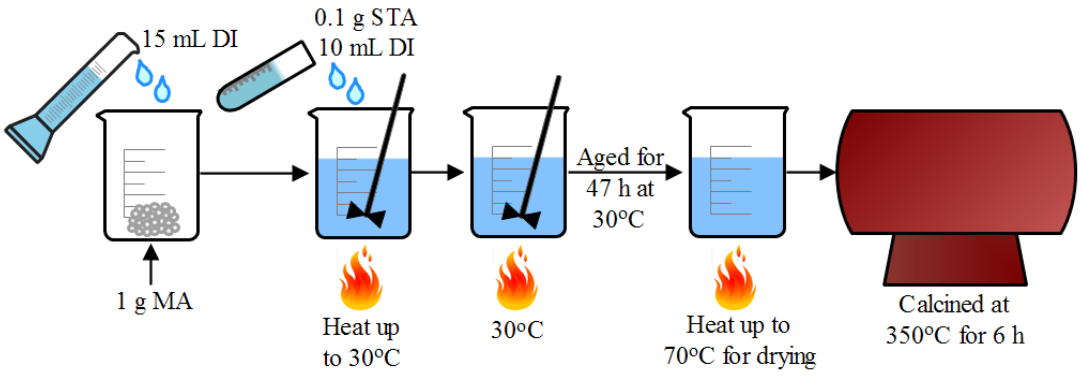

Figure 9. The synthesis procedure for STA impregnated mesoporous alumina

6.2. CHARACTERIZATION METHODS APPLIED FOR THE CATALYSTS

X-ray diffraction (XRD), nitrogen physisorption (BET), Transmission Electron Microscopy (TEM) and Diffusion Reflectance Infrared Fourier Transform Spectroscopy of pyridine adsorption (DRIFTS) were used to characterize the synthesized catalysts.

6.2.1. X-Ray Diffraction (XRD)

The XRD patterns of the synthesized catalysts were obtained by XRD Rigaku Ultima-IV X-Ray diffractometer in the METU-Central laboratory. The radiation source is CuK with a 2θ scanning ranges of small angle between 0.5° and 10°. The wide angle patterns of the synthesized materials and the used catalyst to detect the formation of the agglomerated copper particles were obtained by Philips PW 1840 X-Ray diffractometer in Chemical Engineering Department in METU. The radiation source is CuK with a 2θ scanning ranges of wide angle between 10^o and 80^o.

6.2.2. Nitrogen Physisorption

Nitrogen adsorption-desorption analyses were performed by Quantachrome Corporation, Autosorb-6 device in Central Laboratory in METU. The samples were degassed 120°C for 6 hours and the degassed samples were analyzed at a relative pressure range of $5x10^{-2}$ to 0.99 at liquid nitrogen temperature, 77 K nitrogen adsorption and desorption isotherms, the surface areas and the pore size distributions were determined.

6.2.3. Transmission Electron Microscopy (TEM)

Transmission Electron Microscopy (TEM) analyses with EDX mapping were done in the Middle East Technical University (METU) Central Laboratory by a Jeol 2100F HRTEM TEM high resolution instrument with Orius SC1000 Model 832 11 Megapixel CCCD camera. Before the analyses, samples were suspended in alcohol

by an ultrasonic stirrer for 15 minutes. Then, a drop of each sample was placed over HC300-Cu Holey Carbon film grid and dried overnight.

6.2.4. Diffuse Reflectance Infrared Fourier Transform Spectroscopy (DRIFTS) of Pyridine Adsorption

Diffuse Reflectance Infrared Fourier Transform Spectroscopy of pyridine adsorption analyses were performed by Perkin Elmer Spectrum One instrument at Kinetic Laboratory in Middle East Technical University. The samples were dried in oven at 110^{o}C for 12 hours. 0.035 gr of each sample was adsorbed with 1 mL of pyridine and dried in oven for 2 hours at 40^{o}C. A background spectrum was recorded with KBr. Then, the spectrum of pyridine-adsorbed sample was subtracted from the spectrum of non-adsorbed sample. The present acid sites were determined by the difference spectrum.

6.3. REACTION SET-UP

The activity tests are performed by a high pressure continuous flow system for the direct synthesis of dimethyl ether. The schematic representation of the reaction set-up is given in Figure 10. The bifunctional catalyst mixture of methanol synthesis and methanol dehydration catalysts is placed into stainless steel tubular reactor and supported with glass wool at both ends. The stainless steel tubular reactor has the length of 60 cm and the diameter of 4 mm. The reactor is placed into a tubular furnace and the reaction temperature is adjusted by the temperature controller of the furnace. The reactant gases of CO and H_2 are fed from the pressurized cylinders and their pressures are controlled with regulators and pressure gauges. The pressures of the regulators are adjusted to 60 bar. Flow rates of the feed gases are controlled by the Omega FMA-800A series mass flow controllers. A venting system is placed before the mass flow controllers for evacuation of the lines after the operation. Another pressure gauge is placed after the mass flow controllers to measure the operating system pressure. The line is then connected to the reactor that is placed into the furnace. After the furnace, a metering valve is placed to adjust the flow rate of

the stream. The operating system pressure is selected as 50 bar. The metering valve was closed and the system was filled with feed gases to pressurize the system to 50 bar. At 50 bar, the metering valve was opened and the flow rate was adjusted. The lines before and after the furnace are heated to 150^{o}C and insulated to provide pre-heating and to prevent condensation of the products. An online gas chromatography is used to analyze the outlet stream. A soap bubble flow meter is placed at the end of the line to measure the exit flow rate.

A secondary study was performed by adding various amount of CO_2 to the feed stream with small modifications to the existing system. The flow rate of is measured by metering valve and soap bubble flow meter. The lines starting from the exit of CO_2 the cylinder to the entrance of the reactor are heated and insulated to avoid CO_2 to form ice that occurs at high pressure. The schematic representation of the modified reaction set-up is displayed in Figure 11.

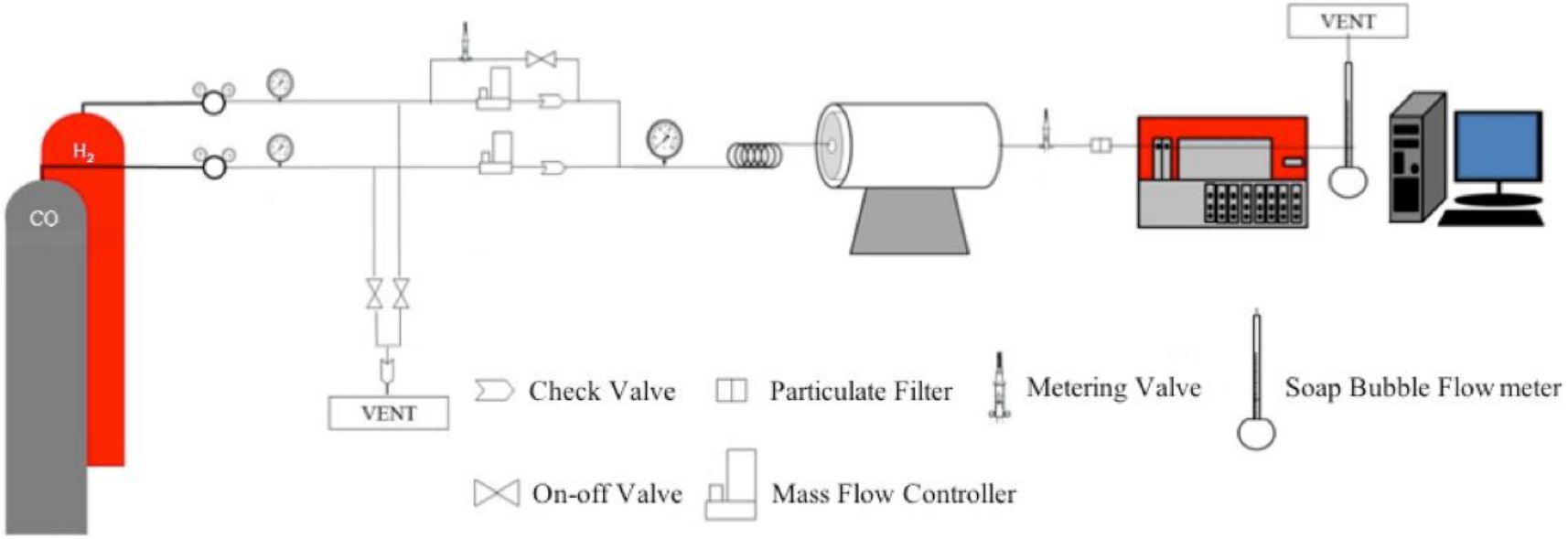

Figure 10. High pressure experimental set-up with reactant gases of CO and H_2

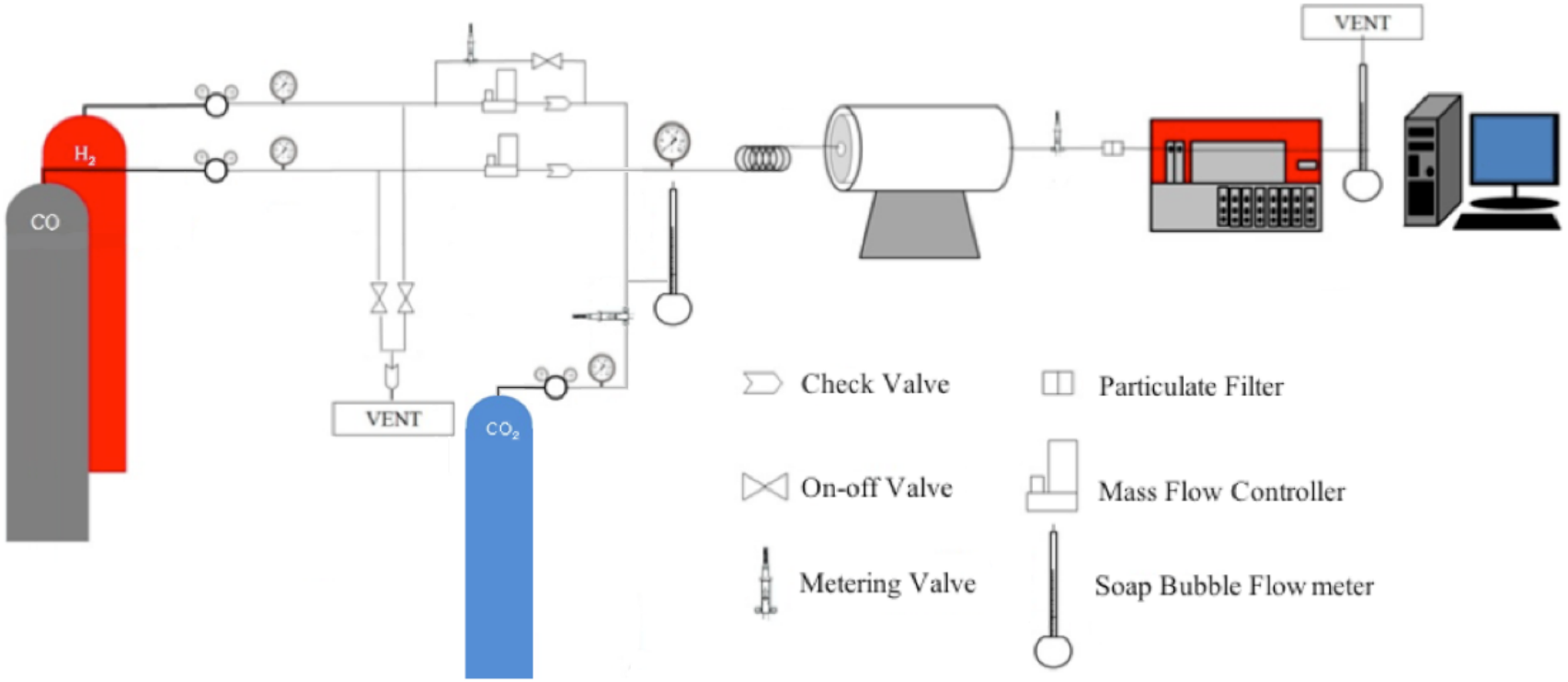

Figure 11. High pressure experimental set-up with reactant gases of CO, CO_2 and H_2

The SRI 3680 multigas #1 gas chromatography (GC) is equipped with a Carbosphere column and a thermal conductivity detector (TCD). Helium is used as the carrier for the GC with the flow rate of 20 cc/min and the pressure of 4 bar. The parameters for the temperature ramped program that is used in the GC are given in Table 7. The calibration factors and the retention times for the gases present in the stream are given in Table 8.

Table 7. Temperature program of gas chromatograph

Initial Temp., ºC	Time, min	Ramp, ºC/min	Final Temp., ºC
130	7	-	130
130	3	40	250
250	18	-	250

Table 8. Calibration factors and retention times of gas chromatograph

Component	Retention Time, min.	Calibration Factor
Carbon Monoxide	1.3 – 1.4	1.00
Methane	2.4 - 2.6	1.36
Carbon Dioxide	4.2 - 4.3	0.83
Formic Acid	11.8 - 11.9	1.80
Methanol	13.9 - 14.2	1.40
Dimethyl Ether	23.3 - 23.5	0.49
Ethanol	25.8 - 26.0	1.44

The connection and construction materials that were used in the reaction set-up have been selected as stainless steel to withstand high pressure. The bifunctional catalyst mixtures of 0.2 or 0.3g that was packed in the middle of the reactor contained mostly equal amounts of methanol synthesis and dehydration catalysts. In some experiments, methanol synthesis catalyst to dehydration catalyst weight ratio was chosen as 1:2. The total flow rate of the feed gas was adjusted as 25 cc/min (measured at room temperature at 1 bar) with a space time of 0.48 g.s/mL or 0.72 g.s/mL. When CO and H_2 were used as feed gases, equal volumetric flow rates of the

gases were selected. When CO_2 was introduced to the system, varying volume ratios of H_2, CO and CO_2 were selected.

Catalytic activity tests were performed generally in the temperature range of 200 to 300^oC with intervals of 25^oC. Steady state was reached in 60 minutes and afterwards three successive analyses were taken for each temperature and the averages of the results of these analyses were used for conversion and selectivity calculations.

CO conversion was defined as the ratio of amount of CO reacted to the amount of CO fed to reactor and product selectivities were defined as the ratio of moles of CO converted to a specific component to total moles of CO converted to the products. According to these definitions, conversion and DME, methanol, and CO_2 selectivities were expressed as;

X = (Moles of CO fed to system - Moles of CO emerged from system)/ Moles of CO fed to system 6.1.

S_{DME} = 2(Moles of DME formed)/ (Moles of CO converted to products) 6.2.

S_{MEOH} = (Moles of MEOH formed)/ (Moles of CO converted to products) 6.3.

S_{CO_2} = (Moles of CO_2 formed)/ (Moles of CO converted to products) 6.4.

CO_2 was observed as the major product together with DME when the feed stream was composed of 50% CO and 50% H_2. In the experiments performed with addition of CO_2 to the feed stream, it was seen that carbon dioxide behaved as the reactant at low temperatures. Therefore, CO and CO_2 conversions were calculated and the product selectivities were calculated by involving the contribution of CO_2. Product selectivities, in this case, were calculated as the ratio of moles CO and CO_2 converted to specific component to total moles of CO and CO_2 converted to products. Accordingly, CO and CO_2 conversions and DME and methanol selectivities were defined as;

X_{CO} = (Moles of CO fed to system – Moles of CO emerged from system)/ Moles of CO fed to system 6.5.

X_{CO_2} = (Moles of CO_2 fed to system – Moles of CO_2 emerged from system)/ Moles of CO_2 fed to system 6.6.

$\underline{S}_{DME}$ = 2(Moles of DME formed)/ (Moles of CO&CO_2 converted to products) 6.7.

$\underline{S}_{MEOH}$= (Moles of MEOH formed)/ (Moles of CO&CO_2 converted to products) 6.8.

DME yields were also calculated for comparison. Yield was expressed as the ratio of moles of desired product formed to moles of reactant fed to the system.

Y_{MEOH}= (Moles of MEOH formed)/ (Moles of CO fed to system) 6.9.

Sample calculations for conversion, selectivity, and yield are presented in the Appendix B.

6.4. OBJECTIVE OF THE STUDY

In the first part of the study, the bifunctional catalysts composed of physical mixtures of the previously synthesized copper-based methanol synthesis catalysts and commercial γ-Al_2O_3 methanol dehydration catalyst were tested with the feed mixture containing 50% CO and 50% H_2. Their performances were compared and the methanol synthesis catalyst that exhibited the best performance was selected.

In the second part of the study, the best catalyst or commercial methanol synthesis catalyst were mixed with MA or STA@MA to compare their performances. This time, methanol synthesis to dehydration catalyst weight ratio was also investigated.

In the third part of the study, best catalyst combination was used for investigating the effect of adding carbon dioxide to the feed gas stream with varying volume ratios of H_2/CO/CO_2.

CHAPTER 7

CHARACTERIZATION RESULTS

In this chapter, characterization results of the synthesized materials are presented. X-Ray diffraction (XRD), nitrogen physisorption, Transmission Electron Microscopy (TEM), and Diffuse Reflectance Infrared Fourier Transform Spectroscopy of pyridine adsorption techniques were used for the characterization of these materials.

7.1. CHARACTERIZATION RESULTS OF METHANOL SYNTHESIS CATALYSTS

The methanol synthesis catalysts that have been used in this study were synthesized by Çelik, G., with mole ratios of Cu/Zn/Promoter = 6/3/1 [11]. The nomenclature of the synthesized catalysts is presented in Table 9. The summary of the characterization results of the catalysts is given in Table 10. Commercial γ -Al_2O_3 from TOYO is used as methanol dehydration catalyst in the first phase of the study and the characterization results of γ-Al_2O_3 is presented in Table 11.

Table 9. The methanol synthesis catalysts (Adapted from [11])

Nomenclature	Content	Aging Time	Washing Water	Calcination Temp., ºC	Reduction Temp., ºC
CZ	Cu-Zn	3 hr	Cold	350	-
CZCe	Cu-Zn-Ce	3 hr	Cold	350	-
CZZr	Cu-Zn-Zr	3 hr	Cold	350	-
CZA-1hr	Cu-Zn-Al	1 hr	Cold	350	-
CZA or CZA-3hr	Cu-Zn-Al	3 hr	Cold	350	-
CZA-6hr	Cu-Zn-Al	6 hr	Cold	350	-
CZA-Hot	Cu-Zn-Al	3 hr	Hot	350	-
CZA-C550	Cu-Zn-Al	3 hr	Cold	550	-
CZZr-C550	Cu-Zn-Zr	3 hr	Cold	550	-
CZA-R225	Cu-Zn-Al	3 hr	Cold	350	225
CZA-R250	Cu-Zn-Al	3 hr	Cold	350	250
MSC	Cu-Zn-Al	-	-	-	-

Table 10. Characterization results of the methanol synthesis catalysts (Adapted from [11])

Catalyst	d_{CuO}, nm	d_{Cu2O}, nm	d_{Cu}, nm	d_{ZnO}, nm	Multipoint BET Surface area, m^2/g	BJH Method Desorption Pore Volume, cc/g	BJH Method Desorption Pore Diameter, nm
CZ	4.3	-	-	4.9	62	0.62	9.6
CZCe	2.8	-	-	-	97	0.77	3.8
CZZr	5.0	-	-	2.5	107	0.51	9.7
CZA-1hr	9.4	-	-	4.0	69	0.49	17.5
CZA-3hr	8.1	-	-	4.1	57	0.45	7.9
CZA-6hr	7.6	-	-	4.7	50	0.37	7.85
CZA-Hot	8.4	-	-	4.3	77	0.51	17.7
CZA-C550	13.0	-	-	8.1	41	0.62	2.1
CZZr-C550	6.9	-	-	5.4	48	0.42	32.0
CZA-R225	-	18.5	-	10.3	22	0.11	2.1
CZA-R250	-	-	26.8	10.6	53	0.27	17.7
MSC	4.6	-	-	3.4	99	0.24	6.5

Table 11. Characterization results of commercial γ-Al_2O_3 (Adapted from [11])

Catalyst	d_{Al2O3}, nm	Multipoint BET Surface area, m^2/g	BJH Method Desorption Pore Volume, cc/g	BJH Method Desorption Pore Diameter, nm
γ-Al_2O_3 TOYO	4.8	148	0.57	9.5

7.2. CHARACTERIZATION RESULTS OF MA AND STA@MA

7.2.1. X-Ray Diffraction (XRD) Results

XRD provides information about the pore structure of the synthesized material. In the case of mesoporous materials, the diffraction patterns provide information about mesostructure of the material in the small angle range (2θ less than 10). The XRD pattern of mesoporous alumina is shown in Figure 12 and has a major peak at 2θ = 1° that correspond to (100) peak and a minor (110) peak close to 2θ = 2°.

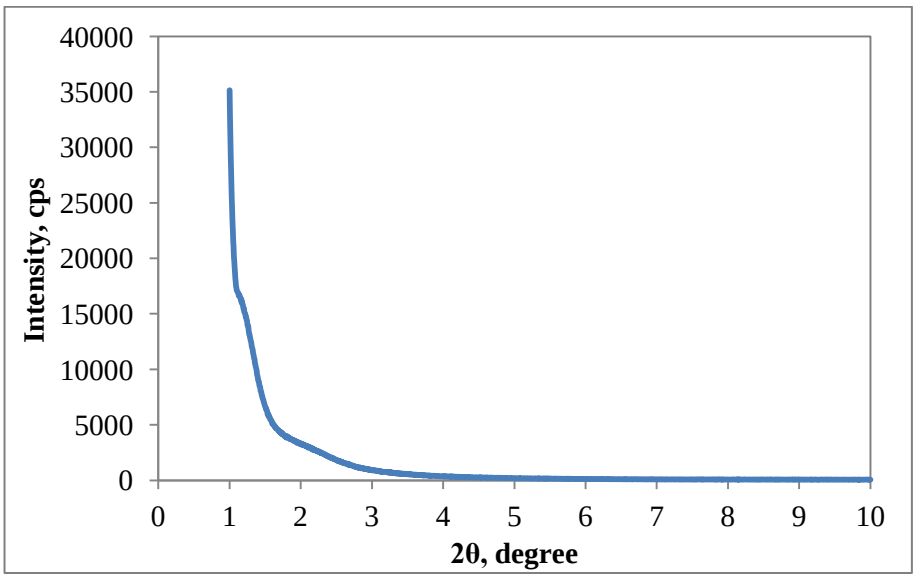

Figure 12. The small angle XRD pattern of MA

The small angle XRD pattern of STA impregnated MA (STA@MA) is shown in Figure 13. Similarly, XRD pattern of STA@MA has a major (100) peak at 1^{o}. However, the minor (110) peak is not visible which means that STA impregnation has disturbed the mesoporous structure of MA.

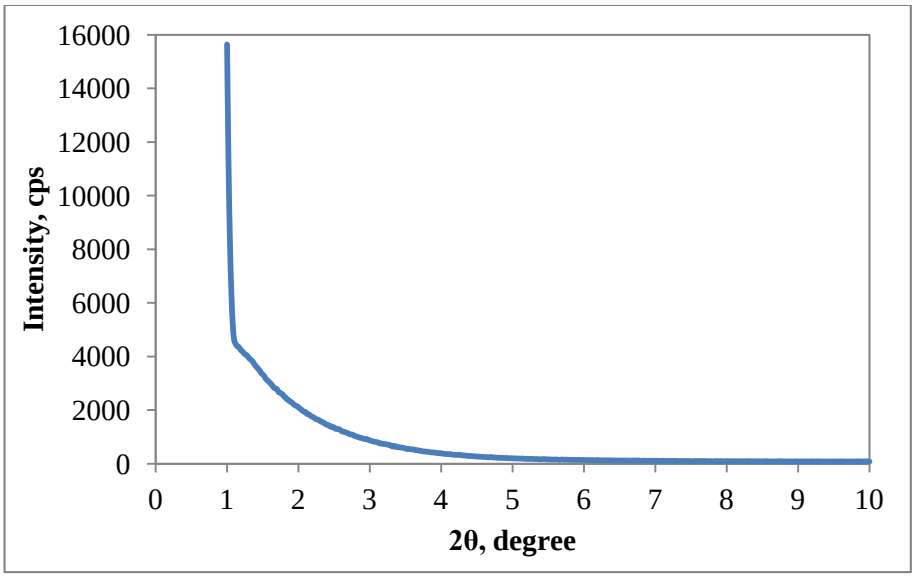

Figure 13. The small angle XRD pattern of STA@MA

The wide angle XRD patterns of MA and STA@MA are presented in Figure 14. Mesoporous alumina possesses amorphous wall when calcined at 400^{o}C, whereas crystalline γ-Al_2O_3 phase forms at higher calcination temperatures [71]. According to the XRD pattern of MA, crystalline γ-Al_2O_3 phase was present with a characteristic peak at a 2θ value of 66. Silicotungstic acid impregnation MA evolved crystalline γ-Al_2O_3 phases with 2θ values of 34, 46 and 66 due to further catalytic treatment.

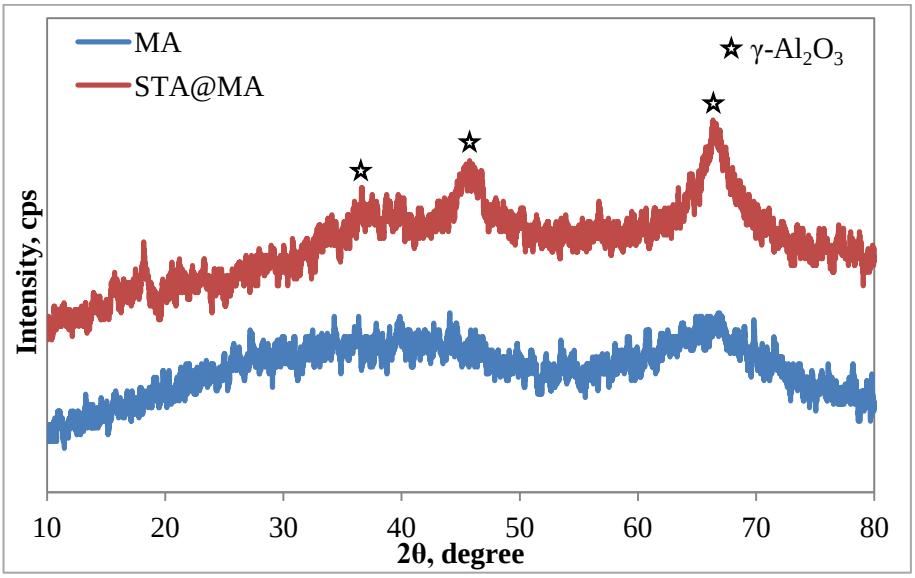

Figure 14. The wide angle XRD patterns of MA and STA@MA

7.2.2. N_2 Physisorption (BET) Results

The surface area, average pore diameter and pore volume and also pore size distributions and nitrogen adsorption desorption isotherms were obtained by nitrogen physisorption results. According to the adsorption-desorption isotherm of MA, which is presented in Figure 15, the synthesized mesoporous alumina had a typical Type IV isotherm in the mesoporous range with relative pressure (P/P_o) between 0.5 and 0.8. Hysteresis loops are formed by capillary condensation of nitrogen in the pores and the adsorption and desorption branches of the hysteresis loop are steep and parallel with Type H1 according to IUPAC classification. This result informs that the synthesized mesoporous alumina possesses uniform, cylindrical, open ended, unconnected pores with a long range order.

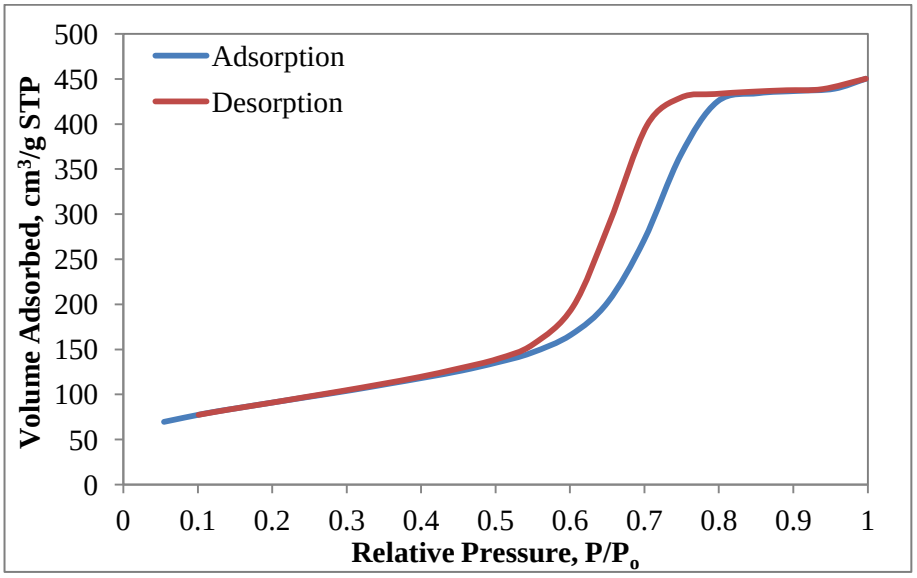

Figure 15. Nitrogen physisorption isotherm of MA

The adsorption-desorption isotherm of STA@MA is presented in Figure 16 and the isotherm is Type IV. However, the hysteresis loop is between Type 1 and 3, since the adsorption and desorption branches are broad and but not very steep. This indicates the disturbance of ordered mesoporosity of mesoporous alumina due to silicotungstic acid impregnation.

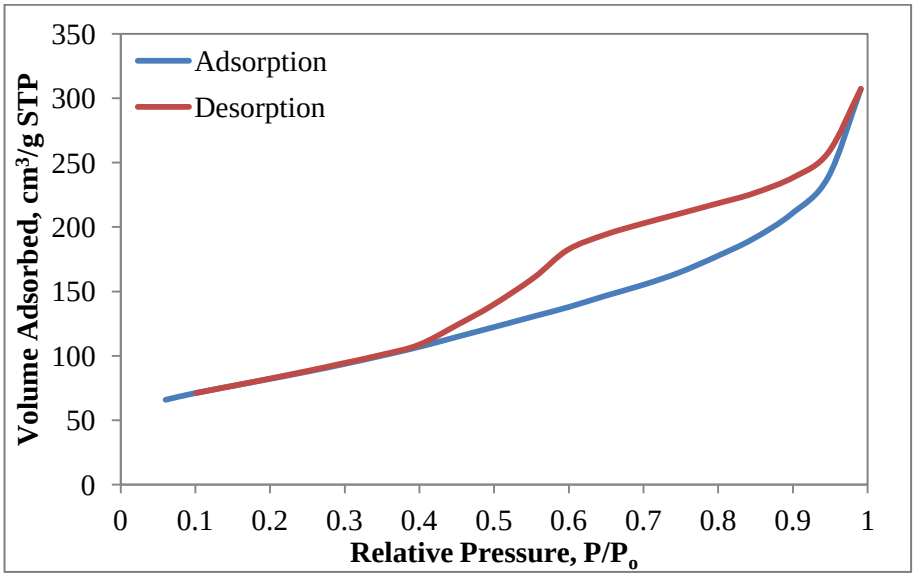

Figure 16. Nitrogen physisorption isotherm of STA@MA

BET and BJH surface area, pore volume, pore size and micropore area data of MA and STA@MA are listed in Table 12. According to Table 12, the surface area of the synthesized mesoporous alumina (323 m^2/g) is obtained as expected in the literature [71]. The synthesized MA is in the mesoporous range with pore diameter of 5.7 nm and mesopore volume of 0.77 cc/g. Silicotungstic acid impregnation on mesoporous alumina caused in decrease of BET and BJH surface area, mesopore volume and pore diameter. The reason of this result could be explained as STA impregnation covered the surface area and plugged the pores of mesoporous alumina. Though, the surface area and pore size reductions were not severe since the amount of STA impregnated on mesoporous alumina was not very high. The pore size distributions of MA and STA@MA are presented in Figure 17 and it is seen that mesoporous alumina has very narrow and uniform pore size distribution. However, STA impregnation on MA disturbed the uniformity of the pore size distribution.

Table 12. BET and BJH surface area, pore volume and size and micropore area data of MA and STA@MA

	MA	STA@MA
BET Surface Area, m²/g	323	289
BJH Surface Area, m²/g	489	309
BJH Mesopore Volume, cc/g	0.77	0.47
BJH Pore Diameter, nm	5.7	4.9
DR Micropore Volume, cc/g	0.16	0.14
DR Micropore Area, m²/g	451	405

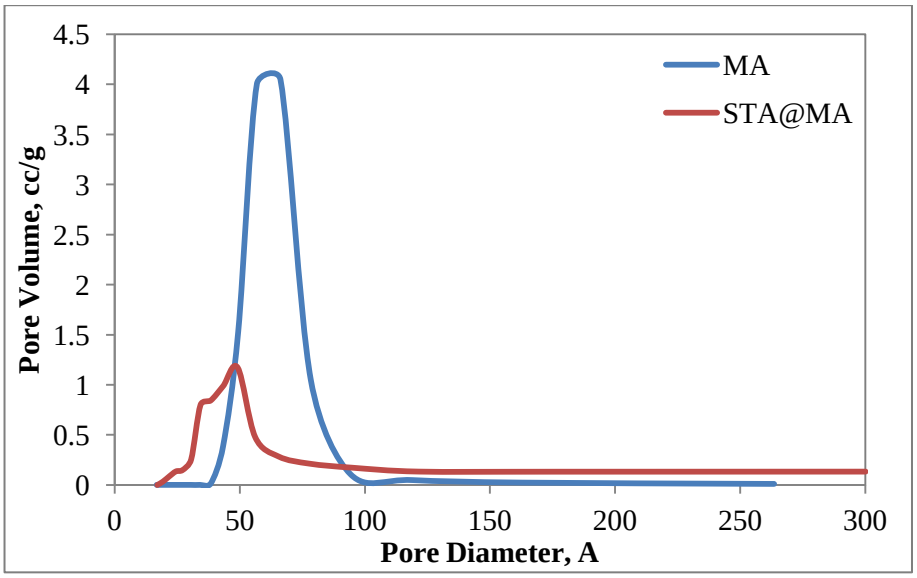

Figure 17. Pore size distribution curves of MA and STA@MA

7.2.3. Transmission Electron Microscopy (TEM) Results

TEM images of mesoporous alumina are displayed in Figures 18 and 19. In the images, pore openings of the material are visibly seen with ordered cylindrical channels as presented in the inset of Figure 18.

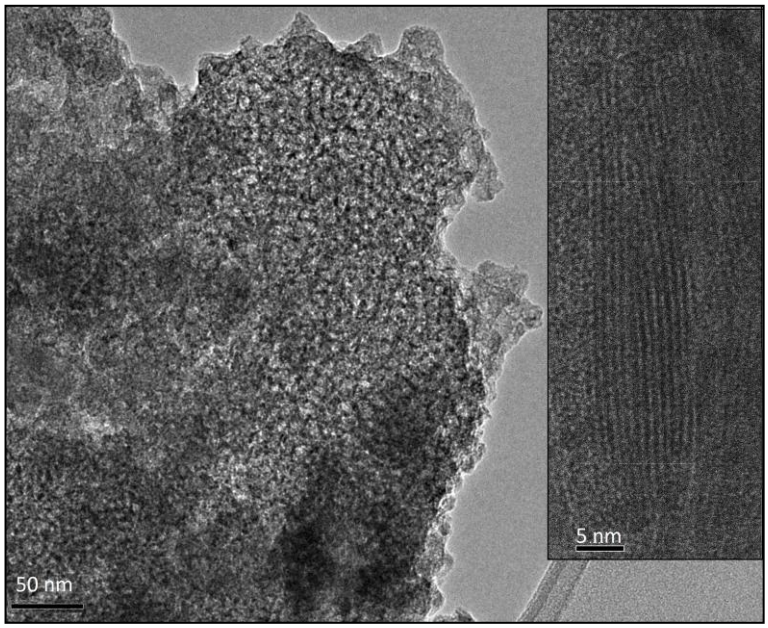

Figure 18. TEM image of MA

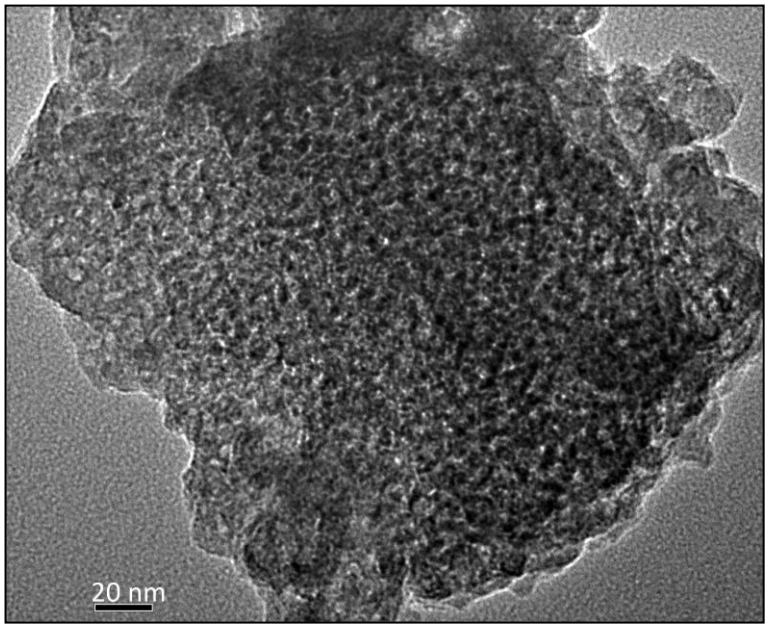

Figure 19. TEM image of MA

TEM images of STA impregnated mesoporous alumina are displayed in Figures 20 and 21. According to the images, the ordered pore openings of the material are visibly seen without significant disturbance due to STA impregnation. Ordered cylindrical channels are also visible as presented in the inset of Figure 20.

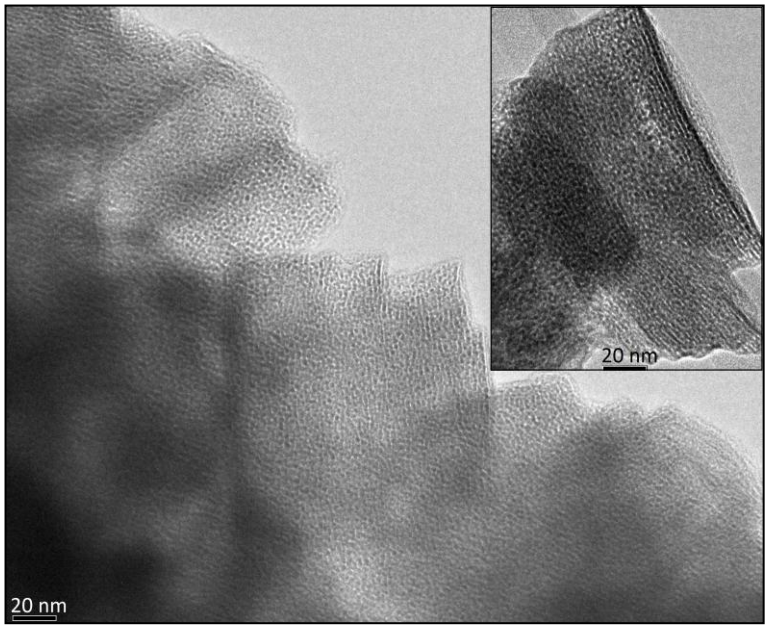

Figure 20. TEM image of STA@MA

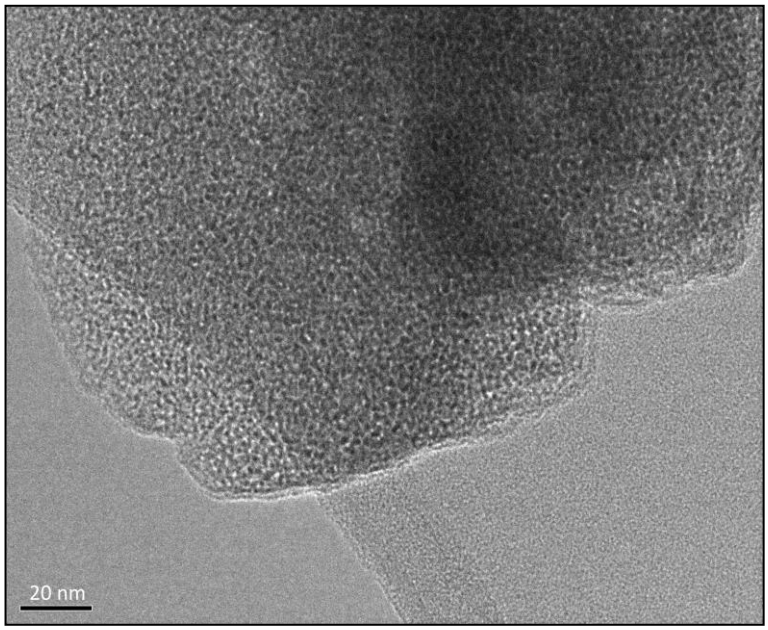

Figure 21. TEM image of STA@MA

The EDX mapping of STA impregnated mesoporous alumina is displayed in Figure 22. In the image, silica (Si) and tungsten (W) are homogeneously dispersed over the surface of mesoporous alumina.

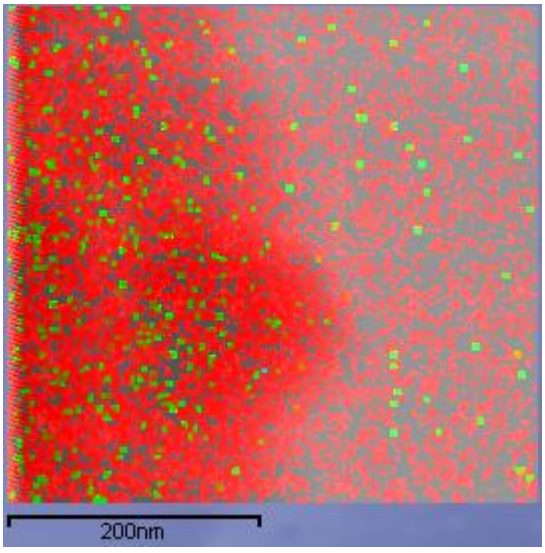

Figure 22. EDX mapping of STA@MA (Si = Red, W = Green)

7.2.4. Diffuse Reflectance Infrared Fourier Transform Spectroscopy of Pyridine Adsorption

DRIFTS analyses were performed for mesoporous alumina, STA impregnated mesoporous alumina and commercial γ-Al_2O_3 to identify the relative strengths of the Brønsted and Lewis acid sites. According to the DRIFTS spectrum, presented in Figure 23, for MA, the Lewis bands at 1445 and 1595 cm^{-1} are very small. In the case of STA@MA, Lewis acid sites at the band positions of 1445 and 1595 cm^{-1} are visibly seen. This means that impregnation of silicotungstic acid enhanced the acidic strength of mesoporous alumina. The commercial γ-Al_2O_3 exhibited stronger Lewis acid sites than that of STA@MA. Brønsted acid sites are present at the band positions of 1540 and 1640 cm^{-1}. However, Brønsted acid sites are not visible for MA, STA@MA and γ-Al_2O_3. The intensity of the bands for Brønsted acid sites could be very low. The band at 1490 cm^{-1} is due to the simultaneous contribution of Brønsted and Lewis acid sites. However, for MA, STA@MA and γ-Al_2O_3, the band at 1490 cm^{-1} was only due to Lewis acid sites since the intensities of the bands for Brønsted acid sites were not very strong. DRIFTS spectra of MA and STA@MA are separately presented in Appendix C.

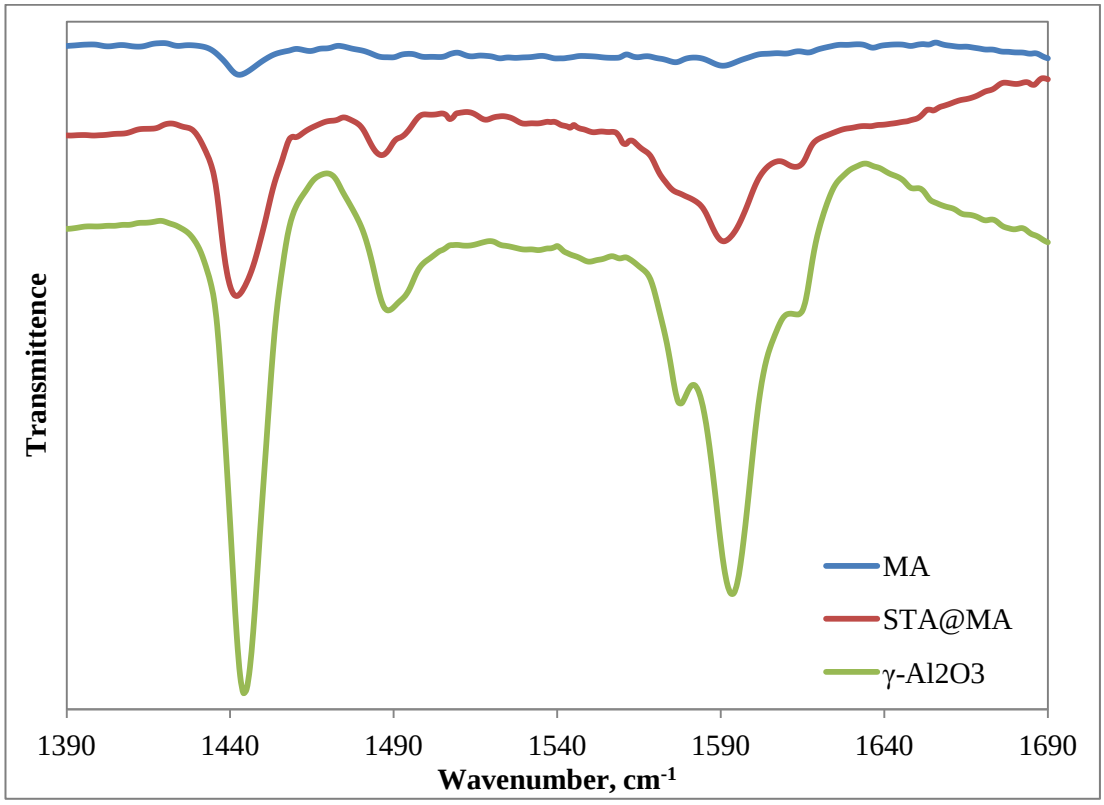

Figure 23. DRIFTS spectra of MA, STA@MA and commercial γ-Al_2O_3

CHAPTER 8

ACTIVITY RESULTS

In this chapter, activity results of the direct synthesis of dimethyl ether using various catalyst mixtures and operation conditions are presented. The performed study was composed of three parts. In the first part, bifunctional catalysts were tested for the direct DME synthesis at 50 bar and within a temperature range of 200-300^{o}C with a feed composition of H_2/CO = 50/50 based on volume ratio. For this purpose, different methanol synthesis catalysts were used as methanol synthesis function while commercial γ-Al_2O_3 was used as methanol dehydration function. Methanol synthesis catalysts were prepared by Çelik [11] at different synthesis conditions such as different promoters, aging time, washing water, calcination and reduction temperatures. After the activity tests, the best methanol synthesis catalyst was selected which was zirconia promoted copper-based catalyst and used in the second part.

In the second part, mesoporous alumina was synthesized to be used as the solid acid catalyst. Zirconia promoted copper-based catalyst was compared with commercial methanol synthesis catalyst. These catalysts were mixed with mesoporous alumina and tested at the same reactions. Silicotungstic acid (STA) was impregnated on mesoporous alumina to enhance the acidic strength. STA impregnated mesoporous alumina was also mixed with zirconia promoted and commercial methanol synthesis catalyst. In addition, weight of STA impregnated mesoporous alumina was increased to twice of methanol synthesis catalyst. The best catalyst mixture was also selected which was the mixture of commercial methanol synthesis catalyst and STA impregnated mesoporous alumina and used in the third part.

In the third part, the effect of presence of carbon dioxide in the feed stream was investigated. The volumetric flow rate ratio of CO, CO_2 and H_2 was selected as H_2/CO/ CO_2 = 50/40/10, 50/25/25 and 50/10/40. Carbon monoxide and carbon dioxide conversion and product distributions are presented with respect to reaction temperature.

8.1. ACTIVITY RESULTS OF THE BIFUNCTIONAL CATALYSTS WITH METHANOL SYNTHESIS CATALYSTS AND γ-Al_2O_3

Methanol synthesis catalysts that were used in this part were listed in Table 9. All of the methanol synthesis catalysts, except for commercial methanol synthesis catalysts (MSC), were physically mixed with commercial γ-Al_2O_3 purchased from TOYO with a weight ratio of 1:1. In total, 0.2 g of catalyst mixtures (0.1 g MeOH synthesis catalyst and 0.1 g γ-Al_2O_3) was loaded in the middle of the stainless steel reactor tube. The feed gas mixture was composed of 50% CO and 50% H_2 in volume basis and the total flow rate was 25 mL/min. Reaction experiments were performed at the operating conditions of 50 bar and within a temperature range of 200-300^{o}C, with intervals of 25^{o}C. For consistency, the bifunctional mixtures were abbreviated as "methanol synthesis catalyst + TOYO".

8.1.1. Promoter Effect

In this section, the effect of addition of promoters was investigated on carbon monoxide conversion and product distribution for the direct synthesis of DME. The promoters added on copper-zinc catalyst were Al, Zr and Ce.

The carbon monoxide conversion results obtained with the mixture of copper-zinc catalyst with no promoter (CZ) and γ-Al_2O_3 (TOYO) are given in Figure 24. According to this figure, carbon monoxide conversion was around 1% at 200°C. Then, the conversion increased with an increase in temperature and reached to 13.4% at 300°C.

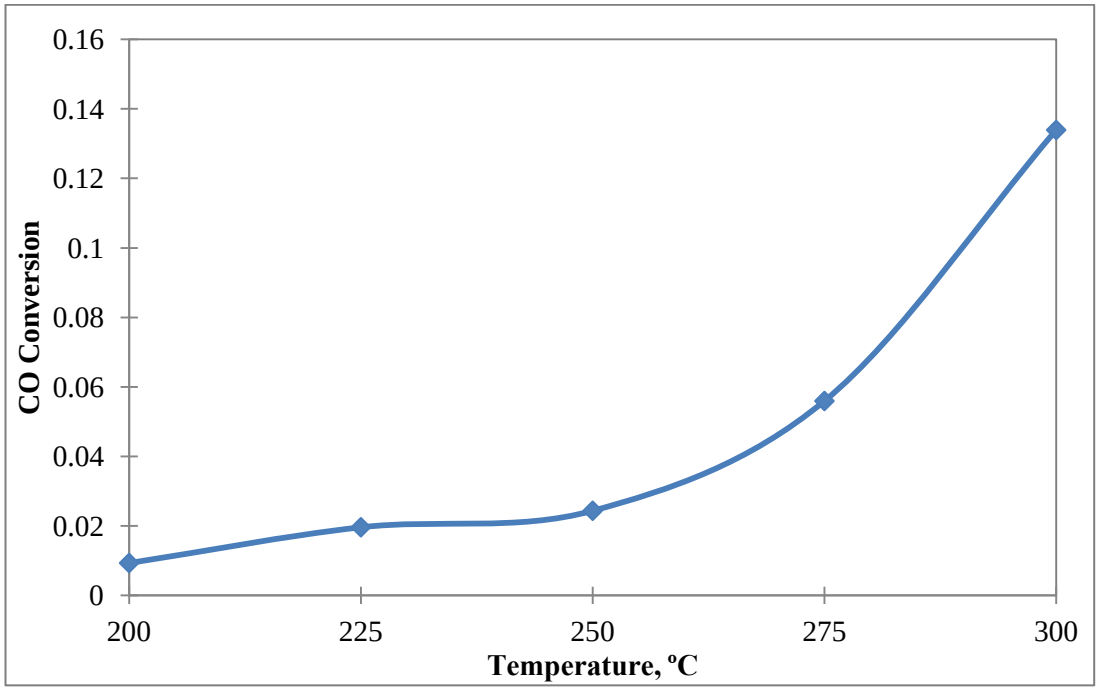

Figure 24. Carbon monoxide conversion obtained with CZ + TOYO (Space time: 0.48 s.gr/cc, catalyst amount: 0.2 gr, feed stream: 50% CO + 50% H_2)

The product distribution obtained with CZ + TOYO catalyst mixture is given in Figure 25. As it is seen in that figure, the highest DME selectivity was achieved at 200°C as 64.8%. DME selectivity remained at about 65% up to 250°C and decreased at higher temperatures. Since the process itself is an exothermic reaction, reverse reactions become more significant at higher temperatures. Besides, formation of side products also gains importance at high temperatures. Significant amount of carbon dioxide formation was observed at all temperatures. Small amount of unconverted methanol also remained in the product stream. At temperatures above 250^{o}C, byproducts, such as methane, ethanol and formic acid were also formed.

Water-gas shift reaction, in which the formed water reacts with CO, could also be responsible for the formation of CO_2. In addition to that, production of CO_2 could be due to reverse dry reforming reaction (Reaction 10), since small amount of CH_4 was also observed at higher temperatures. CH_4 could also be produced by CO hydrogenation (Reaction 11). Both of these reactions are thermodynamically favorable at the operating conditions of this study [85].

$$2CO + 2H_2 \leftrightarrow CH_4 + CO_2 \quad (10)$$

$$CO + 3H_2 \leftrightarrow CH_4 + H_2O \quad (11)$$

The presence of CO_2 could be also due to Boudouard reaction (Reaction 12), especially at low temperatures, since the Boudouard reaction is thermodynamically favorable at reaction conditions [11].

$$2CO \rightarrow CO_2 + C_{(s)} \quad (12)$$

Formations of CO_2, and the side products of methane, ethanol and formic acid through reactions 10, 11, 13, 14 and 15, were responsible for the sharp increase in CO conversion after 250^{o}C [11, 85].

$$2CO + 4H_2 \leftrightarrow C_2H_5OH + H_2O \quad (13)$$

$$3CO + 3H_2 \leftrightarrow C_2H_5OH + CO_2 \quad (14)$$

$$CO_2 + H_2 \leftrightarrow CH_2O_2 \quad (15)$$

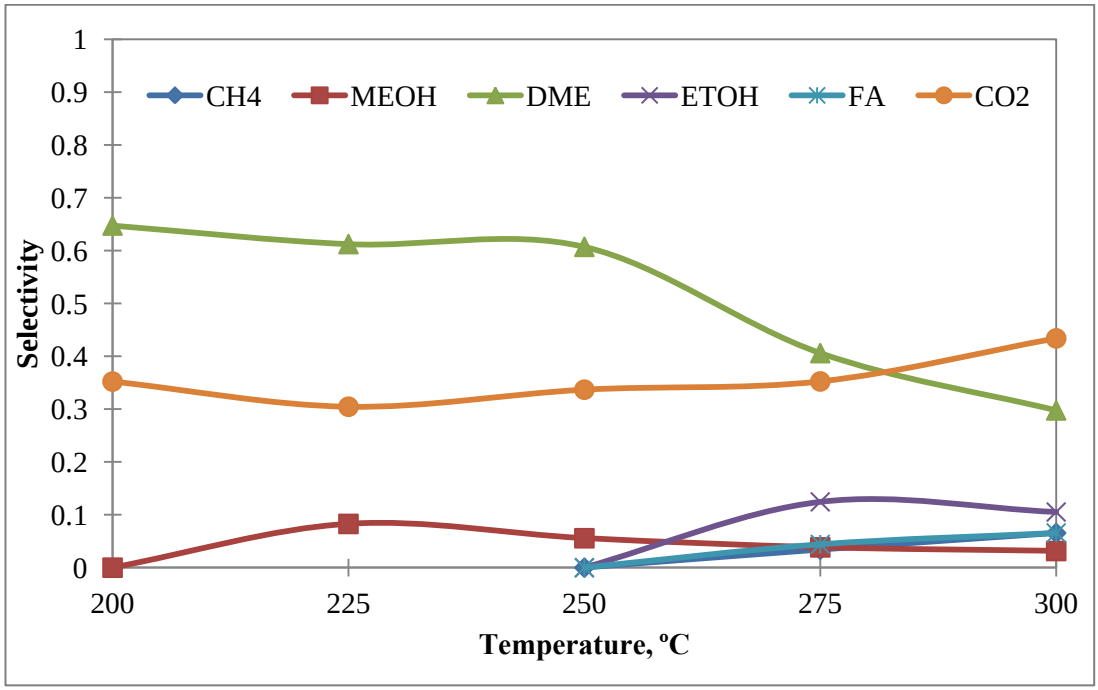

Figure 25. Product distribution obtained with CZ + TOYO (Space time: 0.48 s.gr/cc, catalyst amount: 0.2 gr, feed stream: 50% CO + 50% H_2)

Comparison of carbon monoxide conversion due to promoter effect is given in Figure 26. The promoters added to copper-zinc catalyst were alumina, zirconia and ceria with molar ratio on Cu/Zn/Promoter = 6/3/1. According to this figure, the promoter effect is not visibly seen since there are small differences between the carbon monoxide conversion which is due to both direct synthesis and side reactions. However, the contribution of a promoter on the catalyst performance is observed better in the product distribution.

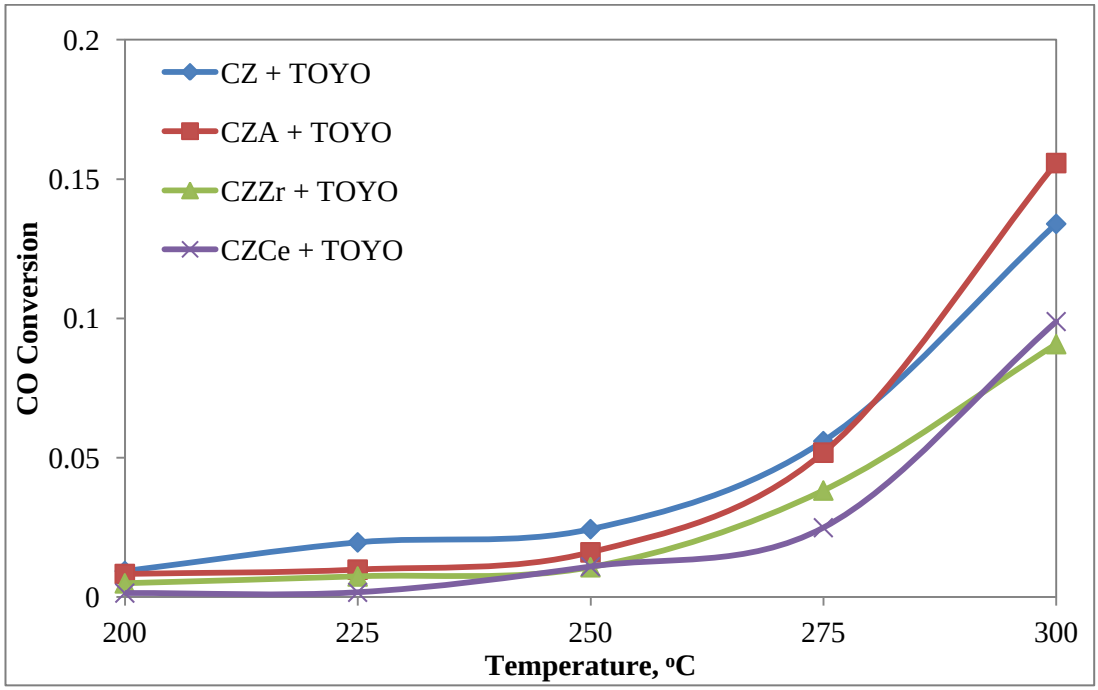

Figure 26. Comparison of carbon monoxide conversions obtained by the promoter effect with the mixtures of CZ, CZA, CZZr and CZCe with γ-Al_2O_3 (TOYO) (Space time: 0.48 s.gr/cc, catalyst amount: 0.2 gr, feed stream: 50% CO + 50% H_2)

When alumina was used as promoter, a better product distribution was obtained as compared to the catalyst without promoter. According to the product distribution of the CZA + TOYO catalyst mixture shown in Figure 27, 68.8% of DME selectivity was obtained at 200°C, which was then decreased only after 250°C due to formation of significant amount of CO_2 and byproducts such as methane, ethanol and formic acid. Methanol was not observed up to 275°C which indicates that CZA + TOYO was sufficient to convert the produced methanol to DME. The presence of methanol at higher temperatures could be due to inhibition of methanol dehydration with byproduct formations. Addition of alumina on copper-zinc increased the catalytic activity and stability. The amount of unconverted methanol was seen at temperatures above 250°C. Therefore, the catalyst mixture containing alumina promoted catalyst exhibited better product distribution as compared to the catalyst mixture containing copper-zinc catalyst.

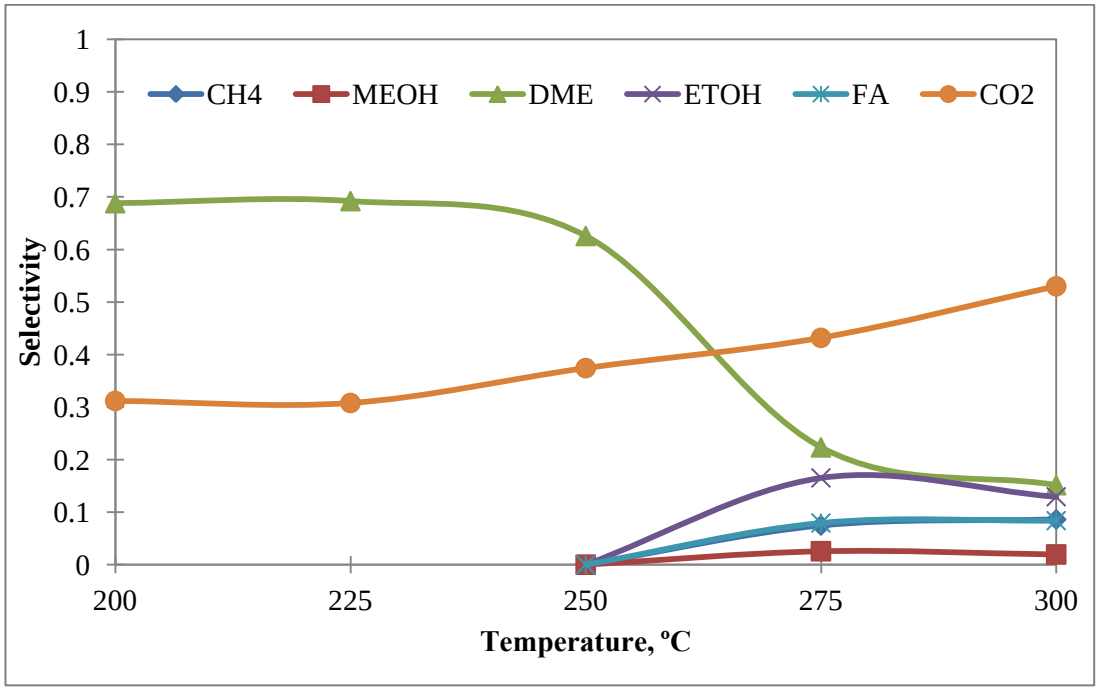

Figure 27. Product distribution obtained with CZA + TOYO (Space time: 0.48 s.gr/cc, catalyst amount: 0.2 gr, feed stream: 50% CO + 50% H_2)

The catalyst mixture with zirconia promoter presented similar product distribution with the catalyst mixture with alumina promoter. The product distribution of CZZr + TOYO mixture is given in Figure 28. The highest DME selectivity was 66.4% at 200°C which decreased much slower as the temperature increased as compared to CZA + TOYO mixture. Less amount of CO_2 formed at higher temperatures with complete dehydration of methanol except for 300°C at which insignificant amount of methanol present. It can be deduced that zirconia promoter enhanced the catalytic activity of the bifunctional catalyst by providing smaller copper particles of 5.0 nm and larger surface area of 107 m^2/g. On the other hand, alumina promoted catalyst possessed the copper particles of 8.1 nm and surface area of 57 m^2/g.

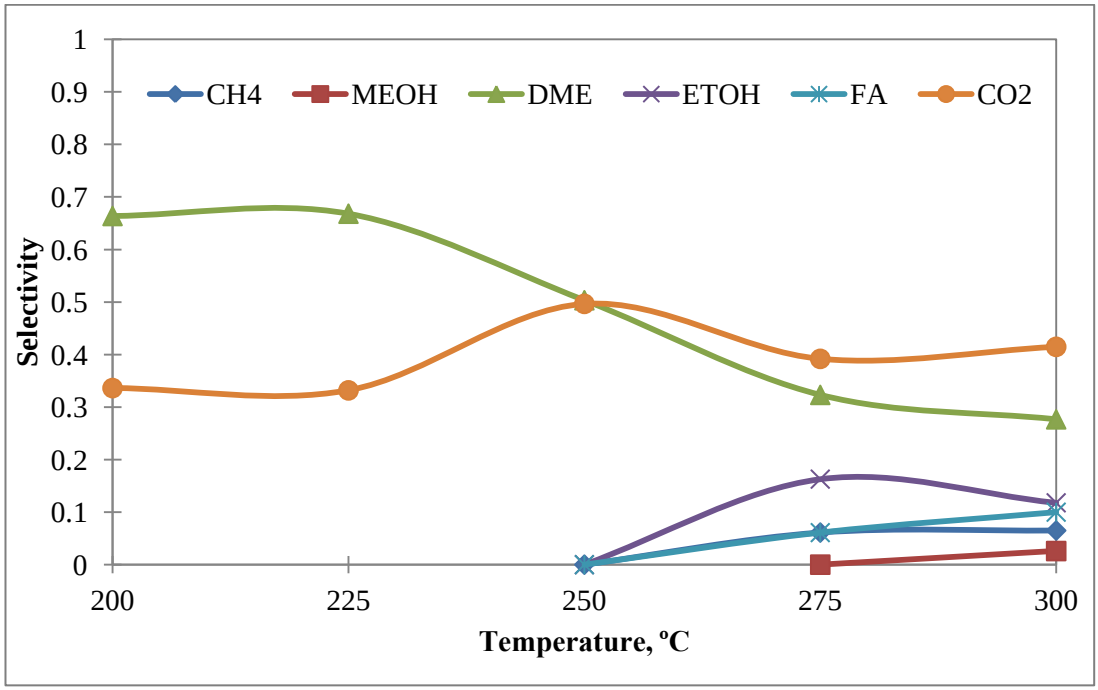

Figure 28. Product distribution obtained with CZZr + γ-Al_2O_3 (Space time: 0.48 s.gr/cc, catalyst amount: 0.2 gr, feed stream: 50% CO + 50% H_2)

The product distribution of the catalyst mixture with ceria promoter is presented in Figure 29. DME formation was not seen until 250°C at which only 10% of DME selectivity was achieved. At higher temperatures, DME selectivity decreased and at 300°C small amount of unconverted methanol was present. Carbon monoxide and hydrogen was converted mostly to carbon dioxide. Carbon dioxide was the only product at 200 and 225°C with 100% selectivity and was produced via water-gas shift and Boudouard reaction since no other side products were formed. The selectivity of carbon dioxide then decreased due to formation of the byproducts. At 250°C, significant amount of ethanol was produced with a selectivity value of 34.5% due to Reactions 13 and 14. Methane and formic acid were produced in small amounts at temperatures higher than 225°C and 250°C, respectively. This result indicates that ceria promoter was not active for methanol synthesis and the overall direct synthesis of DME processes. However, it gave high ethanol yields.

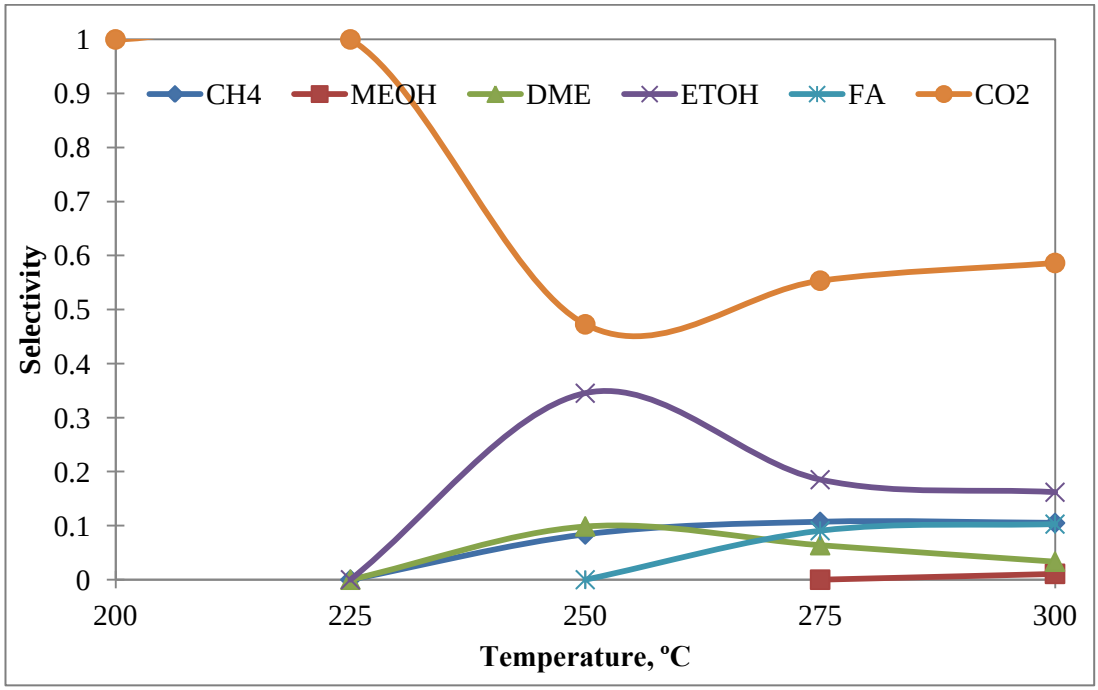

Figure 29. Product distribution obtained with CZCe + TOYO (Space time: 0.48 s.gr/cc, catalyst amount: 0.2 gr, feed stream: 50% CO + 50% H_2)

The DME selectivities of the catalyst mixtures with different promoters were compared in Figure 30. At temperatures lower than 250°C, the performances of alumina and zirconia promoted catalyst mixtures were similar and better than the others. At higher temperatures, zirconia promoted and non-promoted catalyst mixtures were better than the rest. Better performance of zirconia promoted catalyst mixture could be attributed to smaller CuO particle size of 5.0 nm. Significant drop in alumina promoted catalyst mixture could be due to larger CuO particles of 8.1 nm.

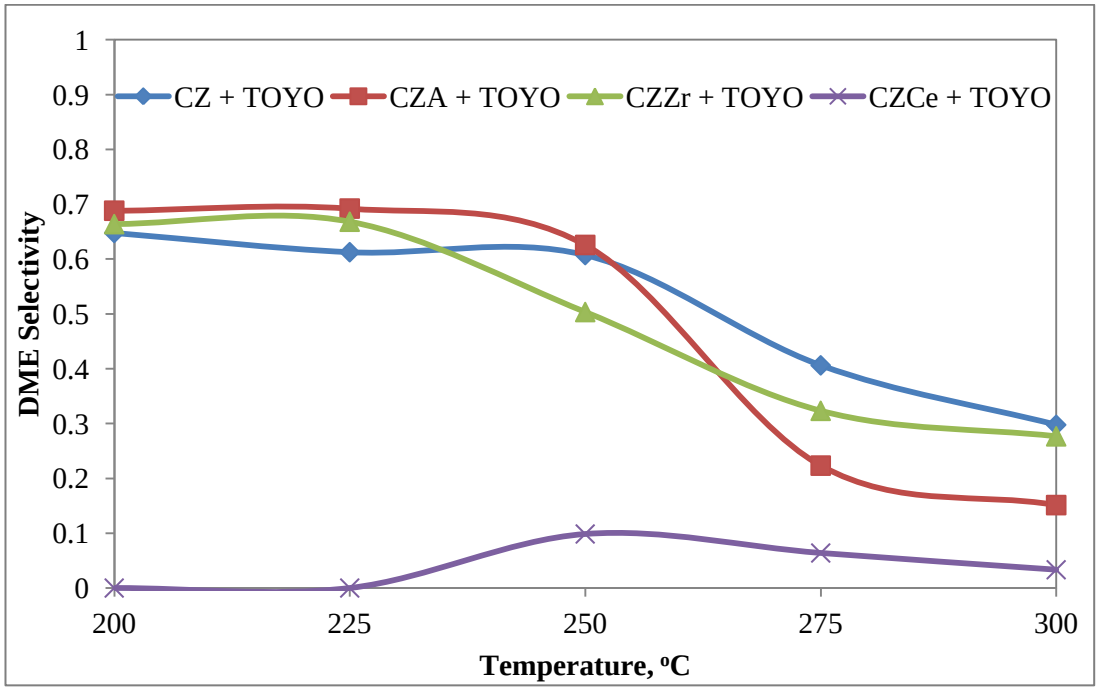

Figure 30. Comparison of DME selectivities of the catalyst mixtures with different promoters; CZ + TOYO, CZA + TOYO, CZZr + TOYO and CZCe + TOYO (Space time: 0.48 s.gr/cc, catalyst amount: 0.2 gr, feed stream: 50% CO + 50% H_2)

8.1.2. Effects of Synthesis Conditions of Cu/Zn/Al Catalyst on Catalytic Performance

The standard aging condition was 3 hours for the copper-zinc based, co-precipitated methanol synthesis catalysts described in the previous section. The alumina promoted methanol synthesis catalysts were synthesized at two different aging times, namely 1 hour and 6 hours. The carbon monoxide conversions of the catalyst mixtures containing CZA catalysts aged for 1, 3 and 6 hours are compared and the results are presented in Figure 31. CZA-3hr is used instead of CZA in this part, for nomenclature consistency. Alumina promoted catalyst mixtures aged for 1 hour, 3 hours and 6 hours exhibited similar carbon monoxide conversion trends. However, the performance of the catalyst aged for 6 hours was the best, giving a CO conversion value of about 21.5% at 300°C. As given in Table 10, as the aging time

increases, CuO particle size decreases. Better performance of 6 hours-aged catalyst mixture could be attributed to smaller particle size.

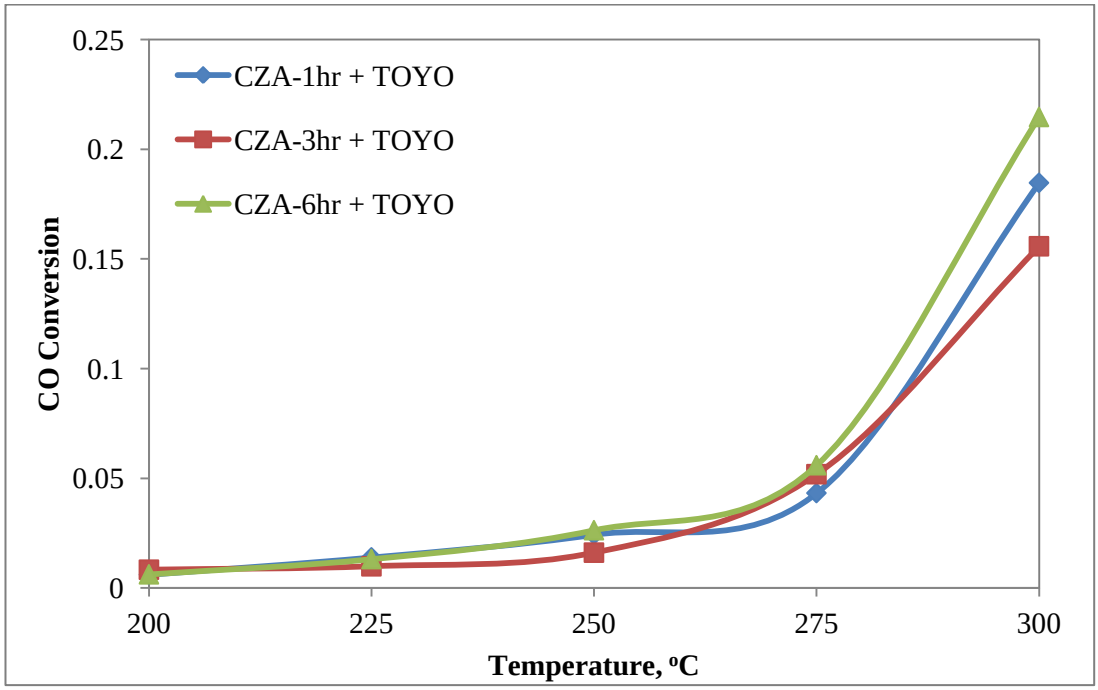

Figure 31. Comparison of carbon monoxide conversions obtained by aging effect on CZA with γ-Al_2O_3 (TOYO) (Space time: 0.48 s.gr/cc, catalyst amount: 0.2 gr, feed stream: 50% CO + 50% H_2)

Product distribution of 1 hour-aged aluminum promoted catalyst mixture is given in Figure 32. According to the results, the highest DME selectivity was obtained as 52.8% at 200°C and the selectivity decreased sharply to 3% at 300°C. This catalyst mixture favored formation of carbon dioxide with steep increase via conversion of carbon monoxide and hydrogen by Boudouard reaction and water-gas shift reaction at low temperature. Ethanol and methane formation reactions also contributed at higher temperatures. 60% of carbon dioxide selectivity was obtained at 300°C. Significant amount of byproducts were produced; methane was formed after 200°C, ethanol and formic acid were produced after 225°C. Small amounts of methanol, which did not dehydrate to DME, were also present at each temperature.

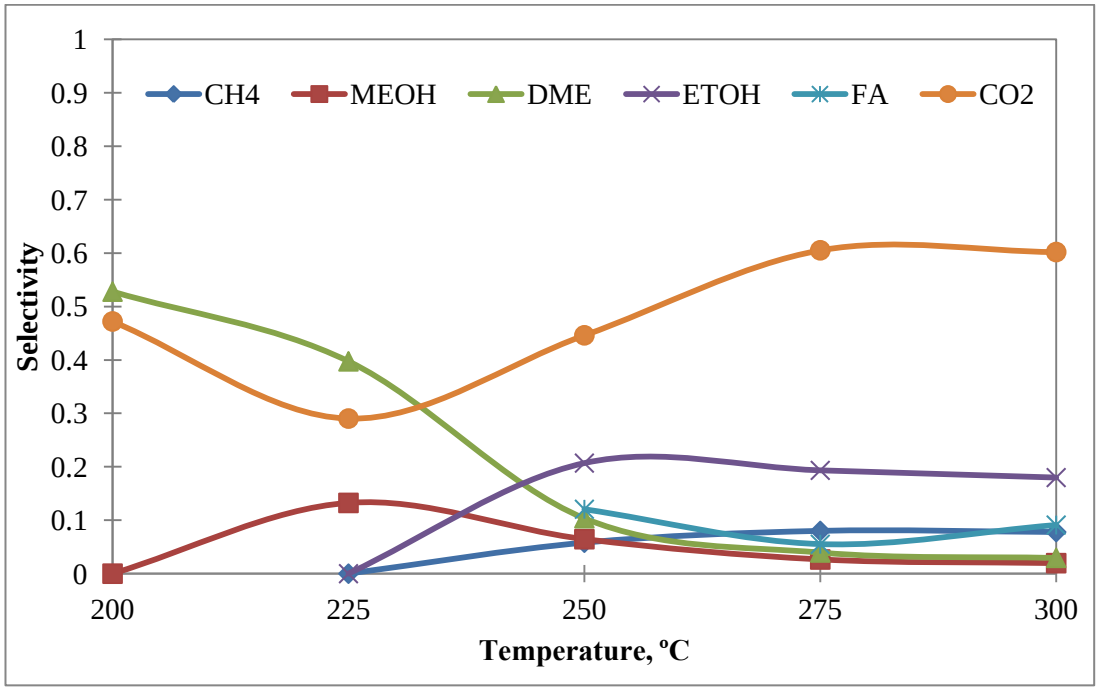

Figure 32. Product distribution obtained with CZA-1hr + TOYO (Space time: 0.48 s.gr/cc, catalyst amount: 0.2 gr, feed stream: 50% CO + 50% H_2)

According to the product distribution of 6 hours-aged aluminum promoted catalyst mixture which is given in Figure 33, the highest DME selectivity was achieved as 57.7% at 200°C and decreased to 10.3% at 300°C. This catalyst mixture also favored formation of carbon dioxide with steady increase up to 56.4% at 300°C with temperature rather than DME synthesis. The presence of carbon dioxide was again due to water-gas shift reaction and Boudouard reaction initially and byproduct formation reactions of ethanol and methane above 225°C.

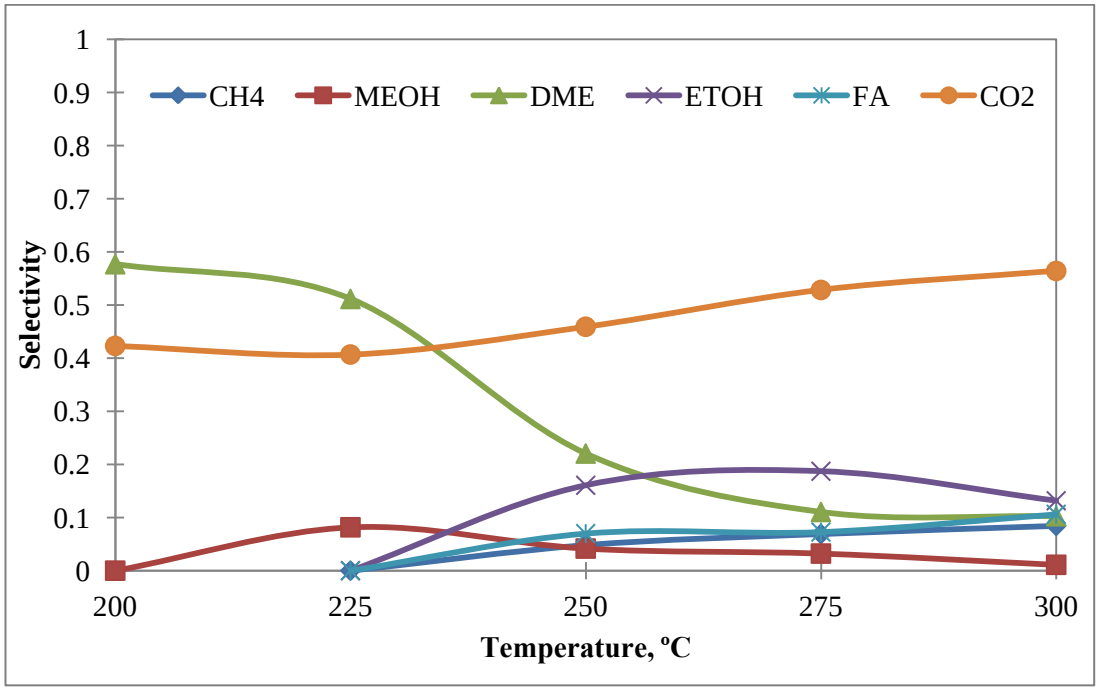

Figure 33. Product distribution obtained with CZA-6hr + TOYO (Space time: 0.48 s.gr/cc, catalyst amount: 0.2 gr, feed stream: 50% CO + 50% H_2)

DME selectivities of catalyst mixtures having alumina promoted catalyst with different aging times were compared and given in Figure 34. As seen from this figure, DME selectivity of CZA-3hr + TOYO catalyst mixture was always higher than that of CZA-6hr + TOYO and CZA-1hr + TOYO catalyst mixtures.

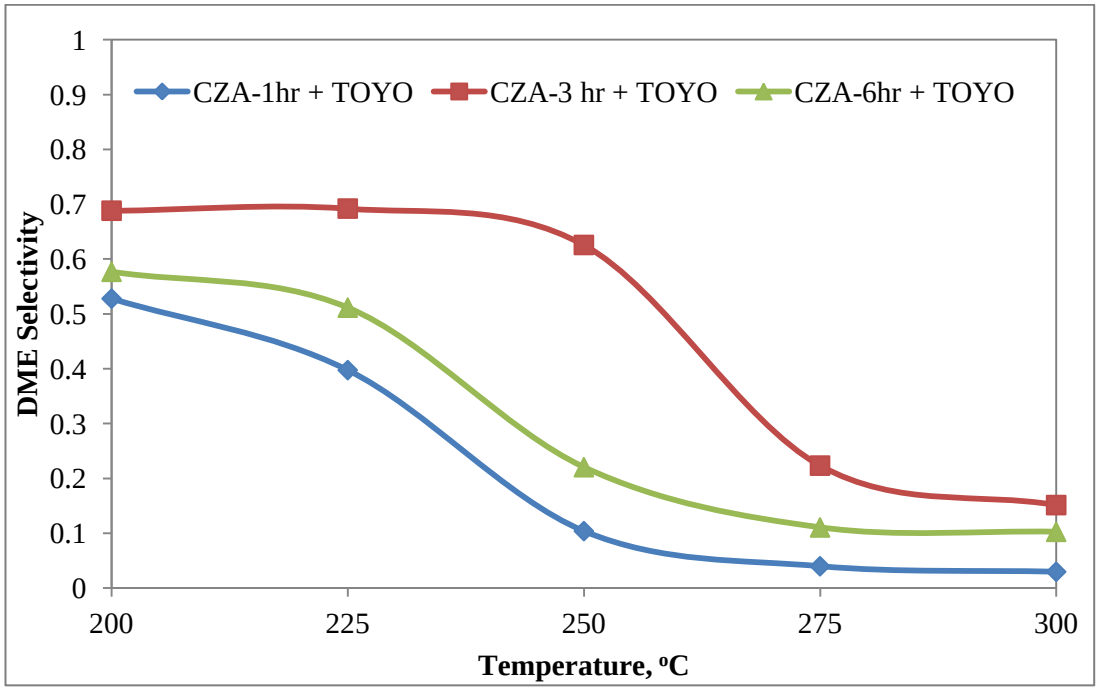

Figure 34. Comparison of DME selectivities of the catalyst mixtures with different aging times; CZA-1hr + TOYO, CZA-3hr + TOYO and CZA-6hr + TOYO (Space time: 0.48 s.gr/cc, catalyst amount: 0.2 gr, feed stream: 50% CO + 50% H_2)

The carbon monoxide conversion of CZA-3hr + TOYO was lower; however, the DME selectivity of this mixture was higher than the rest. This could depend on the particle size and surface area of CZA-3hr. The particle size of CZA-3hr, which was 8.1 nm, was slightly larger than that of CZA-6hr, which was 7.6 nm. However, the surface area of CZA-3hr, which was 57 m^2/g, was larger than that of CZA-6hr, which was 50 m^2/g. The deficiency in particle size of CZA-3hr could be compensated by the surface area.

CZA catalyst was washed with water that at room temperature to remove the undesired and useless ions after the coprecipitation step. It was also investigated that washing with hot water would increase ion exchange efficiency. Therefore, CZA catalyst was washed with hot water [11]. This catalyst was also used and CZA-Hot + TOYO, for consistency CZA is referred as CZA-Cold + TOYO.

The carbon monoxide conversions of the CZA-Cold + TOYO and CZA-Hot + TOYO are presented in Figure 35. The conversion trends were similar for both mixtures. However, the conversion values of CZA-Cold + TOYO were slightly better at higher temperatures.

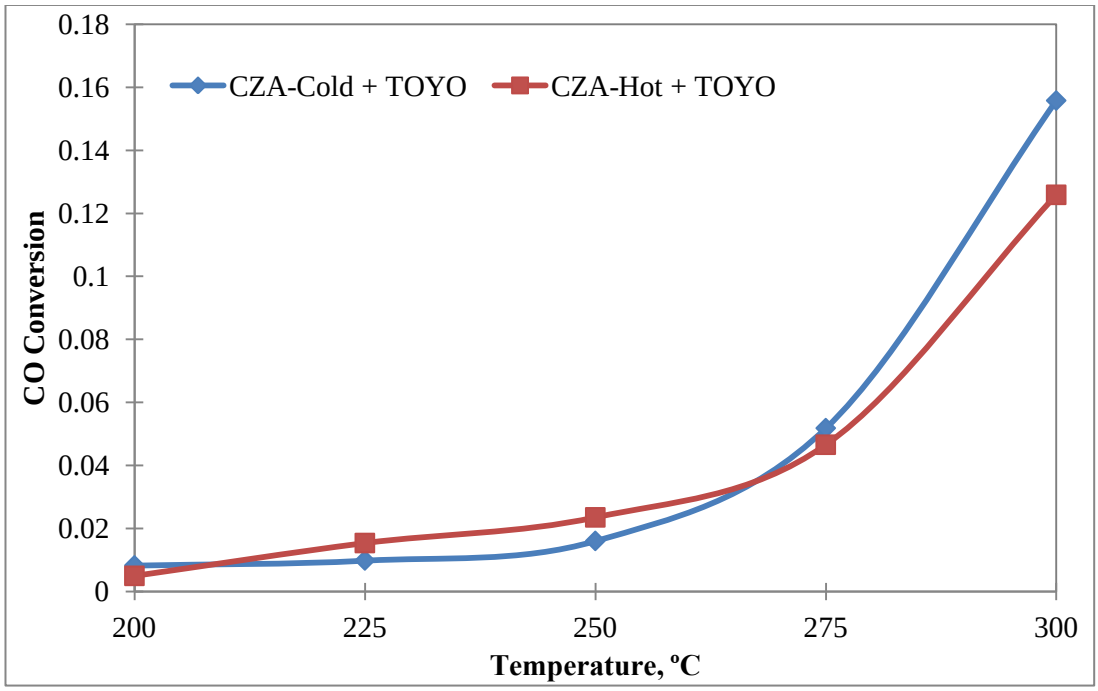

Figure 35. Comparison of carbon monoxide conversions obtained by the washing temperature effect with the mixtures of CZA-Cold and CZA-Hot with γ-Al_2O_3 (TOYO) (Space time: 0.48 s.gr/cc, catalyst amount: 0.2 gr, feed stream: 50% CO + 50% H_2)

Product distribution of the catalyst mixture containing alumina promoter catalyst washed with hot deionized water is given in Figure 36. As it can be seen from the figure, the DME selectivity was 55.4% at 200°C and decreased slowly after 250°C. Carbon dioxide was secondary major product with highest selectivity of 48.1% at 275°C. Methanol and methane were observed after 200°C and small amounts of ethanol and formic acid were produced above 250°C.

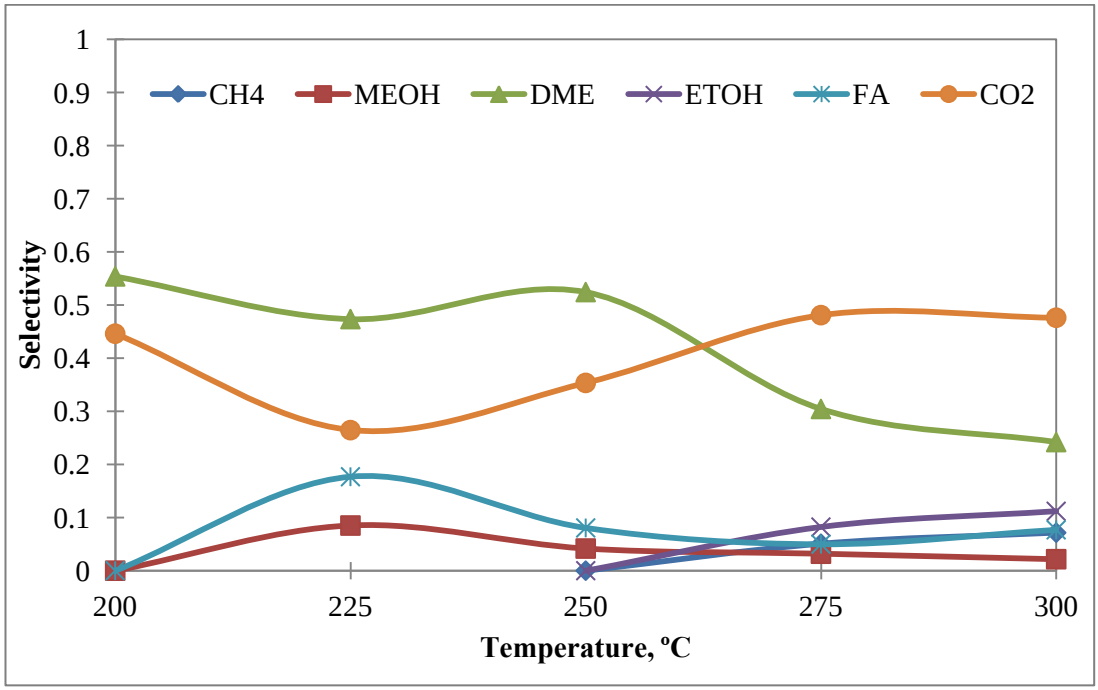

Figure 36. Product distribution obtained with CZA-Hot + TOYO (Space time: 0.48 s.gr/cc, catalyst amount: 0.2 gr, feed stream: 50% CO + 50% H_2)

DME selectivities of CZA-Cold + TOYO and CZA-Hot + TOYO were compared and presented in Figure 37. The DME selectivity of CZA-Cold + TOYO mixture was greater than that of CZA-Hot + TOYO mixture up to 250°C, due to smaller CuO particle size. At higher temperatures, the DME selectivity of CZA-Hot + TOYO was higher due to larger surface area and less amount of byproducts.

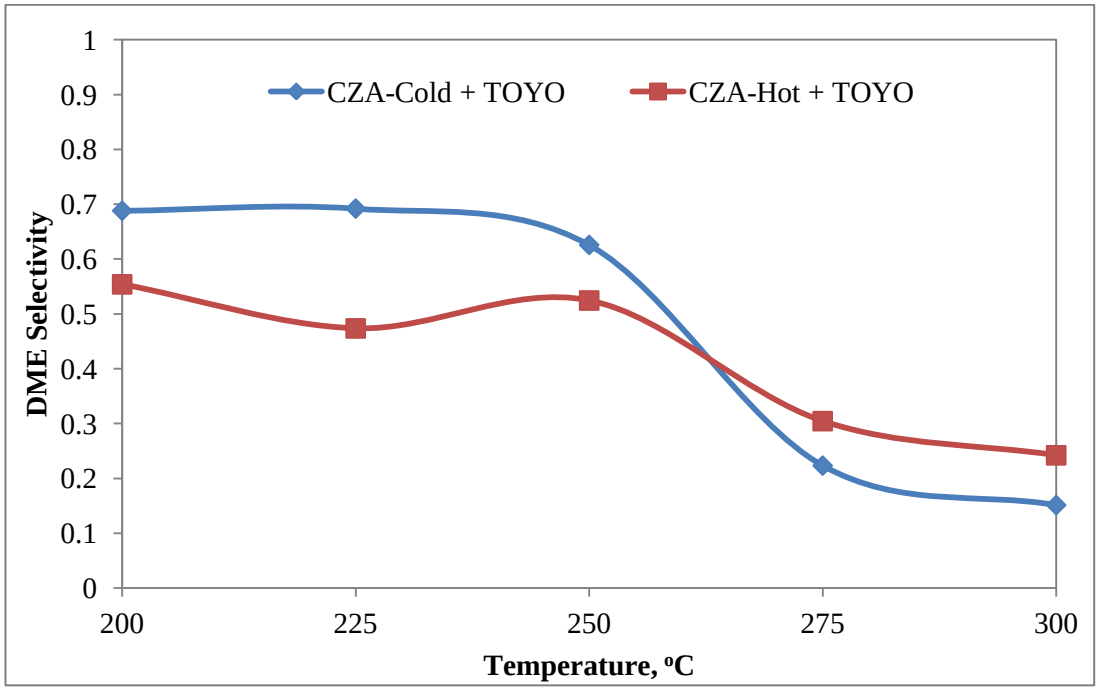

Figure 37. Comparison of DME selectivities of the catalyst mixtures with different washing temperatures; CZA-Cold + TOYO and CZA-Hot + TOYO (Space time: 0.48 s.gr/cc, catalyst amount: 0.2 gr, feed stream: 50% CO + 50% H_2)

8.1.3. Calcination Temperature and Reduction Effect

Effect of calcination temperature and reduction on catalyst performance was also investigated. Calcination temperature is very important for activity of the catalysts. Therefore, calcination was performed at two different temperatures, which were 350°C and 550°C for alumina and zirconia promoted catalysts. The calcination temperature of 350°C was the standard for all catalysts and CZA and CZZr are denoted as "CZA-C350" and "CZZr-C350", respectively. The CZA and CZZr that were calcined at 550°C are denoted as "CZA-C550" and "CZZr-C550", respectively. Reduction effect in which CuO particles were reduced to metallic copper was also investigated for CZA catalyst at different reduction temperatures of 225°C and 250°C. The reduced catalysts are denoted as "CZA-R225" and "CZA-R250" respectively.

Carbon monoxide conversions of CZA-C350 + TOYO and CZA-C550 + TOYO are compared and presented in Figure 38. According to the results, CZA-C350 + TOYO exhibited much better carbon monoxide conversion performance. The reason for poor carbon monoxide conversion of the catalyst calcined at 550^{o}C could be due to larger CuO particle size of 13.0 nm caused by agglomeration of the particles at high calcination temperature. CZA-C550 + TOYO presented a slight increase in carbon monoxide conversion which could be due to smaller surface area as well.

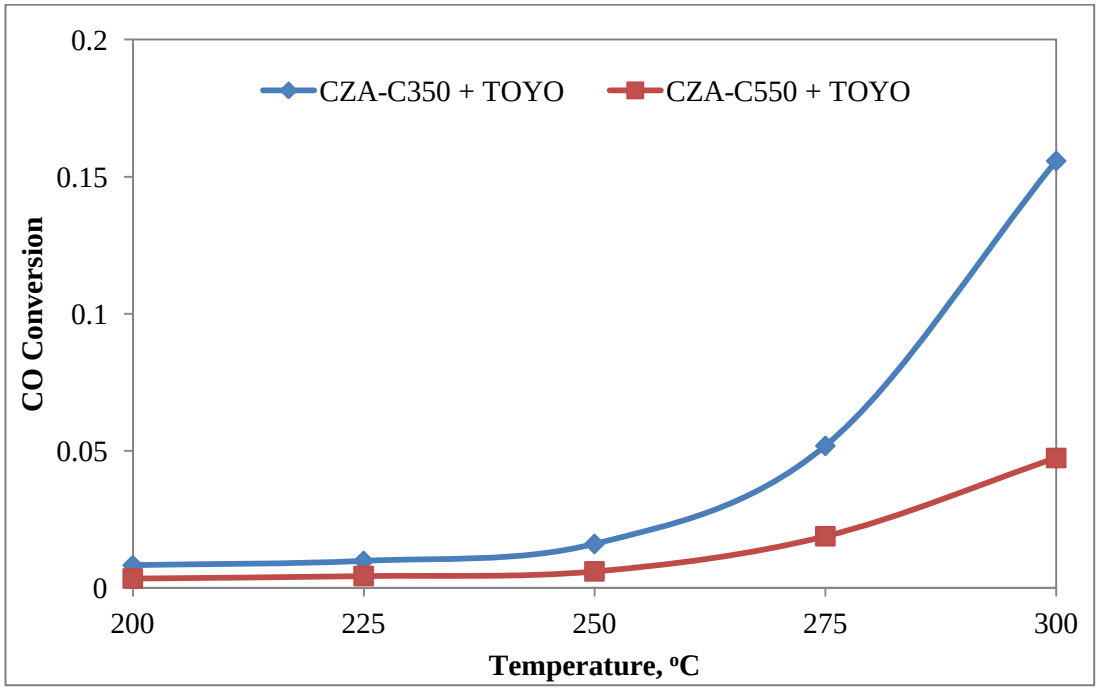

Figure 38. Comparison of carbon monoxide conversions obtained by the calcination temperature effect with the mixtures of CZA-C350 and CZA-C550 with γ-Al_2O_3 (TOYO) (Space time: 0.48 s.gr/cc, catalyst amount: 0.2 gr, feed stream: 50% CO + 50% H_2)

According to the product distribution of CZA-C550 + TOYO given in Figure 39, DME selectivity was quite similar up to 250°C, reached to a maximum value of 59.2%, then decreased to 17.1% at 300°C. Carbon dioxide formation was similar through all temperatures and formed due to water-gas shift and Boudouard reactions up to 250°C. Above 250°C, formation of side products also contributed formation of carbon dioxide. Presence of methanol was not detected for all temperatures.

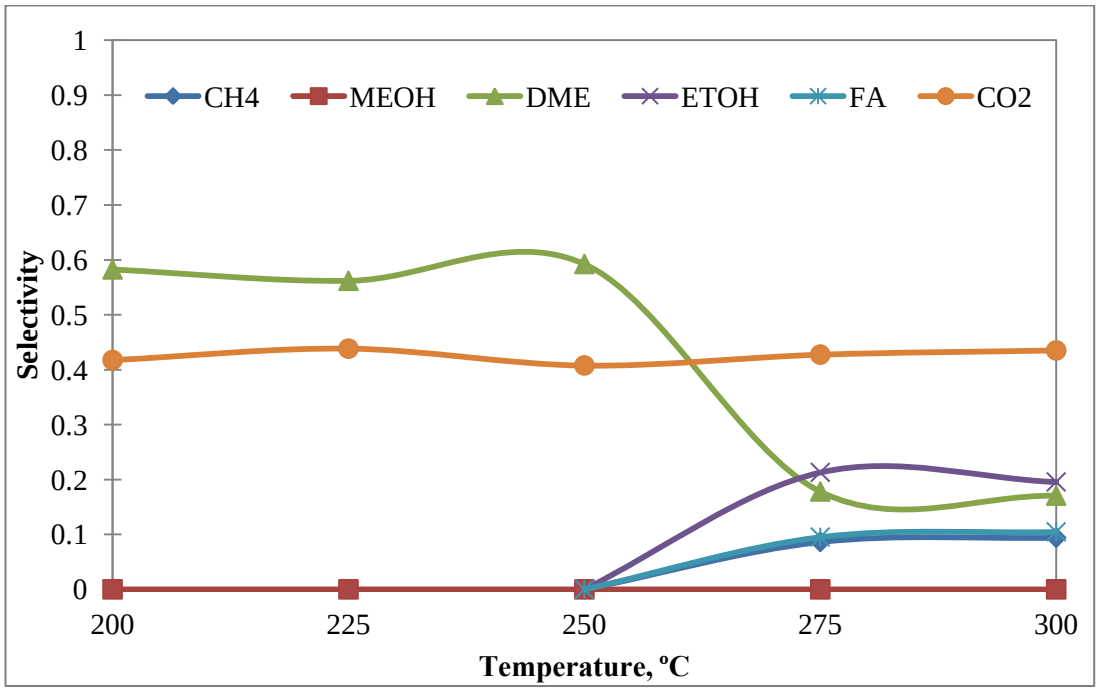

Figure 39. Product distribution obtained with CZA-C550 + TOYO (Space time: 0.48 s.gr/cc, catalyst amount: 0.2 gr, feed stream: 50% CO + 50% H_2)

Comparison of the DME selectivities of CZA-C350 + TOYO and CZA-C550 + TOYO is presented in Figure 40. The selectivity of CZA-C550 + TOYO was slightly lower than that of CZA-C350 + TOYO. This could be attributed to larger particle size and lower surface area of CZA-C550 + TOYO, which was caused by the agglomeration of the particles due to calcination at higher temperature.

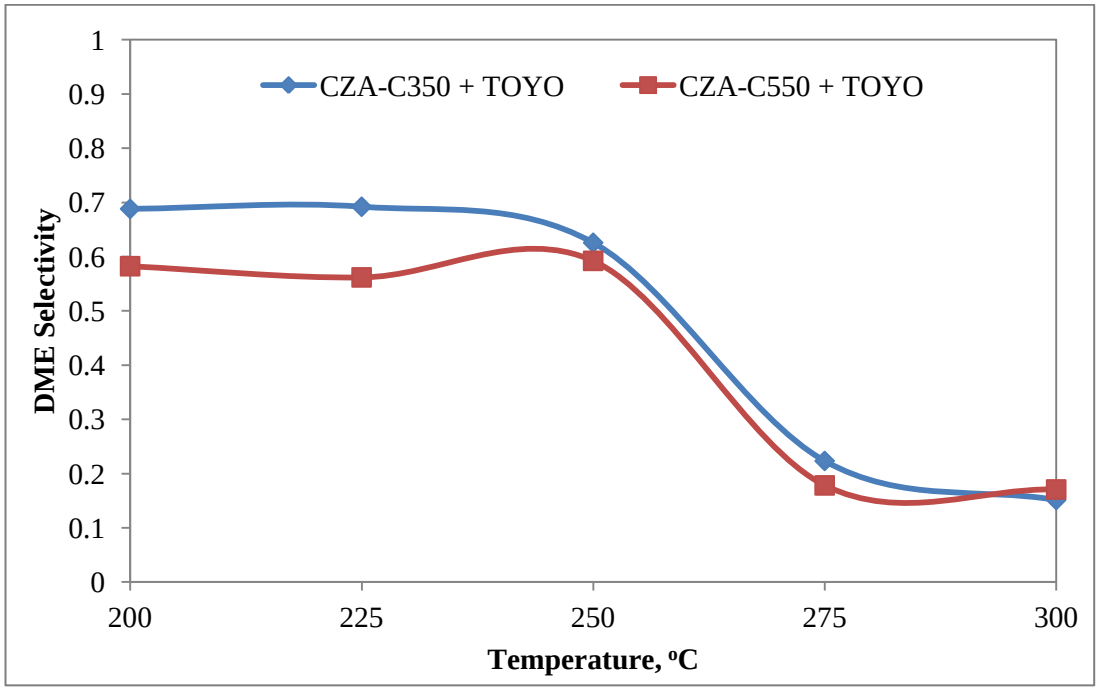

Figure 40. Comparison of DME selectivities of the catalyst mixtures with different calcination temperatures; CZA-C350 + TOYO and CZA-C550 + TOYO (Space time: 0.48 s.gr/cc, catalyst amount: 0.2 gr, feed stream: 50% CO + 50% H_2)

Carbon monoxide conversions of CZZr-C350 + TOYO and CZZr-C550 + TOYO are presented in Figure 41. According to the results, the conversion values of CZZr-C350 + TOYO and CZZr-C550 + TOYO exhibited similar patterns with 9.1% and 10.4% at 300^{o}C, respectively.

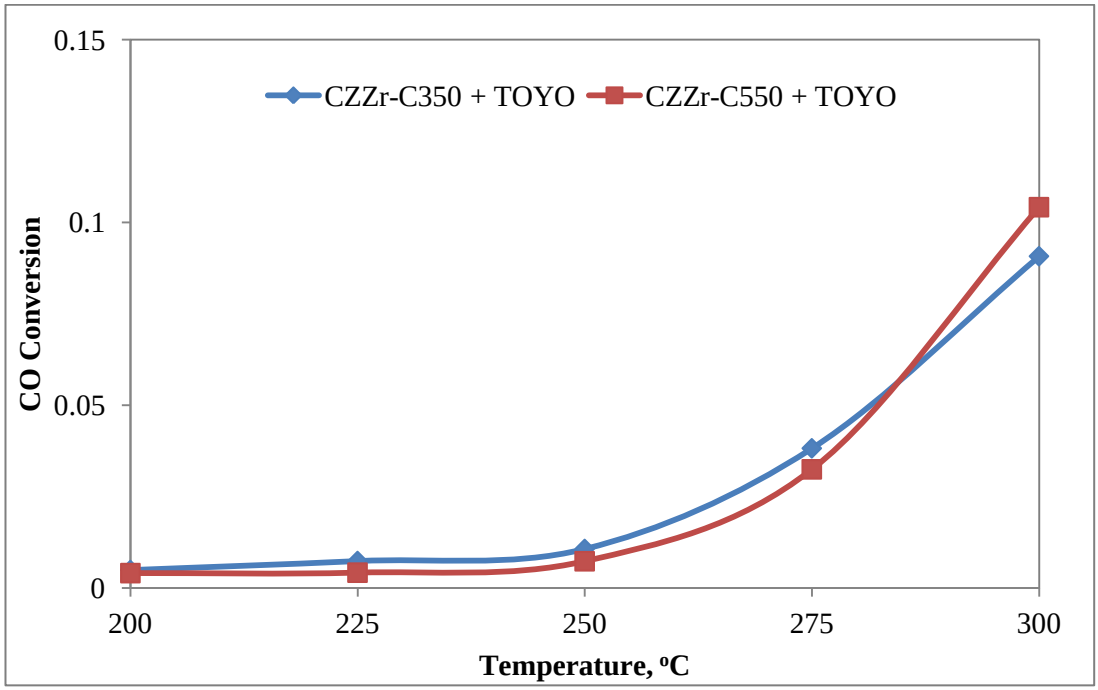

Figure 41. Comparison of carbon monoxide conversions obtained by the calcination temperature effect with the mixtures of CZZr-C350 and CZZr-C550 with γ-Al_2O_3 (TOYO) (Space time: 0.48 s.gr/cc, catalyst amount: 0.2 gr, feed stream: 50% CO + 50% H_2)

The product distribution of CZZr-C550 + TOYO given in Figure 42 and the maximum DME selectivity of 73.9% was achieved at 225°C and decreased sharply. Carbon dioxide was the major secondary product above 200 °C due to in situ formation of byproducts of methane after 225°C and ethanol after 250°C. Insignificant amount of unconverted methanol was detected at 300°C.

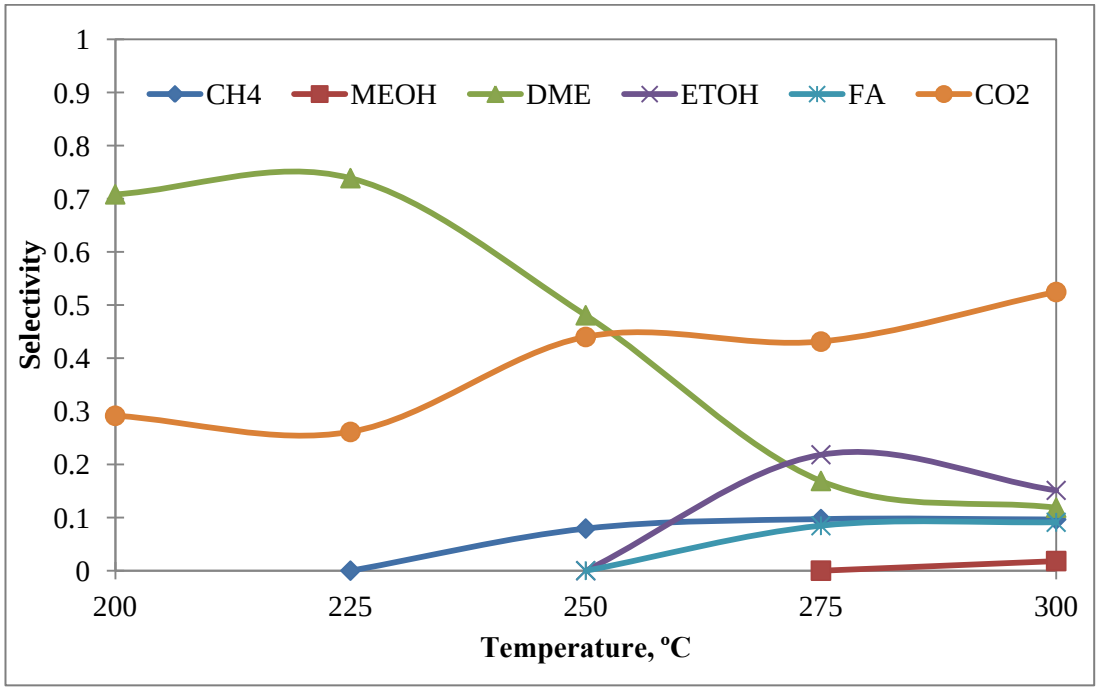

Figure 42. Product distribution obtained with CZZr-C550 + TOYO (Space time: 0.48 s.gr/cc, catalyst amount: 0.2 gr, feed stream: 50% CO + 50% H_2)

DME selectivities of CZZr-C350 + TOYO and are compared and presented in Figure 43. According to the results, CZZr-C550 + TOYO presented higher initial activity between 200 and 250°C than that of CZZr-C350 + TOYO. The DME selectivity of CZZr-C550 + TOYO dropped below that of CZZr-C350 + TOYO above 250 °C. High initial activity could cause coke formation between 200 and 250°C and coking could cause deactivation and followed by the decrease in the activity of CZZr-C550 + TOYO.

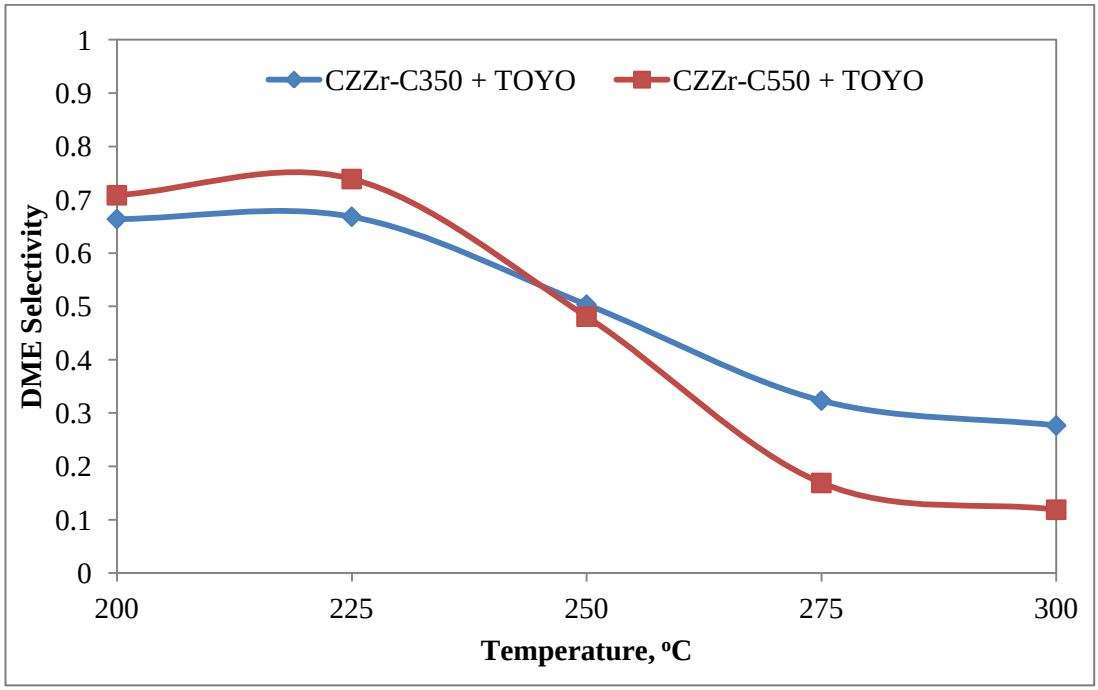

Figure 43. Comparison of DME selectivities of the catalyst mixtures with different calcination temperatures; CZZr-C350 + TOYO and CZZr-C550 + TOYO (Space time: 0.48 s.gr/cc, catalyst amount: 0.2 gr, feed stream: 50% CO + 50% H_2)

Copper, zinc and alumina containing co-precipitated catalyst was reduced with hydrogen at two different temperatures. It was reported that all CuO particles within the catalyst were reduced to metallic copper, completely [11]. The comparison of carbon monoxide conversions for reduced and unreduced catalyst mixtures is given in Figure 44. According to this figure, reduction caused significant decrease in catalyst activity. The lower catalyst activities for the reduced catalyst mixtures could be due to severe decrease in surface areas and increase in particle sizes. For the catalyst reduced at 225°C, copper particle size increased to 18.5 nm and surface area decreased to 22 m^2/g. For the catalyst reduced at 250°C, copper particle size increased to 26.8 nm and surface area decreased to 53 m^2/g. However, the non-reduced catalyst had much smaller copper particle size of 8.1 nm and larger surface area of 57 m^2/g. The maximum conversion achieved for the reduced catalysts mixtures was only 6.8% at 300°C whereas it was 15.6% for the non-reduced catalysts mixtures.

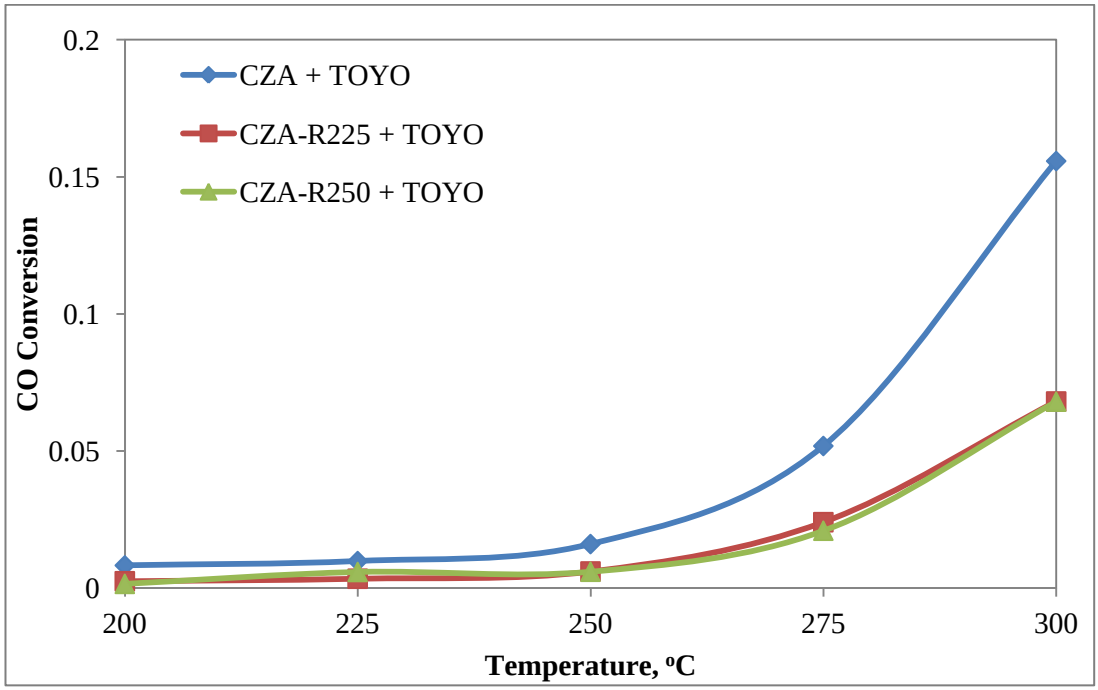

Figure 44. Comparison of carbon monoxide conversions obtained by the reduction effect with the mixtures of CZA, CZA-R225 and CZA-R250 with γ-Al_2O_3 (TOYO) (Space time: 0.48 s.gr/cc, catalyst amount: 0.2 gr, feed stream: 50% CO + 50% H_2)

According to the product distribution of CZA-R225 + TOYO given in Figure 45, DME selectivity was maximum as 75% at 200°C and decreased rapidly at higher temperatures, due to significant amount of ethanol formation between 225 and 250°C with the selectivities of 50% and 46.1%, respectively. Carbon dioxide selectivity also increased above 250 °C and reached 50.5% at 300°C due to in situ formation of byproducts of methane and ethanol. Very low amount of unconverted methanol was detected at 300°C.

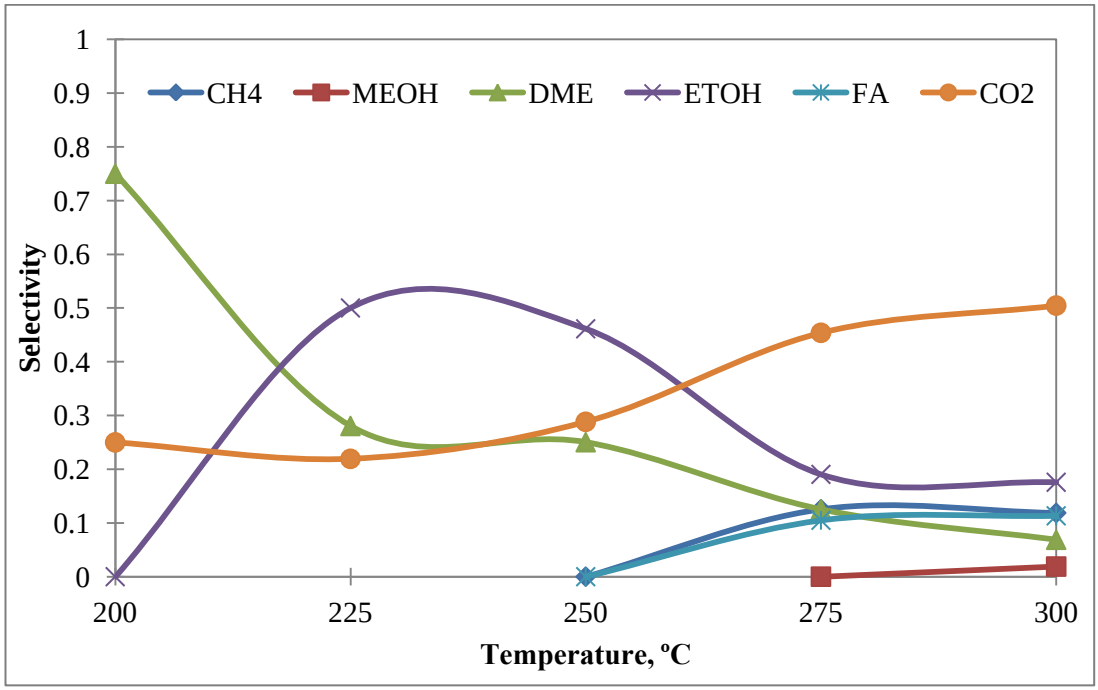

Figure 45. Product distribution obtained with CZA-R225 + TOYO (Space time: 0.48 s.gr/cc, catalyst amount: 0.2 gr, feed stream: 50% CO + 50% H_2)

The product distribution of CZA-R250 + TOYO, given in Figure 46, was very similar to CZA-R225 + TOYO. DME selectivity was maximum as 61.5% at 200^{o}C and a sharp decrease was observed at higher temperatures. Significant amount of ethanol formation was observed at 225^{o}C with the selectivities of 57.3%. Carbon dioxide selectivity also increased above 225 ^{o}C and reached 49.6% at 300^{o}C due to in situ formation of byproducts of methane and ethanol. Very low amount of methanol was present at 300^{o}C.

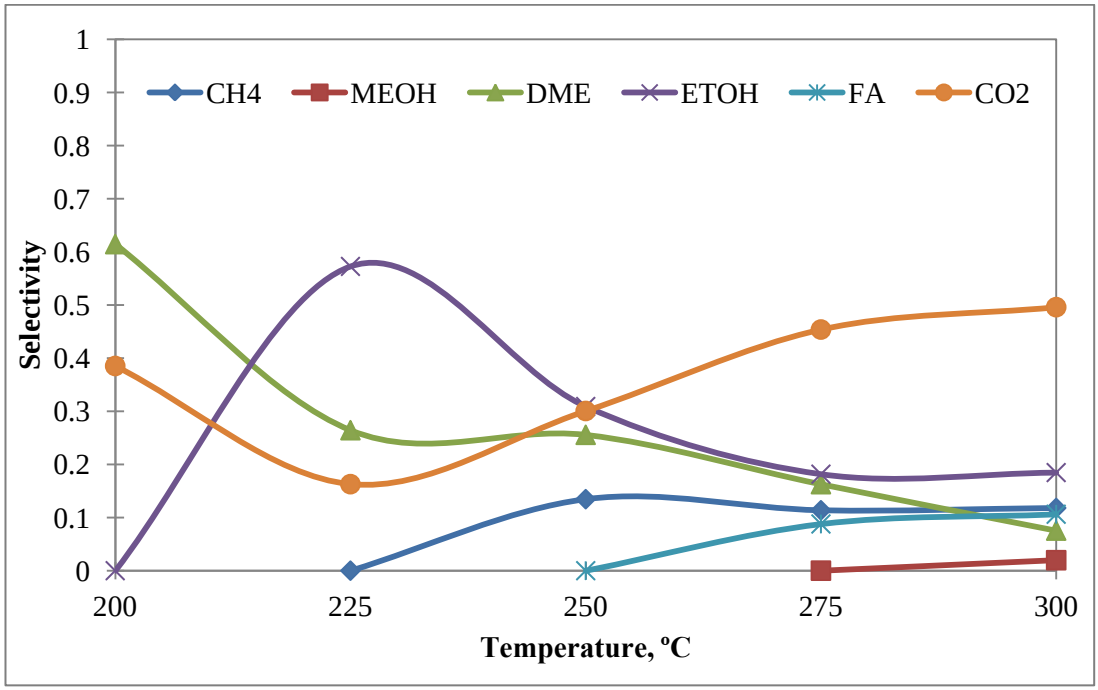

Figure 46. Product distribution obtained with CZA-R250 + TOYO (Space time: 0.48 s.gr/cc, catalyst amount: 0.2 gr, feed stream: 50% CO + 50% H_2)

DME selectivities of CZA + TOYO, CZA-R225 + TOYO and CZA-R250 + TOYO are compared and presented in Figure 47. According to the results, both CZA-R225 + TOYO and CZA-R250 + TOYO exhibited similar DME selectivity patterns and both of them were extremely lower than CZA + TOYO. This result could be due to significant decrease in surface areas and increase in particle sizes. The particle size and the surface area of CZA-R225 were 18.5 nm and 22 m^2/g, respectively, while, the particle size and the surface area of CZA-R225 were 26.8 nm and 53 m^2/g, respectively. The particle size and the surface area of CZA were, on the other hand, 8.1 nm and 57 m^2/g, respectively.

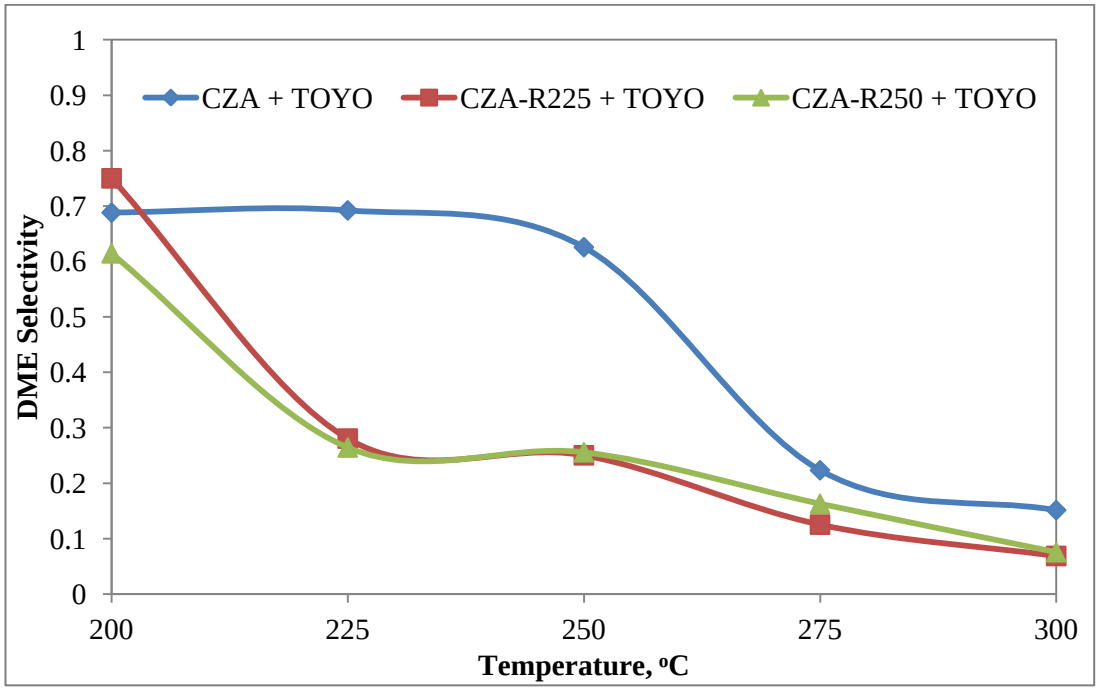

Figure 47. Comparison of DME selectivities of the catalyst mixtures with different reduction temperatures CZA + TOYO, CZA-R225 + TOYO and CZA-R250 + TOYO (Space time: 0.48 s.gr/cc, catalyst amount: 0.2 gr, feed stream: 50% CO + 50% H_2)

In this part, effects of different parameters, such as type of promoter, synthesis conditions, calcination and reduction temperatures, on the activities coprecipitated methanol synthesis catalyst were investigated, when they are mixed with γ-Al_2O_3 as the solid acid catalyst. It was observed that promoter type enhanced the catalytic activity and among them zirconia was better as compared to alumina and ceria. Aging time of the coprecipitated catalyst was also effective, such that 3 hours of aging was the best as far as the DME production was concerned. Washing with hot water decreased the catalytic activity. Calcination at high temperature resulted in activity decrease for alumina promoted catalyst and initial higher activity for zirconia promoted catalyst. Pre-reduction of the CuO had adverse effect on catalyst performance. According to these results; it was decided to select copper-zinc-zirconia catalyst for the following studies.

8.2. ACTIVITY RESULTS OBTAINED WITH THE BIFUNCTIONAL CATALYST MIXTURES COMPOSED OF METHANOL SYNTHESIS CATALYSTS AND MESOPOROUS ALUMINA

In this part, commercial methanol synthesis catalyst (MSC) and copper-zinc-zirconia coprecipitation catalyst (CZZr) were used for the methanol synthesis function of the bifunctional catalyst mixture. For the methanol dehydration function, mesoporous alumina (MA) and silicotungstic acid impregnated mesoporous alumina (STA@MA) were used as solid acid catalysts. The bifunctional catalysts were prepared by physical mixture of 0.1 g of methanol synthesis and 0.1 g of solid catalyst. The bifunctional catalysts with catalyst weight ratio of 1:1 were abbreviated as follows: "MSC + MA", "CZZr + MA", "MSC + STA@MA" and "CZZr + STA@MA". Additional experiments were also performed with a bifunctional catalyst mixture having a catalyst weight ratio of 1:2, that contained 0.1 g of methanol synthesis catalyst and 0.2 g of STA@MA. These bifunctional catalyst mixtures were abbreviated as "MSC + STA@MA (1:2)" and "CZZr + STA@MA (1:2)". The operation conditions were also valid in this part of the study, with a pressure of 50 bar and a temperature range of 200 to 300^{o}C. The feed flow rate was 25 cc/min with 50% CO and 50 % H_2. In Table 13, the studies performed with mesoporous alumina were summarized.

Table 13. The summary of the studies performed with mesoporous alumina

Catalyst Mixture	**Methanol Synthesis Catalyst Weight, g**	**Methanol Dehydration Catalyst Weight, g**
MSC	0.1	-
CZZr	0.1	-
MSC + MA	0.1	0.1
CZZr + MA	0.1	0.1
MSC + STA@MA	0.1	0.1
CZZr + STA@MA	0.1	0.1
MSC + STA@MA (1:2)	0.1	0.2
CZZr + STA@MA (1:2)	0.1	0.2

8.2.1. Activity Results of Bifunctional Catalysts with Mesoporous Alumina; MSC + MA and CZZr + MA

The comparison of the carbon monoxide conversion obtained with the bifunctional catalysts involving methanol synthesis catalysts; MSC and CZZr, which were physically mixed with mesoporous alumina is given in Figure 48. As seen in this figure, carbon monoxide conversion values obtained with MSC + MA and CZZr + MA increased with temperature and reached to 36.6% and 27.2% at 300^{o}C, respectively.

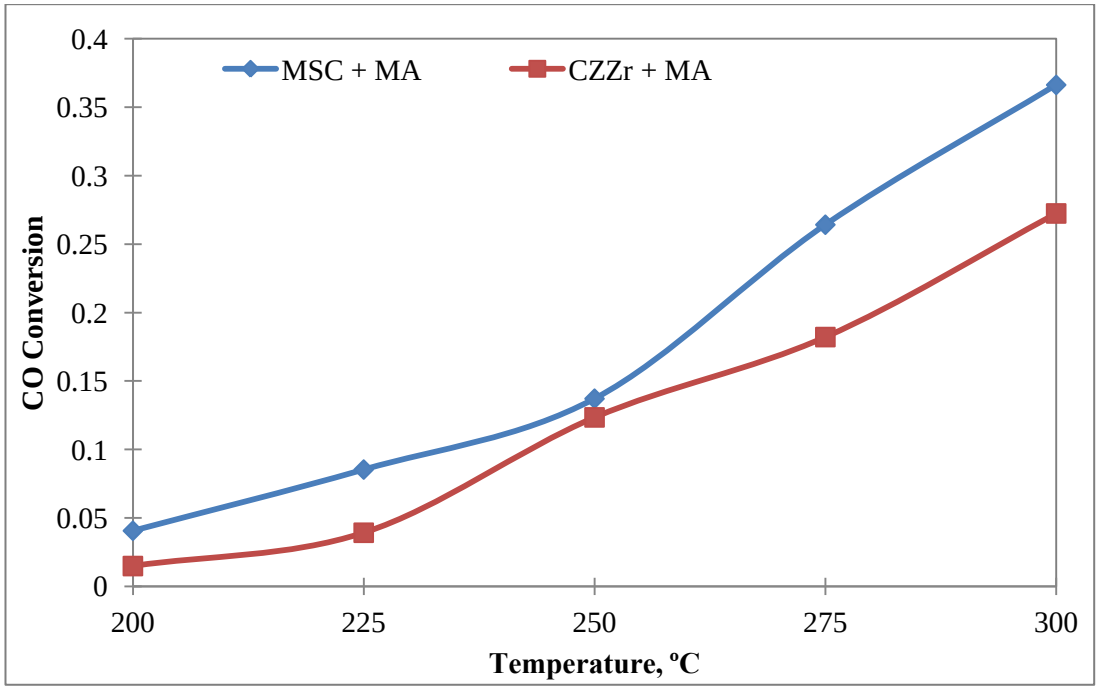

Figure 48. Comparison of carbon monoxide conversions obtained with the mixtures of MSC and CZZr with MA (Space time: 0.48 s.gr/cc, catalyst amount: 0.2 gr, feed stream: 50% CO + 50% H_2)

Product distribution obtained with MSC + MA is presented in Figure 49. According to the results, dehydration of methanol to DME was very low at 200^{o}C with methanol selectivity of 80.1% and DME selectivity of 7.8%. The poor methanol dehydration activity of mesoporous alumina could be attributed to very low Lewis and Brønsted acidic strengths of this material, which were not sufficient enough for dehydration reaction. Brønsted acidic strengths are mostly effective at low temperatures. Since Brønsted acidity of this material is very low, the produced methanol could not be dehydrated to DME effectively at low temperatures. Therefore, the amount of unconverted methanol was very high. However, as the temperature increased, methanol selectivity decreased followed by increase in DME selectivity, which means that at higher temperatures the synthesized methanol was dehydrated more to DME. At 300^{o}C, methanol and DME selectivities were 13.3% and 55.8%, respectively. The increase in DME selectivity could be due to enhanced rate of methanol synthesis reaction and increased catalytic activity of mesoporous alumina for methanol dehydration reaction at higher temperatures [44]. In addition, Lewis acid-base pairs were responsible for dehydration of methanol to DME at higher temperatures. The formation of carbon dioxide was mostly due to water-gas shift reaction, since total byproduct formation was only 2.2% at 300^{o}C.

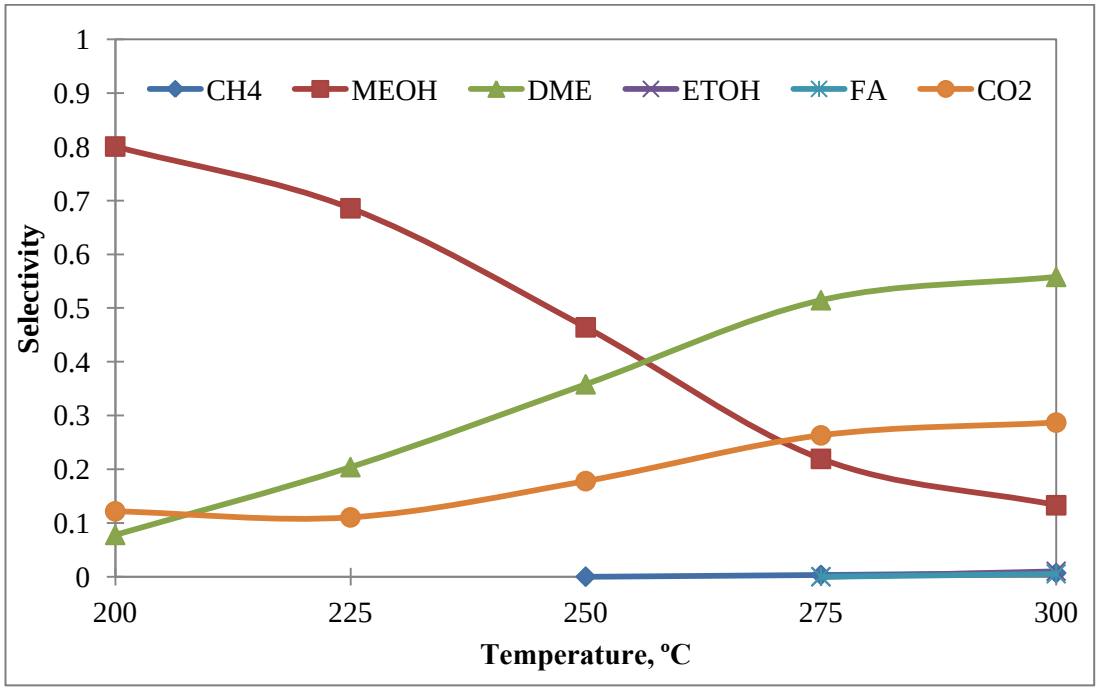

Figure 49. Product distribution obtained with MSC + MA (Space time: 0.48 s.gr/cc, catalyst amount: 0.2 gr, feed stream: 50% CO + 50% H_2)

According to the product distribution obtained with CZZr + MA, which is given in Figure 50, a similar behavior was observed. Initial performance of this catalyst mixture was better than that of MSC + MA, since the selectivities of methanol and DME were 57.3% and 20.5%, respectively at 200^{o}C and reached 16.9% and 52.4%, respectively at 300^{o}C. DME formation was enhanced at higher temperatures due to increased catalytic dehydration activity of mesoporous alumina. Carbon dioxide was considered to be produced mainly via water-gas shift reaction, since very low amounts of byproducts were observed.

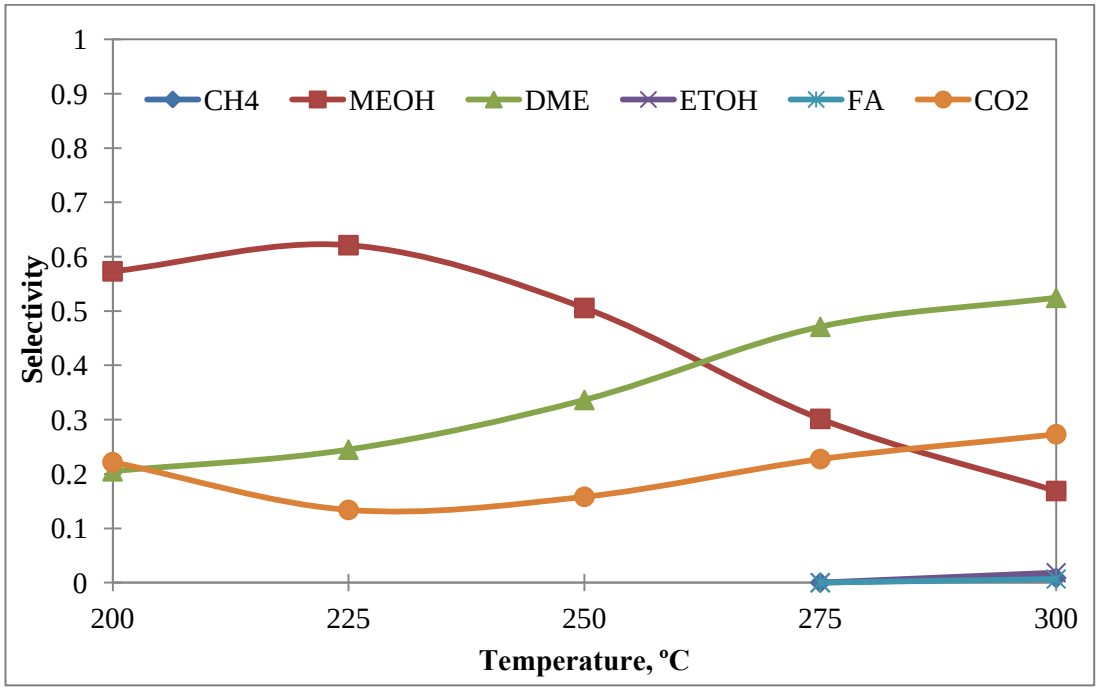

Figure 50. Product distribution obtained with CZZr + MA (Space time: 0.48 s.gr/cc, catalyst amount: 0.2 gr, feed stream: 50% CO + 50% H_2)

In Figure 51, the DME selectivities of MSC + MA and CZZr + MA were compared. The activity of CZZr + MA was higher initially which could be due to higher surface area and then decreased possibly due to coke formation caused by initial high activity and formation of larger copper particles. Copper and copper oxide particle sizes of the used catalysts were calculated by Scherrer's equation by using their wide angle XRD spectra and the results are presented in Table 15 in Section 8.4. Copper and copper oxide particle sizes of the used MSC + MA increased to 4.9 nm and 9.4 nm, respectively, while copper and copper oxide particle sizes of the used CZZr + MA increased to 6.9 nm and 16.9 nm, respectively.

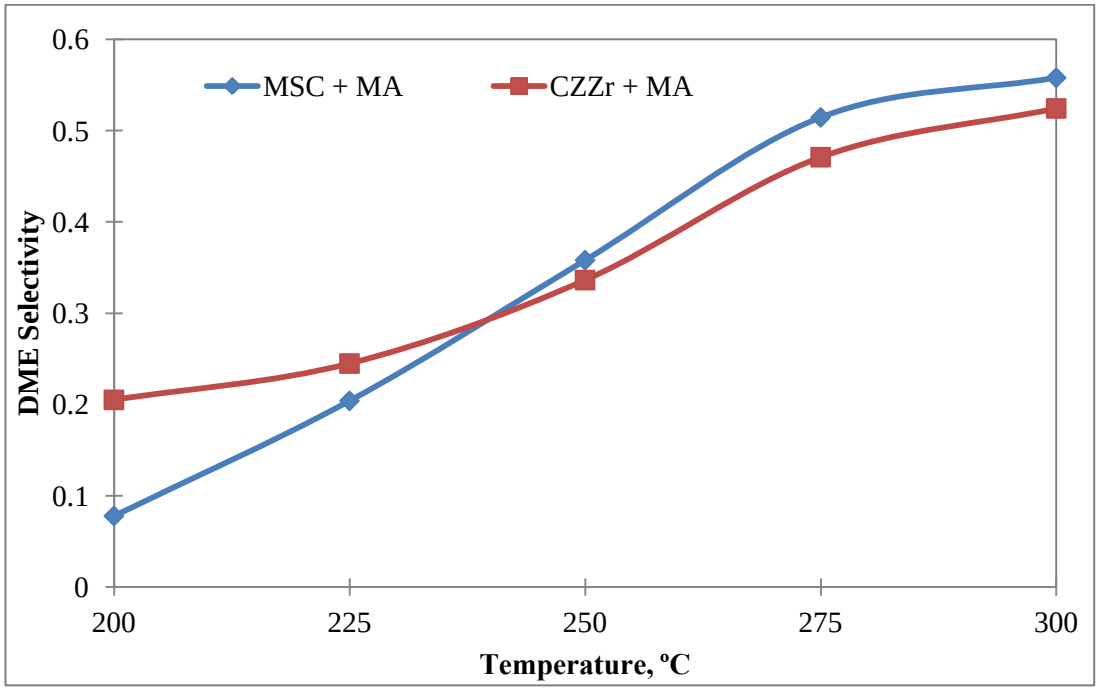

Figure 51. Comparison of DME selectivities of the catalyst mixtures with MSC + MA and CZZr + MA (Space time: 0.48 s.gr/cc, catalyst amount: 0.2 gr, feed stream: 50% CO + 50% H_2)

A comparative study was performed by using only 0.1 g of methanol synthesis catalyst, MSC or CZZr (without the dehydration catalyst) to observe the effect of addition of the solid acid catalyst to the catalyst bed on carbon monoxide conversion. As seen in Figure 52, the carbon monoxide conversions of MSC and CZZr reached 13.1% and 10.9% at 300^{o}C, respectively. On the other hand, introduction of solid acid catalyst, mesoporous alumina in this case, enhanced the carbon monoxide conversions significantly due to the synergetic effect obtained by the cooperation of methanol synthesis, dehydration and water-gas shift reactions. Therefore, the carbon monoxide conversions of MSC + MA and CZZr + MA reached 36.6% and 27.2% at 300^{o}C, respectively.

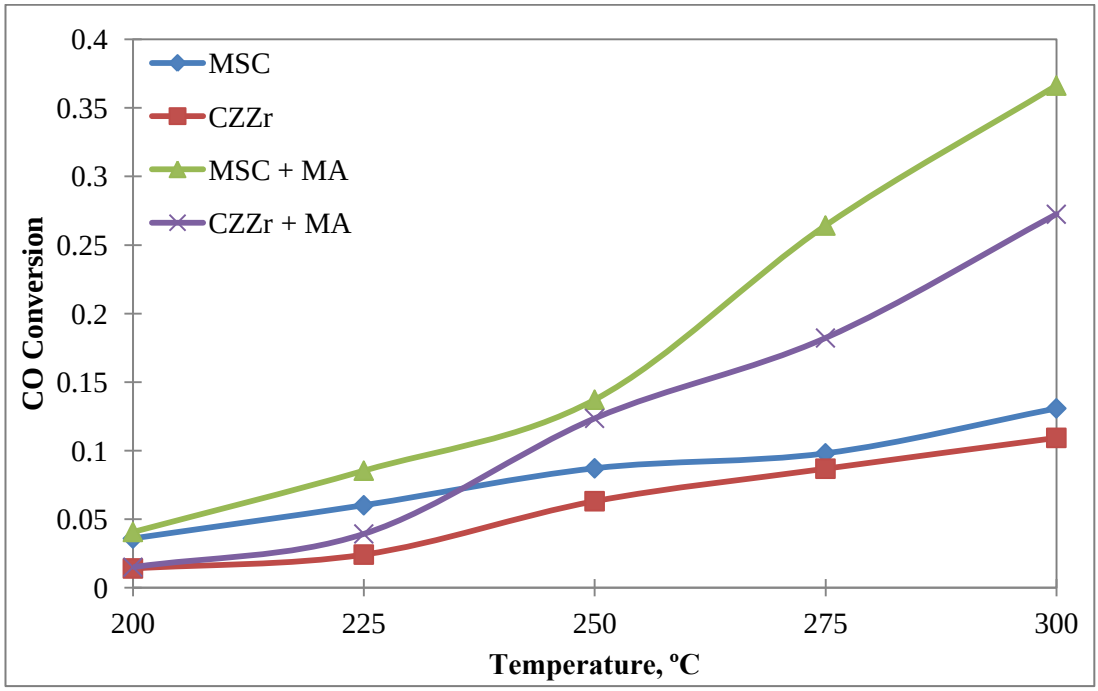

Figure 52. Comparison of carbon monoxide conversions obtained with MSC, CZZr, MSC + MA and CZZr + MA (Feed stream: 50% CO + 50% H_2)

8.2.2. Activity Results of Bifunctional Catalysts with STA Impregnated Mesoporous Alumina; MSC + STA@MA and CZZr + STA@MA

In the previous part, it was observed that the acid strength of Brønsted and Lewis acid sites of mesoporous alumina was not sufficient for methanol dehydration activity. Some literature studies indicated that silicotungstic acid impregnation on such catalyst supports enhanced the dehydration performance of the catalysts [51, 55, 62]. Therefore, STA was impregnated on MA to enhance the acidities correspond to Lewis acidity, as supported by DRIFTS spectrum. Similar to the results with MA, the carbon monoxide conversion of MSC + STA@MA was again higher than that of CZZr + STA@MA as seen in Figure 53. The carbon monoxide conversions were 49.4% and 31.0% for MSC + STA@MA and CZZr + STA@MA, respectively at 300^{o}C.

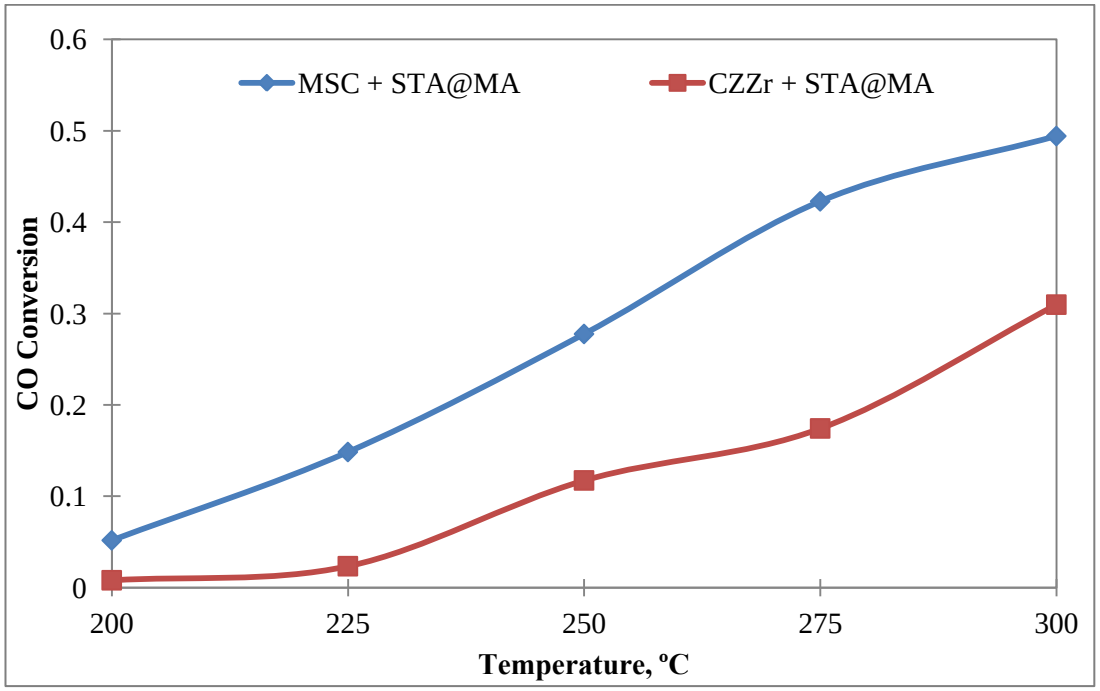

Figure 53. Comparison of carbon monoxide conversions obtained with the mixtures of MSC and CZZr with STA@MA (Space time: 0.48 s.gr/cc, catalyst amount: 0.2 gr, feed stream: 50% CO + 50% H_2)

In Figure 54, product distribution obtained with MSC + STA@MA is given. It is seen that STA impregnation enhanced the activity of mesoporous alumina, since the methanol selectivity was lower with 52.9% and DME selectivity was higher with 31.3% at 200^{o}C as compared to MSC + MA. Higher activity of STA@MA could be due to increase in the strength of Lewis acid sites. DME selectivity increased to 60.8% at 300^{o}C due to increased catalytic activity of mesoporous alumina. At higher temperatures, Lewis acid-base pair would also contribute to methanol dehydration reaction.

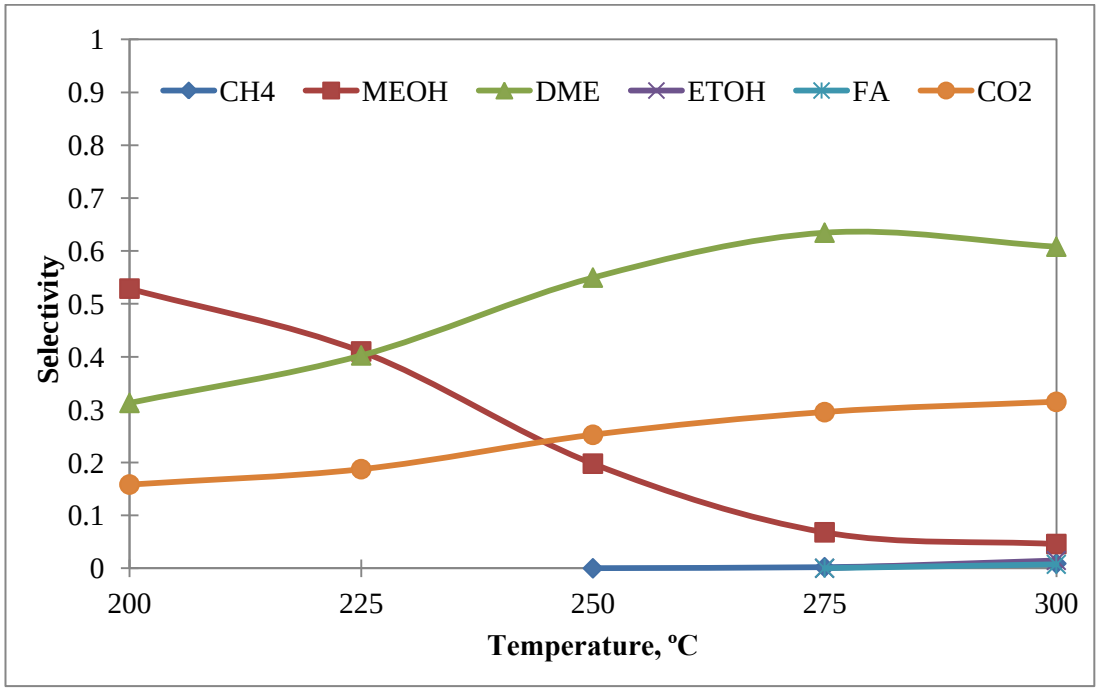

Figure 54. Product distribution obtained with MSC + STA@MA (Space time: 0.48 s.gr/cc, catalyst amount: 0.2 gr, feed stream: 50% CO + 50% H_2)

According to the product distribution obtained with CZZr + STA@MA given in Figure 55, due to enhancing effect of STA on dehydration activity, methanol selectivity dropped to 15.0% and DME selectivity increased to 52.8% at 200°C as compared to CZZr + MA. The selectivities for methanol and DME were 5.1% and 56.6%, respectively at 300°C. The DME formation did not change significantly over the temperature range due to increase in carbon dioxide selectivity. Carbon dioxide was the major secondary product with 33.0% of selectivity at 300°C.

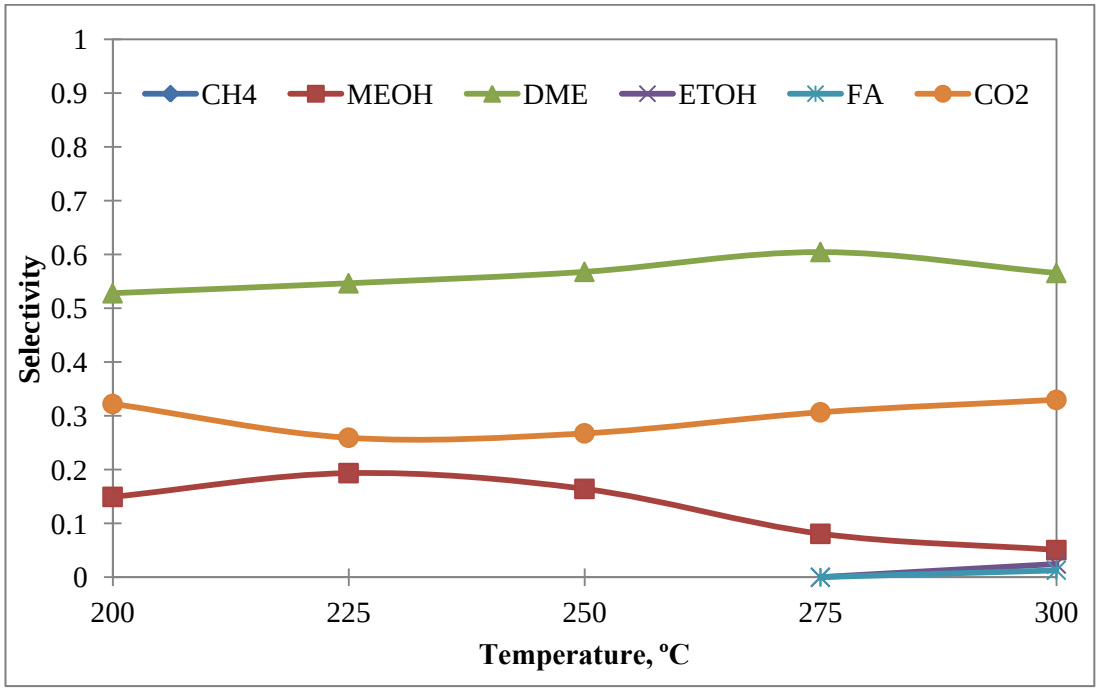

Figure 55. Product distribution obtained with CZZr + STA@MA (Space time: 0.48 s.gr/cc, catalyst amount: 0.2 gr, feed stream: 50% CO + 50% H_2)

In Figure 56, the DME selectivities of MSC + STA@MA and CZZr + STA@MA were compared. A similar behavior was also observed as obtained with MSC + MA and CZZr + MA. The initial activity of CZZr + STA@MA was higher than that of MSC + STA@MA and then decreased at higher temperatures. This could be due to the high initial activity of CZZr + STA@MA at low temperatures. The high initial activity could cause coke formation. Presence of coke could prevent further increase of the activity at higher temperatures.

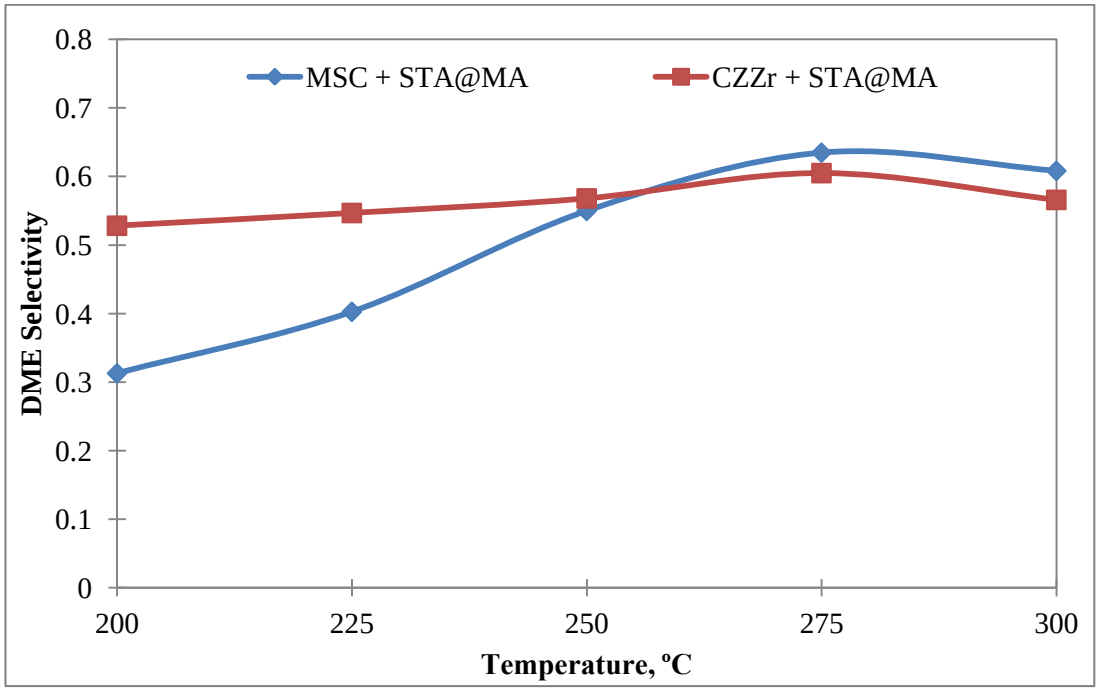

Figure 56. Comparison of DME selectivities of the catalyst mixtures with MSC + STA@MA and CZZr + STA@MA (Space time: 0.48 s.gr/cc, catalyst amount: 0.2 gr, feed stream: 50% CO + 50% H_2)

8.2.3. Activity Results of Bifunctional Catalysts with STA@MA with Different Catalyst Weight Ratio; MSC + STA@MA (1:2) and CZZr + STA@MA (1:2)

In literature, it is stated that when the solid acid catalysts are very active for dehydration of methanol to DME, carbon monoxide conversion becomes independent of acidic strength of the solid acid catalyst which only affects the selectivity of DME. In this case, the methanol synthesis rate is lower and methanol synthesis step becomes the rate limiting step [20, 31, 39, 43]. However, when the acidic strength of the solid acid catalyst is not strong enough for dehydration of the formed methanol to DME, then, methanol dehydration reaction becomes the rate limiting step. The acidic strength of the solid acid catalyst, in this case, has influence on CO conversion and the DME selectivity which could be improved by increasing either the acidic strength or the concentration of the solid acid catalyst [21, 31, 43].

It was seen in the previous parts that the acidic strength of mesoporous alumina was not high enough for efficient dehydration process which became the rate limiting step. Therefore, firstly the acidic strength of the catalyst was enhanced by STA impregnation, now in this part, the content of STA@MA increased to twice of that of methanol synthesis catalyst.

In Figure 57, the carbon monoxide conversions of MSC + STA@MA (1:2), and CZZr + STA@MA (1:2) are compared. The catalytic activity of MSC + STA@MA (1:2) was better as compared to CZZr + STA@MA (1:2) due to smaller CuO particles of the fresh catalyst. CuO particles were 4.6 nm and 5.0 nm for MSC and CZZr, respectively. For both catalysts, carbon monoxide conversions increased with temperature due to enhanced catalytic activity at higher temperatures and reached to 47.1% and 32.6%, respectively at 300^{o}C.

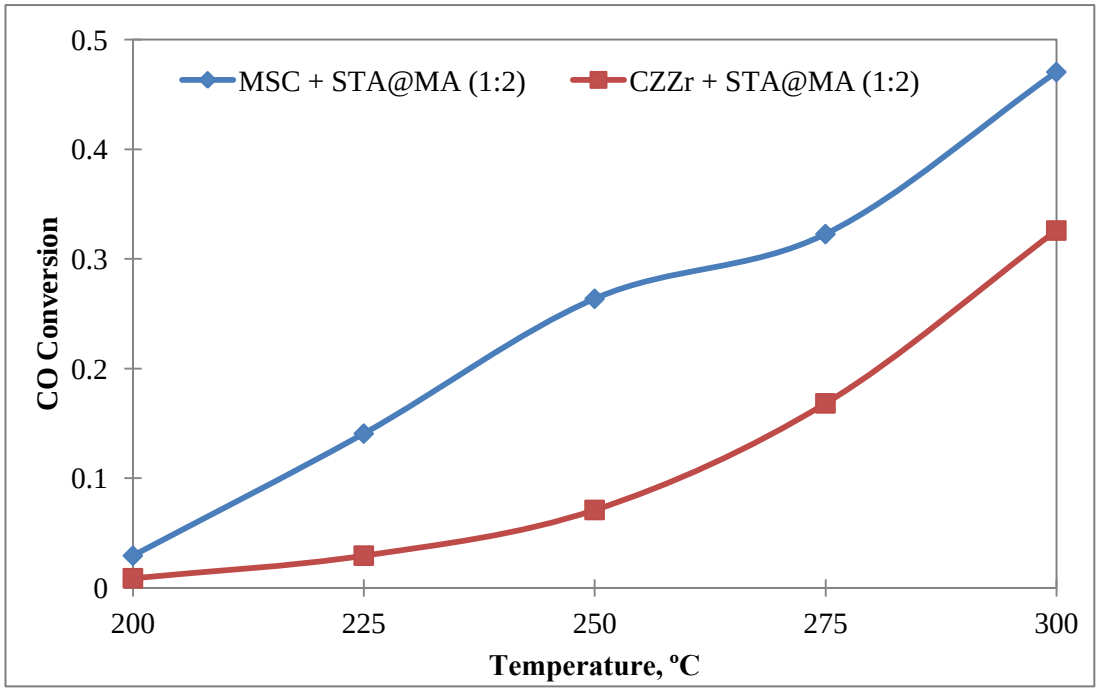

Figure 57. Comparison of carbon monoxide conversions obtained with the mixtures of MSC and CZZr with STA@MA with weight ratio of (1:2) (Space time: 0.72 s.gr/cc, catalyst amount: 0.3 gr, feed stream: 50% CO + 50% H_2)

In Figure 58, the product distribution of MSC + STA@MA (1:2) is given. Since the amount of the methanol dehydration catalyst that is STA@MA, was increased, methanol selectivity dropped to 34.2% and DME selectivity increased to 42.0% at 200°C. Very smooth increase in DME selectivity was observed with a maximum value of 61.1% at 275°C which slightly decreased due to slight increase in carbon dioxide and byproduct formation. Carbon dioxide was produced mostly due to water-gas shift reaction. As seen from the results, carbon dioxide formation was also enhanced parallel with DME formation [12, 21]. Very low amounts of byproducts were produced, methane was observed after 250°C, ethanol and formic acid were formed after 275°C.

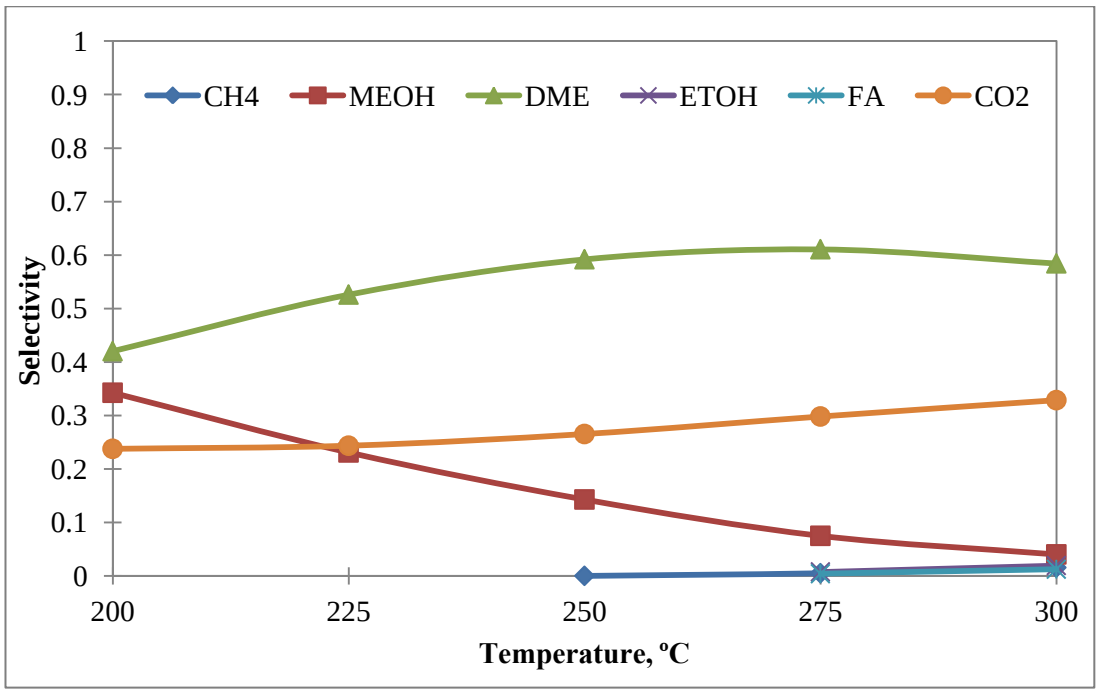

Figure 58. Product distribution obtained with MSC + STA@MA (1:2) (Space time: 0.72 s.gr/cc, catalyst amount: 0.3 gr, feed stream: 50% CO + 50% H_2)

According the product distribution of CZZr + STA@MA (1:2) given in Figure 59, this bifunctional catalyst was almost capable of dehydration of methanol to DME. CO conversion of CZZr was presented previously in Figure 52 and it was lower than that of MSC. This means that lower amount of methanol was produced by CZZr as compared to MSC itself. Therefore, as 0.1 g of CZZr was mixed with 0.2 g of STA@MA, the almost all of the produced methanol was converted to DME. Therefore, methanol was not present at 200°C and observed in very low amounts above 200°C since the activity increased with temperature. DME selectivity increased in slight amounts with temperature with a maximum value of 64.9% at 275°C.

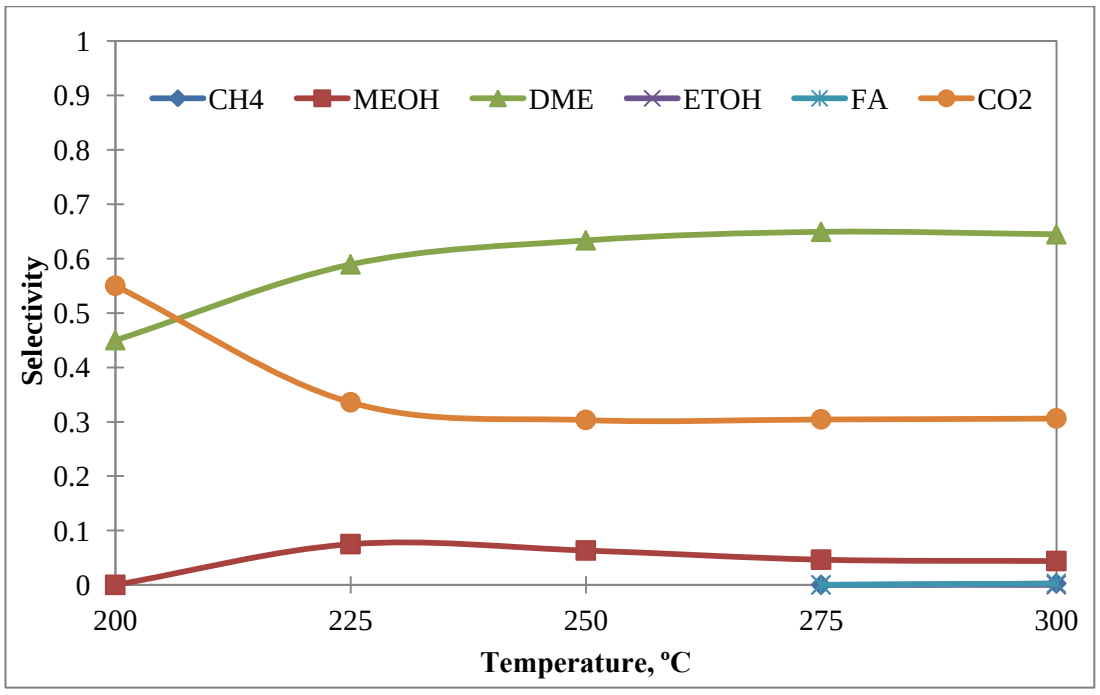

Figure 59. Product distribution obtained with CZZr + STA@MA (1:2) (Space time: 0.72 s.gr/cc, catalyst amount: 0.3 gr, feed stream: 50% CO + 50% H_2)

DME selectivities of MSC + STA@MA (1:2) and CZZr + STA@MA (1:2) were compared in Figure 60. The DME selectivities of MSC + MA (1:2) were slightly lower than that of CZZr + STA@MA (1:2). The particle sizes of Cu^o clusters after reaction of MSC + STA@MA (1:2) and CZZr + STA@MA (1:2) were found as 11.3 nm and 13.0 nm, respectively, as given in Table 15 in Section 8.4. However, lower

activity of MSC + STA@MA (1:2) could be due to catalyst deactivation caused by coke formation.

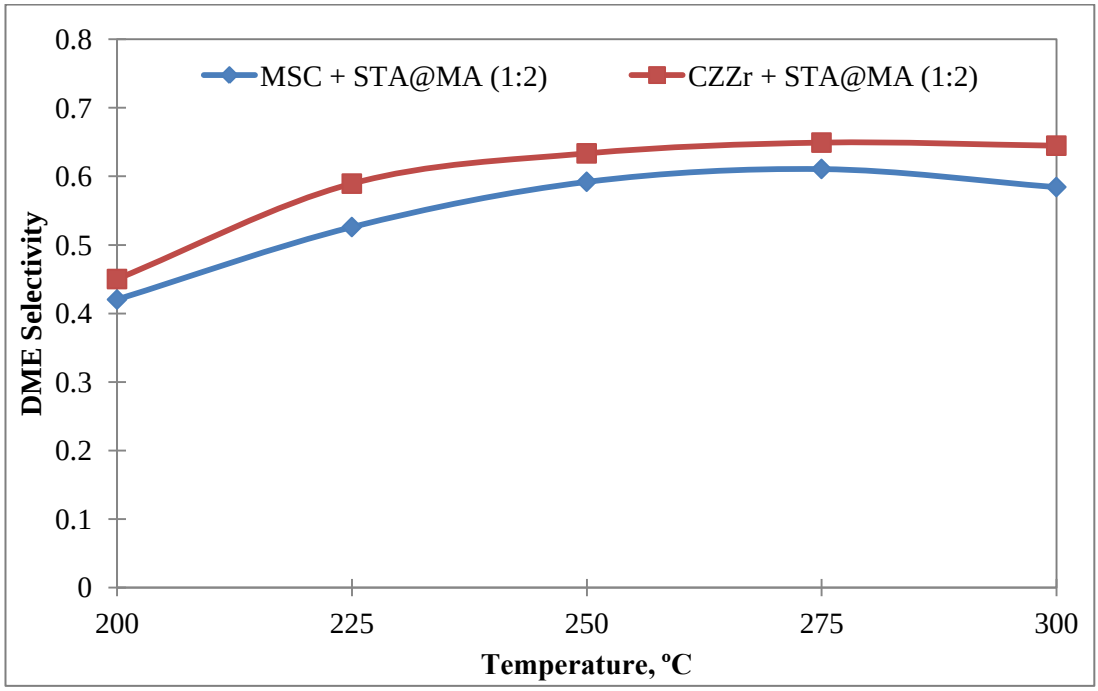

Figure 60. Comparison of DME selectivities of the catalyst mixtures with MSC + STA@MA (1:2) and CZZr + STA@MA (1:2) (Space time: 0.72 s.gr/cc, catalyst amount: 0.3 gr, feed stream: 50% CO + 50% H_2)

The carbon monoxide conversions of all of the studies performed in this part is presented in Figure 61. MSC containing bifunctional catalyst mixtures were better as compared to CZZr containing bifunctional catalyst mixtures. In Figures 62 and 63, the carbon monoxide conversions of the bifunctional catalyst mixtures containing MSC and CZZr are separately presented. As far as the MSC containing bifunctional catalyst mixtures were concerned, the improvement of the catalytic activity by enhancing the acid sites by silicotungstic acid impregnation on mesoporous alumina could be visibly seen for MSC containing bifunctional catalysts. STA impregnation on MA increased CO conversion as compared to MA, as given in Figure 63. However, as the amount of STA@MA was increased to 0.2 g, CO conversion of MSC + STA@MA (1:2) was obtained to be similar to MSC + STA@MA until 250^{o}C. At higher temperatures, CO conversion of MSC + STA@MA (1:2)

decreased. The particle sizes of Cu^{o} clusters obtained after using MSC + STA@MA (1:2) and MSC + STA@MA was found as 11.3 nm and 14.1 nm, respectively as given in Table 15 in Section 8.4. The copper clusters of MSC + STA@MA (1:2) were smaller. The lower activity of this catalyst mixture could not be due to agglomeration of copper clusters. Coking could be a possible cause for deactivation of this catalyst mixture. The impact of the modifications was not obvious for CZZr containing bifunctional catalysts as presented in Figure 63. The methanol synthesis activity of CZZr was already low and the formed methanol was converted to DME by the dehydration catalysts. Modifications like STA impregnation on MA and increasing the amount of STA@MA to 0.2 g did not improve the synergy within the reactions. However, they only improved the amount of methanol converted to DME.

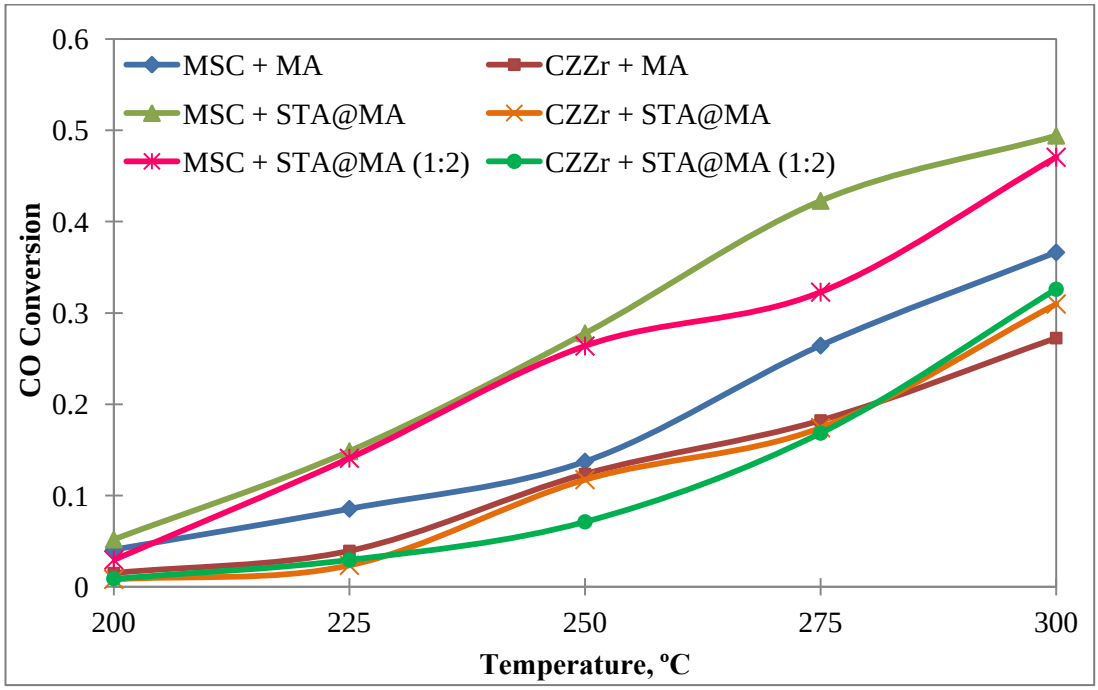

Figure 61. Comparison of carbon monoxide conversions obtained with all of the bifunctional catalyst mixtures (feed stream: 50% CO + 50% H_2)

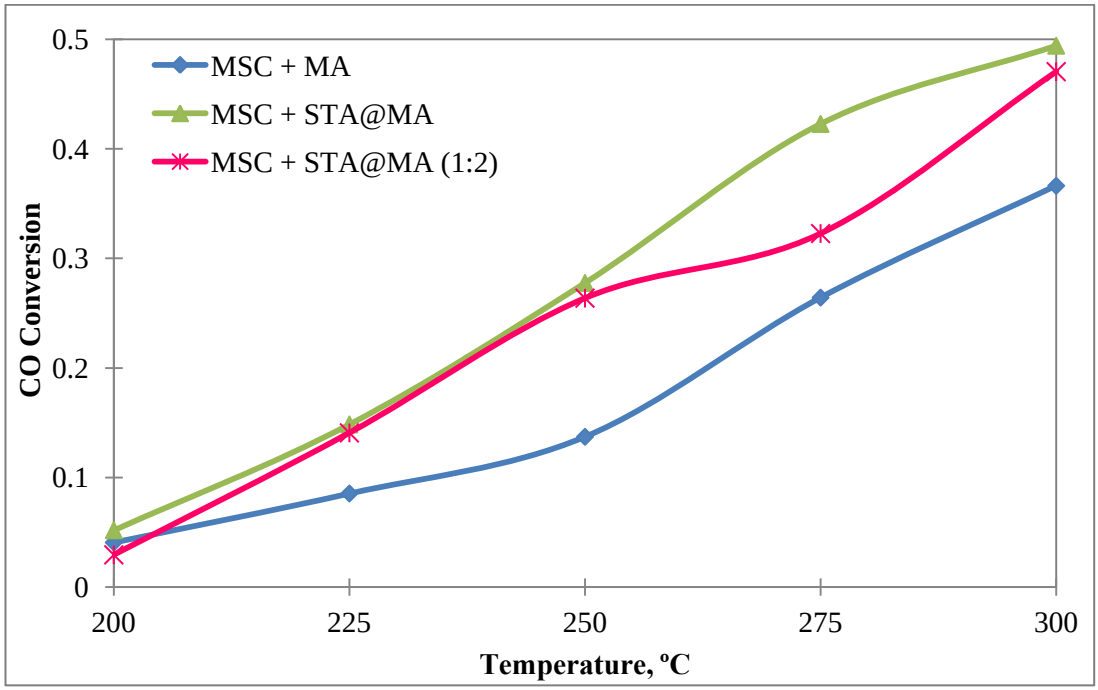

Figure 62. Comparison of carbon monoxide conversions obtained with the bifunctional catalyst mixtures containing MSC (feed stream: 50% CO + 50% H_2)

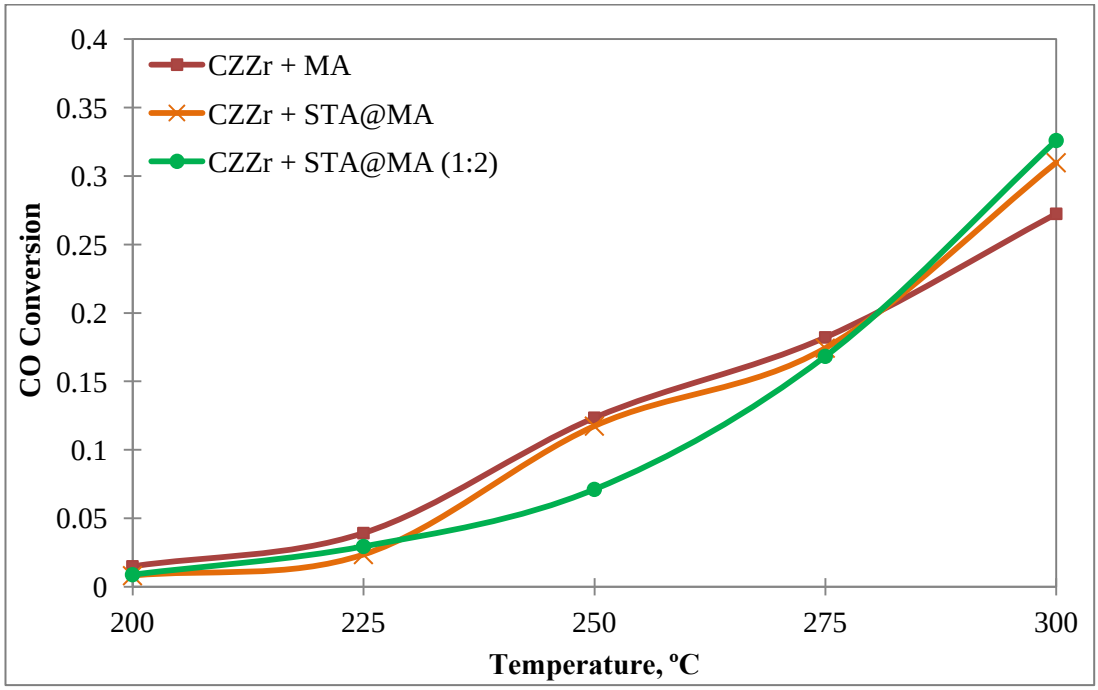

Figure 63. Comparison of carbon monoxide conversions obtained with the bifunctional catalyst mixtures containing CZZr (feed stream: 50% CO + 50% H_2)

The DME selectivities of all the studies performed in this part is presented in Figure 64. According to the results, the improving effects of modifications were positively seen for both MSC and CZZr containing bifunctional catalysts. In Figures 65 and 66, the DME selectivities obtained by the bifunctional catalyst mixtures containing MSC and CZZr are separately presented. The improvement of the catalytic activity by enhancing the acid sites by silicotungstic acid impregnation on mesoporous alumina and increasing the solid acid catalyst amount could be visibly seen for MSC and CZZr containing bifunctional catalysts since the DME selectivities increased with the modifications. As discussed above the modifications on the dehydration catalyst were not effective on CO conversion. However, as seen in Figures 65 and 66, DME selectivities increased with STA impregnation on MA and increasing the amount of STA@MA to 0.2 g. These modifications improved methanol conversion to DME and decreased the amount of unconverted methanol.

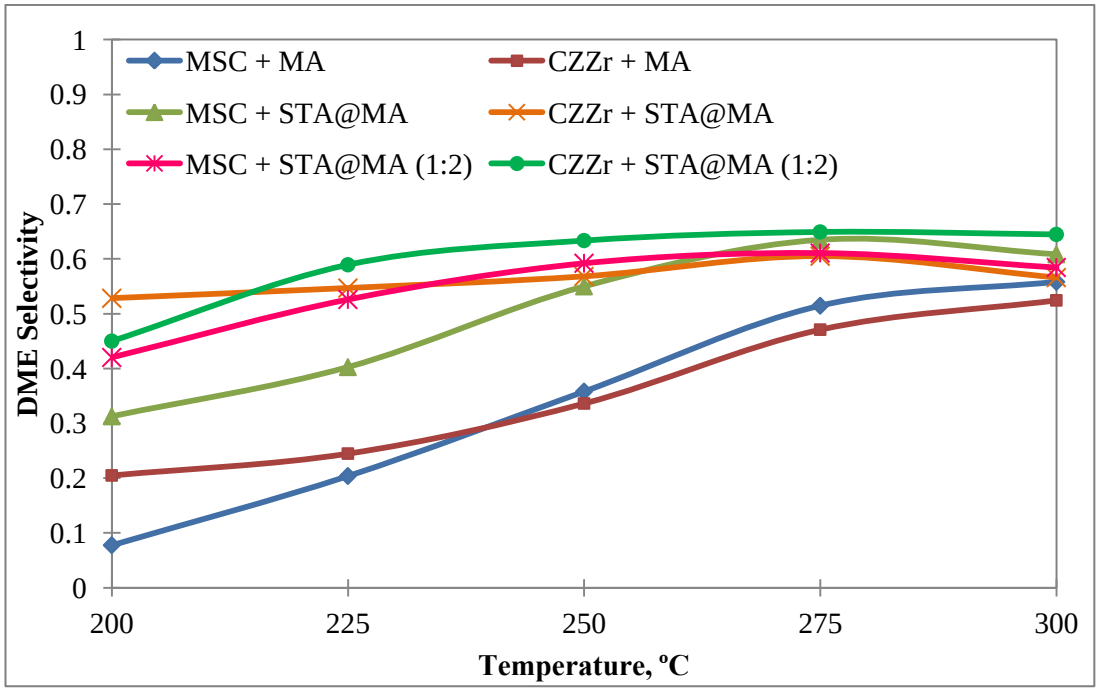

Figure 64. Comparison of DME selectivities obtained with all of the bifunctional catalyst mixtures (feed stream: 50% CO + 50% H_2)

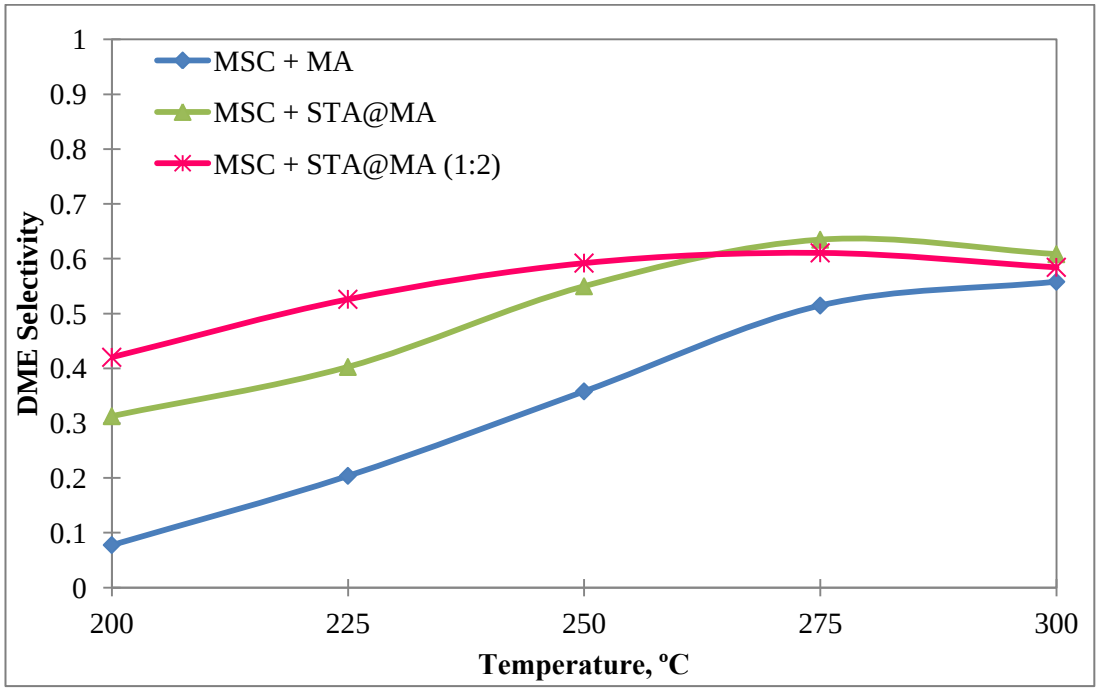

Figure 65. Comparison of DME selectivities obtained with the bifunctional catalyst mixtures containing MSC (feed stream: 50% CO + 50% H_2)

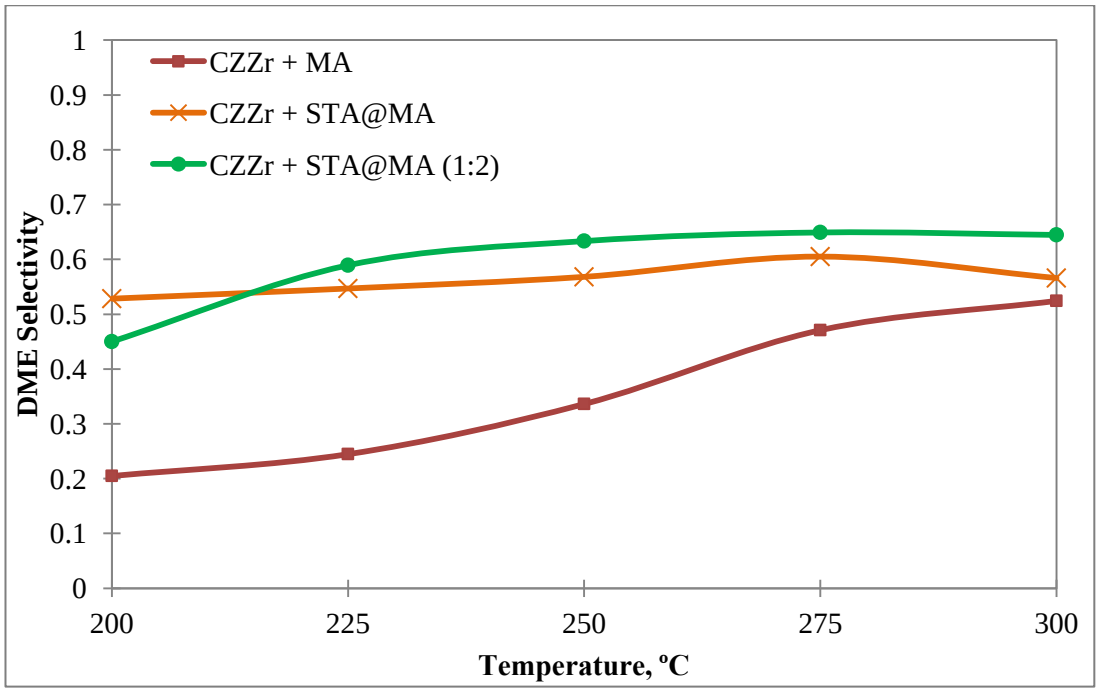

Figure 66. Comparison of DME selectivities obtained with the bifunctional catalyst mixtures containing CZZr (feed stream: 50% CO + 50% H_2)

In Figure 67, DME yield obtained with the bifunctional catalyst mixtures containing MSC is presented. DME yields increased with temperature for all of the bifunctional catalyst mixtures. STA impregnation on MA improved DME yield. Increasing the amount of STA@MA to 0.2 g increased the yield up to 250^{o}C. However, the yield of MSC + STA@MA (1:2) decreased at higher temperatures since both CO conversion and DME selectivity decreased. Also, slightly lower amount of methanol was converted to DME and slightly higher amount of byproducts were formed as compared to MSC + STA@MA. The highest yields achieved using MSC + MA, MSC + STA@MA and MSC + STA@MA (1:2) were as 20.4%, 30.1% and 27.5%, respectively at 300^{o}C.

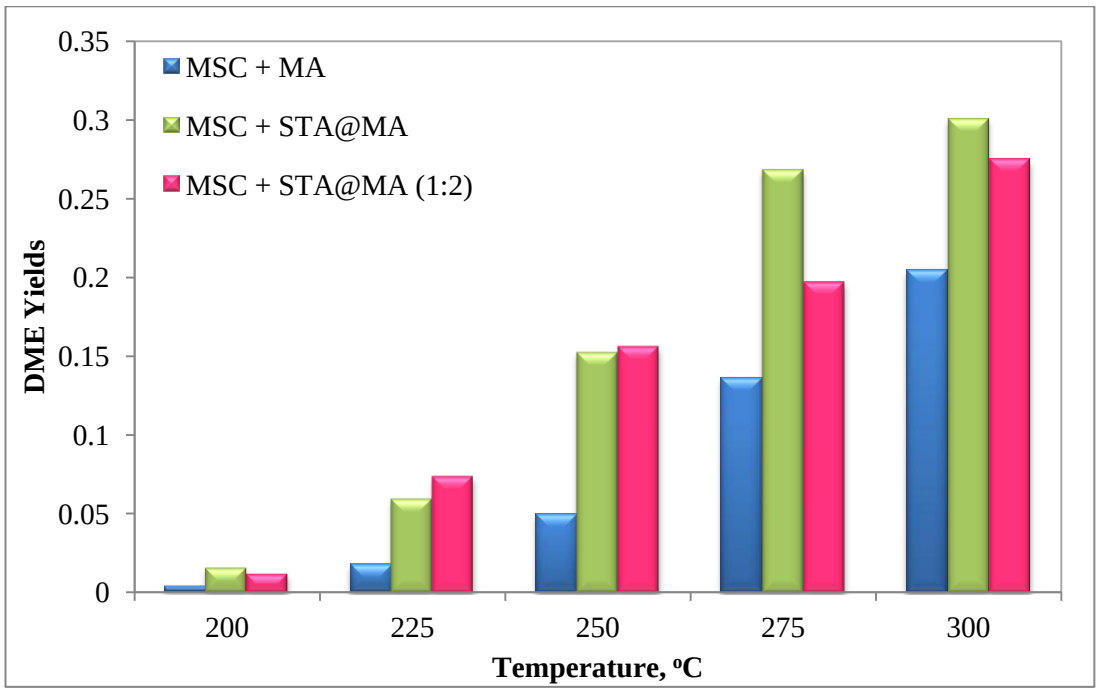

Figure 67. Comparison of DME yields obtained with the bifunctional catalyst mixtures containing MSC (feed stream: 50% CO + 50% H_2)

In Figure 68, DME yield obtained with the bifunctional catalyst mixtures containing CZZr is presented. DME yields increased with temperature for all of the bifunctional catalyst mixtures. STA impregnation on MA and increasing the amount of STA@MA to 0.2 g improved DME yield. The highest yields achieved using CZZr +

MA, CZZr + STA@MA and CZZr + STA@MA (1:2) were as 14.3%, 17.5% and 21.0%, respectively at 300°C.

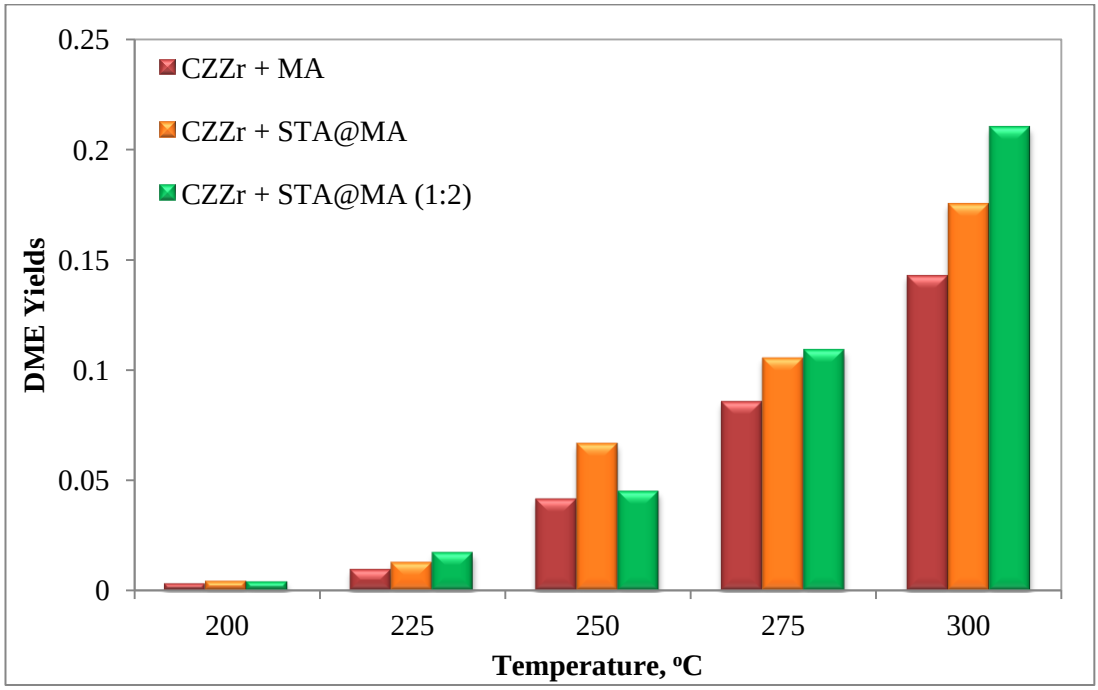

Figure 68. Comparison of DME yields obtained with the bifunctional catalyst mixtures containing CZZr (feed stream: 50% CO + 50% H_2)

8.3. ACTIVITY RESULTS OF THE BIFUNCTIONAL CATALYST MIXTURES COMPOSED OF MSC + STA@MA WITH A FEED STREAM CONTAINING CO_2

In this part, different amounts of CO_2 were added to the feed gas in order to investigate the presence of CO_2 in the feed for the direct synthesis of DME with keeping the flow rate of the feed gas as 25 cc/min. The activity tests were performed at 50 bar within the temperature range of 180 to 300°C. It was reported that CO_2 addition to feed gas promoted methanol synthesis reaction [36]. As the feed contained CO and CO_2 mixture, CO_2 hydrogenation was mainly responsible for methanol synthesis rather than CO hydrogenation since CO_2 hydrogenation rate was

faster than that of CO [2, 86, 87]. It was recently suggested that CO_2 was adsorbed on ZnO sites while the Cu species (either Cu^0 or Cu^{1+}) were the active sites that promoted the reaction [33].

As discussed in the literature, with the feed containing mostly CO_2 and H_2, the main reactions became hydrogenation of CO_2 to methanol and reverse water-gas shift reaction, while, with the feed containing higher amount of CO than CO_2, hydrogenation of CO to methanol was the main reaction. Significant amount of water was formed due to hydrogenation of CO_2 to methanol and reverse water-gas shift reaction [32, 33].

In Table 14, the studies performed in this study with the different feed compositions containing carbon dioxide and using MSC + STA@MA mixture are listed.

Table 14. The feed compositions containing CO_2 with MSC + STA@MA

% H_2	**% CO**	**% CO_2**
50	40	10
50	25	25
50	10	40

The feed gas mixtures contained volumetric ratios of $H_2/CO/CO_2$ = 50/40/10, 50/25/25 and 50/10/40 in these experiments. For that reason, CO and CO_2 conversions were separately calculated and given in Figures 69 and 70, respectively, to see whether CO_2 was also effective in DME formation or not. According to Figure 69, carbon monoxide conversions were negative below 225^{o}C, 250^{o}C and 250^{o}C for the feed gases with CO_2 of 10%, 25% and 40%, respectively. This behavior indicated that carbon dioxide acted as a reactant while carbon monoxide was as a product rather than being a reactant at these temperatures and some amount of CO_2 was converted to CO via reverse water-gas shift reaction. The CO conversions increased with temperature and the highest conversions were obtained as 53.4% at 300^{o}C and

39.4% at 275°C, 43.2% at 275°C for the feed gases containing 10%, 25% and 40% CO_2, respectively. According to Figure 70, it was clearly seen that CO_2 was also involved for DME synthesis and the degree of contribution increased with CO_2 content. For the feed gas with 10% CO_2, CO_2 conversion was negative above 250°C. This indicated that CO_2 behaved as a product; formed more than it was consumed; as a consequence, DME began to be produced via CO route.

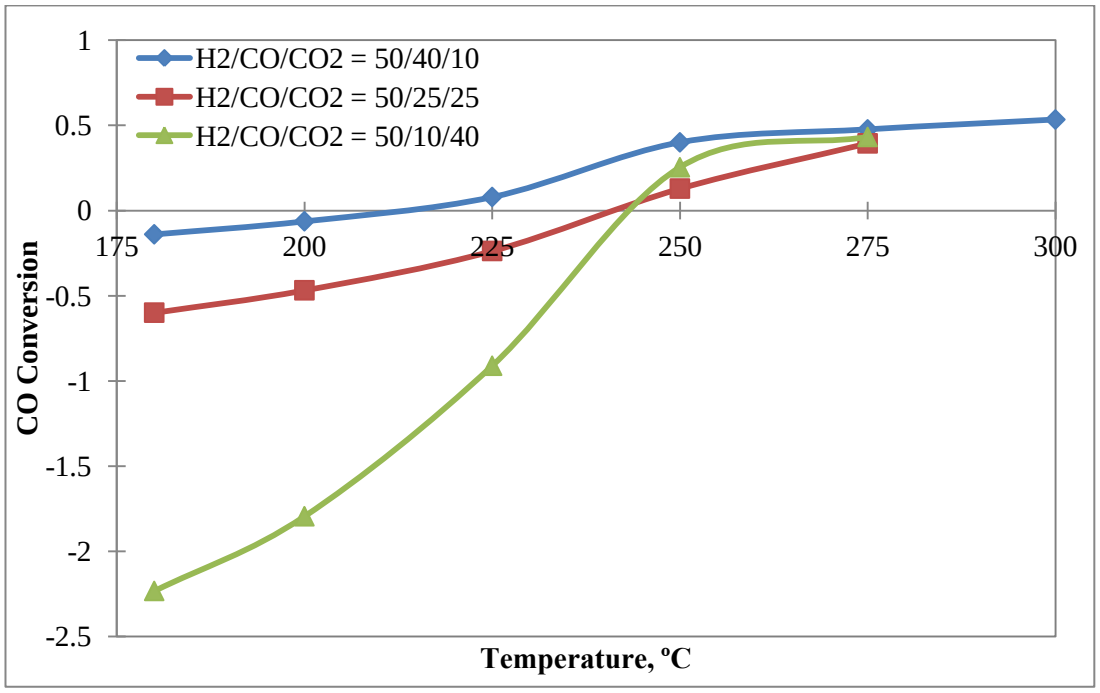

Figure 69. Comparison of carbon monoxide conversions with different feed mixtures using MSC + STA@MA (Space time: 0.48 s.gr/cc, catalyst amount: 0.2 gr)

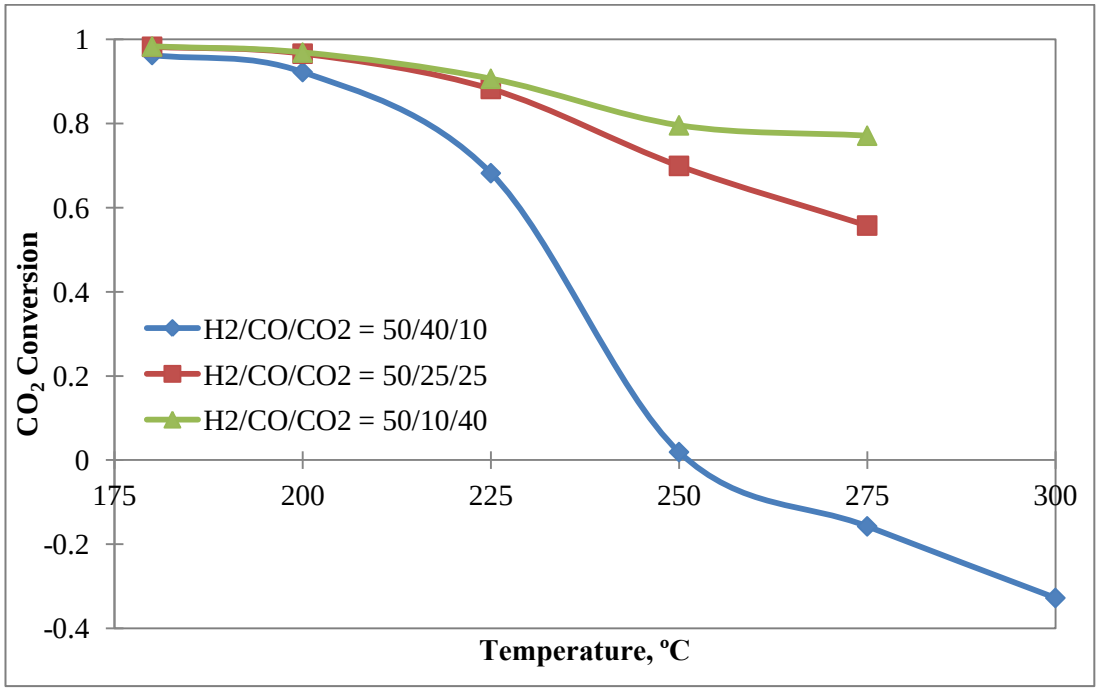

Figure 70. Comparison of carbon dioxide conversions with different feed mixtures using MSC + STA@MA (Space time: 0.48 s.gr/cc, catalyst amount: 0.2 gr)

In Figure 71, the product distribution of MSC + STA@MA with the feed mixture of $H_2/CO/CO_2$ = 50/40/10 is presented. In that figure, the selectivities of the components were calculated with respect to moles of converted carbon monoxide. Therefore, some inconsistencies occurred such as CO_2 selectivities were first higher than one and then decreased below zero, methanol and DME selectivities were negative at low temperatures. The reason for this behavior was that CO was not a reactant at low temperatures. In addition, at higher temperatures CO_2 selectivities were lower than that of DME indicating two conclusions. First, the presence of CO_2 inhibited water-gas shift reaction and CO_2 was not produced through this reaction. Therefore, the amount of CO_2 that was present in the product mixture was less as compared to the feed mixture in the absence of CO_2. Second, the overall DME formation reaction proceeded through the pathway of Reaction 2.

$$2CO + 4H_2 \leftrightarrow CH_3OCH_3 + H_2O \quad (2)$$

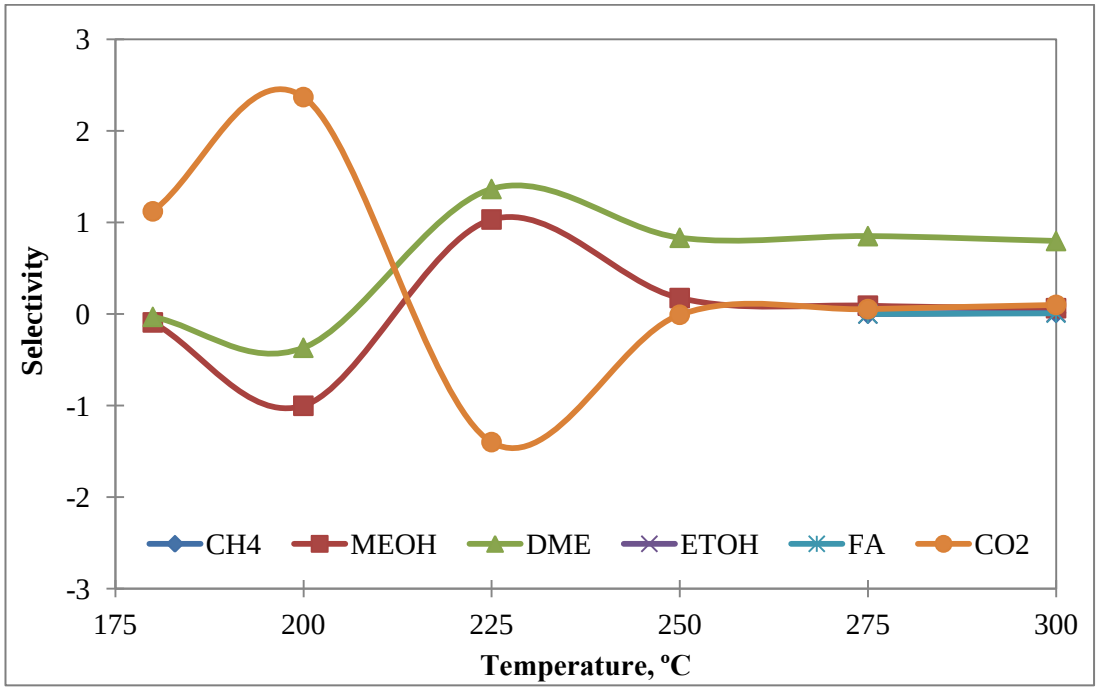

Figure 71. Product distribution obtained with the feed mixture of $H_2/CO/CO_2$ = 50/40/10 based on carbon monoxide with MSC + STA@MA (Space time: 0.48 s.gr/cc, catalyst amount: 0.2 gr)

Due to these inconsistencies which were caused due to the selectivity definition used in Figure 71, selectivities were redefined with respect to total moles of converted CO and CO_2. Sample conversion and selectivity calculations are given in Appendix B. The product distributions with respect to total moles of converted CO and CO_2 for a feed mixture of $H_2/CO/CO_2$ = 50/40/10 is given in Figure 72. According to this figure, methanol and DME selectivities did not change significantly between 180 and 200^oC. In addition, between 180 and 200^oC, almost all of carbon dioxide was consumed as presented before in Figure 70. Therefore, at 180^oC, the presence of CO_2 in the feed gas mixture could promote reverse water-gas shift reaction to produce carbon monoxide. Carbon monoxide conversion was -14.0% at 180^oC as presented before in Figure 69, and this means that carbon monoxide was produced much more rather than it was consumed. Above 200^oC as presented in Figure 72, a very sharp increase in DME selectivity and a corresponding decrease in methanol selectivity were observed. The highest DME selectivity reached to 90% at 275^oC then, slightly decreased to 88.6% at 300^oC, due to byproduct formation and possible

aggregation of copper clusters. Smaller amounts of byproducts were observed than obtained with the feed mixture of CO and H_2. Because, the presence of small amount of CO_2 in the feed mixture inhibited water-gas shift reaction and reverse dry reforming reaction (Reaction 10).

$$2CO + 2H_2 \leftrightarrow CH_4 + CO_2 \quad (10)$$

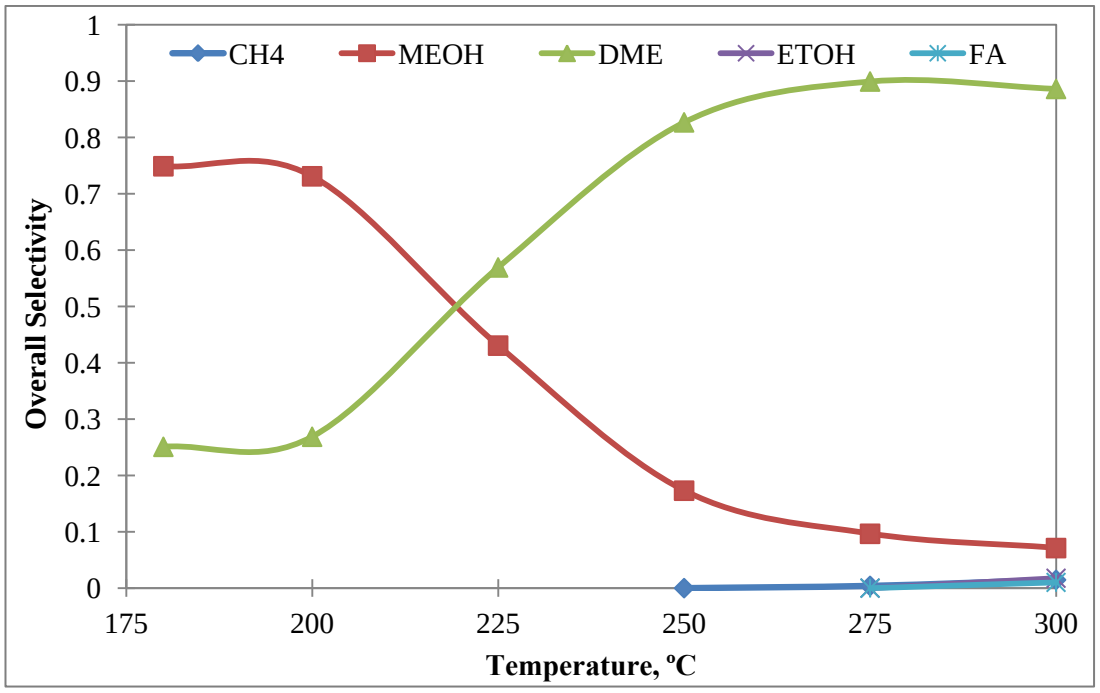

Figure 72. Product distribution obtained with the feed mixture of $H_2/CO/CO_2$ = 50/40/10 based on total moles of converted CO and CO_2 with MSC + STA@MA (Space time: 0.48 s.gr/cc, catalyst amount: 0.2 gr)

Product distributions with respect to total moles of converted CO and CO_2 for feed mixture of $H_2/CO/CO_2$ = 50/25/25 is given in Figure 73. As the temperature increased, methanol selectivity decreased while DME selectivity increased since they follow opposite trends. The maximum DME selectivity was achieved as 82.2% at 275^oC which was somewhat less than that of for the feed mixture of $H_2/CO/CO_2$ = 50/40/10.

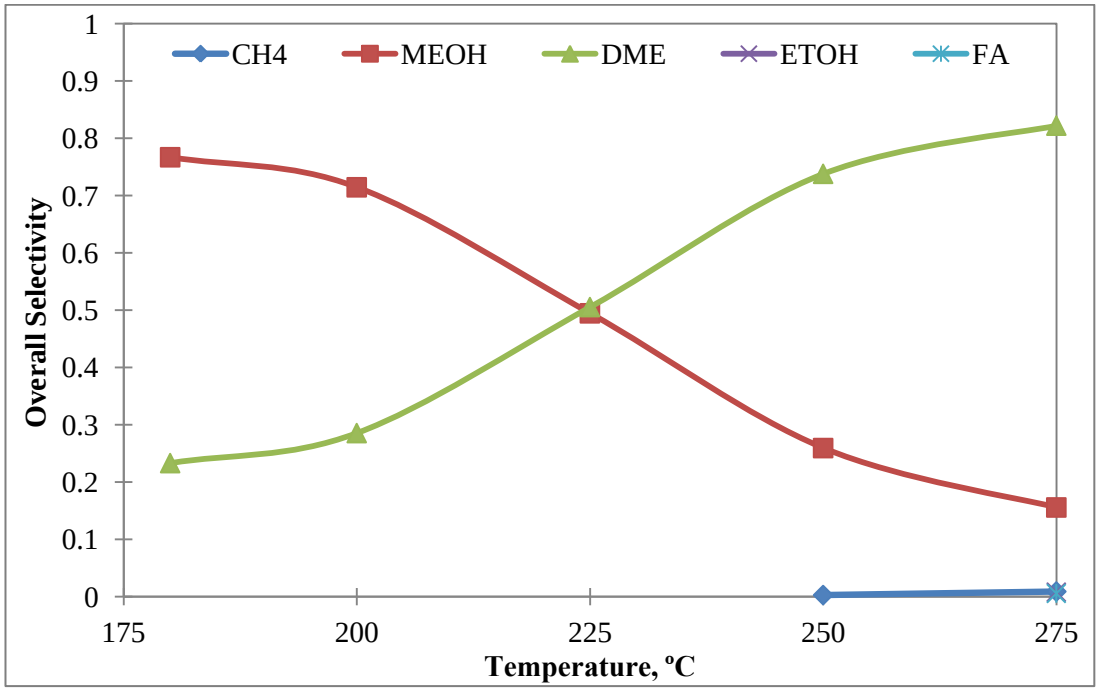

Figure 73. Product distribution obtained with the feed mixture of $H_2/CO/CO_2$ = 50/25/25 based on total moles of converted CO and CO_2 with MSC + STA@MA (Space time: 0.48 s.gr/cc, catalyst amount: 0.2 gr)

Product distributions with respect to total moles of converted CO and CO_2 for feed mixture of $H_2/CO/CO_2$ = 50/10/40 are given in Figure 74. According to this figure, DME selectivity was very low at 180°C. This indicated that methanol dehydration was not favored with high CO_2 presence in the feed stream at low temperatures. Even though DME selectivity increased with temperature, it could merely reached 78.2% at 275°C, which was lower than that of obtained with the feed stream containing less CO_2. The byproduct formation was here insignificant.

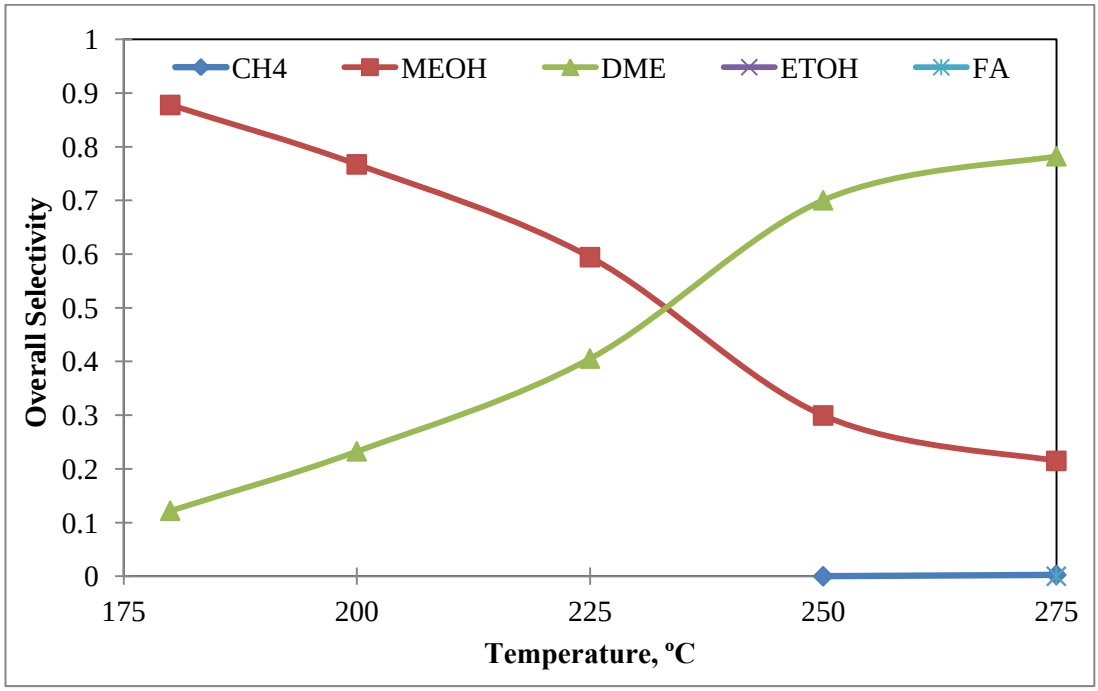

Figure 74. Product distribution obtained with the feed mixture of $H_2/CO/CO_2$ = 50/10/40 based on total moles of converted CO and CO_2 with MSC + STA@MA (Space time: 0.48 s.gr/cc, catalyst amount: 0.2 gr)

It was concluded in literature that the amount of CO_2 in feed gas was beneficial for methanol synthesis up to a certain point. At low concentrations of CO_2, rate of water-gas shift reaction increased and consumed water, which accelerated the methanol dehydration reaction. Also it is stated that, after a threshold value of CO_2, reverse water-gas shift reaction was favored and unconsumed water inhibited the dehydration reaction followed by increase in methanol [46]. The effect of presence and absence of CO_2 in the feed stream on CO conversion and DME selectivity was presented in Figures 75 and 76, respectively. At low temperatures, the CO_2 hydrogenation is the main reaction since the CO hydrogenation is slower. Therefore, with the feed mixture of $H_2/CO/CO_2$ = 50/40/10, carbon monoxide conversion was negative below 225^oC while, with the feed mixtures of $H_2/CO/CO_2$ = 50/25/25 and $H_2/CO/CO_2$ = 50/10/40, carbon monoxide conversions were negative below 250^oC as seen in Figure 75. This indicated that reverse water-gas shift reaction was accelerated more and produced higher amount of carbon monoxide at lower temperatures as the CO_2 content in feed mixture increased. However, the low amount of CO_2 in the feed,

that was 10%, enhanced CO conversion as compared to feed without CO_2 at higher temperatures. Carbon dioxide conversions never dropped below zero for these mixtures, which indicated that it was effective in product formation and mostly promoted reverse water-gas shift reaction. This result could also be inferred from the overall DME selectivities, which was given in Figure 76. For the feed streams with 10% and 25% of CO_2, DME selectivities were lower than that of obtained with the feed stream without CO_2 up to 200^oC, while for the feed stream with 40% of CO_2, DME selectivity was lower up to 225^oC. At higher temperatures, DME selectivities were over than that of obtained without CO_2. As the CO_2 content increased, DME selectivity decreased such that the feed streams with 10% of CO_2 yielded higher DME as compared to feed streams with 25% and 40% of CO_2 even though, the latter compositions resulted in higher CO_2 conversions. These findings suggested that with a feed containing higher amount of CO_2, the synergetic effect decreased and the reverse water-gas shift reaction was favored. Formation of large amount of water inhibited the dehydration reaction and amount of unconverted methanol to DME increased. When the feed contained higher amount of CO, the synergetic effect over bifunctional catalyst increased due to conversion of methanol to DME with high efficiency [88]. The effect of CO_2 on reduction of byproduct formation was also apparent since even lower amounts of byproducts were formed.

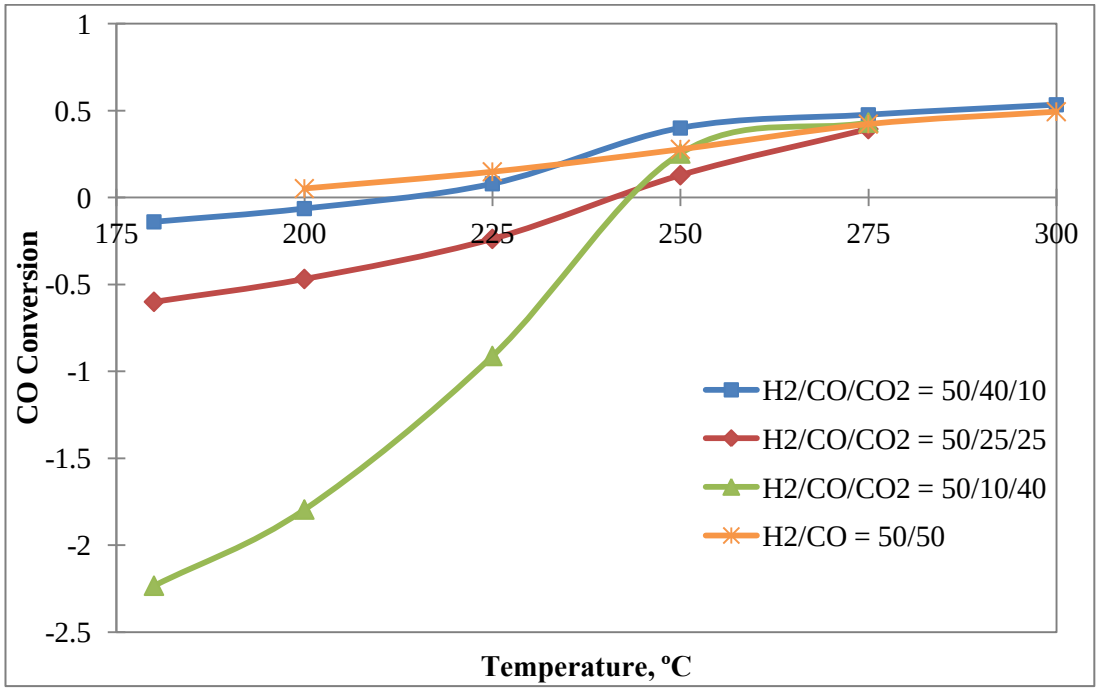

Figure 75. Comparison of carbon monoxide conversions with the effect of carbon dioxide addition to feed stream using MSC + STA@MA (Space time: 0.48 s.gr/cc, catalyst amount: 0.2 gr)

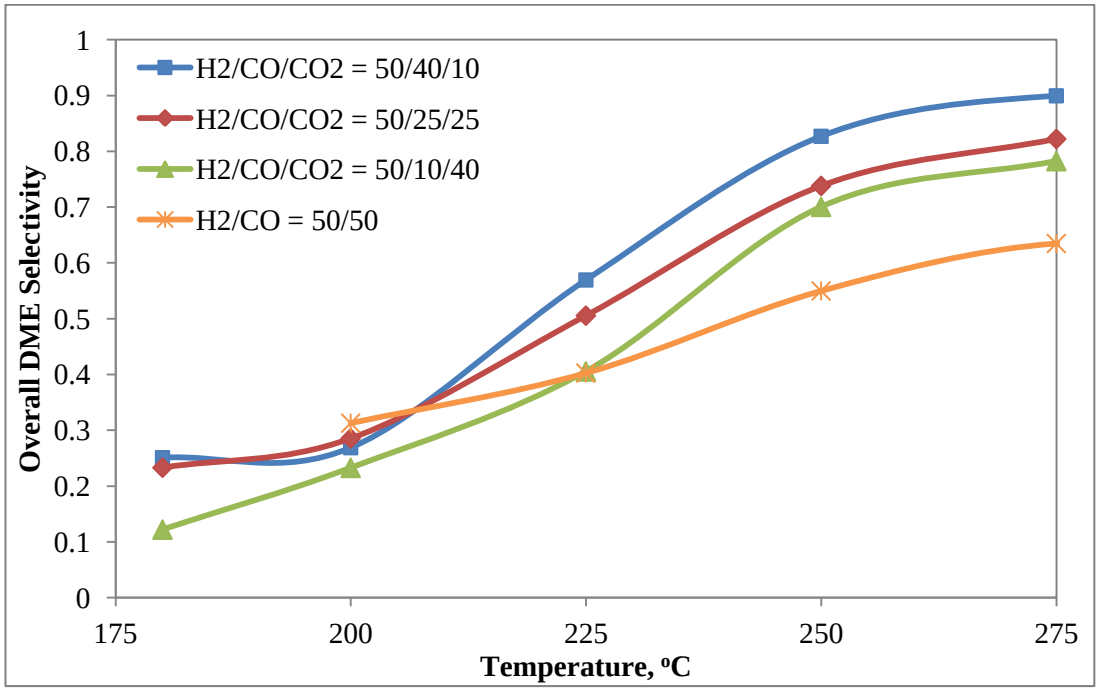

Figure 76. Comparison of DME selectivities with the effect of carbon dioxide addition to feed stream using MSC + STA@MA (Space time: 0.48 s.gr/cc, catalyst amount: 0.2 gr)

8.4. DEACTIVATION ANALYSIS

One of the possible causes for deactivation of Cu/ZnO type catalysts is aggregation of copper crystals that could occur at temperatures above 300^{o}C. The XRD patterns of some of the used catalyst of this work were obtained to investigate the changes in the crystal structure of the catalysts. The wide angle XRD patterns of the used catalysts of CZZr-based, MSC-based and MSC-based with carbon dioxide in the feed stream are given in Figures 77, 78 and 79, respectively. The common trend for all the used catalysts could be seen from the XRD patterns such that the intensities of the main CuO peaks of the fresh catalysts at 2θ value of about 35.6^{o} decreased after reaction that lasted approximately 12 hours. The majority of the CuO crystals of the fresh catalysts were reduced to Cu^{o} with a very sharp XRD peak at around 43^{o} after reaction. 2θ degrees of the peaks of CuO and ZnO were given in Appendix D.

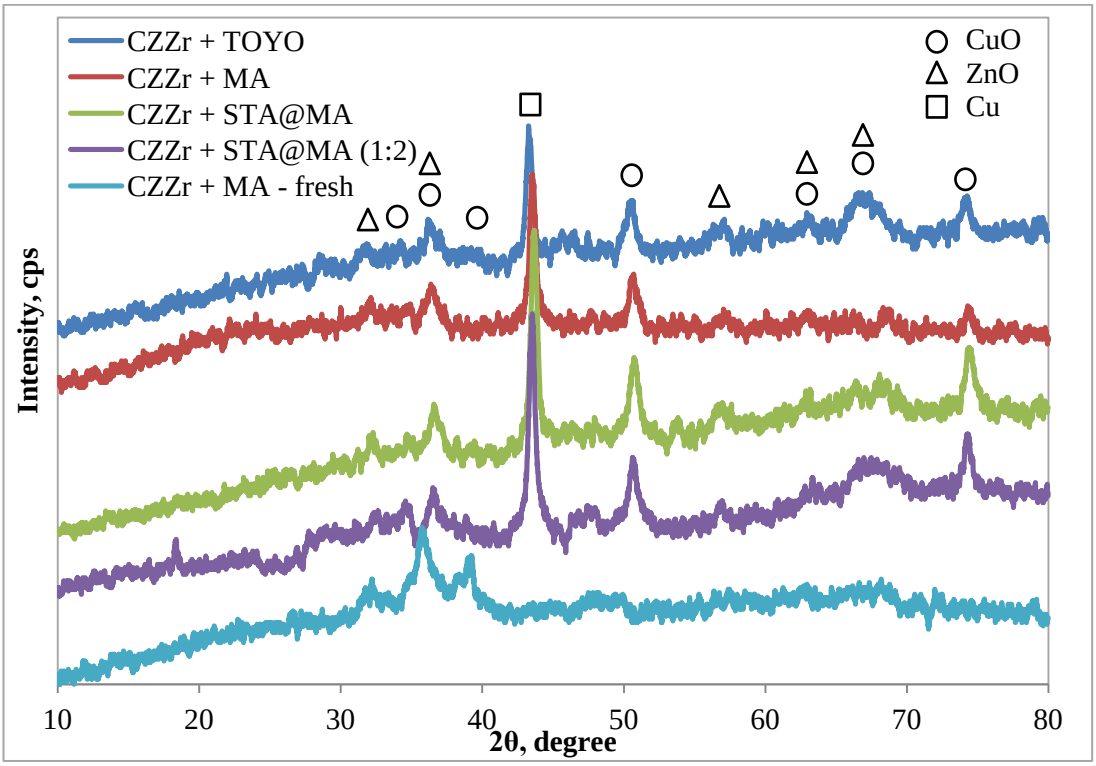

Figure 77. The wide angle XRD patterns of the used and fresh CZZr-based catalysts

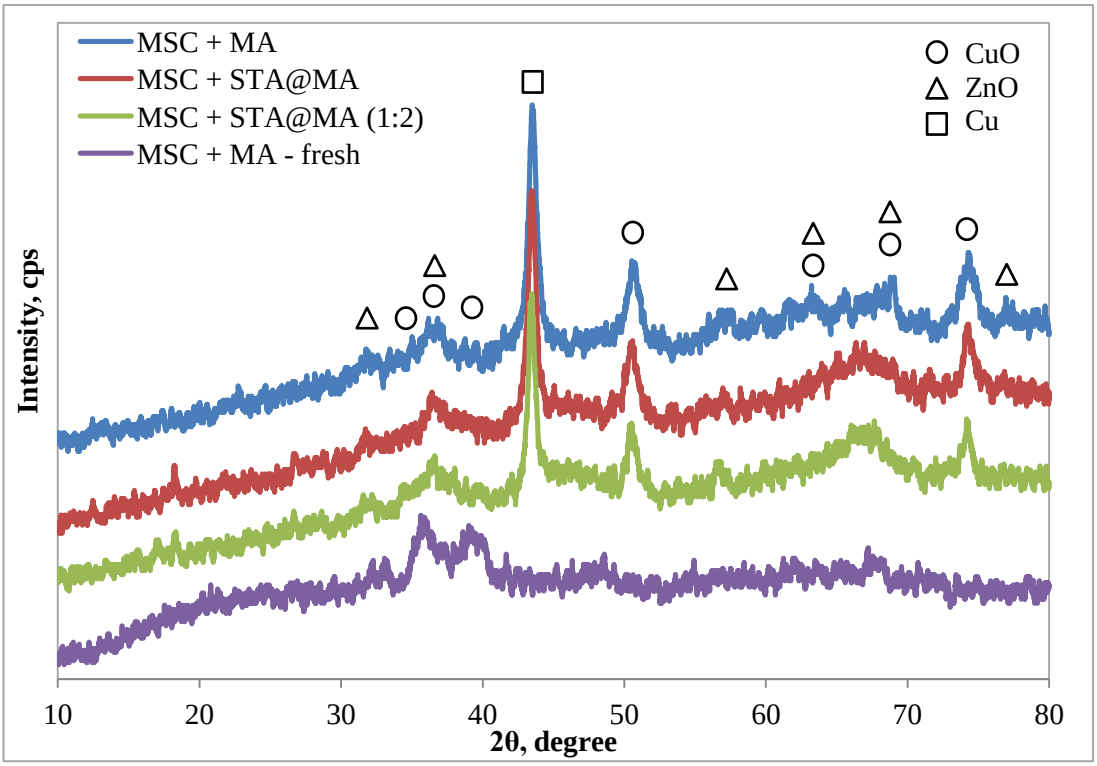

Figure 78. The wide angle XRD patterns of the used and fresh MSC-based catalysts

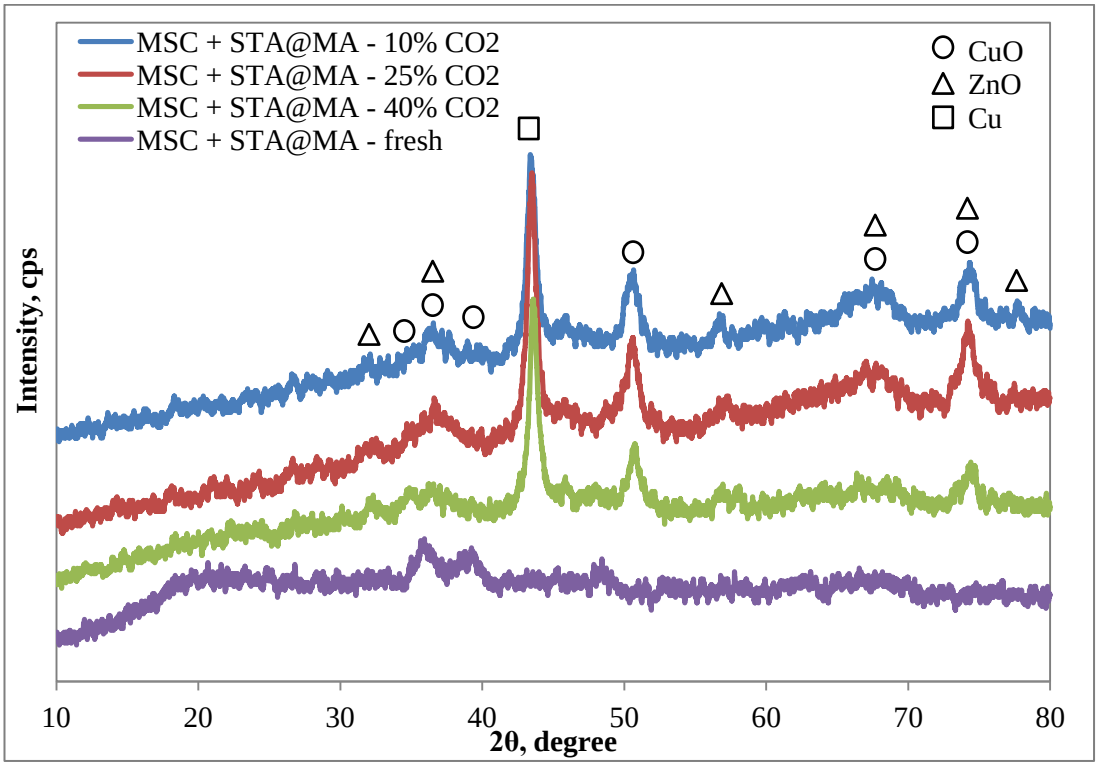

Figure 79. The wide angle XRD patterns of the used and fresh MSC-based catalysts with carbon dioxide in the feed stream

The crystal sizes of CuO and Cu^{o} were calculated using the Scherrer's equation and given in Table 15 and a sample calculation was presented in Appendix E. The particle sizes of CuO clusters in MSC and CZZr fresh catalysts were 4.6 and 5.0 nm, respectively, whereas at the end of the reaction, the particle sizes of Cu clusters increased to 9.4 and 16.9 nm, respectively. These results indicated that CuO clusters were agglomerated and reduced to larger Cu clusters at the end of the reaction.

Table 15. Particle sizes for metals and metal oxides calculated from Scherrer's equation

Catalyst	**Peak**	**Particle Size, nm**
MSC - fresh	CuO	4.6
CZZr - fresh	CuO	5.0
CZZr + TOYO	CuO	5.5
	Cu	13.0
MSC + MA	CuO	4.9
	Cu	9.4
CZZr + MA	CuO	6.9
	Cu	16.9
MSC + STA@MA	CuO	4.6
	Cu	14.1
CZZr + STA@MA	CuO	8.3
	Cu	14.1
MSC + STA@MA (1:2)	CuO	4.1
	Cu	11.3
CZZr + STA@MA (1:2)	CuO	6.9
	Cu	13.0
MSC + STA@MA - 10% CO_2	CuO	3.9
	Cu	14.1
MSC + STA@MA - 25% CO_2	CuO	2.8
	Cu	10.6
MSC + STA@MA - 40% CO_2	CuO	3.0
	Cu	9.9

TEM image of the used MSC + STA@MA catalyst at a feed composition of $H_2/CO/CO_2$ = 50/40/10 is given in Figure 80. Presence of carbon nanotubes over the surface of the used catalyst indicates coke formation. The EDX mapping of the used MSC + STA@MA catalyst is given in Figure 81. Homogeneous distribution of silica and tungsten suggests that there was no major disturbance on the distribution of active sites during reaction that lasted approximately 12-14 hours as the catalyst was exposed to high pressure and temperature up to 300^{o}C.

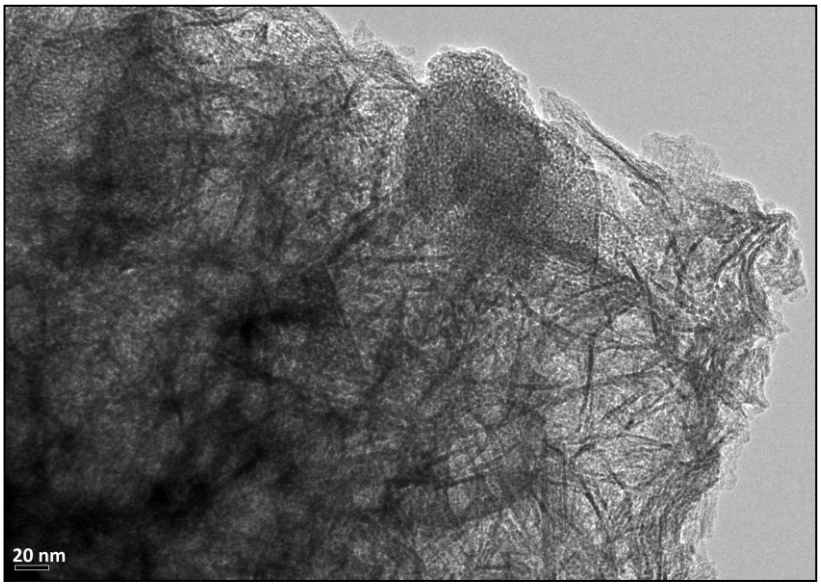

Figure 80. TEM image of the used MSC + STA@MA catalyst at feed composition of $H_2/CO/CO_2$ = 50/40/10

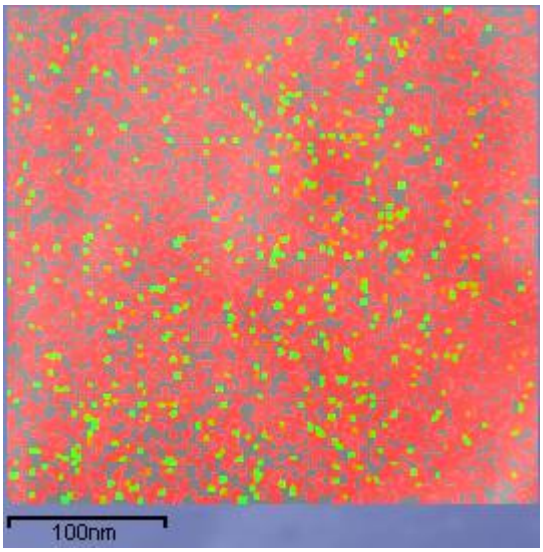

Figure 81. EDX mapping of used MSC + STA@MA catalyst at feed composition of $H_2/CO/CO_2$ = 50/40/10 (Si = Red, W = Green)

CHAPTER 9

THERMODYNAMIC ANALYSES FOR THE CONDUCTED STUDIES

The thermodynamic analyses were performed for the studies conducted throughout this work. The intention for these analyses was to observe the behavior of the results obtained during activity analyses and to investigate whether or not the experimental results ever exceeded the thermodynamic equilibrium. In this respect, thermodynamic equilibrium conversions and also compositions were evaluated considering occurance of all possible reactions, using a special Chemical Equilibrium Program; Gaseq, considering the operation conditions of the activity analyses and the results were given in Appendix F.

The molar compositions of each feed gas mixture were used as the inlet stream at the pressure of 50 bar and for the product stream, the considered species were CO, CO_2, H_2, methanol, DME and water. The reason for neglecting the side products of methane, ethanol and formic acid was that they were formed in trace amounts during the reaction processes. Therefore, the program considered the only possible reactions that could proceed through the available species. These reactions could be hydrogenation of carbon monoxide and carbon dioxide, methanol dehydration, water-gas shift and reverse water-gas shift reactions. In addition, the equilibrium conversion of carbon dioxide and hydrogen to formic acid was separately evaluated using Gaseq. The amount of formic acid formed was found to be zero at the operating conditions which meant that formation of formic acid was not favorable.

The equilibrium carbon monoxide conversions of different feed gas compositions with respect to temperature were displayed in Figure 82. As seen in this figure, the addition of carbon dioxide to the feed stream enhanced the equilibrium carbon

monoxide conversions at low temperatures by providing extra carbon monoxide via reverse water-gas shift reaction. However, as the temperature increased, equilibrium conversions for all feed mixtures decreased with temperature due to exothermic nature of the reactions. The equilibrium carbon monoxide conversions also decreased with CO_2 content at higher temperatures possibly due to inhibition of methanol dehydration via excess build up of water.

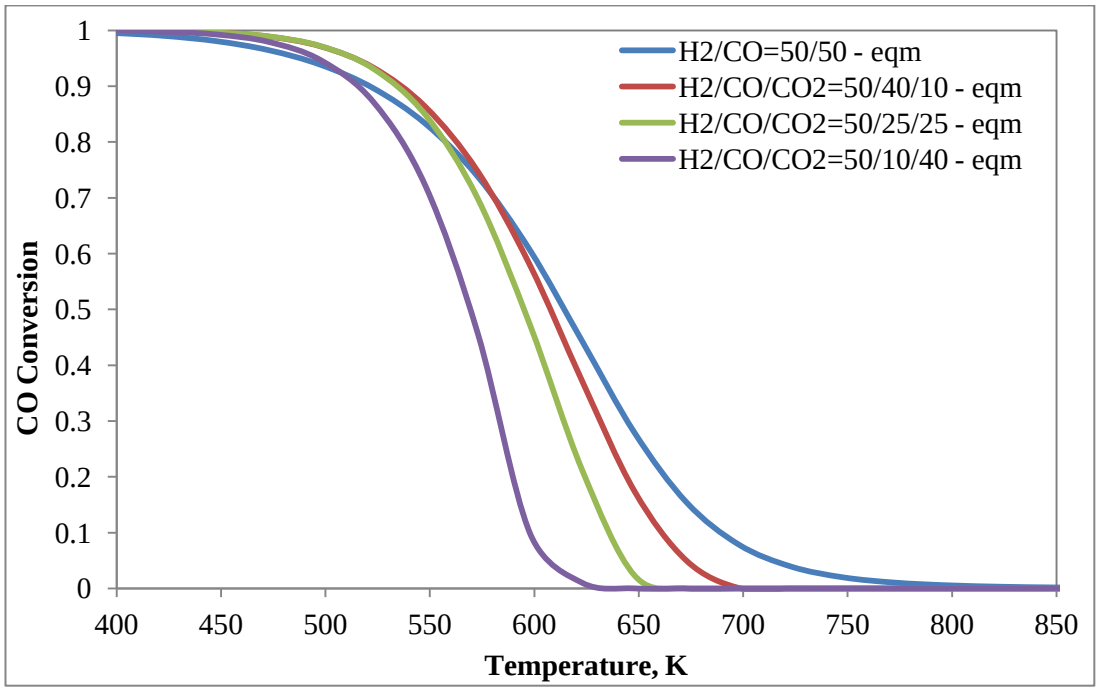

Figure 82. The equilibrium carbon monoxide conversions of different feed gas compositions with respect to temperature

In Figure 83, the equilibrium carbon monoxide conversions and the experimental values obtained over different catalyst pairs were compared for the feed mixture of H_2/CO = 50/50 with respect to temperature, at 50 bar. As seen from the figure, the carbon monoxide conversions obtained using catalyst mixtures containing MA and STA@MA were below the equilibrium conversions. CO conversions achieved by the catalytic reactions could not approach to the equilibrium as seen from the figure. However, CO conversions achieved by the catalytic reactions did not to exceed the equilibrium either. This suggested that the CO conversion calculations were presumed to be valid from both experimental and thermodynamic point of view.

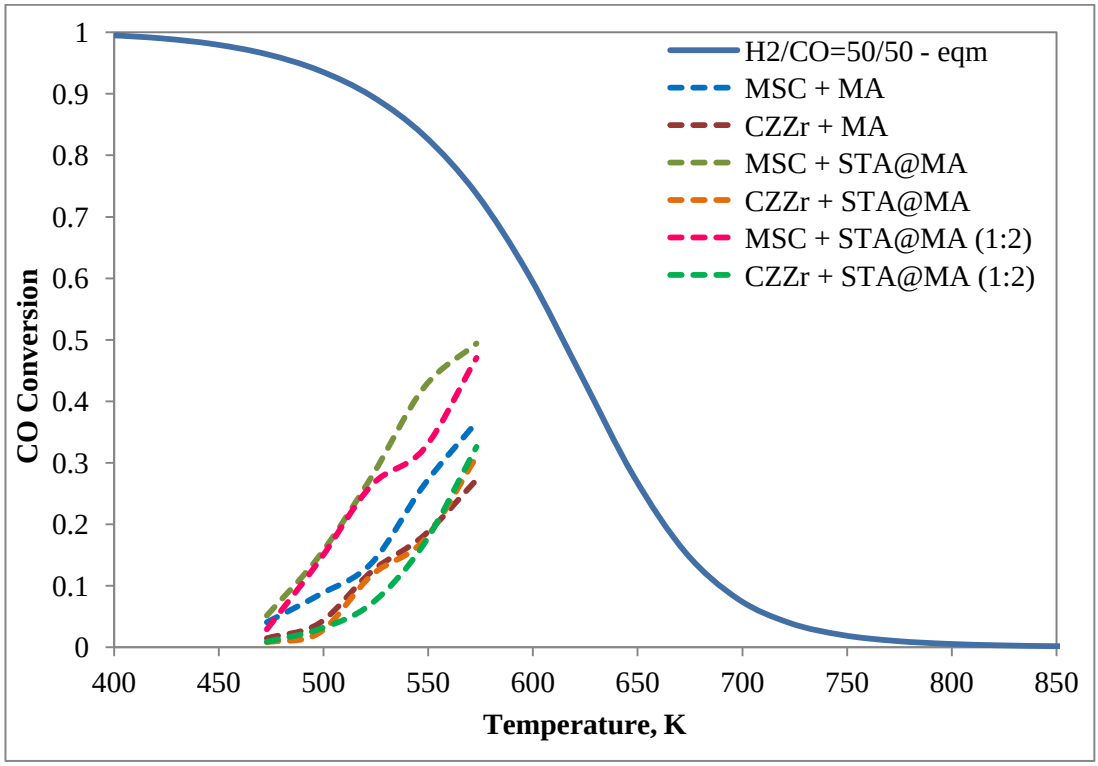

Figure 83. CO conversions of the equilibrium and reactions over different catalysts for feed mixture of H_2/CO = 50/50 with respect to temperature

In Figure 84, equilibrium conversions of carbon monoxide are compared with the experimental conversions obtained over MSC + STA@MA for different CO_2 contents in the feed mixture. According to this figure, the carbon monoxide conversions obtained at each feed mixture were below their corresponding equilibrium conversions.

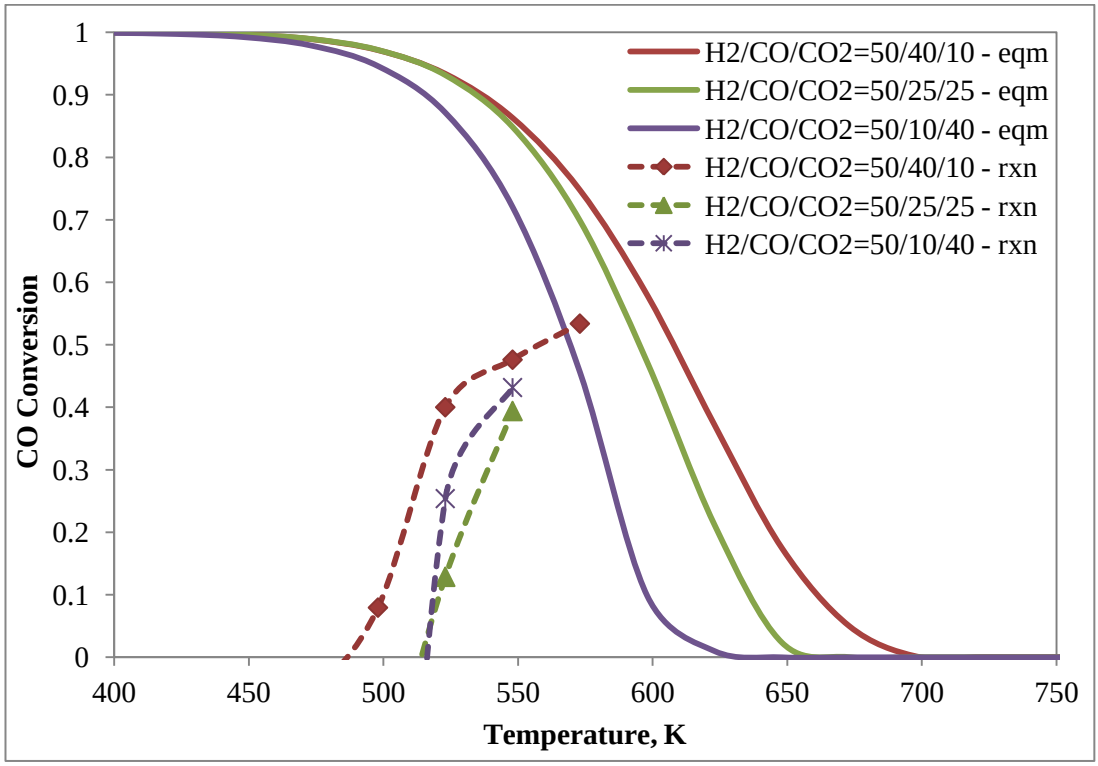

Figure 84. CO conversions of the equilibrium and reactions over MSC + STA@MA for different CO_2 content in feed mixture

However, the setback here was simultaneous consumption and production of carbon monoxide and carbon dioxide due to synergy among the reactions. The calculation of CO conversion was based on the moles of carbon monoxide in the inlet and outlet streams. Carbon monoxide could be consumed by CO hydrogenation and can be produced by reverse water-gas shift reaction from carbon dioxide and hydrogen as well. In addition, equilibrium CO_2 conversions were found as negative within the temperature range. Therefore, the evaluation of the thermodynamic analyses based on carbon monoxide conversion was meaningless and futile for the feed mixtures containing carbon dioxide. In order to overcome this difficulty, another approach was considered in which equilibrium compositions of carbon monoxide and carbon dioxide and experimental product composition values were compared for different feed gas compositions and catalyst mixtures. Equilibrium compositions involved only carbon containing species.

The equilibrium carbon monoxide compositions of different feed streams are given in Figure 85. According to this figure, at equilibrium, carbon monoxide compositions in the product stream were expected to be very small at low temperatures for each gas mixture. This indicated that almost all of carbon monoxide should be converted to products, from thermodynamic point of view. As the temperature increased, the carbon monoxide compositions at equilibrium increased as well, suggesting that carbon monoxide was produced more than it was consumed. The equilibrium carbon monoxide compositions for all feed gas mixtures followed similar patterns.

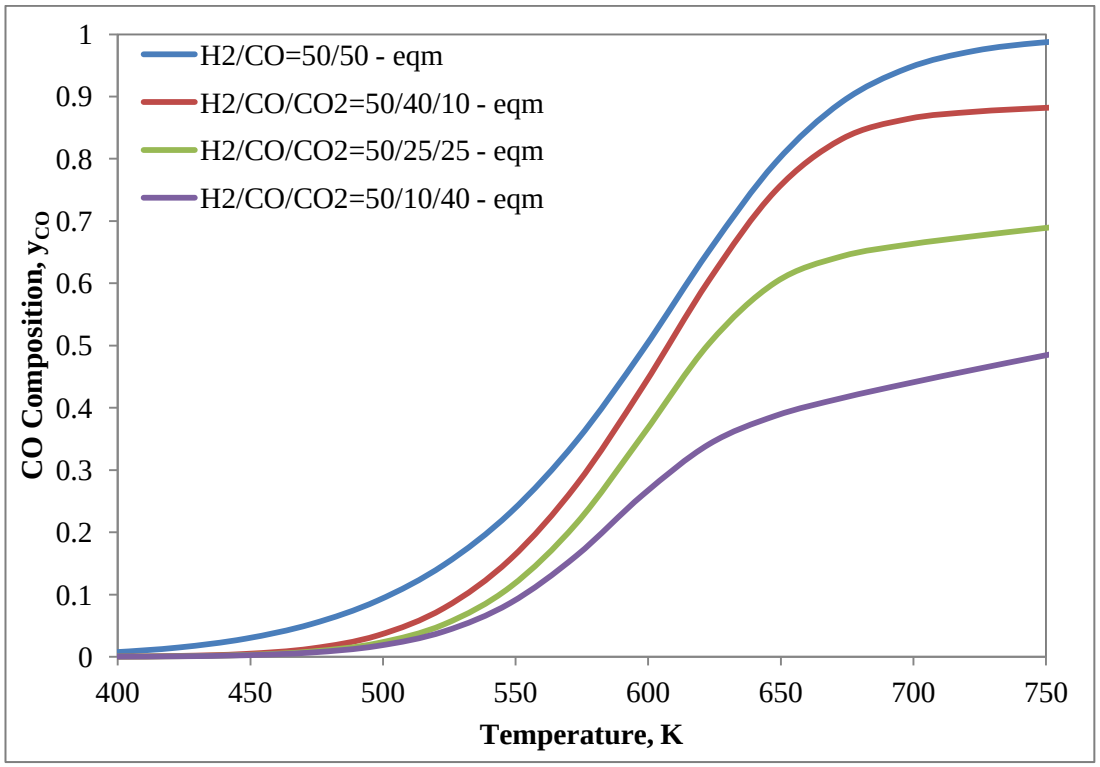

Figure 85. Equilibrium CO compositions based on carbon containing species at different feed compositions

The equilibrium carbon dioxide compositions of different feed gas compositions with respect to temperature are given in Figure 86. At equilibrium, carbon dioxide compositions in the product stream were higher at low temperatures for each gas mixtures and decreased as the temperature increased. From the thermodynamic point of view, consumption of CO_2 becomes more significant and contributes to the formation of CO at higher temperatures.

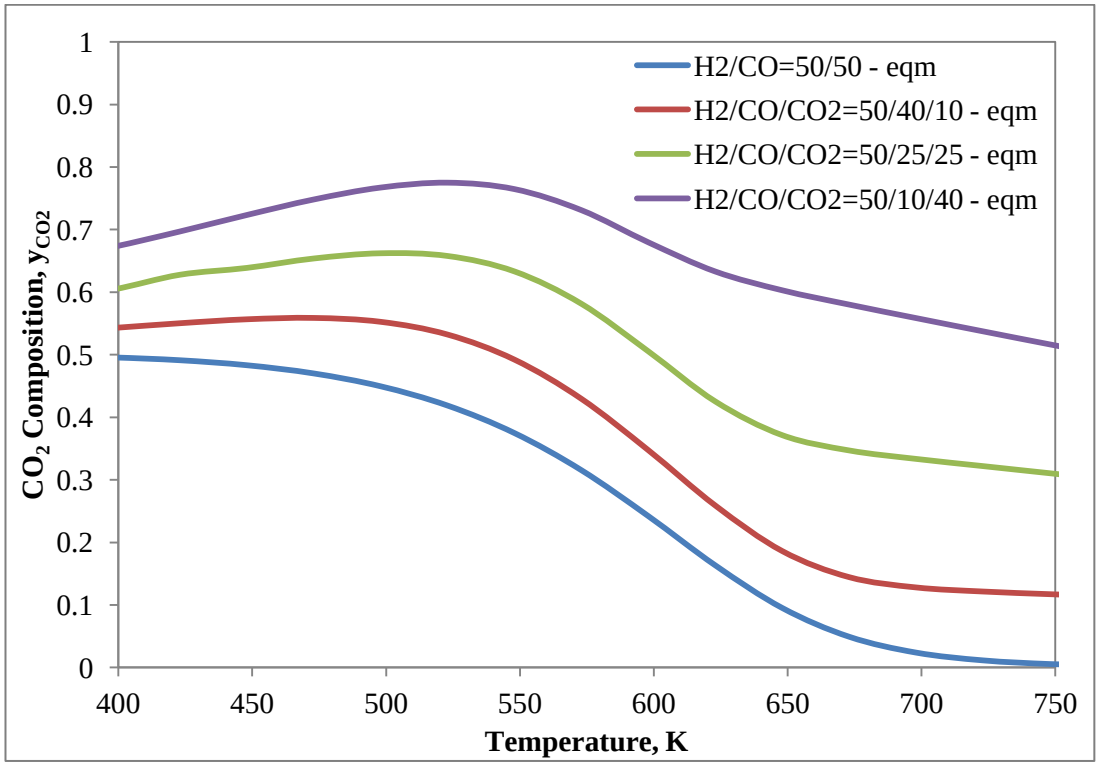

Figure 86. Equilibrium CO_2 compositions based on carbon containing species at different feed compositions

In Figure 87, equilibrium carbon monoxide compositions and the experimentally found results obtained over different catalysts were presented for the feed mixture of H_2/CO = 50/50 with respect to temperature, at 50 bar. As seen from this figure, carbon monoxide conversions obtained using catalyst mixtures containing MA and STA@MA were above the equilibrium compositions. This was an expected result. Since the CO conversions were small at low temperatures due to nature of the catalyst mixtures, more unconverted CO were present in the outlet stream. As reaction temperature was increased, more CO was consumed and its composition in the outlet stream decreased and approached to equilibrium as expected.

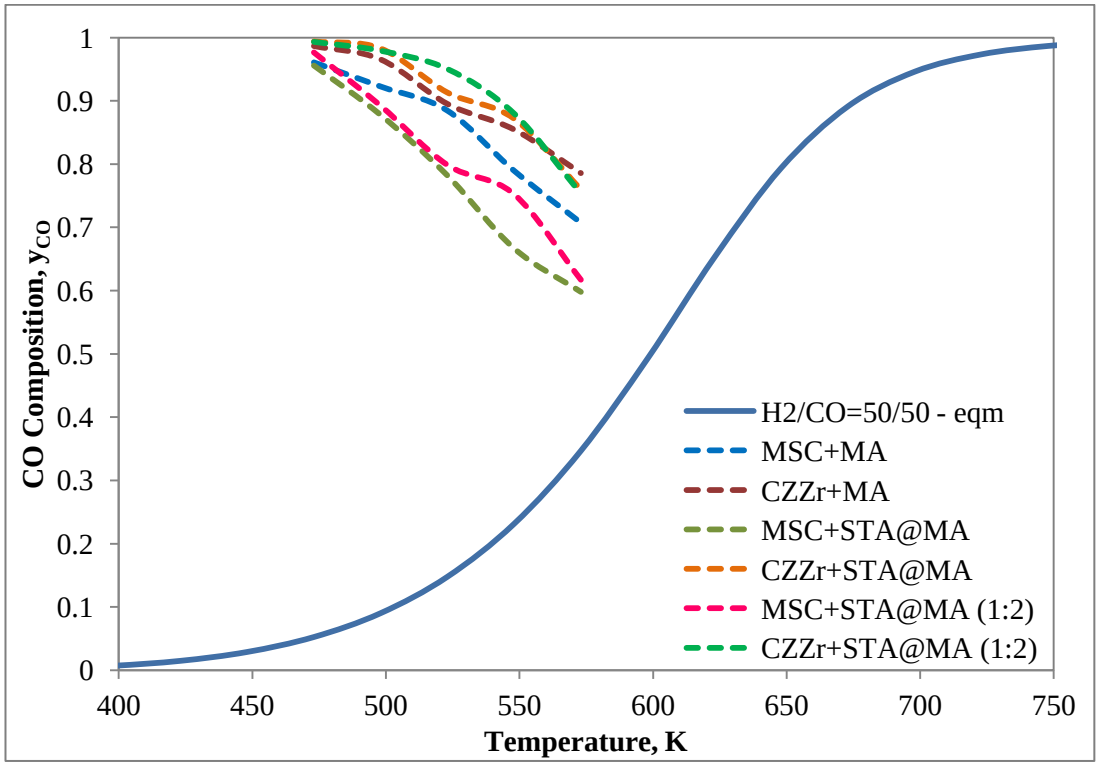

Figure 87. CO compositions of the equilibrium and reactions based on carbon containing species over different catalysts for feed mixture of H_2/CO = 50/50

In Figure 88, equilibrium carbon dioxide compositions and the experimental values obtained over different catalysts were presented for the feed mixture of H_2/CO = 50/50, with respect to temperature, at 50 bar. According to this figure, carbon dioxide conversions obtained using catalyst mixtures containing MA and STA@MA were all below the equilibrium conversions, which was also an expected result. Even though CO_2 was found to be secondary major product, the compositions were very small at low temperatures due to presence of significant amount of unconverted CO at the outlet. As the reaction temperature increased, more CO_2 was produced and CO conversion increased, therefore, CO_2 composition in the outlet stream increased towards equilibrium. Compositions of both CO and CO_2 obtained from experimental studies did not pass across their corresponding equilibrium values which indicated that the deduction were viable.

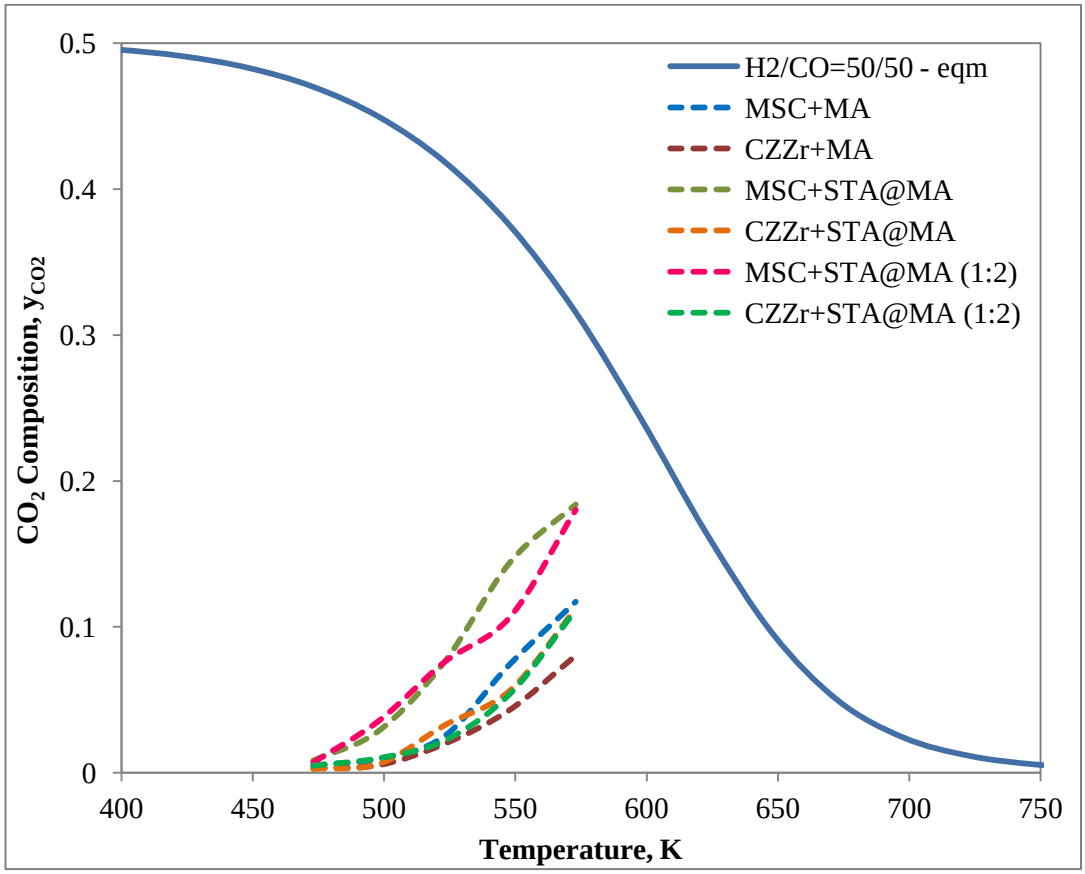

Figure 88. CO_2 compositions of the equilibrium and reactions based on carbon containing species over different catalysts for feed mixture of H_2/CO = 50/50

In Figure 89, equilibrium carbon monoxide compositions and the experimental values obtained over MSC + STA@MA catalyst mixtures were compared for different CO_2 content in feed mixture with respect to temperature, at 50 bar. According to this figure, carbon monoxide compositions obtained at each feed mixture composition were above their corresponding equilibrium values since carbon monoxide behaved as a product rather than a reactant at low temperatures. As the temperature increased, carbon monoxide conversion was increased and the composition in the outlet stream decreased and approached towards equilibrium compositions.

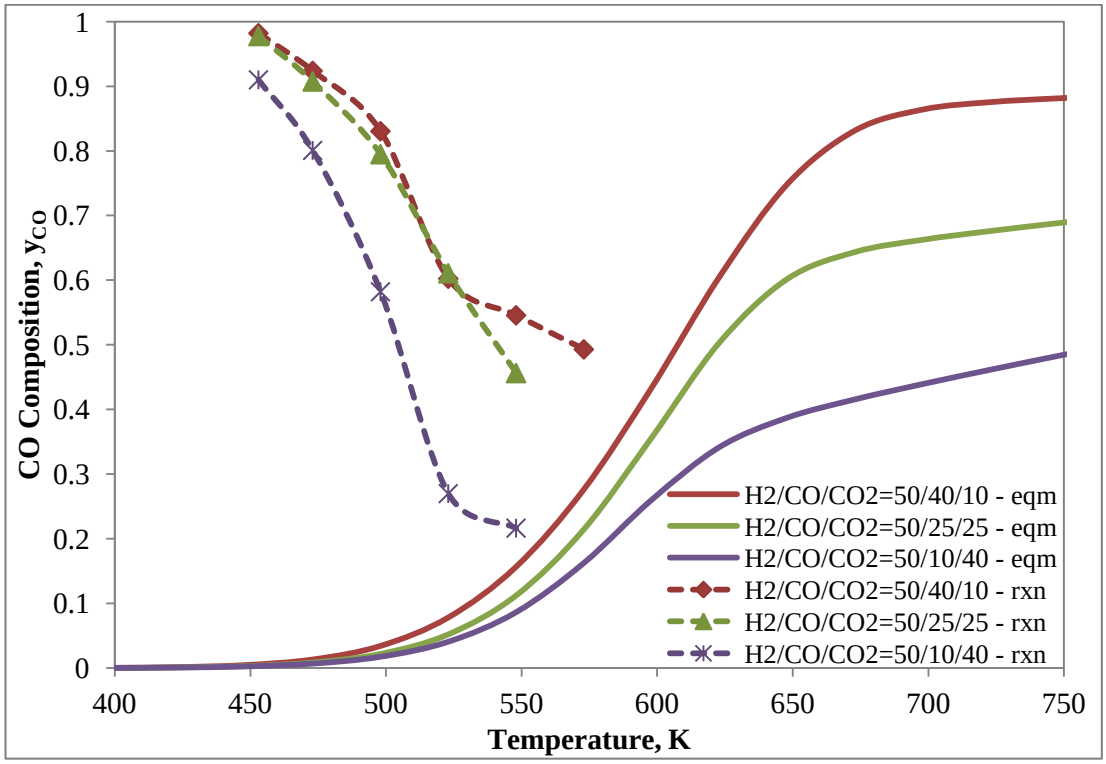

Figure 89. CO compositions of the equilibrium and reactions based on carbon containing species over MSC + STA@MA for different CO_2 content in feed mixture

In Figure 90, equilibrium carbon dioxide compositions and experimental values obtained over MSC + STA@MA catalyst mixtures were compared for different CO_2 content in feed mixture with respect to temperature, at 50 bar. Carbon dioxide compositions obtained at each feed mixture were below their corresponding equilibrium conversions. At lower temperatures, carbon dioxide conversions were almost complete and their compositions at the outlet were smaller. As the temperature increased, carbon dioxide conversion decreased and also its production decreased due to contribution of carbon monoxide hydrogenation. For the studies with varying CO_2 composition content in the feed, the compositions of both CO and CO_2 did not exceed their corresponding equilibrium values.

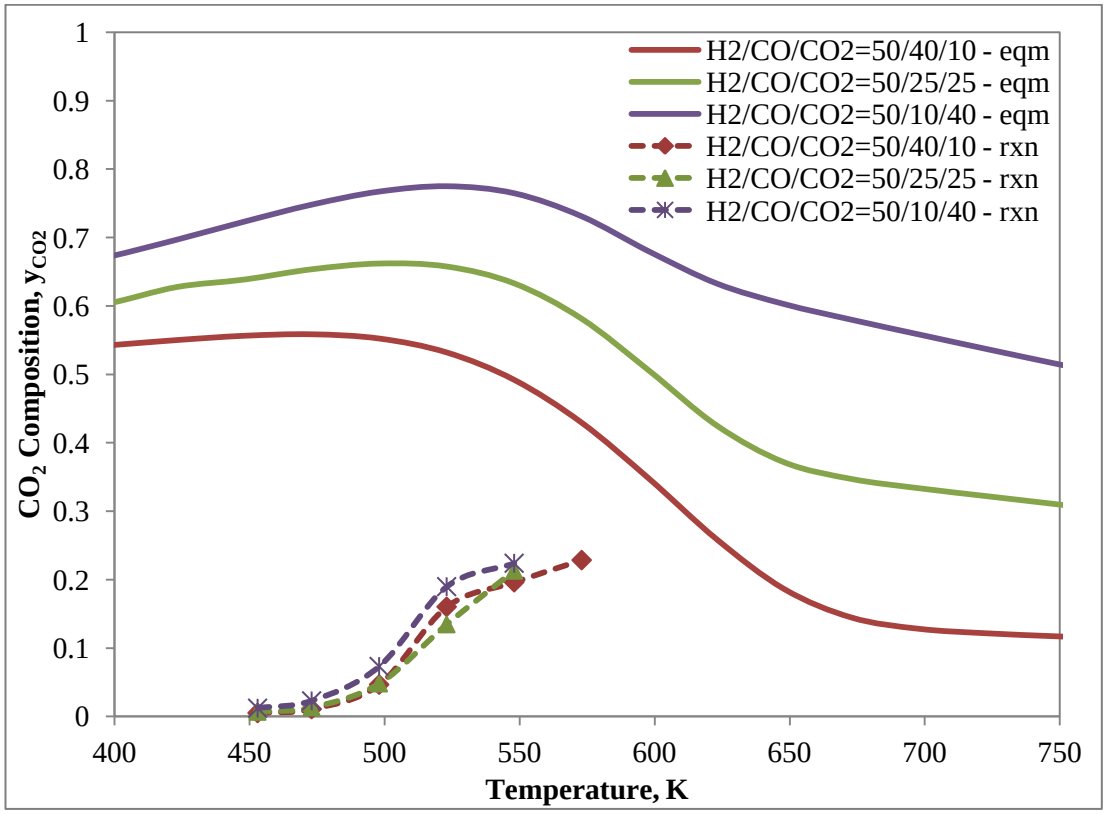

Figure 90. CO_2 compositions of the equilibrium and reactions based on carbon containing species over MSC + STA@MA for different CO_2 content in feed mixture

CHAPTER 10

CONCLUSIONS

In the first part of this study, different methanol synthesis catalysts were used as methanol synthesis function of the bifunctional catalyst mixture, while commercial γ-Al_2O_3 (TOYO) was used as methanol dehydration function. The promoters added on copper-zinc based methanol synthesis catalysts were Al (CZA), Zr (CZZr) and Ce (CZCe) and were aged for 3 hours, washed with cold water and calcined at 350^oC. These catalysts were mixed with commercial γ-Al_2O_3 for direct synthesis of DME from synthesis gas. The highest CO conversion was 15.6% at 300^oC and was achieved by using CZA + TOYO. As DME selectivities were compared, CZA + TOYO and CZZr + TOYO provided the highest selectivities of 68.8% and 66.4%, respectively at 200°C. DME selectivities decreased with increase in temperature, however CZZr + TOYO was observed to be more stable. Ceria promoter was not active for methanol synthesis and the overall direct synthesis of DME processes. Carbon monoxide and hydrogen was converted mostly to carbon dioxide and gave high ethanol yields. Basing on these results, it was concluded that zirconia promoted copper-zinc catalyst (CZZr) mixed with γ-Al_2O_3 (TOYO) was the best in direct DME synthesis from syngas.

6 hours-aged alumina promoted catalyst mixture provided the highest CO conversion, which was 21.5% at 300^oC as compared to 1 hour and 3 hours-aged catalysts. However, the highest DME selectivity was 57.7% for this catalyst at 200°C, which was lower than that of 3 hours-aged alumina promoted catalyst mixture. Bifunctional catalyst mixtures containing alumina promoter washed with hot water resulted in lower DME selectivity of 55.4% at 200°C as compared to cold

water-washed catalyst. Calcination of CZA at 550^{o}C was not beneficial for CO conversion and DME selectivity. Calcination at high temperatures caused partial sintering of copper and formation of larger clusters. The highest values for CO conversion and DME selectivity were smaller than that of obtained using CZA calcined at 350^{o}C. Reduction of CZA caused significant decrease in DME selectivity and promoted formation of byproducts, especially ethanol. Therefore, it was decided to select copper-zinc-zirconia catalyst calcined at 350^{o}C for the following studies, since it was more stable and presented good activity.

In the second part of the study, ordered mesoporous alumina (MA) was synthesized by EISA method. The characterization results indicated that mesoporous alumina was successfully synthesized by preserving the ordered mesoporous structure with very narrow and uniform pore size distribution. The synthesized mesoporous alumina calcined at 700^{o}C had the surface area of 323 m^2/g, with pore diameter of 5.7 nm and mesopore volume of 0.77 cc/g. Silicotungstic acid was impregnated on mesoporous alumina to improve acidic strength which resulted in decrease of surface area to 289 m^2/g, mesopore volume to 0.47 cc/g and pore diameter to 4.9 nm.

The synthesized mesoporous alumina was physically mixed with commercial methanol synthesis catalyst (MSC) and copper-zinc-zirconia catalyst (CZZr). Carbon monoxide conversion values obtained with MSC + MA and CZZr + MA increased with temperature and reached to 36.6% and 27.2% at 300^{o}C, respectively. Better performance of MSC + MA could be attributed to better dispersion of smaller CuO particle. Methanol and DME selectivities were obtained using MSC + MA as 80.1% and 7.8%, respectively at 200^{o}C. Using CZZr + MA, methanol and DME selectivities were 57.3% and 20.5%, respectively. The poor methanol dehydration activity of mesoporous alumina could be attributed to its low Lewis and Brønsted acidic strengths. However, as the temperature increased, methanol selectivity decreased, followed by increase in DME selectivity. This means that Lewis acid-base pairs could promote methanol dehydration to DME at high temperatures. Highest DME selectivities were obtained using MSC + MA and CZZr + MA as 55.8% and 52.4%, respectively at 300^{o}C. STA impregnation on MA (STA@MA) improved the activity

of MA. The highest carbon monoxide conversions were 49.4% and 31.0% for MSC + STA@MA and CZZr + STA@MA, respectively at 300^{o}C. Highest DME selectivities were 63.5% and 60.5% for MSC + STA@MA and CZZr + STA@MA, respectively at 275^{o}C. The catalyst weight ratio of methanol synthesis catalyst to STA@MA was increased from (1:1) to (1:2). The highest carbon monoxide conversions were obtained as 47.1% and 32.6% for MSC + STA@MA (1:2) and CZZr + STA@MA (1:2), respectively at 300^{o}C. Highest DME selectivities were 61.1% and 64.9% for MSC + STA@MA (1:2) and CZZr + STA@MA (1:2), respectively at 275^{o}C. The best bifunctional catalyst mixture was selected to be MSC + STA@MA with highest DME yield of 30.1% at 300^{o}C.

Mixing of MA with MSC or CZZr enhanced the carbon monoxide conversions significantly due to the synergetic effect obtained by the cooperation of methanol synthesis, dehydration and water-gas shift reactions. Therefore, the carbon monoxide conversions of MSC + MA and CZZr + MA reached to 36.6% and 27.2% at 300^{o}C, respectively while CO conversions for MSC and CZZr were only 13.1% and 10.9% at 300^{o}C, respectively.

In the third part of the study, different amounts of CO_2 were added to the feed gas in order to investigate the presence of CO_2 in the feed for direct synthesis of DME. The feed gas mixtures contained the volumetric ratios of H_2/CO/CO_2 = 50/40/10, 50/25/25 and 50/10/40 in these experiments. It was found that the presence of carbon dioxide mostly promoted reverse water-gas shift reaction at low temperatures, such as 180^{o}C and 200^{o}C. Carbon monoxide was produced more than it was consumed since carbon monoxide conversions were negative below 250^{o}C. CO conversions increased with temperature. The highest conversions were obtained as 53.4% at 300^{o}C and 39.4% at 275^{o}C, 43% at 275^{o}C for the feed gases containing 10%, 25% and 40% CO_2, respectively. For the feed gases containing 10% CO_2, methanol and DME selectivities were 74.9% and 25.1%, respectively at 180^{o}C. At low temperatures, DME was mostly produced via CO_2 hydrogenation. As the temperature increased, methanol selectivity decreased sharply and DME selectivity increased rapidly. Highest DME selectivity was achieved to 90% at 275^{o}C. The maximum

DME selectivities using the feed gases with CO_2 of 25% and 40% were achieved as 82.2% and 78.2%, respectively at 275^{o}C. These results indicated that feed gas mixture containing 10% of CO_2 was favorable for DME selectivity and could be considered as the best feed gas composition. Higher CO_2 content resulted in decrease in DME selectivity since reverse water-gas shift reaction was favored and unconsumed water inhibited the dehydration reaction followed by increase in methanol. In addition, presence of CO_2 in the feed gas inhibited formation of byproducts.

Thermodynamic analyses were performed for the studies conducted throughout this work. CO conversion values and experimental CO and CO_2 mol fractions were compared with the equilibrium values. None of the experimental values were found to exceed their corresponding equilibrium CO conversion, CO and CO_2 compositions, while equilibrium was approached at higher temperatures.

According to the data obtained throughout this work, MSC + STA@MA was recommended as the best bifunctional catalyst mixture for the direct synthesis of DME from syngas.

REFERENCES

[1] Tokay K.C., Dogu T., Dogu G., Dimethyl Ether Synthesis over Alumina Based Catalysts, Chemical Engineering Journal, 184: 278–285, 2012.

[2] Zha F., Ding J., Chang Y., Ding J., Wang J., Ma J., Cu-Zn-Al Oxide Cores Packed by Metal-Doped Amorphous Silica-Alumina Membrane for Catalyzing the Hydrogenation of Carbon Dioxide to Dimethyl Ether, Industrial & Engineering Chemistry Research, 51: 345–352, 2012.

[3] Naik S.P., Du H., Wan H., Bui V., Miller J.D., Zmierczak W.W., A Comparative Study of ZnO-CuO-Al_2O_3/SiO_2-Al_2O_3 Composite and Hybrid Catalysts for Direct Synthesis of Dimethyl Ether from Syngas, Industrial & Engineering Chemistry Research, 47: 9791–9794, 2008.

[4] Yoon E.S., Han C., A Review of Sustainable Energy - Recent Development and Future Prospects of Dimethyl Ether (DME), 10th International Symposium on Process Systems Engineering - PSE2009, 27: 169–175, 2009.

[5] Marchionna M., Patrini R., Sanfilippo D., Migliavacca G., Fundamental Investigations on Di-methyl Ether (DME) as LPG Substitute or Make-up for Domestic Uses, Fuel Processing Technology, 89: 1255–1261, 2008.

[6] Song J., Huang Z., Qiao X., Wang W., Performance of a Controllable Premixed Combustion Engine Fueled with Dimethyl Ether, Energy Conversion and Management, 45: 2223–2232, 2004.

[7] Semelsberger T.A., Borup R.L., Greene H.L., Dimethyl Ether (DME) as an Alternative Fuel, Journal of Power Sources, 156: 497–511, 2006.

[8] Fleisch T.H., Basu A., Gradassi M.J., Masin J.G., Dimethyl Ether: A Fuel for the 21st Century, Studies in Surface Science and Catalysis, 107: 117–125, 1998.

[9] Ereña J., Garoña R., Arandes J.M., Aguayo A.T., Bilbao J., Effect of Operating Conditions on the Synthesis of Dimethyl Ether over a CuO-ZnO-Al_2O_3/NaHZSM-5 Bifunctional Catalyst, Catalysis Today, 107-108: 467–473, 2005.

[10] Chen W.-H., Lin B.-J., Lee H.-M., Huang M.-H., One-Step Synthesis of Dimethyl Ether from the Gas Mixture Containing CO_2 with High Space Velocity, Applied Energy, 98: 92–101, July 2012.

[11] Celik G., Bi-Functional Nanostructured Novel Catalysts for Dimethyl Ether Synthesis, M. Sc. Thesis, Middle East Technical University, 2012.

[12] Ramos F.S., Duarte de Farias A.M., Borges L.E.P., Monteiro J.L., Fraga M.A., Sousa-Aguiar, E.F., Appel, L.G., Role of Dehydration Catalyst Acid Properties on One-Step DME Synthesis over Physical Mixtures, Catalysis Today, 101: 39–44, 2005.

[13] Arkharov A.M., Glukhov S.D., Grekhov L.V., Zherdev A.A., Ivashchenko N.A., Kalinin D.N., Use of Dimethyl Ether as a Motor Fuel and a Refrigerant, Chemical and Petroleum Engineering, 39: 330–336, 2003.

[14] Ahlgren S., Baky A., Bernesson S., Nordberg A., Noren O., Hansson P.A., Future Fuel Supply Systems for Organic Production based on Fischer-Tropsch Diesel and Dimethyl Ether from on-Farm-Grown Biomass, Bioprocess and Biosystems Engineering, 99: 145–155, 2008.

[15] Mollavali M., Yaripour F., Atashi H., Sahebdelfar S., Intrinsic Kinetics Study of Dimethyl Ether Synthesis from Methanol on γ-Al_2O_3 Catalysts, Industrial & Engineering Chemistry Research, 47: 3265–3273, 2008.

[16] Sierra I., Ereña J., Aguayo A.T., Arandes J.M., Bilbao J., Regeneration of CuO-ZnO-Al_2O_3/γ-Al_2O_3 Catalyst in the Direct Synthesis of Dimethyl Ether, Applied Catalysis B: Environmental, 94: 108–116, 2010.

[17] Pop G., Bozga G., Ganea R., Natu N., Methanol Conversion to Dimethyl Ether over H-SAPO-34 Catalyst, Industrial & Engineering Chemistry Research, 48: 7065–7071, 2009.

[18] Bonura G., Arena F., Mezzatesta G., Cannilla C., Spadaro L., Frusteri F., Role of the Ceria Promoter and Carrier on the Functionality of Cu-based Catalysts in the CO_2-to-Methanol Hydrogenation Reaction, Catalysis Today, 171: 251–256, 2011.

[19] An X., Zuo Y.-Z., Zhang Q., Wang D., Wang J.-F., Dimethyl Ether Synthesis from CO_2 Hydrogenation on a CuO-ZnO-Al_2O_3-ZrO_2/HZSM-5 Bifunctional Catalyst, Industrial & Engineering Chemistry Research, 47: 6547–6554, 2008.

[20] Yoo K.S., Kim J.-H., Park M.-J., Kim S.-J., Joo O.-S., Jung K.-D., Influence of Solid Acid Catalyst on DME Production Directly from Synthesis Gas over the Admixed Catalyst of Cu/ZnO/Al_2O_3 and Various SAPO Catalysts, Applied Catalysis A: General, 330: 57–62, 2007.

[21] Bae J.-W., Potdar H.S., Kang S.-H., Jun K.-W., Coproduction of Methanol and Dimethyl Ether from Biomass-Derived Syngas on a Cu-ZnO-Al_2O_3/γ-Al_2O_3 Hybrid Catalyst, Energy & Fuels, 22: 223–230, 2008.

[22] Flores J.H., Peixoto D.P.B., Appel L.G., de Avillez R.R., Pais da Silva M.I., The Influence of Different Methanol Synthesis Catalysts on Direct Synthesis of DME from Syngas, Catalysis Today, 172: 218–225, 2011.

[23] Ereña J., Sierra I., Olazar M., Gayubo A.G., Aguayo A.T., Deactivation of a CuO-ZnO-Al_2O_3/γ-Al_2O_3 Catalyst in the Synthesis of Dimethyl Ether, Industrial & Engineering Chemistry Research, 47: 2238–2247, 2008.

[24] Wang L., Fang D., Huang X., Zhang S., Qi Y., Liu Z., Influence of Reaction Conditions on Methanol Synthesis and WGS Reaction in the Syngas-to-DME Process, Journal of Natural Gas Chemistry, 15: 38–44, 2006.

[25] Zhang Y., Fei J., Yu Y., Zheng X., Methanol Synthesis from CO_2 Hydrogenation over Cu Based Catalyst Supported on Zirconia Modified γ-Al_2O_3, Energy Conversion and Management, 47: 3360–3367, 2006.

[26] Ogawa T., Inoue N., Shikada T., Inokoshi O., Ohno Y., Direct Dimethyl Ether (DME) Synthesis from Natural Gas, Studies in Surface Science and Catalysis, 147: 379–384, 2004.

[27] Lu W.-Z., Teng L.-H., Xiao W.-D., Theoretical Analysis of Fluidized-Bed Reactor for Dimethyl Ether Synthesis from Syngas, International Journal of Chemical Reactor Engineering, Note S2, 2003.

[28] García-Trenco A., Martínez A., Direct Synthesis of DME from Syngas on Hybrid CuZnAl/ZSM-5 Catalysts: New Insights into the Role of Zeolite Acidity, Applied Catalysis A: General, 411-412: 170–179, 2012.

[29] Moradi G., Ahmadpour J., Nazari M., Yaripour F., Effects of Feed Composition and Space Velocity on Direct Synthesis of Dimethyl Ether from Syngas, Industrial & Engineering Chemistry Research, 47: 7672–7679, 2008.

[30] Peng X.D., Wang A.W., Toseland B.A., Tijm P.J.A., Single-Step Syngas-to-Dimethyl Ether Processes for Optimal Productivity, Minimal Emissions, and Natural Gas-Derived Syngas, Industrial & Engineering Chemistry Research, 38: 4381–4388, 1999.

[31] Mao D., Yang W., Xia J., Zhang B., Song Q., Chen Q., Highly Effective Hybrid Catalyst for the Direct Synthesis of Dimethyl Ether from Syngas with Magnesium Oxide-Modified HZSM-5 as a Dehydration Component, Journal of Catalysis, 230: 140–149, 2005.

[32] Pontzen F., Liebner W., Gronemann V., Rothaemel M., Ahlers B., CO_2-Based Methanol and DME-Efficient Technologies for Industrial Scale Production, Catalysis Today, 171: 242–250, 2011.

[33] Naik S.P., Ryu T., Bui V., Miller J.D., Drinnan N.B., Zmierczak W., Synthesis of DME from CO_2/H_2 Gas Mixture, Chemical Engineering Journal, 167: 362–368, 2011.

[34] Inui T., Hara H., Takeguchi T., Kim J.-B., Structure and Function of Cu-Based Composite Catalysts for Highly Effective Synthesis of Methanol by Hydrogenation of CO_2 and CO, Catalysis Today, 36: 25–32, 1997.

[35] Sloczynski J., Grabowski R., Olszewski P., Kozlowska A., Stoch J., Lachowska M., Skrzypek J., Effect of Metal Oxide Additives on the Activity and Stability of $Cu/ZnO/ZrO_2$ Catalysts in the Synthesis of Methanol from CO_2 and H_2, Applied Catalysis A: General, 310: 127–137, 2006.

[36] Zhang Q., Zuo Y.-Z., Han M.-H., Wang J.-F., Jin Y., Wei F., Long Carbon Nanotubes Intercrossed Cu/Zn/Al/Zr Catalyst for CO/CO_2 Hydrogenation to Methanol/Dimethyl Ether, Catalysis Today, 150: 55–60, 2010.

[37] Sierra I., Ereña J., Aguayo A.T., Olazar M., Bilbao J., Deactivation Kinetics for Direct Dimethyl Ether Synthesis on a $CuO\text{-}ZnO\text{-}Al_2O_3/\gamma\text{-}Al_2O_3$ Catalyst, Industrial & Engineering Chemistry Research, 49: 481–489, 2010.

[38] Liu X.-M., Lu G.Q., Yan Z.-F., Beltramini J., Recent Advances in Catalysts for Methanol Synthesis via Hydrogenation of CO and CO_2, Industrial & Engineering Chemistry Research, 42: 6518–6530, 2003.

[39] Kim J.-H., Park M.J., Kim S.J., Joo O.-S., Jung K.-D., DME Synthesis from Synthesis Gas on the Admixed Catalysts of $Cu/ZnO/Al_2O_3$ and ZSM-5, Applied Catalysis A: General, 264: 37–41, 2004.

[40] Nie R., Lei H., Pan S., Wang L., Fei J., Hou Z., Core-Shell Structured CuO-ZnO@H-ZSM-5 Catalysts for CO Hydrogenation to Dimethyl Ether, Fuel, 96: 419–425, 2012.

[41] Fei J., Hou Z., Zhu B., Lou H., Zheng X., Synthesis of Dimethyl Ether (DME) on Modified HY Zeolite and Modified HY Zeolite-supported Cu-Mn-Zn Catalysts, Applied Catalysis A: General, 304: 49–54, 2006.

[42] Sofianos A.C., Scurrell M.S., Conversion of Synthesis Gas to Dimethyl Ether over Bifunctional Catalytic Systems, Industrial & Engineering Chemistry Research, 30: 2372–2378, 1991.

[43] Mao D., Yang W., Xia J., Zhang B., Lu G., The Direct Synthesis of Dimethyl Ether from Syngas over Hybrid Catalysts with Sulfate-modified γ-Alumina as Methanol Dehydration Components, Journal of Molecular Catalysis A: Chemical, 250: 138–144, 2006.

[44] Jiang H., Bongard H., Schmidt W., Schüth F., One-pot Synthesis of Mesoporous Cu-γ-Al_2O_3 as Bifunctional Catalyst for Direct Dimethyl Ether Synthesis, Microporous Mesoporous Materials, 164: 3–8, 2012.

[45] Phan X.K., Bakhtiary-Davijany H., Myrstad R., Pfeifer P., Venvik H.J., Holmen A., Preparation and Performance of Cu-based Monoliths for Methanol Synthesis, Applied Catalysis A: General, 405: 1–7, 2011.

[46] Lim H.-W., Park M.-J., Kang S.-H, Chae H.-J., Bae J.W., Jun K.-W., Modeling of the Kinetics for Methanol Synthesis Using Cu/ZnO/Al_2O_3/ZrO_2 Catalyst: Influence of Carbon Dioxide during Hydrogenation, Industrial & Engineering Chemistry Research, 48: 10448–10455, 2009.

[47] Rase H.F., Handbook of Commercial Catalysts: Heterogeneous Catalysts, CRC Press, 428–437, 2000.

[48] Baltes C., Vukojevic S., Schüth F., Correlations Between Synthesis, Precursor, and Catalyst Structure and Activity of a Large Set of CuO/ZnO/Al_2O_3 Catalysts for Methanol Synthesis, Journal of the American Chemical Society, 258: 334–344, 2008.

[49] Hassanpour S., Taghizadeh M., Yaripour F., Preparation, Characterization and Activity Evaluation of H-ZSM-5 Catalysts in Vapor-Phase Methanol Dehydration to Dimethyl Ether, Industrial & Engineering Chemistry Research, 49: 4063–4069, 2010.

[50] Ciftci A., Varisli D., Tokay K.C., Sezgi N.A., Dogu T., Dimethyl Ether, Diethyl Ether & Ethylene from Alcohols over Tungstophosphoric Acid based Mesoporous Catalysts, Chemical Engineering Journal, 207-208: 85–93, 2012.

[51] Ciftci A., Varisli D., Dogu T., Dimethyl Ether Synthesis over Novel Silicotungstic Acid Incorporated Nanostructured Catalysts, International Journal of Chemical Reactor Engineering, 8: Article A45, 2010.

[52] Ciftci A., Sezgi N.A., Dogu T., Nafion-Incorporated Silicate Structured Nanocomposite Mesoporous Catalysts for Dimethyl Ether Synthesis, Industrial & Engineering Chemistry Research, 49: 6753–6762, 2010.

[53] Xu M., Lunsford J.H., Goodman D.W., Bhattacharyya A., Synthesis of Dimethyl Ether (DME) from Methanol over Solid-Acid Catalysts, Applied Catalysis A: General, 149: 289–301, 1997.

[54] Jin D., Zhu B., Hou Z., Fei J., Lou H., Zheng X., Dimethyl Ether Synthesis via Methanol and Syngas over Rare Earth Metals Modified Zeolite Y and Dual Cu-Mn-Zn Catalysts, Fuel, 86: 2707–2713, 2007.

[55] Varisli D., Dogu T., Dogu G., Silicotungstic Acid Impregnated MCM-41-like Mesoporous Solid Acid Catalysts for Dehydration of Ethanol, Industrial & Engineering Chemistry Research, 47: 4071–4076, 2008.

[56] Blaszkowski S.R., van Santen R.A., The Mechanism of Dimethyl Ether Formation from Methanol Catalyzed by Zeolitic Protons, Journal of the American Chemical Society, 118: 5152–5153, 1996.

[57] Kubelkova L., Novakova J., Nedomova K., Reactivity of Surface Species on Zeolites in Methanol Conversion, Journal of Catalysis, 124: 441–450, 1990.

[58] Bandiera J., Naccache C., Kinetics of Methanol Dehydration on Dealuminated H-mordenite- Model with Acid and Basic Active Centers, Applied Catalysis, 69: 139–148, 1991.

[59] Yaripour F., Baghaei F., Schmidt I., Perregaard J., Catalytic Dehydration of Methanol to Dimethyl Ether (DME) over Solid-Acid Catalysts, Chemical Communications, 6: 147–152, 2005.

[60] Vishwanathan V., Jun K.-W., Kim J.-W., Roh H.-S., Vapour Phase Dehydration of Crude Methanol to Dimethyl Ether over Na-Modified H-ZSM-5 Catalysts, Applied Catalysis A: General, 276: 251–255, 2004.

[61] Mao D., Xia J., Zhang B., Lu G., Highly Efficient Synthesis of Dimethyl Ether from Syngas over the Admixed Catalyst of CuO-ZnO-Al_2O_3 and Antimony Oxide Modified HZSM-5 Zeolite, Energy Conversion and Management, 51: 1134–1139, 2010.

[62] Varisli D., Tokay K.C., Ciftci A., Dogu T., Dogu G., Methanol Dehydration Reaction to Produce Clean Diesel Alternative Dimethylether over Mesoporous Aluminosilicate-based Catalysts, Turkish Journal of Chemistry, 33: 355–366, 2009.

[63] Haber J., Pamin L., Matachowski L., Napruszewska B., Poltowicz J., Potassium and Silver Salts of Tungstophosphoric Acid as Catalysts in Dehydration of Ethanol and Hydration of Ethylene, Journal of Catalysis, 207: 296–306, 2002.

[64] Ciftci A., Nanocomposite Nafion and Heteropolyacid Incorporated Mesoporous Catalysts for Dimethyl Ether Synthesis from Methanol, M. Sc. Thesis, Middle East Technical University, 2009.

[65] Wang Y., Liu J., Wenzhao L., Synthesis of 2-Butoxy Ethanol with Narrow-range Distribution Catalyzed by Supported Heteropolyacids, Journal of Molecular Catalysis A: Chemical, 159: 71–75, 2000.

[66] Verhoef M.J., Kooyman P.J., Peters J.A., Bekkum H., A Study on the Stability of MCM-41 Supported Heteropoly Acids under Liquid and Gas Phase Esterification Conditions, Microporous Mesoporous Materials, 27: 365–371, 1999.

[67] Thomas A., Dablemont C., Basset J.M., Lefebvre F., Comparison of $H_3PW_{12}O_{40}$ and $H_4SiW_{12}O_{40}$ Heteropolyacids Supported on Silica by 1H MAS NMR, Comptes Rendus Chimie, 8: 1969–1974, 2005.

[68] Obalı Z., Heteropolyacid Catalysts for Etherification of Isoolefins, M. Sc. Thesis, Middle East Technical University, 2003.

[69] Varisli D., Dogu T., Dogu G., Petrochemicals from Ethanol over a W–Si-based Nanocomposite Bidisperse Solid Acid Catalyst, Chemical Engineering Science, 65: 153–159, 2010.

[70] Sandler S.I., Chemical and Engineering Thermodynamics, 3th Ed., Wiley, New York, 1999.

[71] Yuan Q., Yin A.-X., Luo C., Sun L.-D., Zhang Y.-W., Duan W.-T., Liu H.-C., Yan C.-H., Facile Synthesis for Ordered Mesoporous gamma-Aluminas with High Thermal Stability, Journal of the American Chemical Society, 130: 3465–3472, 2008.

[72] Oye G., Sjöblom J., Stöcker M., Synthesis, Characterization and Potential Applications of New Materials in the Mesoporous Range, Advances in Colloid and Interface Science, 89-90: 439–466, 2001.

[73] Corma A., From Microporous to Mesoporous Molecular Sieve Materials and Their Use in Catalysis, Chemical Reviews, 97: 2373–2419, 1997.

[74] Hartmann S., Sachse A., Galarneau A., Challenges and Strategies in the Synthesis of Mesoporous Alumina Powders and Hierarchical Alumina Monoliths, Materials, 5: 336–349, 2012.

[75] Márquez-Alvarez C., Žilková N., Pérez-Pariente J., Čejka J., Synthesis, Characterization and Catalytic Applications of Organized Mesoporous Aluminas, Catalysis Reviews Science and Engineering, 50: 222–286, 2008.

[76] Pal N., Bhaumik A., Soft Templating Strategies for the Synthesis of Mesoporous Materials: Inorganic, Organic-Inorganic Hybrid and Purely Organic Solids, Advances in Colloid and Interface Science, 189-190: 21–41, 2013.

[77] Morris S.M., Fulvio P.F., Jaroniec M., Ordered Mesoporous Alumina-Supported Metal Oxides, Journal of the American Chemical Society, 130: 15210–15216, 2008.

[78] Lesaint C., Kleppa G., Arla D., Glomm W.R., Øye G., Synthesis and Characterization of Mesoporous Alumina Materials with Large Pore Size Prepared by a Double Hydrolysis Route, Microporous Mesoporous Materials, 119: 245–251, 2009.

[79] Zhang Z., Pinnavaia T.J., Mesostructured gamma-Al_2O_3 with a Lathlike Framework Morphology, Journal of the American Chemical Society, 124: 12294–12301, 2002.

[80] Tian B., Yang H., Liu X., Xie S., Yu C., Fan J., Tu B., Zhao D., Fast Preparation of Highly Ordered Nonsiliceous Mesoporous Materials via Mixed Inorganic Precursors, Chemical Communications (Cambridge, England), 1824–1825, 2002.

[81] Niesz K., Yang P., Somorjai G.A., Sol-gel Synthesis of Ordered Mesoporous Alumina, Chemical Communications (Cambridge, England), 1986–1987, 2005.

[82] Kuemmel M., Grosso D., Boissière C., Smarsly B., Brezesinski T., Albouy P.A, Amenitsch H., Sanchez C., Thermally Stable Nanocrystalline gamma-Alumina Layers with Highly Ordered 3D Mesoporosity, Angewandte Chemie International Edition, 44: 4589–4592, 2005.

[83] Brinker J.C., Lu Y., Sellinger A., Fan H., Evaporation-Induced Self-Assembly: Nanostructures Made Easy, Advanced Materials, 11: 579–585, 1999.

[84] Yang P., Zhao D., Margolese D.I., Chmelka B.F., Stucky G.D., Generalized Syntheses of Large-Pore Mesoporous Metal Oxides with Semicrystalline Frameworks, Nature, 396: 152–155, 1998.

[85] Celik G., Arinan A., Bayat A., Ozbelge H.O., Dogu,T., Varisli D., Performance of Silicotungstic Acid Incorporated Mesoporous Catalyst in Direct Synthesis of Dimethyl Ether from Syngas in the Presence and Absence of CO_2, Topics in Catalysis, 56: 1764–1774, 2013.

[86] Chinchen G.C., Denny P.J., Parker D.G., Spencer M.S., Whan D.A., Mechanism of Methanol Synthesis from $CO/CO/H_2$ Mixtures over Copper/Zinc Oxide/ Alumina Catalysts: Use of 14C-Labelled Reactants, Applied Catalysis, 30: 333–338, 2004.

[87] Vanden Bussche K.M., Froment G.F., A Steady-State Kinetic Model for Methanol Synthesis and the Water Gas Shift Reaction on a Commercial $Cu/ZnO/Al_2O_3$ Catalyst, Journal of Catalysis, 10: 1–10, 1996.

[88] Ng K.L., Chadwick D., Toseland B.A., Kinetics and Modelling of Dimethyl Ether Synthesis from Synthesis Gas, Chemical Engineering Science, 54: 3587–3592, 1999.

[89] Pan L., Zhang Z., Preparation, Electrocatalytic and Photocatalytic Performances of Nanoscaled CuO/Co_3O_4 Composite Oxides, Journal of Materials Science: Materials in Electronics, 21:1262–1269, 2010.

[90] Xu Z., Hwang J.-Y., Li B., Huang X., Wang H., The Characterization of Various ZnO Nanostructures Using Field-Emission SEM, Journal of Operations Management: 29-32, 2008.

APPENDIX A

FUGACITY COEFFICIENTS OF THE SPECIES INVOLVED IN METHANOL AND DME SYNTHESES

Fugacity coefficients of the species involved in methanol and DME syntheses were calculated by Peng Robinson equation of state given in Equation A1.

$$P = \frac{R * T}{V - b} - \frac{a}{V(V + b) + b(V - b)} \quad [A1]$$

where

$$a = ac * \propto \quad [A2]$$

$$b = \frac{0.0778 * R * T_C}{P_C} \quad [A3]$$

$$ac = \frac{0.457235 * R^2 * {T_C}^2}{P_C} \quad [A4]$$

$$bc = \frac{0.077796 * R * T_C}{P_C} \quad [A5]$$

$$\propto = \left(1 + \kappa * (1 - Tr^{0,5})\right)^2 \quad [A6]$$

$$\kappa = 0.37464 + 1.54226w - 0.26992w^2 \quad [A7]$$

$$Tr = \frac{T}{Tc} \quad [A8]$$

$$\mathcal{A} = \frac{a * P}{R^2 * T^2} \quad [A9]$$

$$\mathcal{B} = \frac{b * P}{R * T} \qquad \text{[A10]}$$

Then, Peng Robinson equation of state can be written as in Equation A11.

$$Z^3 - (1 - \mathcal{B}) * Z^2 + (\mathcal{A} - 2 * \mathcal{B} - 3 * \mathcal{B}^2) * Z - (\mathcal{A} * \mathcal{B} - \mathcal{B}^2 - \mathcal{B}^3) = 0 \qquad \text{[A11]}$$

Equation A11 was derived from Peng Robinson equation of state as follows:

$$P = \frac{R * T}{V - b} - \frac{a}{V(V + b) + b(V - b)}$$

$$P = \frac{R * T}{V - b} - \frac{a}{V^2 + Vb + bV - b^2} = \frac{RT}{V - b} - \frac{a}{V^2 + 2Vb - b^2}$$

$$P = \frac{RT(V^2 + 2Vb - b^2) - a(V - b)}{V^3 + 2V^2b - Vb^2 - bV^2 - 2Vb^2 + b^3}$$

$$P = \frac{RTV^2 + 2VbRT - b^2RT - aV + ab}{V^3 + V^2b - 3Vb^2 + b^3} \qquad V = \frac{ZRT}{P}$$

$$P\left[\frac{Z^3R^3T^3}{P^3} + \frac{bZ^2R^2T^2}{P^2} - \frac{3ZRTb^2}{P} + b^3\right]$$
$$= RT\left(\frac{Z^2R^2T^2}{P^2}\right) + 2\left(\frac{ZRT}{P}\right)bRT - b^2RT - \frac{aZRT}{P} + ab$$

$$\frac{Z^3R^3T^3}{P^2} + \frac{bZ^2R^2T^2}{P} - 3ZRTb^2 + Pb^3$$
$$= \frac{Z^2R^3T^3}{P^2} + \frac{2ZR^2T^2b}{P} - b^2RT - \frac{aZRT}{P} + ab \qquad / \frac{R^3T^3}{P^2}$$

$$Z^3 + \frac{bZ^2P}{RT} - \frac{3Zb^2P^2}{R^2T^2} + \frac{P^3b^3}{R^3T^3} = Z^2 + \frac{2ZPb}{RT} - \frac{b^2P^2}{R^2T^2} - \frac{aZP}{R^2T^2} + \frac{abP^2}{R^3T^3}$$

$$Z^3 + Z^2\mathcal{B} - 3Z\mathcal{B}^2 + \mathcal{B}^3 = Z^2 + 2Z\mathcal{B} - \mathcal{B}^2 - Z\mathcal{A} + \mathcal{A}\mathcal{B}$$

$$Z^3 + Z^2\mathcal{B} - 3Z\mathcal{B}^2 + \mathcal{B}^3 - Z^2 - 2Z\mathcal{B} + \mathcal{B}^2 + Z\mathcal{A} - \mathcal{A}\mathcal{B} = 0$$

$$Z^3 + (\mathcal{B} - 1)Z^2 + (\mathcal{A} - 2\mathcal{B} - 3\mathcal{B}^2)Z + (\mathcal{B}^3 + \mathcal{B}^2 - \mathcal{A}\mathcal{B}) = 0$$

Finally,

$$Z^3 - (1 - \mathcal{B}) * Z^2 + (\mathcal{A} - 2 * \mathcal{B} - 3 * \mathcal{B}^2) * Z - (\mathcal{A} * \mathcal{B} - \mathcal{B}^2 - \mathcal{B}^3) = 0 \quad \text{[A11]}$$

Fugacity coefficient is given in Equation A12.

$$ln\phi_i = \frac{b_i}{b_m} * (Z - 1) - \ln(Z - \mathcal{B}) + \frac{\mathcal{A}}{2\sqrt{2} * \mathcal{B}} * \left(\frac{2 * \sum_k y_k * a_{ik}}{a_m} - \frac{b_i}{b_m}\right) * \ln\left(\frac{Z + \mathcal{B} * (1 - 2\sqrt{2})}{Z + \mathcal{B} * (1 + 2\sqrt{2})}\right) \quad \text{[A12]}$$

$$a_m = \sum_i \sum_j y_i y_j a_{ij} \quad \text{[A13]}$$

$$b_m = \sum_i y_i b_i \quad \text{[A14]}$$

Because all the components are taken as pure, so b_i/b_m term in Equation A12 is equal to 1. And also Equation A13, $a_m = a_m$ and $\sum_k y_k * a_{ik} = a_m$. Therefore,

$$\frac{2 * \sum_k y_k * a_{ik}}{a_m} = 2$$

$$\left(\frac{2 * \sum_k y_k * a_{ik}}{a_m} - \frac{b_i}{b_m}\right) = 2 - 1 = 1$$

Then, fugacity coefficient is simplified as in Equation A14.

$$ln\phi_i = \frac{b_i}{b_m} * (Z - 1) - \ln(Z - \mathcal{B}) + \frac{\mathcal{A}}{2\sqrt{2} * \mathcal{B}} * \ln\left(\frac{Z + \mathcal{B} * (1 - 2\sqrt{2})}{Z + \mathcal{B} * (1 + 2\sqrt{2})}\right) \quad \text{[A15]}$$

Fugacity coefficients of the species were calculated by Peng Robinson equation of state in the temperature range of 100-400°C and in the pressure range of 1-70 bar. Fugacity coefficients are presented in Tables 16-20.

Table 16. Fugacity coefficients of the species involved in methanol and DME syntheses calculated by Peng Robinson equation of state at 1 bar

T,°C	ϕ_{CO}	ϕ_{CO2}	ϕ_{H2}	ϕ_{DME}	ϕ_{H2O}	ϕ_{CH3OH}
100	1.000	0.997	1.000	0.991	0.991	0.988
125	1.000	0.998	1.000	0.993	0.993	0.990
150	1.000	0.998	1.000	0.994	0.994	0.992
175	1.000	0.999	1.000	0.995	0.995	0.993
200	1.000	0.999	1.000	0.996	0.996	0.994
225	1.000	0.999	1.000	0.996	0.996	0.995
250	1.000	0.999	1.000	0.997	0.997	0.996
275	1.000	0.999	1.000	0.997	0.997	0.997
300	1.000	1.000	1.000	0.998	0.997	0.997
325	1.000	1.000	1.000	0.998	0.998	0.998
350	1.000	1.000	1.000	0.998	0.998	0.998
375	1.000	1.000	1.000	0.999	0.998	0.998
400	1.000	1.000	1.000	0.999	0.998	0.999
425	1.000	1.000	1.000	0.999	0.999	0.999
450	1.000	1.000	1.000	0.999	0.999	0.999

Table 17. Fugacity coefficients of the species involved in methanol and DME syntheses calculated by Peng Robinson equation of state at 10 bar

T,°C	ϕ_{CO}	ϕ_{CO2}	ϕ_{H2}	ϕ_{DME}	ϕ_{H2O}	ϕ_{CH3OH}
100	1.000	0.974	1.003	1.001	0.914	0.883
125	1.001	0.979	1.003	1.001	0.928	0.904
150	1.002	0.983	1.003	1.001	0.939	0.921
175	1.002	0.987	1.003	1.001	0.948	0.934
200	1.003	0.989	1.003	1.001	0.955	0.945
225	1.003	0.992	1.003	1.001	0.962	0.954
250	1.003	0.994	1.003	1.001	0.967	0.962
275	1.003	0.995	1.003	1.001	0.971	0.968
300	1.003	0.996	1.003	1.001	0.975	0.973
325	1.003	0.997	1.002	1.000	0.978	0.977
350	1.003	0.998	1.002	1.000	0.981	0.981
375	1.003	0.999	1.002	1.000	0.983	0.984
400	1.003	0.999	1.002	1.000	0.985	0.987
425	1.003	1.000	1.002	1.000	0.987	0.989
450	1.003	1.000	1.002	1.000	0.988	0.991

Table 18. Fugacity coefficients of the species involved in methanol and DME syntheses calculated by Peng Robinson equation of state at 30 bar

T,°C	ϕ_{CO}	ϕ_{CO2}	ϕ_{H2}	ϕ_{DME}	ϕ_{H2O}	ϕ_{CH3OH}
100	1.000	0.923	1.009	1.003	0.736	0.134
125	1.003	0.939	1.009	1.003	0.782	0.268
150	1.005	0.951	1.009	1.003	0.817	0.764
175	1.007	0.961	1.009	1.002	0.845	0.806
200	1.008	0.969	1.008	1.002	0.867	0.839
225	1.009	0.976	1.008	1.002	0.886	0.866
250	1.009	0.981	1.008	1.002	0.901	0.887
275	1.010	0.985	1.008	1.002	0.914	0.905
300	1.010	0.989	1.008	1.002	0.925	0.920
325	1.010	0.992	1.007	1.001	0.934	0.933
350	1.010	0.995	1.007	1.001	0.942	0.944
375	1.010	0.997	1.007	1.001	0.949	0.953
400	1.010	0.998	1.007	1.001	0.955	0.960
425	1.010	1.000	1.007	1.001	0.960	0.967
450	1.010	1.001	1.007	1.001	0.965	0.973

Table 19. Fugacity coefficients of the species involved in methanol and DME syntheses calculated by Peng Robinson equation of state at 50 bar

T,°C	ϕ_{CO}	ϕ_{CO2}	ϕ_{H2}	ϕ_{DME}	ϕ_{H2O}	ϕ_{CH3OH}
100	1.002	0.875	1.015	0.508	0.018	0.083
125	1.006	0.901	1.015	0.663	0.043	0.166
150	1.009	0.921	1.015	0.725	0.676	0.294
175	1.012	0.937	1.014	0.772	0.737	0.474
200	1.014	0.950	1.014	0.809	0.778	0.733
225	1.015	0.961	1.014	0.839	0.810	0.779
250	1.016	0.969	1.013	0.864	0.836	0.816
275	1.017	0.977	1.013	0.885	0.858	0.845
300	1.017	0.982	1.013	0.903	0.876	0.870
325	1.017	0.987	1.012	0.918	0.891	0.891
350	1.017	0.991	1.012	0.931	0.905	0.908
375	1.018	0.995	1.012	0.941	0.916	0.923
400	1.017	0.998	1.012	0.951	0.926	0.936
425	1.017	1.000	1.011	0.959	0.935	0.946
450	1.017	1.002	1.011	0.966	0.942	0.956

Table 20. Fugacity coefficients of the species involved in methanol and DME syntheses calculated by Peng Robinson equation of state at 70 bar

T,ºC	ϕ_{CO}	ϕ_{CO2}	ϕ_{H2}	ϕ_{DME}	ϕ_{H2O}	ϕ_{CH3OH}
100	1.004	0.830	1.022	0.385	0.013	0.061
125	1.010	0.865	1.021	0.514	0.031	0.122
150	1.014	0.893	1.021	0.624	0.064	0.217
175	1.017	0.915	1.020	0.691	0.120	0.349
200	1.020	0.932	1.020	0.742	0.673	0.515
225	1.021	0.947	1.019	0.783	0.731	0.692
250	1.023	0.958	1.019	0.817	0.770	0.746
275	1.024	0.968	1.018	0.845	0.801	0.788
300	1.024	0.976	1.018	0.869	0.827	0.822
325	1.025	0.983	1.018	0.889	0.849	0.851
350	1.025	0.989	1.017	0.906	0.868	0.875
375	1.025	0.993	1.017	0.921	0.884	0.895
400	1.025	0.997	1.016	0.934	0.897	0.912
425	1.025	1.000	1.016	0.945	0.909	0.927
450	1.024	1.003	1.015	0.955	0.920	0.940

APPENDIX B

CONVERSION AND SELECTIVITY CALCULATIONS

In the activity tests, the gaseous species in the outlet stream of the reactor were analyzed with an online GC connected to experimental set-up. From GC analyses, the species detected in terms of peaks at different retention times, which were found by calibration. The related retention times and calibration factors which were obtained with respect to the reference calibration component; CO, are given in Tables 7 and 8. In this part, sample calculations for conversion and selectivity are presented for two different feed gas compositions.

B1. ACTIVITY RESULTS OF MSC + STA@MA WITH 50% H_2, 50% CO

Catalytic activity tests were performed in the temperature range of 200 to 300^{o}C with intervals of 25^{o}C. Steady state was reached in 60 minutes and afterwards three successive analyses were taken for each temperature and the averages of the results of these analyses were used for conversion and selectivity calculations and the results are given in Table 21.

Table 21. Average of the peak areas for each species obtained from GC analyses

T, ^{o}C	A_{CO}	A_{CH4}	A_{CO2}	A_{FA}	A_{MeOH}	A_{DME}	A_{EtOH}
200	368.70	0	3.84	0	7.60	6.42	0
225	361.91	0	14.25	0	18.48	25.92	0
250	339.26	0	39.66	0	18.43	73.15	0
275	295.13	0.32	76.92	0	10.51	140.04	0
300	270.61	1.74	100.27	1.11	8.66	164.13	1.36

The peak areas obtained from GC analyses were converted to the mole numbers by multiplying the peak areas with the calibration factors using equation B1.

$$n_i = A_i * \beta_i \quad [B1]$$

Sample calculations for 300^oC are given below and the calculated mole numbers at all temperatures were tabulated in Table 22.

$n_{CO} = A_{CO} \times \beta_{CO} = 270.61 \times 1.00 = 270.61$

$n_{CH_4} = A_{CH_4} \times \beta_{CH_4} = 1.74 \times 1.36 = 2.37$

$n_{CO_2} = A_{CO_2} \times \beta_{CO_2} = 100.27 \times 0.83 = 83.22$

$n_{FA} = A_{FA} \times \beta_{FA} = 1.11 \times 1.80 = 1.99$

$n_{MeOH} = A_{MEOH} \times \beta_{MEOH} = 8.66 \times 1.40 = 12.12$

$n_{DME} = A_{DME} \times \beta_{DME} = 164.13 \times 0.49 = 80.42$

$n_{EtOH} = A_{ETOH} \times \beta_{ETOH} = 1.36 \times 1.44 = 1.96$

Table 22. Mole numbers for each species obtained from GC analyses

T, ^oC	n_{CO}	n_{CH4}	n_{CO2}	n_{FA}	n_{MeOH}	n_{DME}	n_{EtOH}
200	368.70	0	3.19	0	10.64	3.15	0
225	361.91	0	11.83	0	25.87	12.70	0
250	339.26	0	32.92	0	25.80	35.84	0
275	295.13	0.43	63.84	0	14.71	68.62	0
300	270.61	2.37	83.22	1.99	12.12	80.42	1.96

The amount of CO that was fed to reactor ($n_{CO,0}$) is found from Equation B2 by performing a total carbon balance. The species CO, CH_4, CO_2, FA and methanol contain one carbon atom while DME and ethanol contain two carbon atoms. Therefore, mole numbers of DME and ethanol were multiplied by 2.

$$n_{CO,0} = n_{CO} + n_{CH_4} + n_{CO_2} + n_{FA} + n_{MeOH} + 2 * n_{DME} + 2 * n_{EtOH} \quad [B2]$$

CO conversion was defined as the ratio of the amount of CO reacted to the amount of CO fed to the system and expressed as in 6.1 and the equation for CO conversion is given with B3.

X = (Moles of CO fed to system – Moles of CO emerged from system) / Moles of CO fed to system [6.1]

$$X = \frac{n_{CO,0} - n_{CO}}{n_{CO,0}} \quad [B3]$$

Sample calculations for total numbers of CO fed to system and CO conversions at 300^{o}C are given below and the results for all temperatures were tabulated in Table 23.

$$n_{CO,0} = n_{CO} + n_{CH_4} + n_{CO_2} + n_{FA} + n_{MeOH} + 2 * n_{DME} + 2 * n_{EtOH}$$
$$= 270.61 + 2.37 + 83.22 + 1.99 + 12.12 + 2 * 80.42 + 2 * 1.96$$
$$= 535.07$$

$$X = \frac{535.07 - 270.61}{535.07} = 0.494$$

Table 23. Total numbers of CO fed to system and CO conversions

T, ^{o}C	**$n_{CO,0}$**	**X**
200	388.82	0.052
225	424.99	0.148
250	469.67	0.278
275	511.35	0.423
300	535.07	0.494

Product selectivities were defined as the ratio of moles of CO converted to a specific component to total moles of CO converted to the products. The selectivities of DME methanol and CO_2 were expressed as;

S_{DME} = 2(Moles of DME formed)/ (Moles of CO converted to products) 6.2.

S_{MEOH}= (Moles of MEOH formed)/ (Moles of CO converted to products) 6.3.

S_{CO_2} = (Moles of CO_2 formed)/ (Moles of CO converted to products) 6.4.

The equations for selectivities of DME methanol and CO_2 were expressed as;

$$S_{DME} = \frac{2 * n_{DME}}{n_{CO,0} - n_{CO}} \quad [B4]$$

$$S_{MEOH} = \frac{n_{MEOH}}{n_{CO,0} - n_{CO}} \quad [B5]$$

$$S_{CO_2} = \frac{n_{CO_2}}{n_{CO,0} - n_{CO}} \quad [B6]$$

Sample calculations for product selectivities at 300^{o}C are given below and the results for all temperatures were tabulated in Table 24.

$$S_{DME} = \frac{2 * n_{DME}}{n_{CO,0} - n_{CO}} = \frac{2 * 80.42}{535.07 - 270.61} = 0.608$$

$$S_{MEOH} = \frac{n_{MEOH}}{n_{CO,0} - n_{CO}} = \frac{12.12}{535.07 - 270.61} = 0.046$$

$$S_{CO_2} = \frac{n_{CO_2}}{n_{CO,0} - n_{CO}} = \frac{83.22}{535.07 - 270.61} = 0.315$$

Table 24. Product selectivities defined with respect to moles of CO converted to products

T, ^{o}C	S_{CH4}	S_{CO2}	S_{FA}	S_{MeOH}	S_{DME}	S_{EtOH}
200	0	0.158	0	0.529	0.313	0
225	0	0.187	0	0.410	0.403	0
250	0	0.252	0	0.198	0.550	0
275	0.002	0.295	0	0.068	0.635	0
300	0.009	0.315	0.008	0.046	0.608	0.015

Yields were calculated by multiplying the selectivity of any component with its conversion and can be expressed as the ratio of moles of desired product formed to moles of reactant fed to the system. The results for selectivity, conversion and yields of DME are given in Table 25.

$$Y = S \times X \quad [B7]$$

Table 25. The results for selectivity, conversion and yields of DME

T, ^{o}C	S_{DME}	X	Yield
200	0.313	0.052	0.016
225	0.403	0.148	0.060
250	0.550	0.278	0.153
275	0.635	0.423	0.268
300	0.608	0.494	0.301

B2. ACTIVITY RESULTS OF MSC + STA@MA WITH 50% H_2, 40% CO, 10%CO_2

Catalytic activity tests were performed in the temperature range of 180 to 300^{o}C with feed mixture of H_2/CO/CO_2 = 50/40/10. Steady state was reached in 60 minutes and afterwards three successive analyses were taken for each temperature and the averages of the results of these analyses were used for conversion and selectivity calculations and the results are given in Table 26.

Table 26. Average of the peak areas for each species obtained from GC analyses

T, ^{o}C	A_{CO}	A_{CH4}	A_{CO2}	A_{FA}	A_{MeOH}	A_{DME}	A_{EtOH}
180	337.09	0	2.14	0	2.69	1.29	0
200	332.62	0	4.76	0	14.18	7.45	0
225	316.15	0	21.41	0	20.11	37.99	0
250	249.43	0	80.00	0	20.72	141.47	0
275	218.94	0.55	94.89	0	12.98	172.81	0
300	200.32	2.23	111.91	1.17	10.49	186.77	1.26

The peak areas obtained from GC analyses were converted to the mole numbers by multiplying the peak areas with the calibration factors using equation B1.

$$n_i = A_i * \beta_i \qquad [B1]$$

Sample calculations for 300^{o}C are given below and the calculated mole numbers at all temperatures were tabulated in Table 27.

$n_{CO} = A_{CO} \times \beta_{CO} = 200.32 \times 1.00 = 200.32$

$n_{CH_4} = A_{CH_4} \times \beta_{CH_4} = 2.23 \times 1.36 = 3.03$

$n_{CO_2} = A_{CO_2} \times \beta_{CO_2} = 111.91 \times 0.83 = 92.89$

$n_{FA} = A_{FA} \times \beta_{FA} = 1.17 \times 1.80 = 2.11$

$n_{MeOH} = A_{MEOH} \times \beta_{MEOH} = 10.49 \times 1.40 = 14.69$

$n_{DME} = A_{DME} \times \beta_{DME} = 186.77 \times 0.49 = 91.52$

$n_{EtOH} = A_{ETOH} \times \beta_{ETOH} = 1.26 \times 1.44 = 1.81$

Table 27. Mole numbers for each species obtained from GC analyses

T, °C	n_{CO}	n_{CH4}	n_{CO2}	n_{FA}	n_{MeOH}	n_{DME}	n_{EtOH}
180	337.09	0	1.78	0	3.77	0.63	0
200	332.62	0	3.95	0	19.86	3.65	0
225	316.15	0	17.77	0	28.16	18.62	0
250	249.43	0	66.40	0	29.01	69.32	0
275	218.94	0.75	78.75	0	18.17	84.68	0
300	200.32	3.03	92.89	2.11	14.69	91.52	1.81

The inlet amount of carbon that was fed to reactor ($n_{C,0}$) is found from Equation B8 by performing a total carbon balance. The species CO, CH_4, CO_2, FA and methanol contain one carbon atom while DME and ethanol contain two carbon atoms. Therefore, mole numbers of DME and ethanol were multiplied by 2.

$$n_{C,0} = n_{CO} + n_{CH_4} + n_{CO_2} + n_{FA} + n_{MeOH} + 2 * n_{DME} + 2 * n_{EtOH} \quad [B8]$$

The feed composition was adjusted on volume basis; therefore the feed composition is converted to mole basis as follows:

$$\dot{n}_{CO} = Q_{CO} * \rho_{CO} * \frac{1}{MW_{CO}} \quad [B9]$$

$$\dot{n}_{CO_2} = Q_{CO_2} * \rho_{CO_2} * \frac{1}{MW_{CO_2}} \quad [B10]$$

$$y_{CO} = \frac{\dot{n}_{CO}}{\dot{n}_{CO} + \dot{n}_{CO_2}} \quad [B11]$$

$$y_{CO_2} = \frac{\dot{n}_{CO_2}}{\dot{n}_{CO} + \dot{n}_{CO_2}} \quad [B12]$$

$$n_{CO,0} = n_{C,0} * y_{CO} \quad [B13]$$

$$n_{CO_2,0} = n_{C,0} * y_{CO_2} \quad [B14]$$

CO conversion was defined as the ratio of the amount of CO reacted to the amount of CO fed to the system and expressed as in Equation 6.1 and the equation for CO conversion is given with B3.

X = (Moles of CO fed to system – Moles of CO emerged from system) / Moles of CO fed to system [6.1]

$$X_{CO} = \frac{n_{CO,0} - n_{CO}}{n_{CO,0}} \quad [B3]$$

Similarly, CO_2 conversion was defined as the ratio of the amount of CO_2 reacted to the amount of CO_2 fed to system and expressed as in Equation 6.6 and the equation for CO_2 conversion is given with B15.

X_{CO_2} = (Moles of CO_2 fed to system – Moles of CO_2 emerged from system)/ Moles of CO_2 fed to system [6.6]

$$X_{CO_2} = \frac{n_{CO_2,0} - n_{CO_2}}{n_{CO_2,0}} \quad [B15]$$

Sample calculations for inlet amount of carbon that was fed to reactor and CO and CO_2 conversions at 300^{o}C are given below and the results for all temperatures were tabulated in Table 28.

$$n_{C,0} = n_{CO} + n_{CH_4} + n_{CO_2} + n_{FA} + n_{MeOH} + 2 * n_{DME} + 2 * n_{EtOH}$$
$$= 200.32 + 3.03 + 92.89 + 2.11 + 14.69 + 2 * 91.52 + 2 * 1.81$$
$$= 499.71$$

Total flow rate = 25cc/min

Feed composition: $H_2/CO/CO_2 = 50/40/10$

$$Q_{CO} = 25\ cc/min * 0.4 = 10\ cc/min$$

$$Q_{CO_2} = 25\ cc/min * 0.1 = 2.5\ cc/min$$

$$\dot{n}_{CO} = Q_{CO} * \rho_{CO} * \frac{1}{MW_{CO}}$$
$$= 10\frac{cc}{min} * 67.79\frac{kg}{m^3} * \frac{1}{28\,g/mol} * \frac{1000g}{kg} * \frac{1m^3}{1000L} * \frac{1L}{1000mL}$$
$$= 0.024\frac{mol}{min}$$

$$\dot{n}_{CO_2} = Q_{CO_2} * \rho_{CO_2} * \frac{1}{MW_{CO_2}}$$
$$= 2.5\frac{cc}{min} * 69.07\frac{kg}{m^3} * \frac{1}{44\,g/mol} * \frac{1000g}{kg} * \frac{1m^3}{1000L} * \frac{1L}{1000mL}$$
$$= 0.004\frac{mol}{min}$$

$$y_{CO} = \frac{\dot{n}_{CO}}{\dot{n}_{CO} + \dot{n}_{CO_2}} = \frac{0.024}{0.024 + 0.004} = 0.86$$

$$y_{CO_2} = \frac{\dot{n}_{CO_2}}{\dot{n}_{CO} + \dot{n}_{CO_2}} = \frac{0.004}{0.024 + 0.004} = 0.014$$

$$n_{CO,0} = n_{C,0} * y_{CO} = 499.71 * 0.86 = 429.75$$

$$n_{CO_2,0} = n_{C,0} * y_{CO_2} = 499.71 * 0.14 = 69.96$$

$$X_{CO} = \frac{n_{CO,0} - n_{CO}}{n_{CO,0}} = \frac{429.75 - 200.32}{429.75} = 0.534$$

$$X_{CO_2} = \frac{n_{CO_2,0} - n_{CO_2}}{n_{CO_2,0}} = \frac{69.96 - 92.89}{69.96} = -0.33$$

Table 28. The total amount of carbon, CO and CO_2 fed to reactor and CO and CO_2 conversions

T, °C	$\mathbf{n_{C,0}}$	$\mathbf{n_{CO,0}}$	$\mathbf{n_{CO_2,0}}$	$\mathbf{n_{CO}}$	$\mathbf{n_{CO_2}}$	$\mathbf{X_{CO}}$	$\mathbf{X_{CO_2}}$
180	343.91	295.76	48.15	337.09	1.78	-0.14	0.96
200	363.72	312.80	50.92	332.62	3.95	-0.06	0.92
225	399.30	343.40	55.90	316.15	17.77	0.08	0.68
250	483.48	415.79	67.69	249.43	66.40	0.40	0.02
275	485.97	417.93	68.04	218.94	78.75	0.48	-0.16
300	499.71	429.75	69.96	200.32	92.89	0.53	-0.33

Product selectivities were defined as the ratio of moles of CO converted to a specific component to total moles of CO converted to the products. The selectivities of DME and CO_2 were expressed as;

S_{DME} = 2(Moles of DME formed)/ (Moles of CO converted to products) 6.2.

S_{CO_2} = (Moles of CO_2 formed)/ (Moles of CO converted to products) 6.4.

The equations for selectivities of DME methanol and CO_2 were expressed as;

$$S_{DME} = \frac{2 * n_{DME}}{n_{CO,0} - n_{CO}} \quad [B4]$$

$$S_{CO_2} = \frac{n_{CO2} - n_{CO_2,0}}{n_{CO,0} - n_{CO}} \quad [B6]$$

Sample calculations for product selectivities at 300^{o}C are given below and the results for all temperatures were tabulated in Table 29.

$$S_{DME} = \frac{2 * n_{DME}}{n_{CO,0} - n_{CO}} = \frac{2 * 91.52}{429.75 - 200.32} = 0.798$$

$$S_{CO_2} = \frac{n_{CO2} - n_{CO_2,0}}{n_{CO,0} - n_{CO}} = \frac{92.89 - 69.96}{429.75 - 200.32} = 0.100$$

Table 29. Product selectivities defined with respect to moles of CO converted to products

T, ^{o}C	**S_{DME}**	**S_{CO_2}**	**S_{MeOH}**	**S_{CH_4}**	**S_{FA}**	**S_{EtOH}**
180	-0.031	1.122	-0.091	0	0	0
200	-0.368	2.370	-1.002	0	0	0
225	1.366	-1.399	1.033	0	0	0
250	0.833	-0.008	0.174	0	0	0
275	0.851	0.054	0.091	0.004	0	0
300	0.798	0.100	0.064	0.013	0.009	0.016

According to the results of CO conversion given in Table 28, carbon monoxide conversions were negative below 225^{o}C which indicated that carbon dioxide acted as a reactant while carbon monoxide acted as a product rather than being a reactant at these temperatures and some amount of CO_2 was converted to CO via reverse water-gas shift reaction. In addition, CO_2 conversion was negative above 250^{o}C, which indicated that CO_2 behaved as a product; formed more than it was consumed. The selectivities of the components were calculated with respect to moles of converted carbon monoxide. Therefore, some inconsistencies occurred such as CO_2 selectivities were first higher than one and then decreased below zero, methanol and DME selectivities were negative at low temperatures. Therefore, selectivities were defined with respect to and expressed as;

$\underline{S}_{DME}$ = 2(Moles of DME formed) / (Moles of CO&CO_2 converted to products) 6.7.

$\underline{S}_{MEOH}$= (Moles of MEOH formed) / (Moles of CO&CO_2 converted to products) 6.8.

The equations for selectivities of DME and methanol with respect to total moles of converted CO and CO_2 were expressed as;

$$S_{DME} = \frac{2 * n_{DME}}{n_{C,0} - (n_{CO} + n_{CO_2})} \quad [B16]$$

$$S_{MEOH} = \frac{n_{MEOH}}{n_{C,0} - (n_{CO} + n_{CO_2})} \quad [B17]$$

Sample calculations for product selectivities which were defined with respect to total moles of converted CO and CO_2 at 300^{o}C are given below and the results for all temperatures were tabulated in Table 30.

$$S_{DME} = \frac{2 * n_{DME}}{n_{C,0} - (n_{CO} + n_{CO_2})} = \frac{2 * 91.52}{499.71 - (200.32 + 92.89)} = 0.886$$

$$S_{MEOH} = \frac{n_{MEOH}}{n_{C,0} - (n_{CO} + n_{CO_2})} = \frac{14.69}{499.71 - (200.32 + 92.89)} = 0.071$$

Table 30. Product selectivities defined with respect to total moles of CO&CO_2 converted to products

T, ^{o}C	S_{DME}	S_{CO_2}	S_{MeOH}	S_{CH_4}	S_{FA}	S_{EtOH}
180	0.251	-9.210	0.749	0	0	0
200	0.269	-1.730	0.731	0	0	0
225	0.569	-0.583	0.431	0	0	0
250	0.827	-0.008	0.173	0	0	0
275	0.900	0.057	0.096	0.004	0	0
300	0.886	0.111	0.071	0.015	0.010	0.018

APPENDIX C

DRIFTS SPECTRA OF MA AND STA@MA

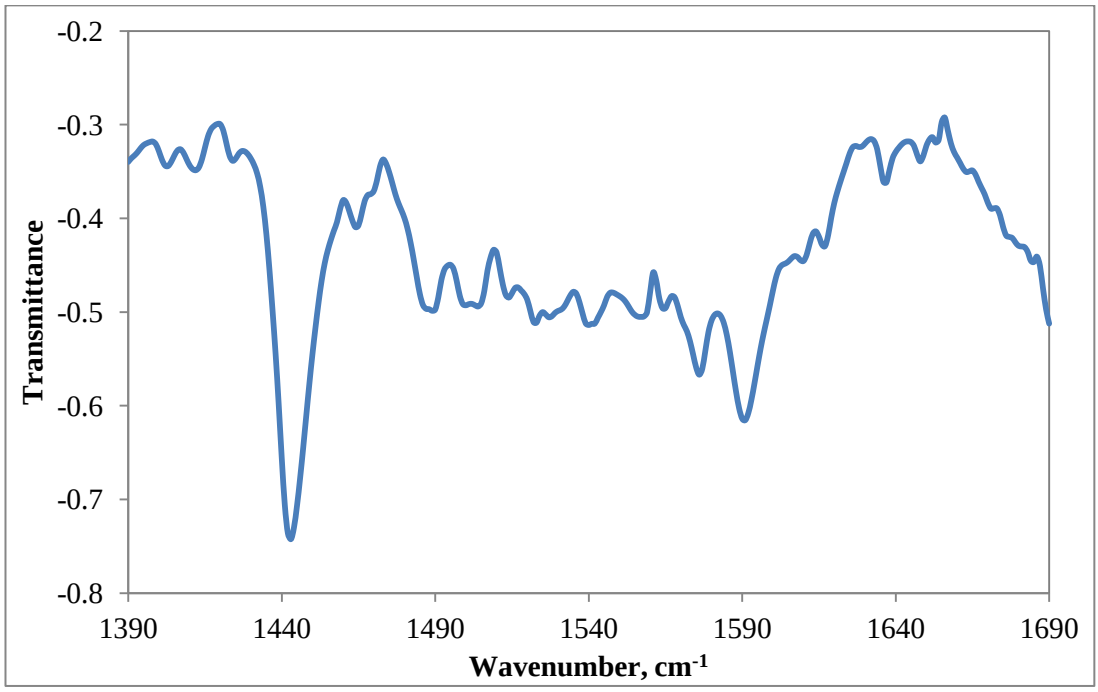

Figure 91. DRIFTS spectrum of MA

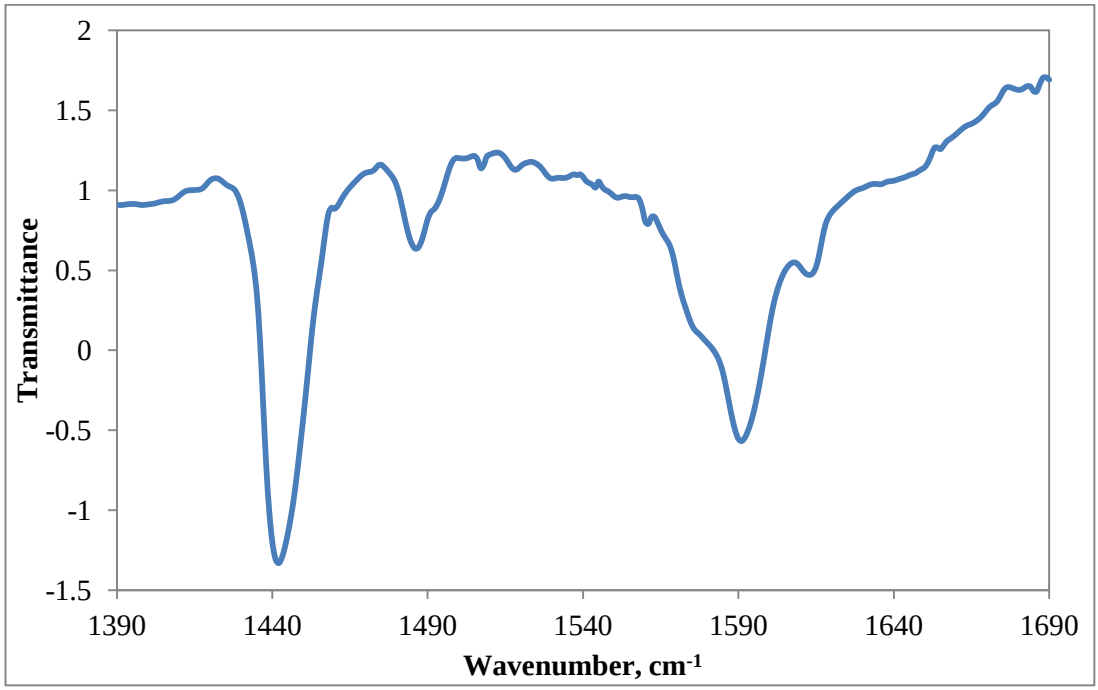

Figure 92. DRIFTS spectrum of STA@MA

APPENDIX D

XRD PEAKS OF CuO AND ZnO

Table 31. 2θ degree of CuO on XRD Pattern [89]

2θ, degree	**Peak**
33	110
36	002
39	200
49	202
54	020
58	202
62	113
66	311
68	220

Table 32. 2θ degree of CuO on XRD Pattern [90]

2θ, degree	**Peak**
32	100
35	002
36	101
48	102
57	110
63	103
67	200
68	112
69	201
73	004
77	202

APPENDIX E

PARTICLE SIZE CALCULATIONS

For the used catalysts, particle sizes of the copper and copper oxide were calculated using Scherrer's equation [23].

$$d_i = \frac{K \times \lambda}{\beta \times \cos(\theta)} \qquad [E1]$$

where, d_i = particle size of i,
K = shape factor
λ = X-Ray wavelength
β = Full width at half max (FWHM)
θ = Bragg's angle

Particle sizes of CuO and Cu calculated from the peaks of 2θ at around 35^o for CuO, and 43^o Cu for Scherrer's equation. X-Ray wavelength and shape factor were taken as 0.154 nm and 0.89, respectively.

For CZZr + TOYO used catalyst, CuO particle size was calculated for 2θ angle of 36.2^o. FWHM was 1.5^o according to the XRD results. FWHM and 2θ values were converted to radians.

$$\text{FWHM (radians)} = \frac{\text{FWHM}(°) \times \pi}{180} = \frac{1.5 \times \pi}{180} = 0.026$$

$$2\theta(\text{radians}) = \frac{2\theta(°) \times \pi}{180} = \frac{36.2 \times \pi}{180} = 0.632$$

$$d_i = \frac{0.89 \times 0.154}{0.026 \times \cos(0.632/2)} = 5.5 \text{ nm}$$

The related particle sizes for copper and copper oxide were calculated from Equation E1 similarly and the results were compiled in Table 33.

Table 33. Particle sizes for metals and metal oxides calculated from Scherrer's equation

Catalyst	**Peak**	**2θ, °**	**FWHM, °**	**Particle Size, nm**
CZZr + TOYO	CuO	36.2	1.50	5.51
	Cu	43.3	0.65	13.00
MSC + MA	CuO	36.8	1.70	4.87
	Cu	43.5	0.90	9.39
CZZr + MA	CuO	36.4	1.20	6.89
	Cu	43.5	0.50	16.91
MSC + STA@MA	CuO	36.2	1.80	4.59
	Cu	43.2	0.60	14.08
CZZr + STA@MA	CuO	36.5	1.00	8.27
	Cu	43.6	0.60	14.10
MSC + STA@MA (1:2)	CuO	36.2	2.00	4.13
	Cu	43.5	0.75	11.27
CZZr + STA@MA (1:2)	CuO	36.4	1.20	6.89
	Cu	43.5	0.65	13.01
MSC + STA@MA - 10% CO_2	CuO	36.1	2.10	3.93
	Cu	43.4	0.60	14.08
MSC + STA@MA - 25% CO_2	CuO	36.6	3.00	2.76
	Cu	43.5	0.80	10.57
MSC + STA@MA - 40% CO_2	CuO	36.5	2.75	3.01
	Cu	43.6	0.85	9.95

APPENDIX F

THERMODYNAMIC EQUILIBRIUM RESULTS

Table 34. Thermodynamic equilibrium results for feed mixture of $H_2/CO = 50/50$

T, K	n_{CO}	n_{CO_2}	n_{DME}	n_{MeOH}	y_{CO}	y_{CO_2}	$x_{CO_{eq}}$
373	0.002	0.332	0.333	0.000	0.003	0.498	0.998
398	0.005	0.331	0.332	0.001	0.007	0.496	0.995
423	0.010	0.329	0.330	0.002	0.015	0.491	0.990
448	0.020	0.326	0.326	0.002	0.029	0.483	0.980
473	0.036	0.319	0.321	0.004	0.053	0.470	0.964
498	0.062	0.310	0.311	0.006	0.090	0.449	0.938
523	0.104	0.294	0.297	0.008	0.148	0.419	0.896
548	0.168	0.271	0.276	0.010	0.231	0.375	0.832
573	0.262	0.238	0.244	0.012	0.347	0.315	0.738
598	0.394	0.194	0.200	0.013	0.493	0.242	0.606
623	0.557	0.139	0.146	0.012	0.653	0.163	0.443
648	0.721	0.086	0.092	0.009	0.794	0.095	0.279
673	0.846	0.047	0.050	0.006	0.891	0.049	0.154
698	0.922	0.023	0.026	0.004	0.946	0.024	0.078
723	0.961	0.011	0.013	0.002	0.973	0.011	0.039
748	0.980	0.006	0.006	0.001	0.987	0.006	0.020
773	0.990	0.003	0.003	0.001	0.993	0.003	0.010

Table 35. Thermodynamic equilibrium results for feed mixture of $H_2/CO/CO_2$ = 50/40/10

T, K	n_{CO}	n_{CO_2}	n_{DME}	n_{MeOH}	y_{CO}	y_{CO_2}	$x_{CO_{eq}}$
373	0.000	0.178	0.147	0.007	0.000	0.535	1.000
398	0.000	0.182	0.145	0.008	0.000	0.543	1.000
423	0.000	0.186	0.143	0.009	0.001	0.550	0.999
448	0.002	0.189	0.140	0.009	0.005	0.557	0.996
473	0.005	0.191	0.138	0.009	0.013	0.559	0.989
498	0.012	0.191	0.134	0.009	0.034	0.552	0.971
523	0.028	0.187	0.128	0.009	0.078	0.532	0.933
548	0.057	0.178	0.118	0.009	0.157	0.492	0.863
573	0.104	0.162	0.102	0.009	0.277	0.429	0.747
598	0.174	0.139	0.079	0.008	0.434	0.347	0.579
623	0.260	0.111	0.051	0.007	0.605	0.259	0.371
648	0.341	0.085	0.024	0.005	0.749	0.186	0.174
673	0.392	0.068	0.008	0.003	0.832	0.144	0.050
698	0.413	0.061	0.002	0.002	0.864	0.128	0.001
723	0.420	0.058	0.000	0.001	0.876	0.121	0.000
748	0.423	0.056	0.000	0.001	0.881	0.117	0.000
773	0.425	0.054	0.000	0.000	0.886	0.113	0.000

Table 36. Thermodynamic equilibrium results for feed mixture of $H_2/CO/CO_2$ = 50/25/25

T, K	n_{CO}	n_{CO_2}	n_{DME}	n_{MeOH}	y_{CO}	y_{CO_2}	$x_{CO_{eq}}$
373	0.000	0.193	0.123	0.011	0.000	0.589	1.000
398	0.000	0.200	0.118	0.013	0.000	0.604	1.000
423	0.000	0.209	0.113	0.010	0.001	0.628	0.999
448	0.001	0.219	0.108	0.015	0.003	0.639	0.996
473	0.003	0.227	0.103	0.015	0.008	0.654	0.989
498	0.008	0.234	0.097	0.014	0.022	0.662	0.972
523	0.019	0.237	0.090	0.014	0.052	0.658	0.931
548	0.041	0.234	0.081	0.013	0.112	0.633	0.848
573	0.082	0.223	0.066	0.012	0.215	0.581	0.698
598	0.144	0.204	0.046	0.010	0.356	0.505	0.472
623	0.215	0.182	0.023	0.008	0.504	0.425	0.212
648	0.267	0.165	0.007	0.005	0.602	0.372	0.024
673	0.289	0.156	0.002	0.003	0.644	0.347	0.000
698	0.298	0.150	0.000	0.001	0.662	0.334	0.000
723	0.304	0.145	0.000	0.001	0.676	0.322	0.000
748	0.310	0.140	0.000	0.000	0.688	0.311	0.000
773	0.315	0.135	0.000	0.000	0.700	0.299	0.000

Table 37. Thermodynamic equilibrium results for feed mixture of $H_2/CO/CO_2$ = 50/10/40

T, K	n_{CO}	n_{CO_2}	n_{DME}	n_{MeOH}	y_{CO}	y_{CO_2}	$x_{CO_{eq}}$
373	0.000	0.207	0.098	0.013	0.000	0.651	1.000
398	0.000	0.218	0.091	0.015	0.000	0.672	0.999
423	0.000	0.232	0.084	0.016	0.001	0.697	0.998
448	0.001	0.246	0.076	0.017	0.003	0.723	0.993
473	0.002	0.261	0.068	0.017	0.007	0.748	0.979
498	0.006	0.273	0.060	0.017	0.018	0.767	0.946
523	0.015	0.283	0.052	0.016	0.041	0.775	0.872
548	0.032	0.287	0.042	0.014	0.086	0.765	0.721
573	0.063	0.283	0.029	0.012	0.163	0.731	0.457
598	0.104	0.273	0.015	0.009	0.260	0.680	0.098
623	0.141	0.260	0.005	0.006	0.342	0.633	0.010
648	0.161	0.250	0.001	0.003	0.387	0.603	0.000
673	0.173	0.241	0.000	0.002	0.416	0.580	0.000
698	0.183	0.232	0.000	0.001	0.440	0.558	0.000
723	0.192	0.224	0.000	0.000	0.462	0.537	0.000
748	0.201	0.215	0.000	0.000	0.483	0.516	0.000
773	0.210	0.206	0.000	0.000	0.504	0.496	0.000